1. General Experimental Information

Unless otherwise stated, all reagents were purchased from commercial sources (Acros Organics, Alfa Aesar, Fisher Scientific, FluoroChem, Sigma Aldrich and VWR) and used without further purification. $[Cu(CH_3CN)_4]PF_6$ was prepared as described by Pigorsch and Köckerling.[1] Anhydrous solvents were purchased from Acros Organics. Petrol refers to the fraction of petroleum ether boiling in the range 40-60 °C. IPA refers to isopropanol. THF refers to tetrahydrofuran. EDTA-NH_3 solution refers to an aqueous solution of NH_3 (17% w/w) saturated with sodium-ethylenediaminetetraacetate. IBX = 2-iodoxybenzoic acid. $CDCl_3$ (without stabilising agent) was distilled over $CaCl_2$ and K_2CO_3 prior to use. Unless otherwise stated, all reaction mixtures were performed in oven dried glassware under an inert N_2 atmosphere with purchased anhydrous solvents. Unless otherwise stated experiments carried out in sealed vessels were performed in CEM microwave vials, with crimped aluminium caps, with PTFE septa. Young's tap vessels and Schlenk techniques were used where specified.

Flash column chromatography was performed using Biotage Isolera-4 or Isolera-1 automated chromatography system. SiO_2 cartridges were purchased commercially Biotage (SNAP or ZIP (50 μm), or Sfär (60 μm) irregular silica, default flow rates). Neutralised SiO_2 refers to ZIP cartridges which were eluted with petrol-NEt_3 (99 : 1, 5 column volumes), followed by petrol (5 column volumes). Analytical TLC was performed on pre-coated silica gel plates on aluminum (0.25 mm thick, 60F254, Merck, Germany) and observed under UV light (254 nm) or visualised with $KMnO_4$ stain.

All melting points were determined using a Griffin apparatus. NMR spectra were recorded on Bruker AV400 or AV500 instrument, at a constant temperature of 298 K. Chemical shifts are reported in parts per million from low to high field and referenced to residual solvent. Coupling constants (*J*) are reported in Hertz (Hz). Standard abbreviations indicating multiplicity were used as follows: m = multiplet, quint = quintet, q = quartet, t = triplet, d = doublet, s = singlet, app. = apparent, br = broad, sept = septet. Signal assignment was carried out using 2D NMR methods (COSY, NOESY, HSQC or HMBC) where necessary. In some cases, complex multiplets with multiple contributing proton signals, exact assignment was not possible. In interlocked compounds, all proton signals corresponding to axle components are in lower case, and all proton signals corresponding to the macrocycle components are in upper case.

Low resolution mass spectrometry was carried out by the mass spectrometry services at University of Southampton (Waters TQD mass spectrometer equipped with a triple quadrupole analyser with UHPLC injection [BEH C18 column; CH_3CN -H_2O gradient (0.2% formic acid)]). High resolution mass spectrometry was carried out by the mass spectrometry services at the University of Southampton (MaXis, Bruker Daltonics, with a Time of Flight (TOF) analyser; samples were introduced to the mass spectrometer via a Dionex Ultimate 3000 autosampler and uHPLC pump in a gradient of 20% CH_3CN in hexane to 100% acetonitrile (0.2% formic acid) over 5-10 min at 0.6 mL/min; column: Acquity UPLC BEH C18 (Waters) 1.7 micron 50 × 2.1mm).

Circular dichroism spectra were acquired on an Applied Photo-physics Chirascan spectropolarimeter, recorded using Applied Photophysics software Ver. 4.2.0 in dried spectroscopic grade $CHCl_3$, following

overnight desiccation of the sample, at a concentration range of <50 μM, in a quartz cell of 1 cm path length, at a temperature of 293 K.

Stereochemical purity was determined by Chiral Stationary Phase HPLC on a Waters Acquity Arc Instrument at 303 K, with *n*-hexane-^{i}PrOH or *n*-hexane-EtOH isocratic eluents. Regis Technologies (S,S)-Whelk-O1 (1-(3,5-dinitrobenzamido)-1,2,3,4-tetrahydrophenanthrene stationary phase), RegisPack (tris-(3,5-dimethylphenyl) carbamoyl amylose stationary phase), RegisPackCLA-1 (tris-(5-chloro-2-methylphenyl)carbamoyl amylose), and RegisCell (tris-(3,5-dimethylphenyl) carbamoyl cellulose stationary phase) columns were used throughout (5 micron, column dimensions 25 cm x 4.6 mm). Unless otherwise shown, racemic samples were prepared employing the same synthetic proceedures and auxiliary strategy but starting from racemic **S1**.

The following compounds were synthetized according to literature procedures: (*R*)-**S1**,[2] **S3**,[3] **S11**,[4] **8**.[5]

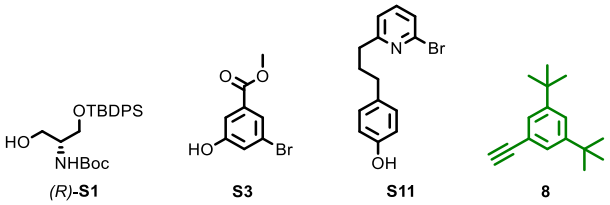

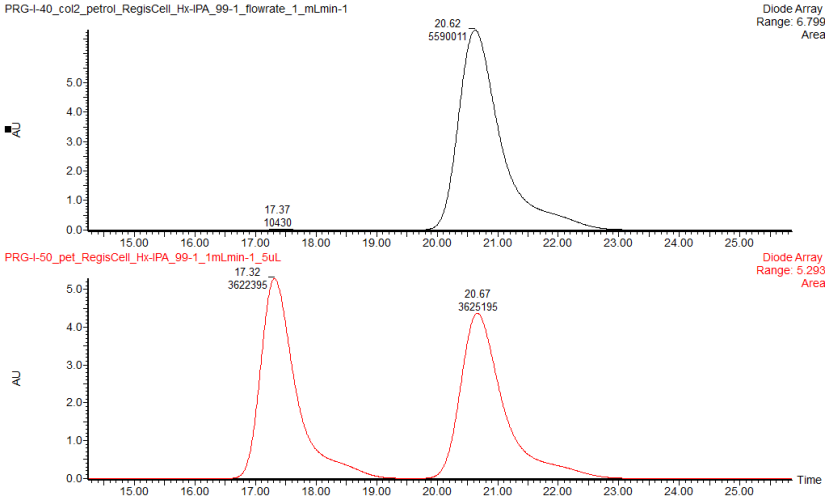

Figure 1: CSP-HPLC of (*R*)-**S1** (loaded in petrol). RegisCell, *n*-hexane-IPA 99 : 1, flowrate 1 mLmin^{-1}. (Top) (*R*)-**S1**, (*S*)-**S1** (17.37 min, 10430, 0.2%), (*R*)-**S1** (20.62 min, 5590011, 99.8%), (Bottom) *rac*-**S1**, (*S*)-**S1** (17.32 min, 3622395, 50.0%), (*R*)-**S1** (20.67 min, 3625195, 50.0%).

2. Compounds leading to catenane pre-macrocycle 1

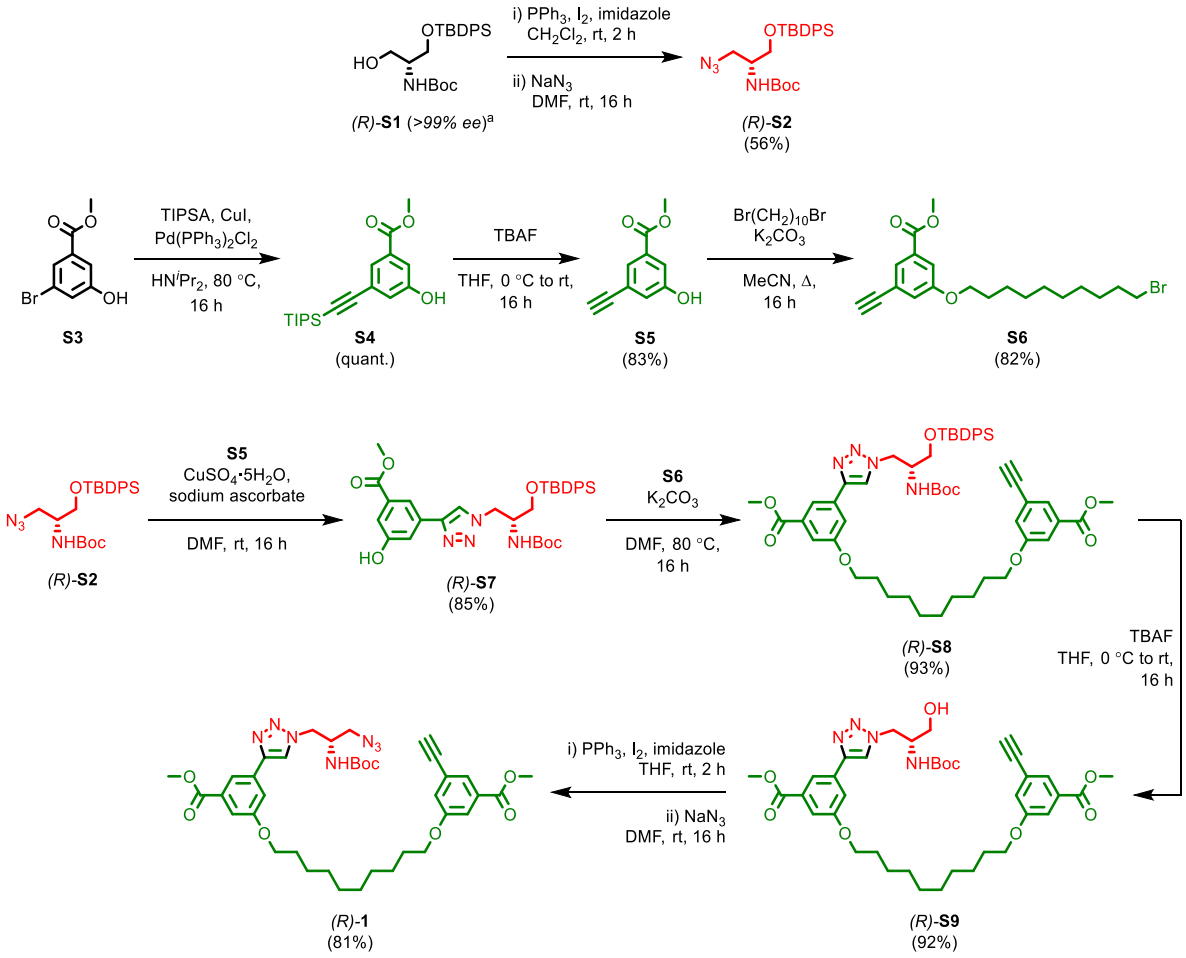

Scheme 1: Synthetic route to catenane pre-macrocycle (*R*)-**1**. [a]stereochemical purity was assessed by CSP-HPLC, Fig.S1.

2.1. Compound (*R*)-S2

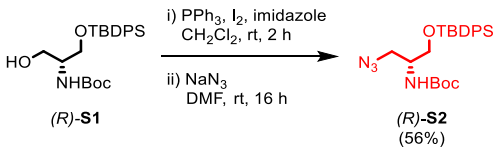

To a solution of PPh_3 (2.50 g, 9.53 mmol, 3.0 eq.) and imidazole (1.08 g, 15.86 mmol, 5.0 eq.) in CH_2Cl_2 (27 mL) was added I_2 (2.42 g, 9.53 mmol, 3.0 eq.) in 1 portion at 0 °C. After stirring for 10 min, a solution of (*R*)-**S1** (1.37 g, 3.19 mmol, 1.0 eq.) in CH_2Cl_2 (7 mL) was added dropwise. The reaction mixture was allowed to warm to ambient temperature and stirred for 2 h. The crude mixture was filtered through Celite®, washing with CH_2Cl_2, and concentrated *in vacuo*. The residue was purified by column chromatography (SiO_2, petrol-EtOAc 0→10%). The resultant oil was immediately dissolved in DMF (16 mL) and NaN_3 (1.04 g, 16.00 mmol, 5.0 eq.) was added. After stirring for 16 h at ambient temperature, the reaction mixture was diluted with EtOAc (10 mL), washed with H_2O (10 mL) and 1 M $Na_2S_2O_3·5H_2O$ (5 mL). The aqueous layer was extracted with EtOAc (3 x 10 mL). The combined organic fractions were washed with 5% LiCl (3 x 10 mL), and brine (10 mL) then dried over $MgSO_4$, filtered, and concentrated *in vacuo*. The residue was purified by column chromatography (SiO_2, petrol-Et_2O 0→20%) to yield (*R*)-**S2** (808.6 mg, 1.78 mmol, 56% over two steps) as a colourless oil.

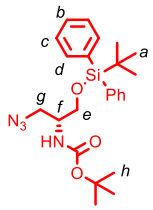

δ_H ($CDCl_3$, 400 MHz) 7.68 – 7.60 (m, 4H, H_b), 7.47 – 7.37 (m, 6H, H_c, H_d), 4.75 (d, J = 8.8, 1H, H_{NHBoc}), 3.85 (br s, 1H, H_f), 3.73 (dd, J = 10.3, 4.0, 1H, H_e), 3.64 (dd, J = 10.3, 5.5, 1H, H_e), 3.57 (dd, J = 12.1, 5.0, 1H, H_g), 3.47 (dd, J = 12.0, 6.2, 1H, H_g), 1.44 (s, 9H, H_h), 1.07 (s, 9H, H_a); δ_C ($CDCl_3$, 101 MHz) 135.7, 133.0, 130.1, 128.0, 79.8 (HMBC), 63.1, 51.6, 51.3, 28.5, 27.01, 19.5, peak corresponding to carbonyl not observed; HR-ESI-MS (+ve) m/z = 477.2290 $[M+Na]^+$ (calc. m/z for $C_{24}H_{34}N_4NaO_3Si$ 477.2292).

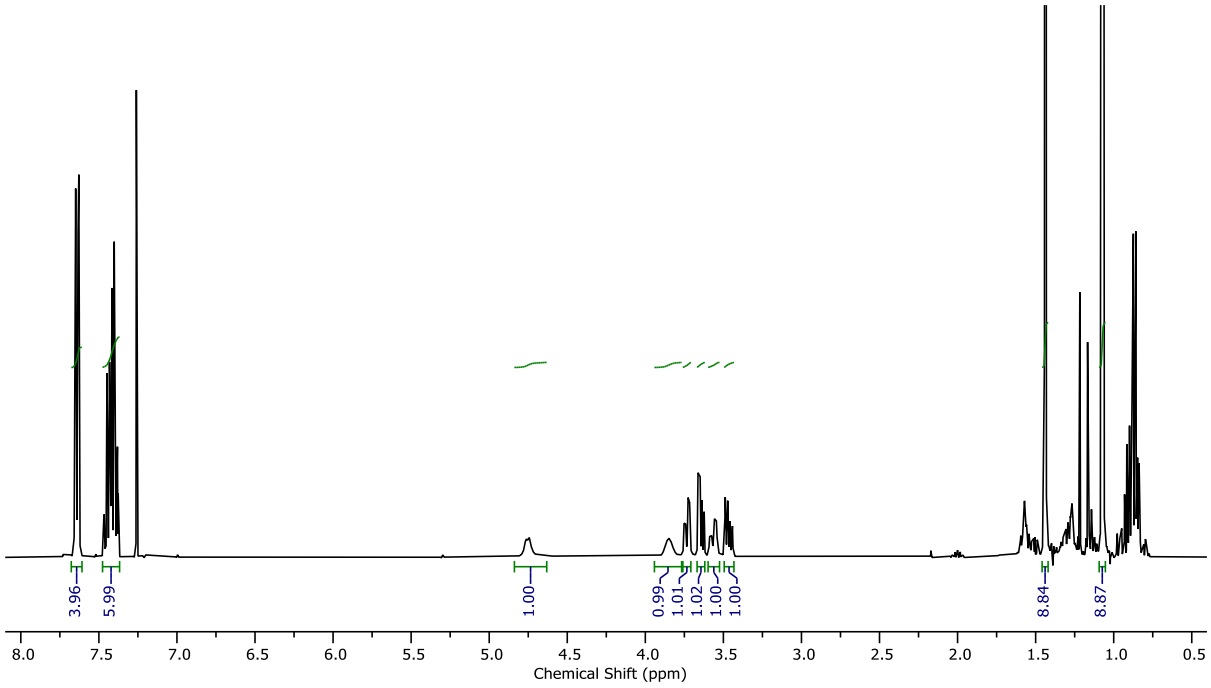

Figure 2: ^1H NMR ($CDCl_3$, 400 MHz) of **S2**.

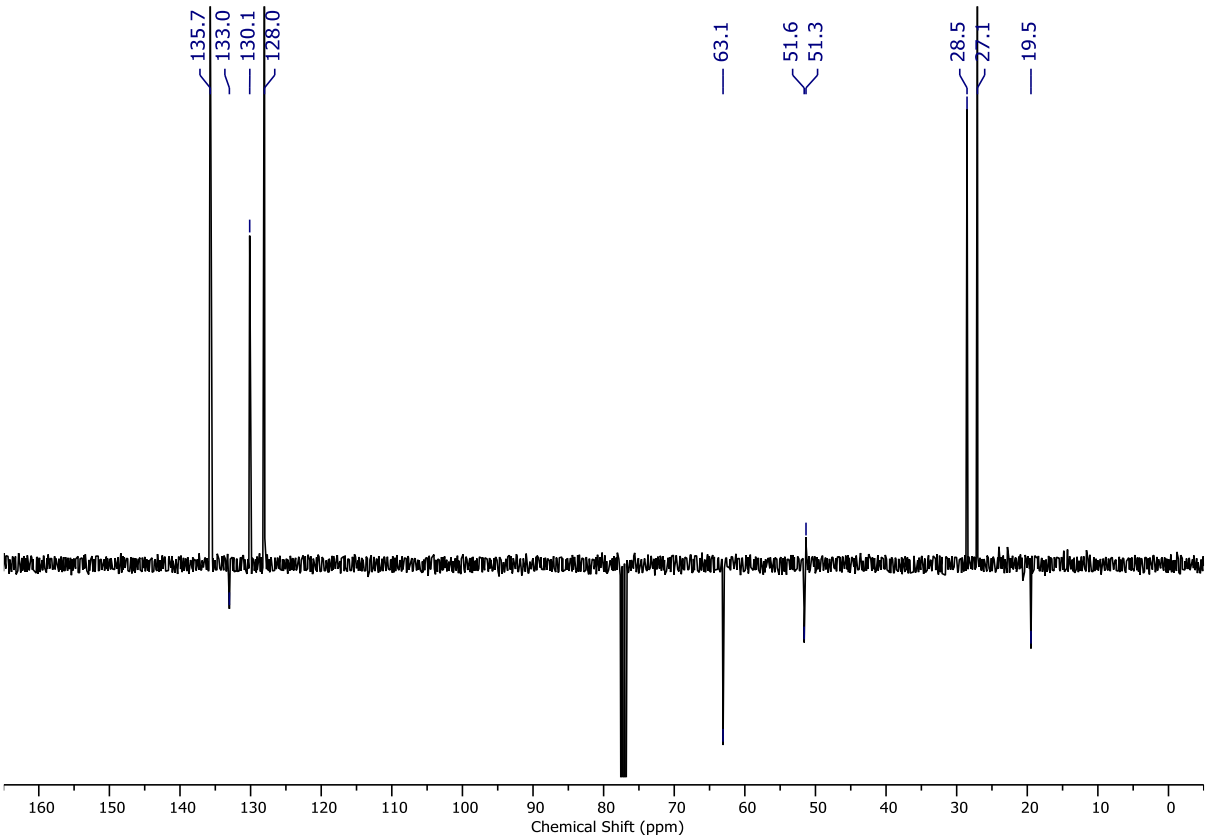

Figure 3: JMOD NMR ($CDCl_3$, 101 MHz) of **S2**.

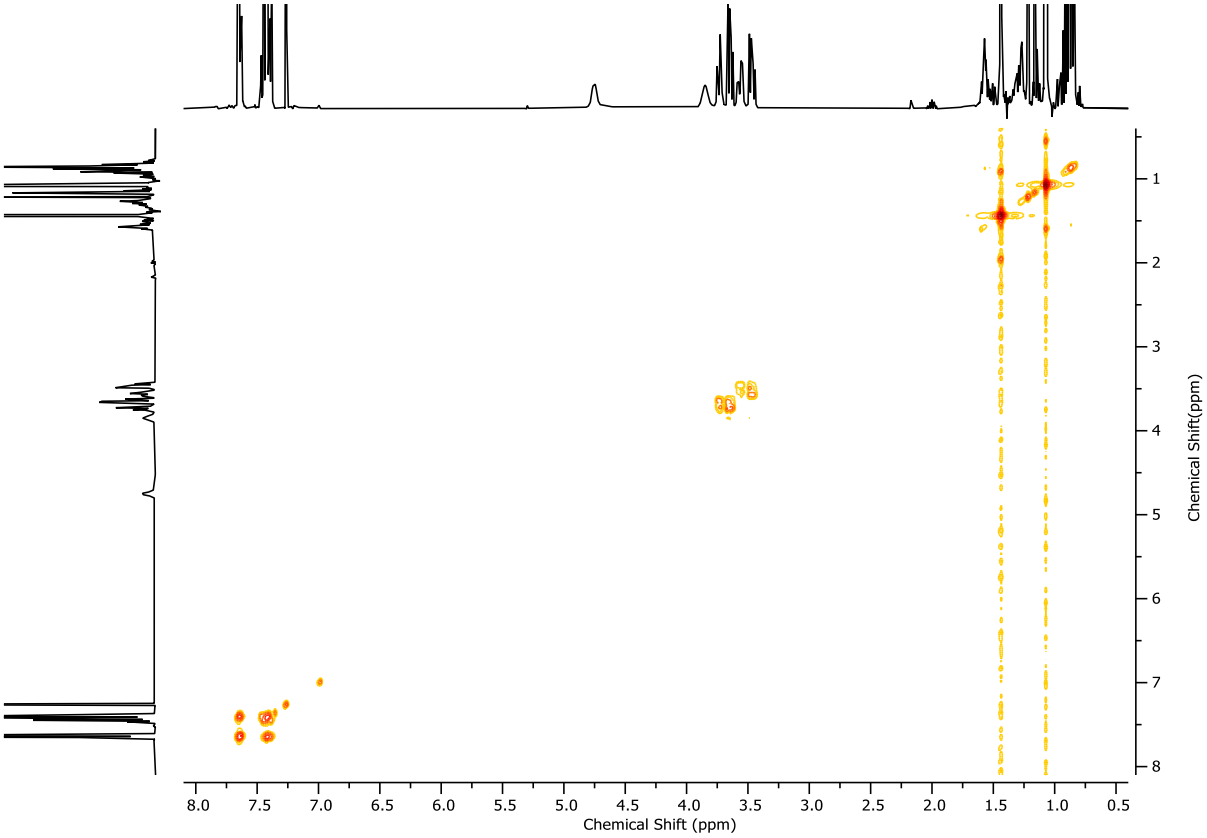

Figure 4: ^1H COSY NMR ($CDCl_3$, 400 MHz) of **S2**.

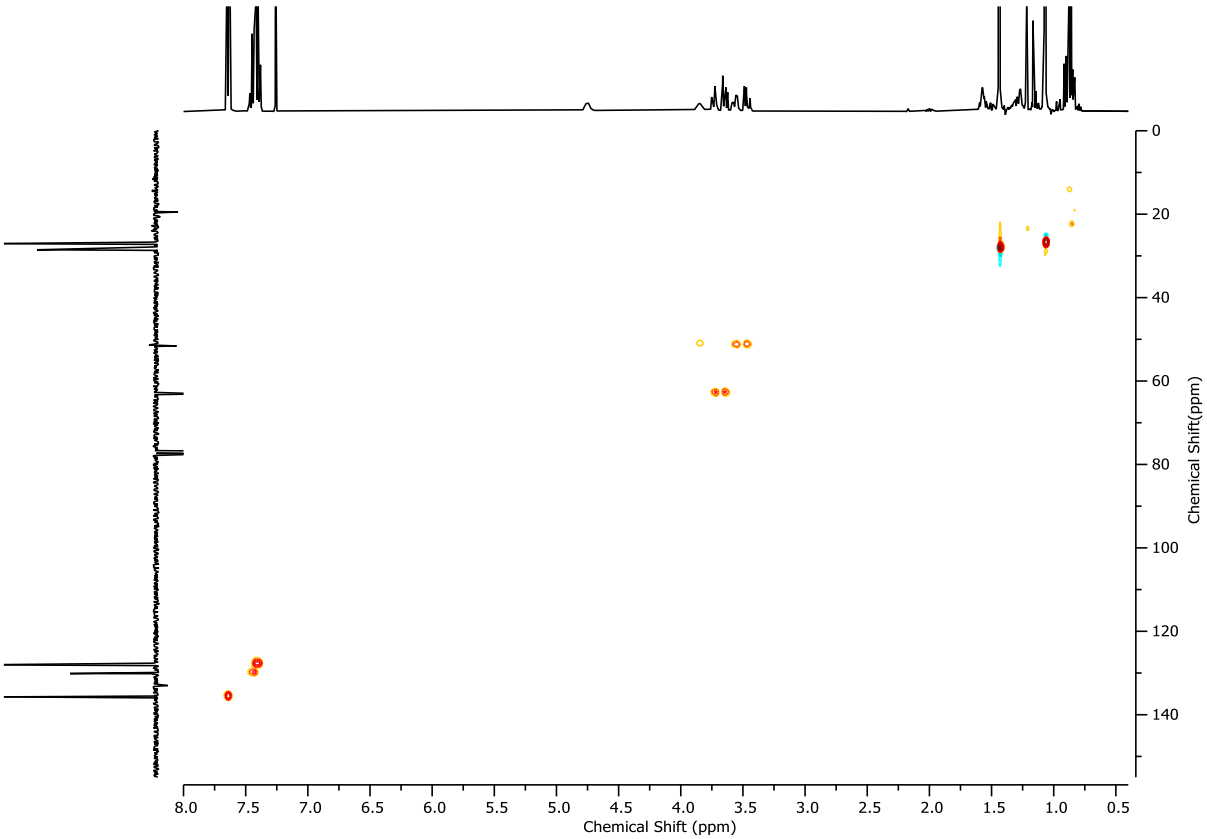

Figure 5: HSQC NMR ($CDCl_3$, 400 MHz) of **S2**.

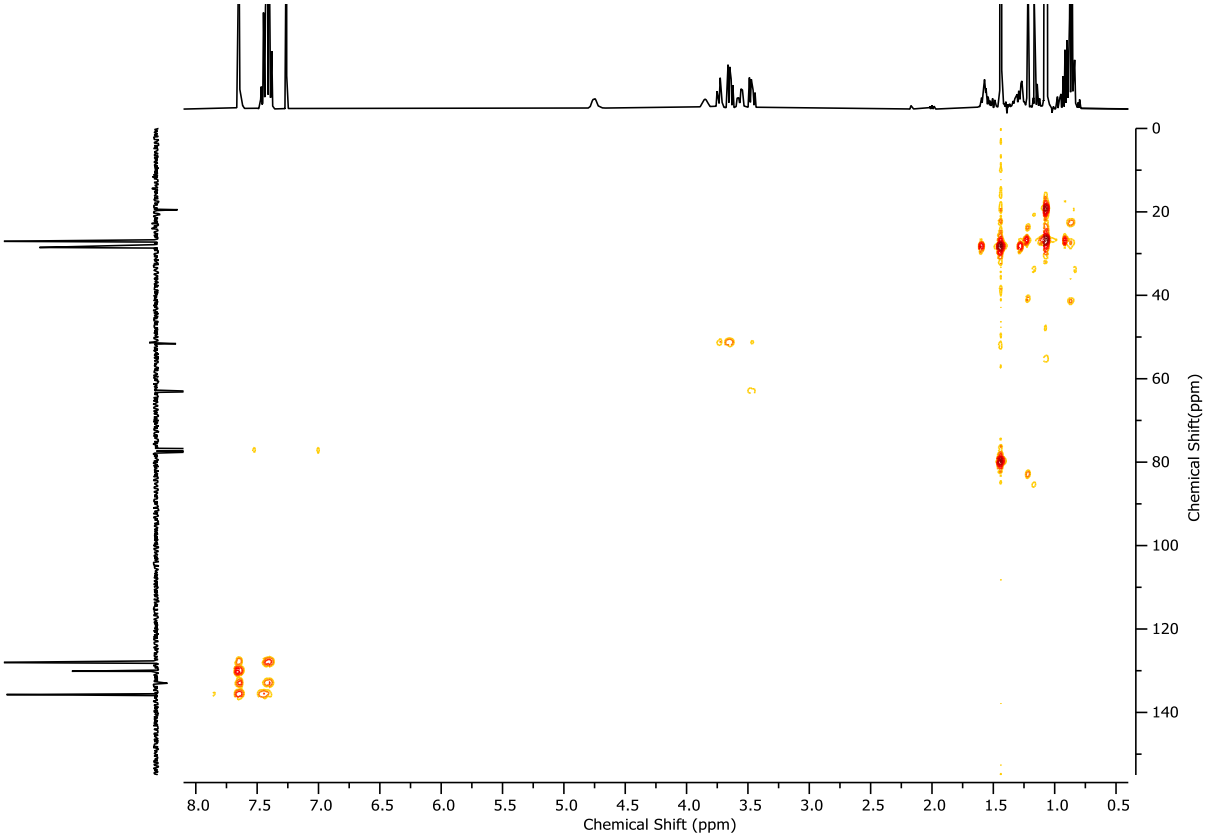

Figure 6: HMBC NMR ($CDCl_3$, 400 MHz) of **S2**.

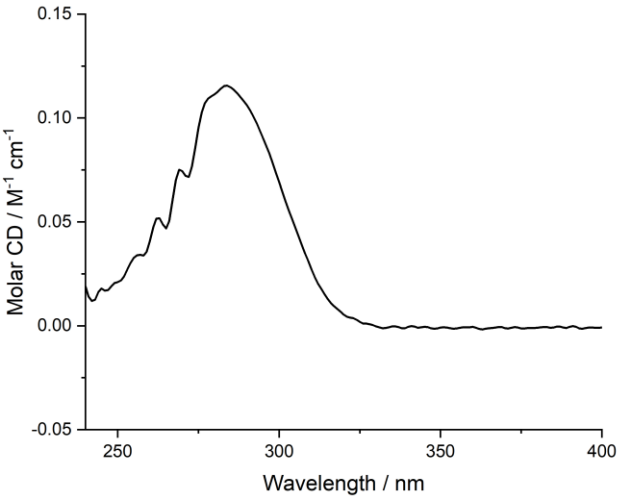

Figure 7: Circular Dichroism Spectra of (*R*)-**S2** (1.3 mM) at 293 K in $CHCl_3$.

2.2. Compound S4

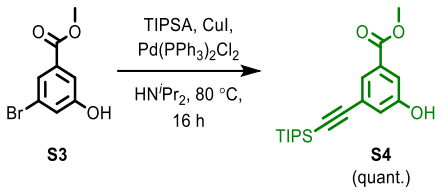

To a solution of **S3** (668 mg, 2.89 mmol, 1.0 eq.), $PdCl_2(PPh_3)_2$ (42.2 mg, 0.06 mmol, 0.02 eq.), CuI (23 mg, 0.12 mmol, 0.04 eq.) in degassed HN^iPr_2 (11.6 mL) was added (triisopropylsilyl)acetylene (1.30 mL, 5.78 mmol, 2.0 eq.), and the reaction mixture was heated at 80 °C for 16 h. After cooling to ambient temperature, and concentration *in vacuo*, the residue was purified by column chromatography (SiO_2, petrol-Et_2O 0→40%) to yield **S4** (970 mg, 2.92 mmol, quant.) as a yellow oil.

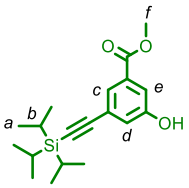

δ_H ($CDCl_3$, 400 MHz) 7.69 (t, *J* = 1.4, 1H, H_c), 7.51 (dd, *J* = 2.6, 1.4, 1H, H_e), 7.15 (dd, *J* = 2.6, 1.4, 1H, H_d), 5.99 (s, 1H, H_{OH}), 3.92 (s, 3H, H_f), 1.16 – 1.04 (m, 21H, H_a, H_b); δ_C ($CDCl_3$, 101 MHz) 166.8, 155.8, 131.6, 125.7, 125.3, 123.5, 116.8, 105.7, 92.0, 52.6, 18.8, 11.4; HR-ESI-MS (+ve) m/z = 333.1883 $[M+H]^+$ (calc. m/z for $C_{19}H_{29}O_3Si$ 333.1880).

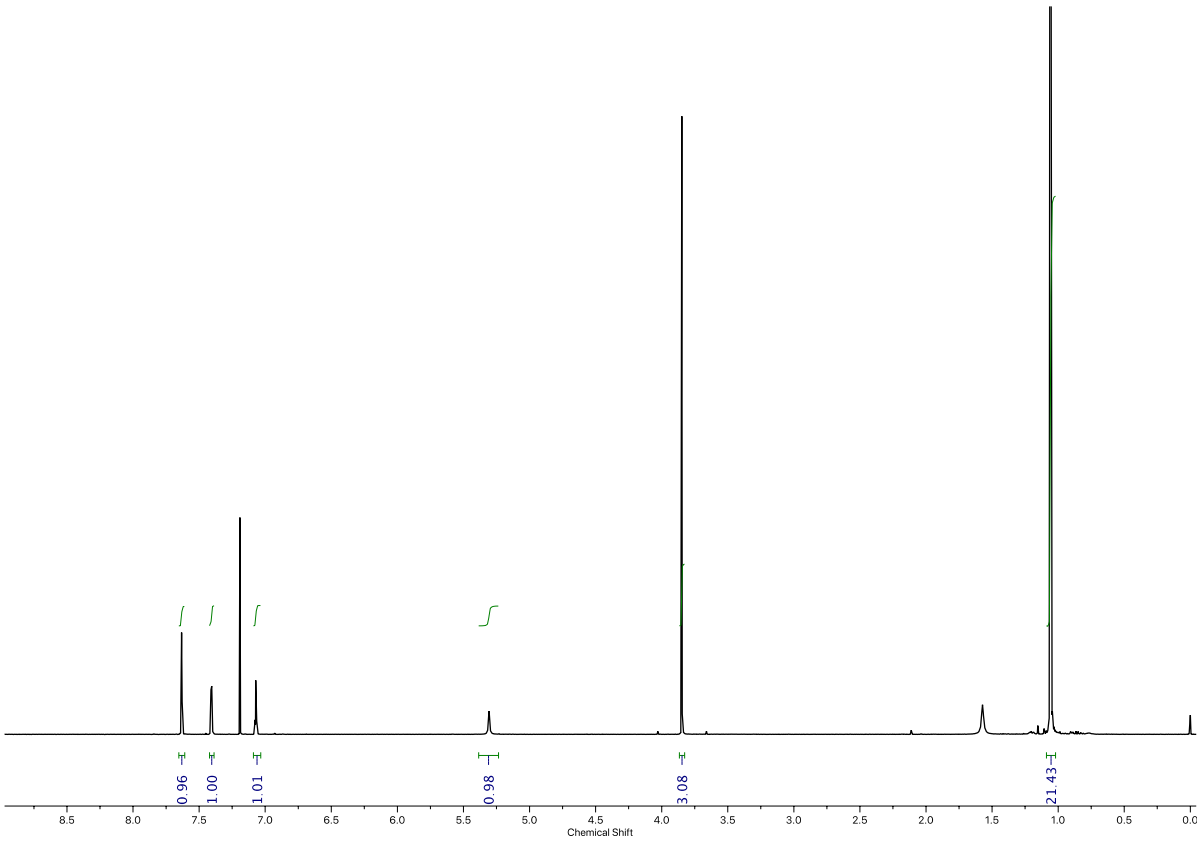

Figure 8: ^{1}H NMR ($CDCl_3$, 400 MHz) of **S4**.

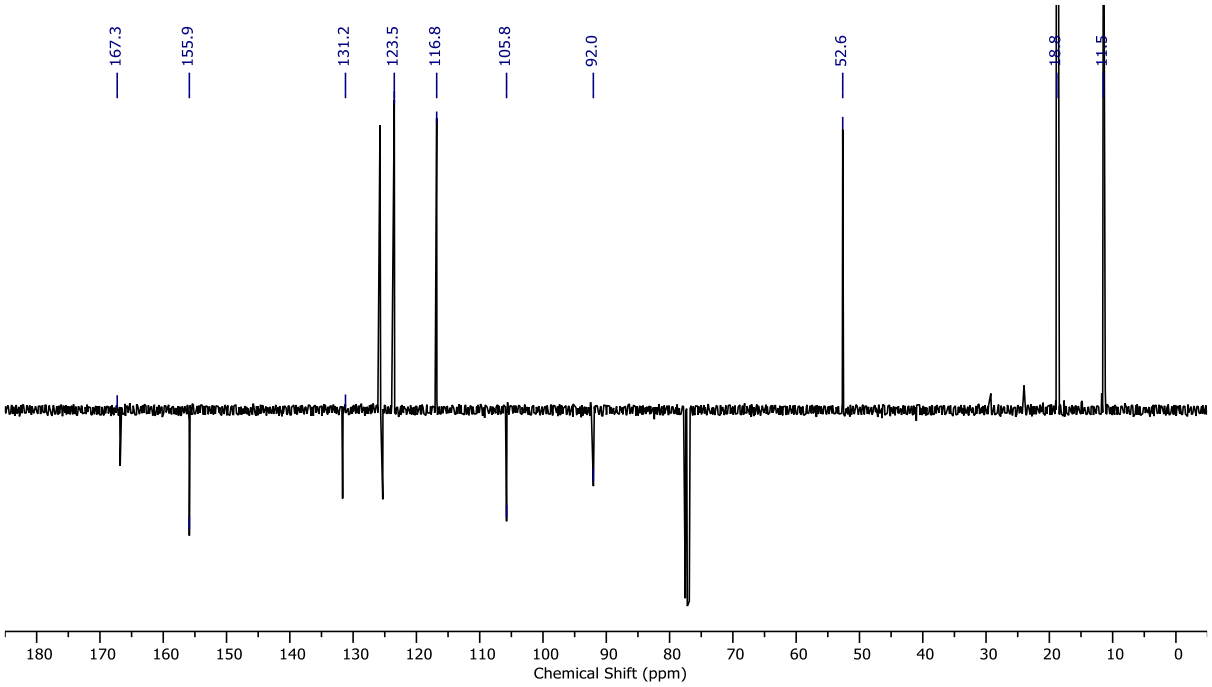

Figure 9: JMOD NMR ($CDCl_3$, 101 MHz) of **S4**.

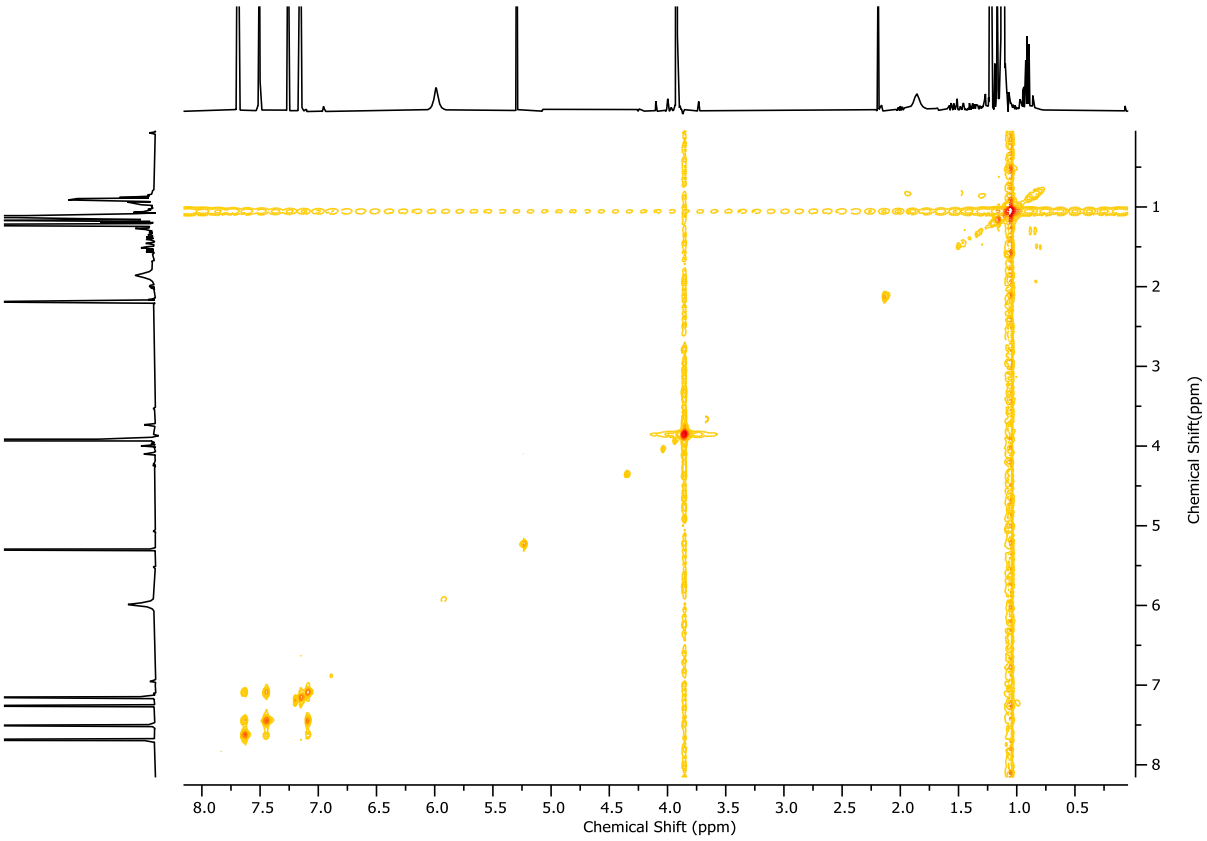

Figure 10: ^{1}H COSY NMR ($CDCl_3$, 400 MHz) of **S4**.

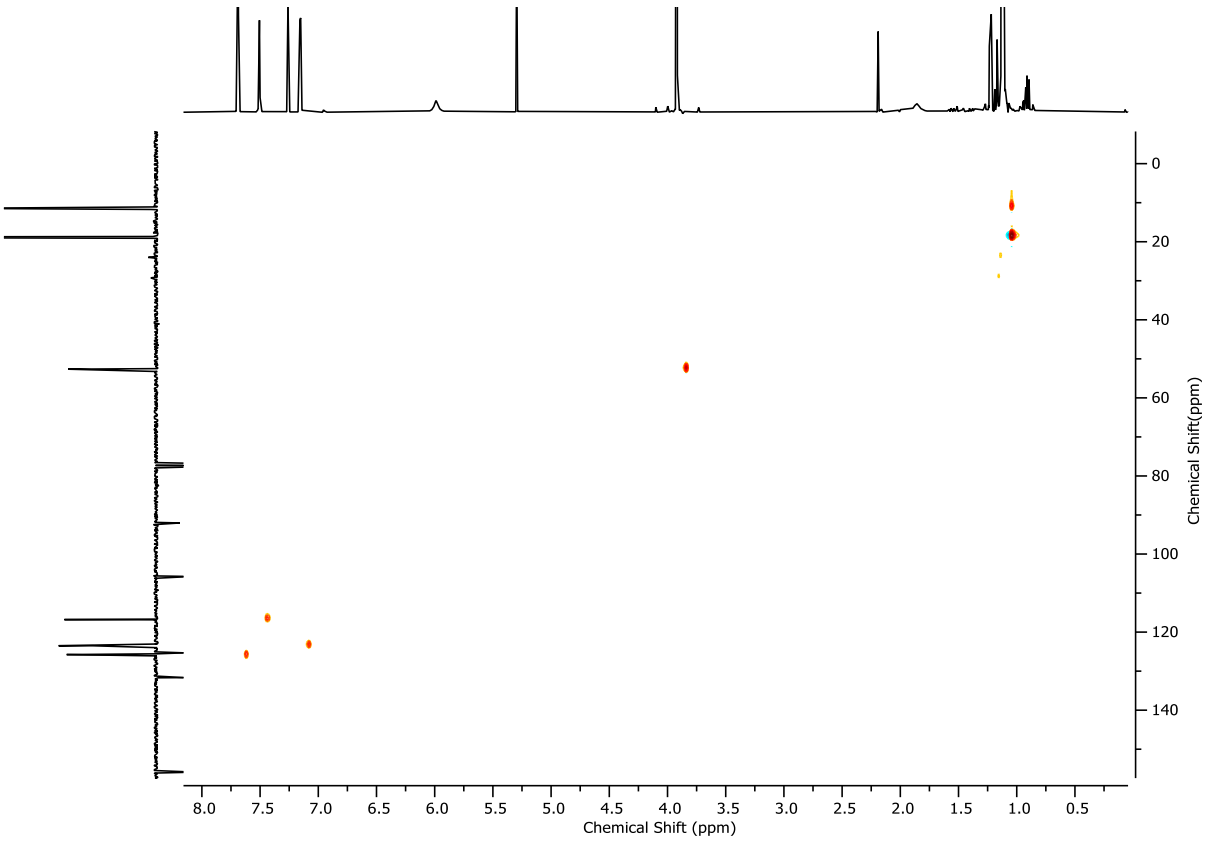

Figure 11: HSQC NMR ($CDCl_3$, 400 MHz) of **S4**.

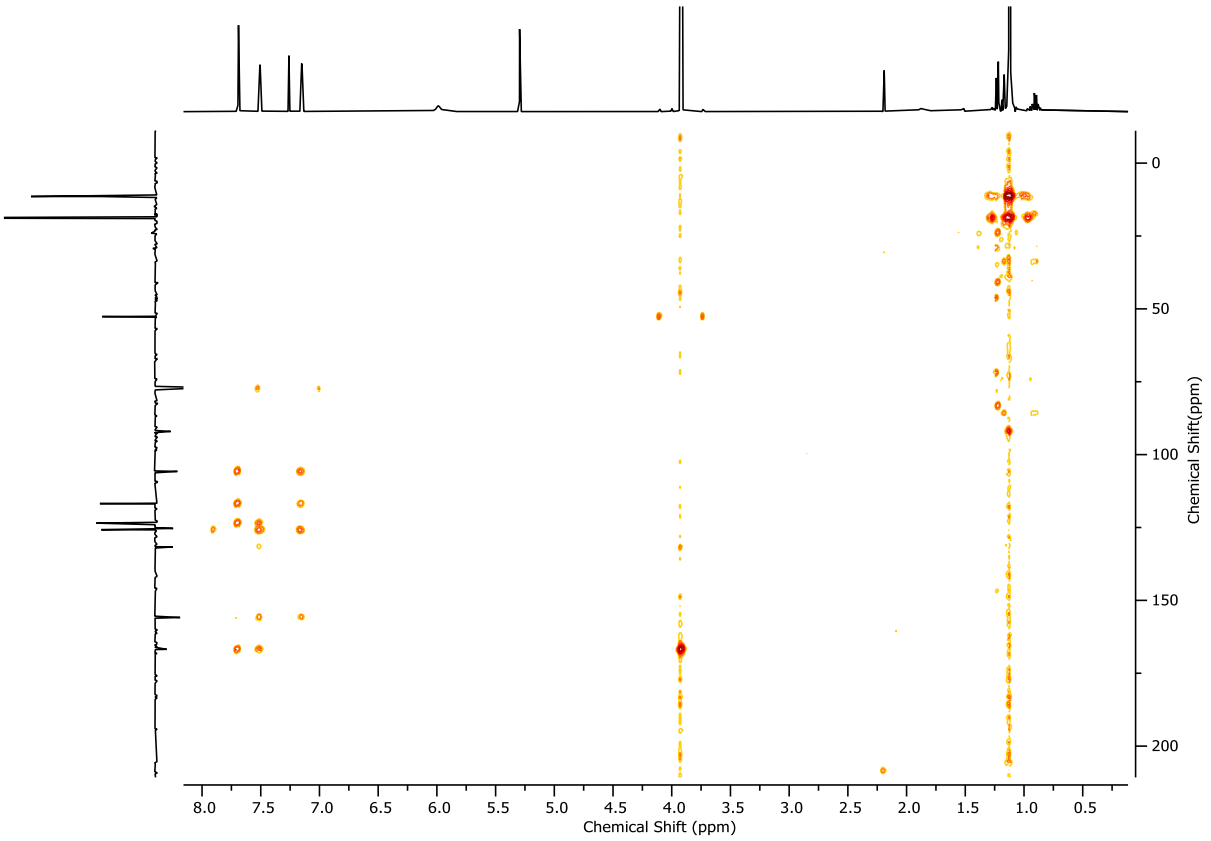

Figure 12: HMBC NMR ($CDCl_3$, 400 MHz) of **S4**.

2.3. Compound S5

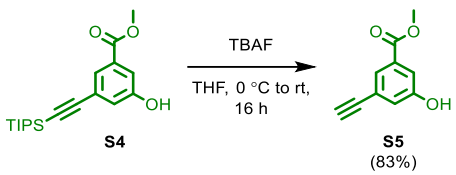

A solution of **S4** (703 mg, 2.11 mmol, 1.0 eq.) in THF (10.5 mL) was cooled to 0 °C, and a 1.0 M THF solution of TBAF (2.33 mL, 2.33 mmol, 1.1 eq.) was added dropwise. After warming to ambient temperature, the reaction mixture was stirred for 16 h before concentrating *in vacuo*. The crude material was dissolved in EtOAc (10 mL) and washed with H_2O (5 mL). The aqueous phase was extracted with EtOAc (2 x 5 mL), and the combined organics were washed with brine (5 mL), dried over $MgSO_4$, filtered and concentrated *in vacuo*. The residue was purified by column chromatography (SiO_2, petrol-EtOAc 0→20%) to yield **S5** (310 mg, 1.76 mmol, 83%) as a yellow solid.

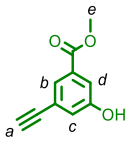

δ_H ($CDCl_3$, 400 MHz) 7.71 (t, J = 1.4, 1H, H_b), 7.58 (dd, J = 2.5, 1.5, 1H, H_d), 7.18 (dd, J = 2.5, 1.4, 1H, H_c), 6.45 (s, 1H, H_{OH}), 3.92 (s, 3H, H_e), 3.10 (s, 1H, H_a); δ_C ($CDCl_3$, 101 MHz) 166.2, 156.8, 132.7, 125.0, 123.5, 123.0, 115.6, 52.8; HR-ESI-MS (-ve) m/z = 175.0403 $[M-H]^-$ (calc. m/z for $C_{10}H_7O_3$ 15.0401); Melting point 102-104 °C.

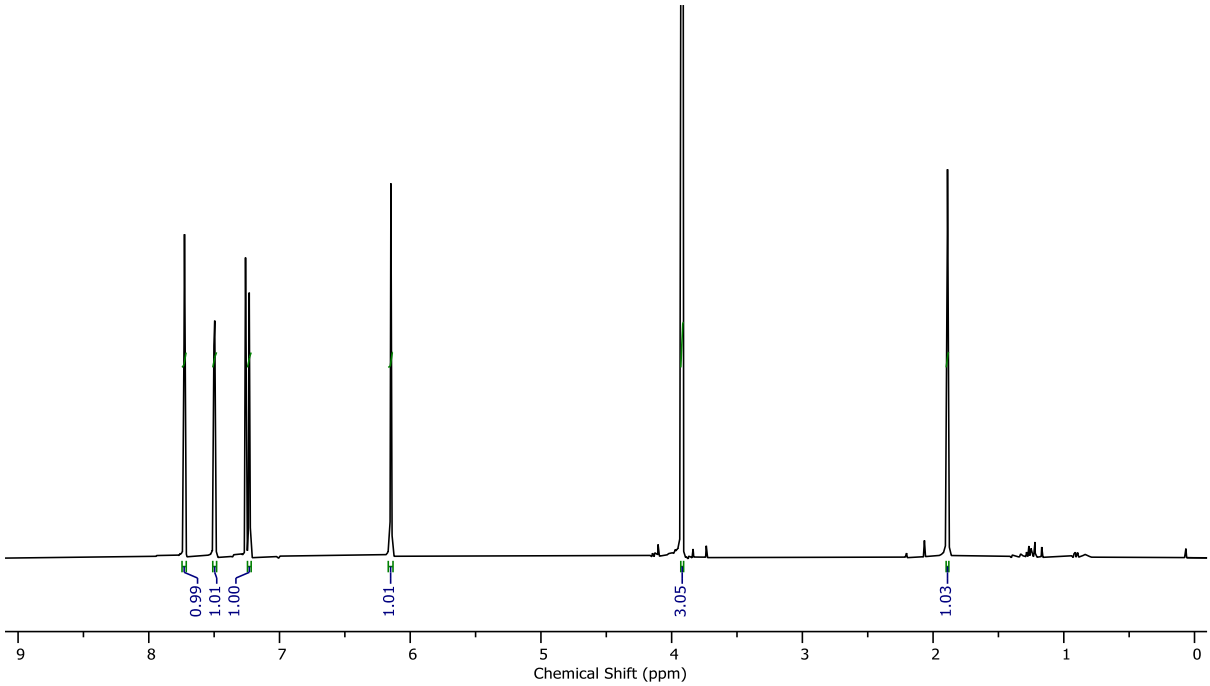

Figure 13: ^1H NMR ($CDCl_3$, 400 MHz) of **S5**.

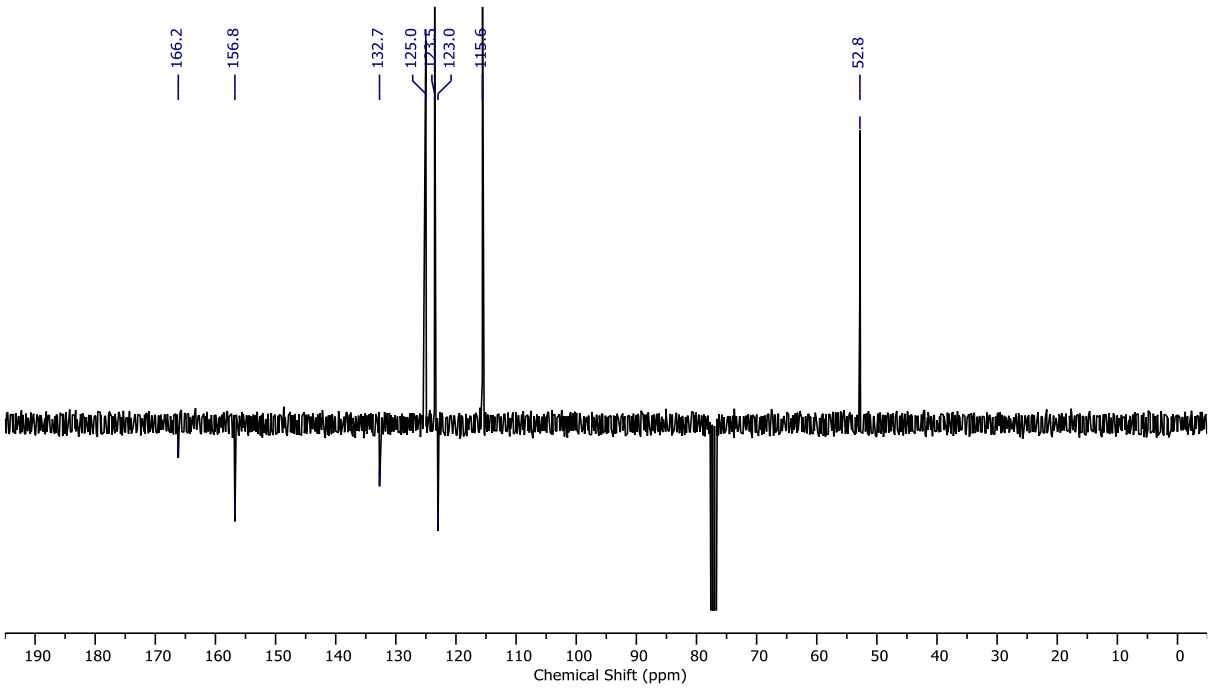

Figure 14: JMOD NMR ($CDCl_3$, 101 MHz) of **S5**.

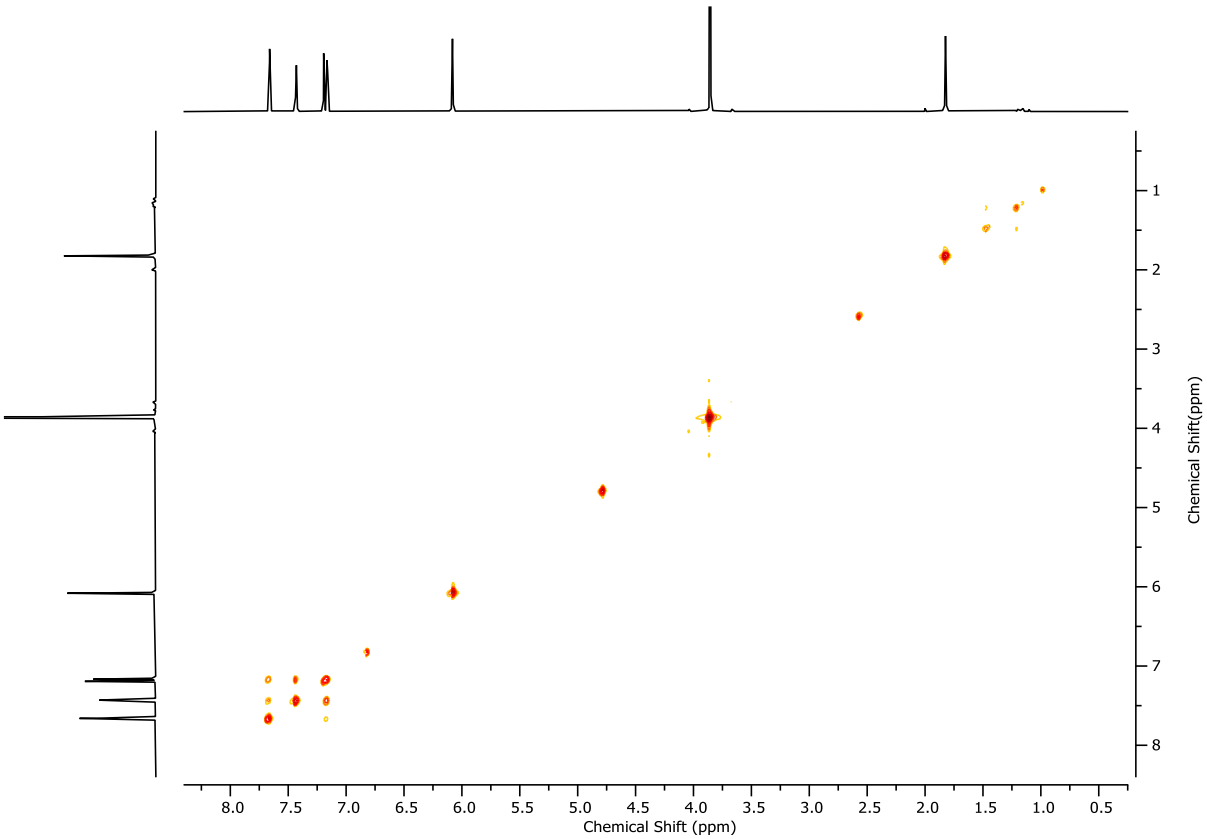

Figure 15: ^{1}H COSY NMR ($CDCl_3$, 400 MHz) of **S5**.

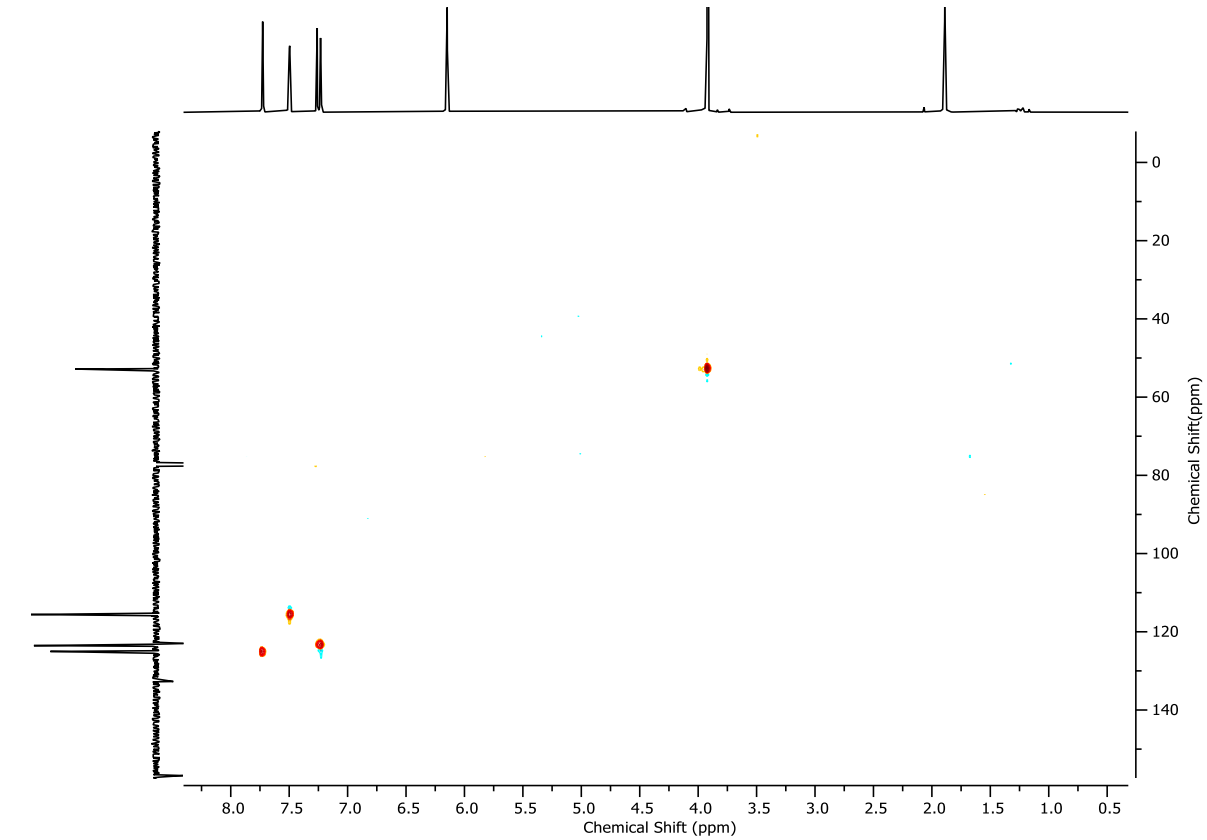

Figure 16: HSQC NMR ($CDCl_3$, 400 MHz) of **S5**.

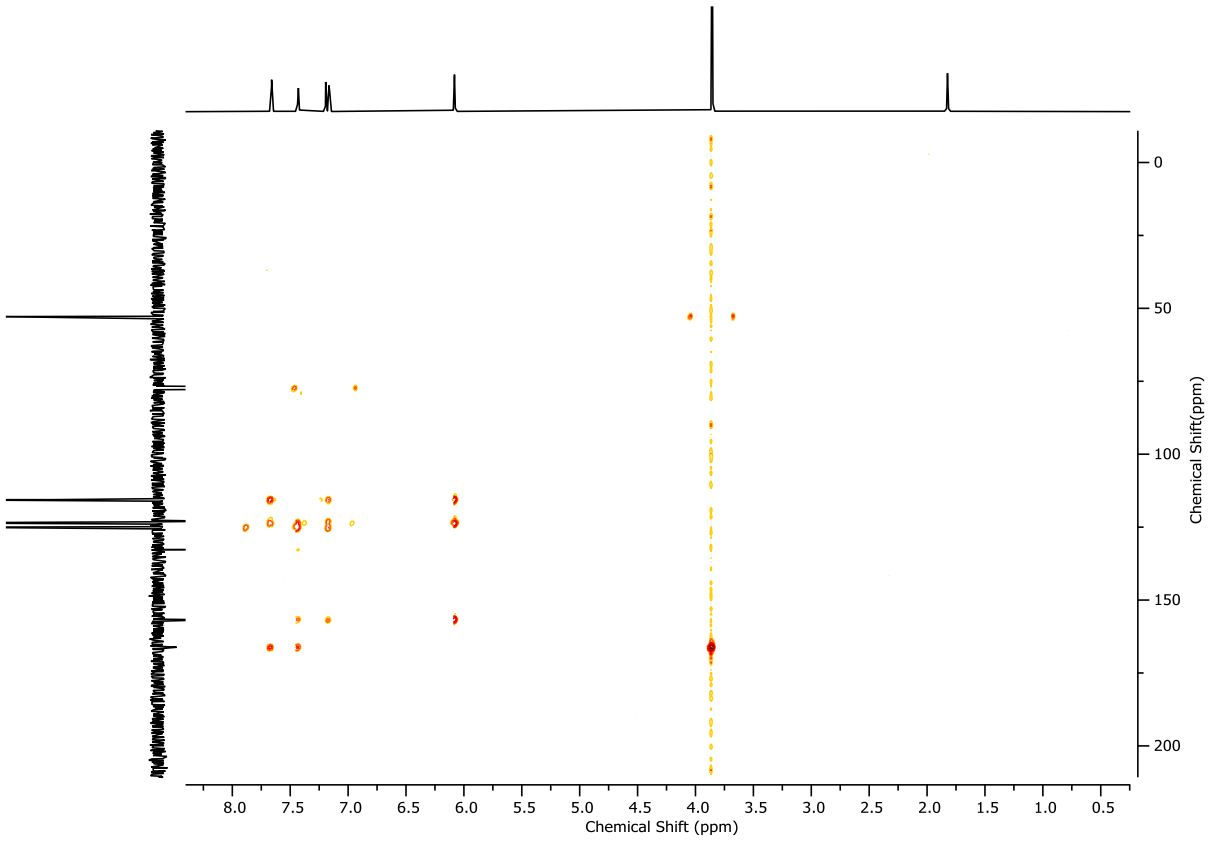

Figure 17: HMBC NMR ($CDCl_3$, 400 MHz) of **S5**.

2.4. Compound S6

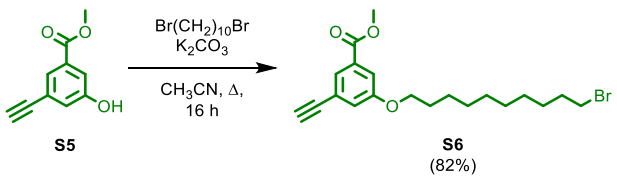

To a solution of **S5** (499 mg, 2.83 mmol, 1.0 eq.) in CH_3CN (28.3 mL) were added K_2CO_3 (1.17 g, 8.49 mmol, 3.0 eq.) and 1,10-dibromodecane (1.17 g, 14.2 mmol, 5.0 eq.), and the reaction mixture was stirred at reflux for 16 h. After cooling to ambient temperature, the reaction mixture was filtered through Celite®, washing with CH_2Cl_2, and concentrated *in vacuo*. The residue was purified by column chromatography (SiO_2, petrol-EtOAc 0→5%) to yield **S6** (960 mg, 2.43 mmol, 86%) as a white solid.

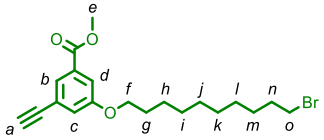

δ_H ($CDCl_3$, 400 MHz) 7.73 (t, J = 1.5, 1H, H_b), 7.53 (dd, J = 2.6, 1.5, 1H, H_d), 7.17 (dd, J = 2.6, 1.5, 1H, H_c), 3.97 (t, J = 6.5, 2H, H_f), 3.90 (s, 3H, H_e), 3.40 (t, J = 6.8, 2H, H_o), 3.08 (s, 1H, H_a), 1.90 – 1.71 (m, 4H, H_g, H_n), 1.49 – 1.26 (m, 12H, H_h, H_i, H_j, H_k, H_l, H_m); δ_C ($CDCl_3$, 101 MHz) 166.4, 159.1, 131.8, 125.7, 123.5, 122.7, 116.1, 82.8, 77.9, 68.6, 52.5, 34.2, 33.0, 29.6, 29.5, 29.4, 29.2, 28.9, 28.3, 26.1; HR-ESI-MS (+ve) m/z = 395.1211 $[M+H]^+$ (calc. m/z for $C_{20}H_{28}BrO_3$ 395.1216); Melting point 65-67 °C.

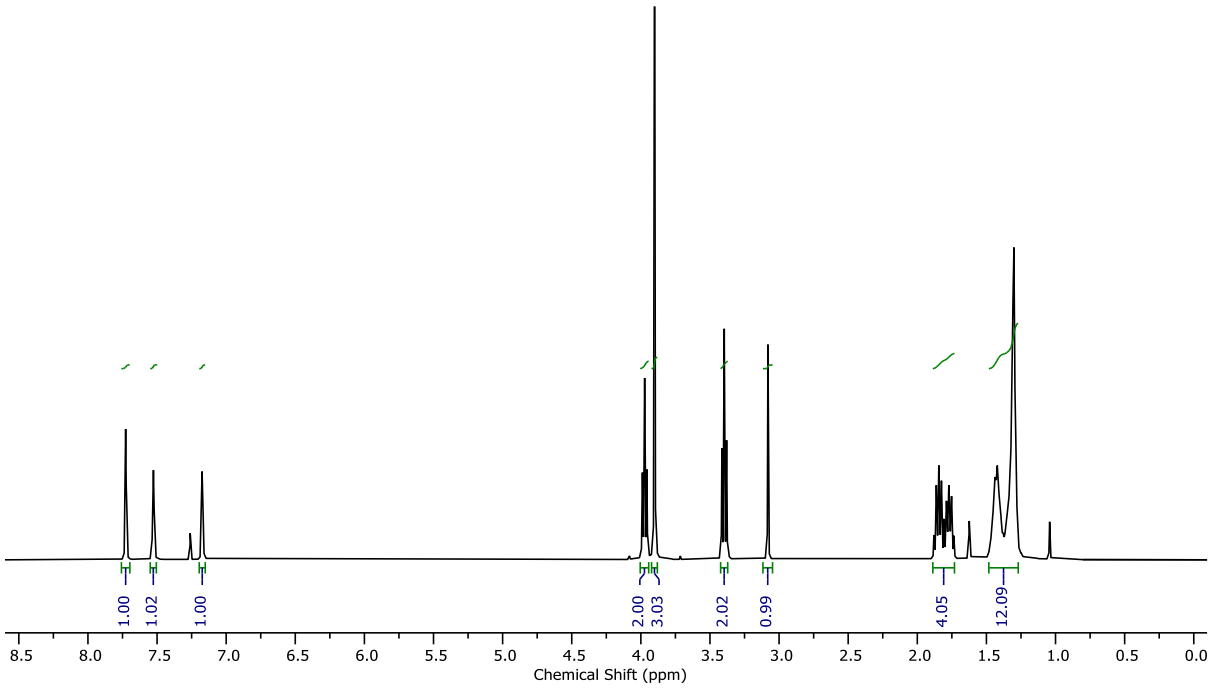

Figure 18: ^{1}H NMR ($CDCl_3$, 400 MHz) of **S6**.

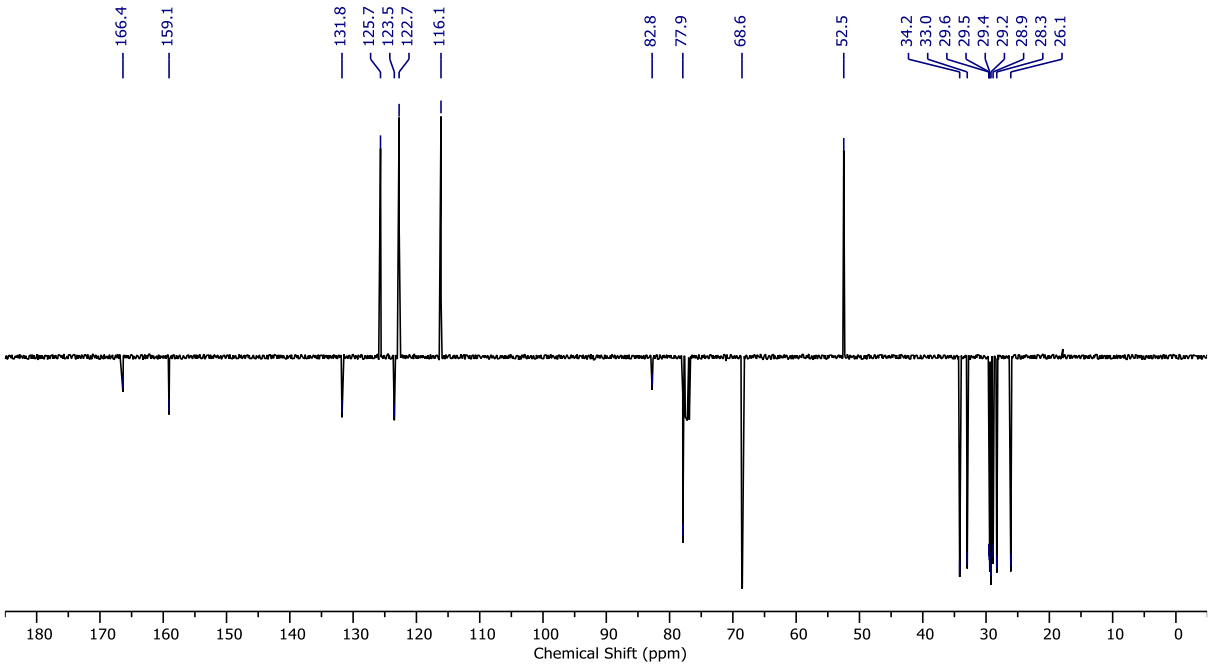

Figure 19: JMOD NMR ($CDCl_3$, 101 MHz) of **S6**.

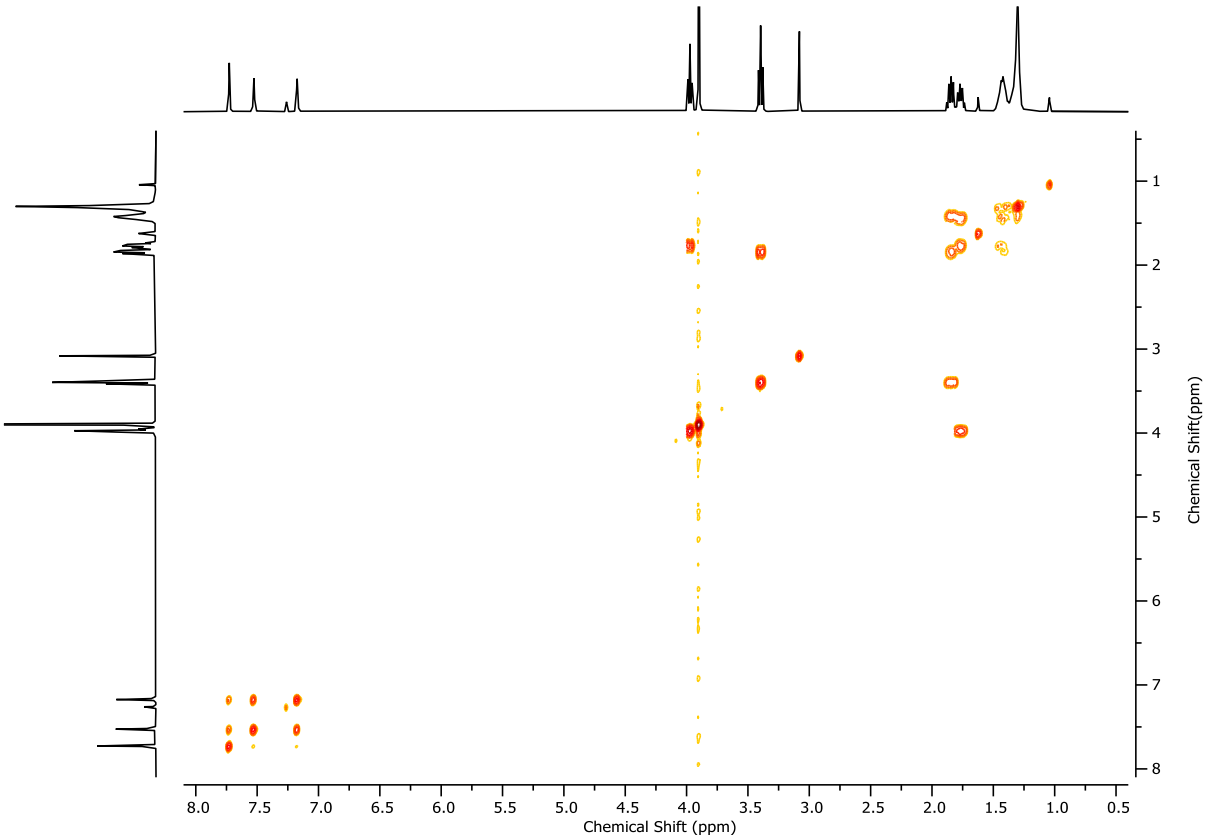

Figure 20: ^{1}H COSY NMR ($CDCl_3$, 400 MHz) of **S6**.

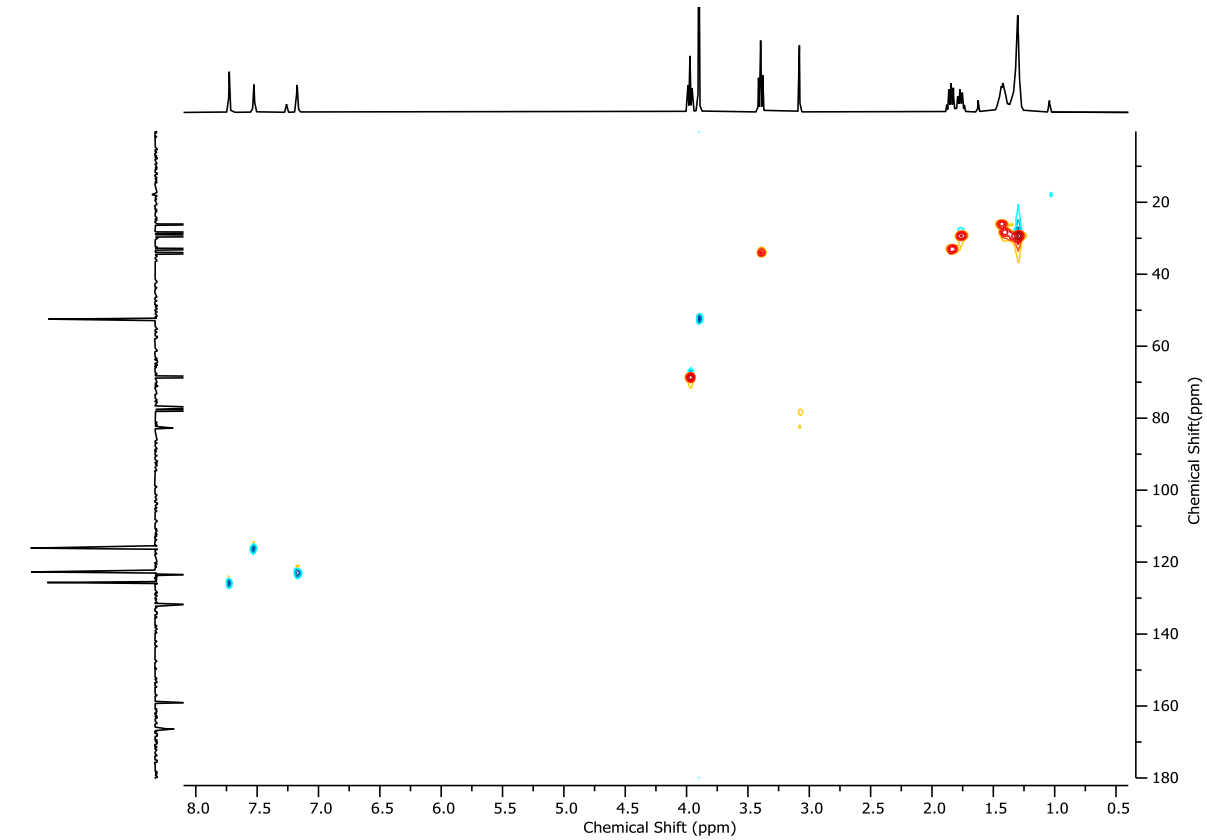

Figure 21: HSQC NMR ($CDCl_3$, 400 MHz) of **S6**.

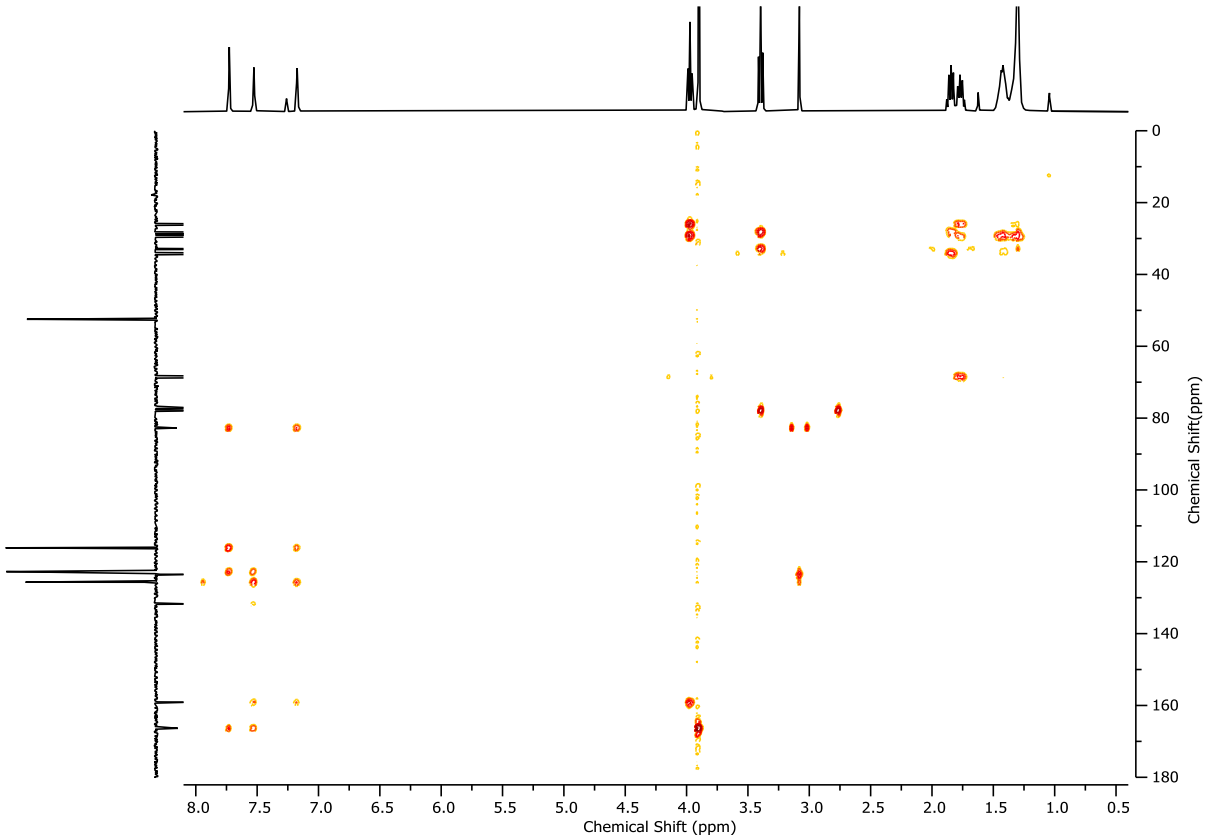

Figure 22: HMBC NMR ($CDCl_3$, 400 MHz) of **S6**.

2.5. Compound (*R*)-S7

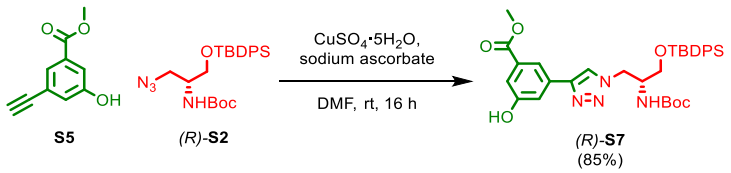

To a solution of (*R*)-**S1** (640.0 mg, 1.41 mmol, 1.0 eq.), alkyne **S5** (298.8 mg, 1.70 mmol, 1.2 eq.) and sodium ascorbate (336.4 mg, 1.70 mmol, 1.2 eq.) in DMF (7.0 mL) was added copper(II) sulfate pentahydrate (353.4 mg, 1.41 mmol, 1.0 eq.) .), and the reaction mixture was stirred at ambient temperature for 16 h. The reaction mixture was diluted with EtOAc (20 mL) and washed with a saturated EDTA/NH_3 solution (25 mL). The aqueous layer was extracted with EtOAc (3 x 15 mL). The combined organic fractions were washed with 5% LiCl (3 x 15 mL), and brine (15 mL) then dried over $MgSO_4$, filtered, and concentrated *in vacuo*. The residue was purified by column chromatography (SiO_2, petrol-EtOAc 0→20%) to yield (*R*)-**S7** (755.2 mg, 1.20 mmol, 85%) as a white foam.

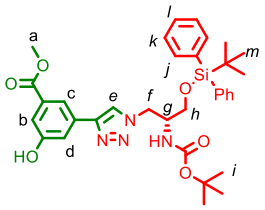

δ_H ($CDCl_3$, 400 MHz) 8.73 (s, 1H, H_{OH}), 7.95 – 7.87 (m, 2H, H_d, H_e), 7.69 (s, 1H, H_c), 7.66 – 7.60 (m, 4H, H_j), 7.59 – 7.55 (m, 1H, H_b), 7.44 – 7.33 (m, 6H, H_k, H_l), 5.26 (br s, 1H, H_{NHBoc}), 4.73 – 4.55 (m, 2H, H_f), 4.28 – 4.14 (m, 1H, H_g), 3.86 (s, 3H, H_a), 3.80 – 3.63 (m, 2H, H_h), 1.39 (s, 9H, H_i), 1.10 (s, 9H, H_m); δ_C ($CDCl_3$, 101 MHz) 167.0, 157.5, 155.8, 147.1, 135.6, 135.6, 132.8, 132.5, 132.0, 131.8, 130.2, 130.2, 128.1, 128.1, 121.6, 118.6, 117.4, 116.6, 80.6, 63.0, 52.3, 52.2, 50.9, 28.4, 27.0, 19.4; HR-ESI-MS (+ve) m/z = 631.2953 $[M+H]^+$ (calc. m/z for $C_{34}H_{43}N_4O_6Si$ 631.2946).

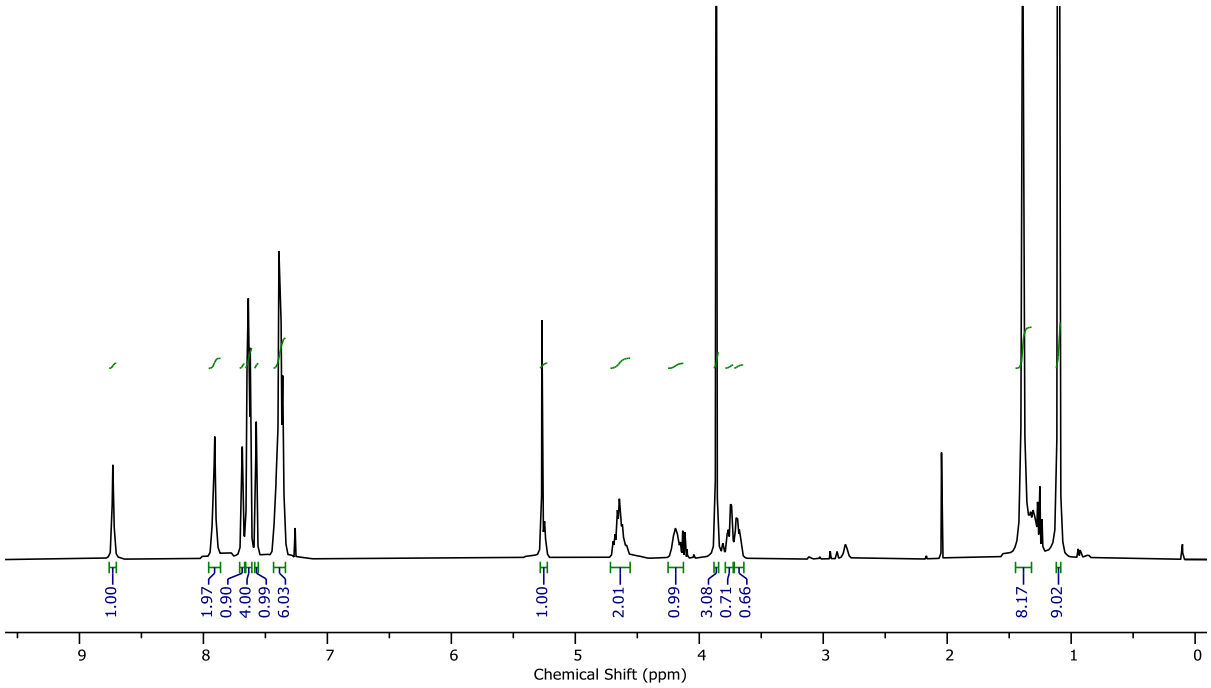

Figure 23: ^1H NMR ($CDCl_3$, 400 MHz) of (*R*)-**S7**.

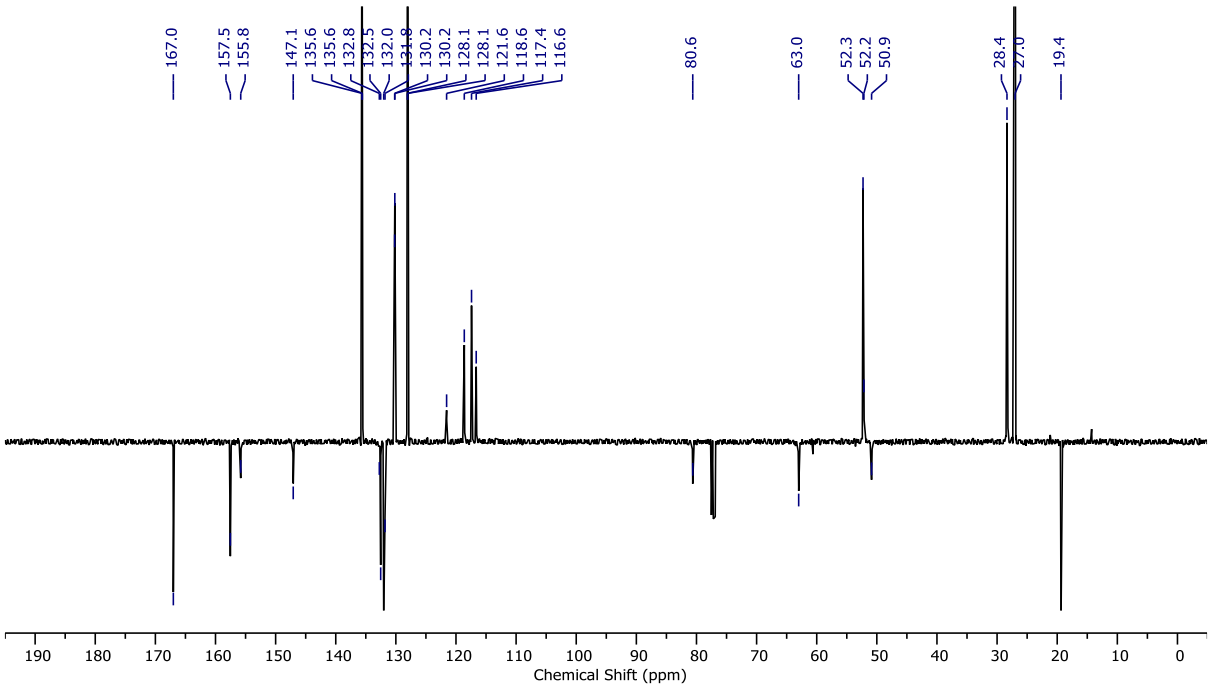

Figure 24: JMOD NMR ($CDCl_3$, 101 MHz) (*R*)-**S7**

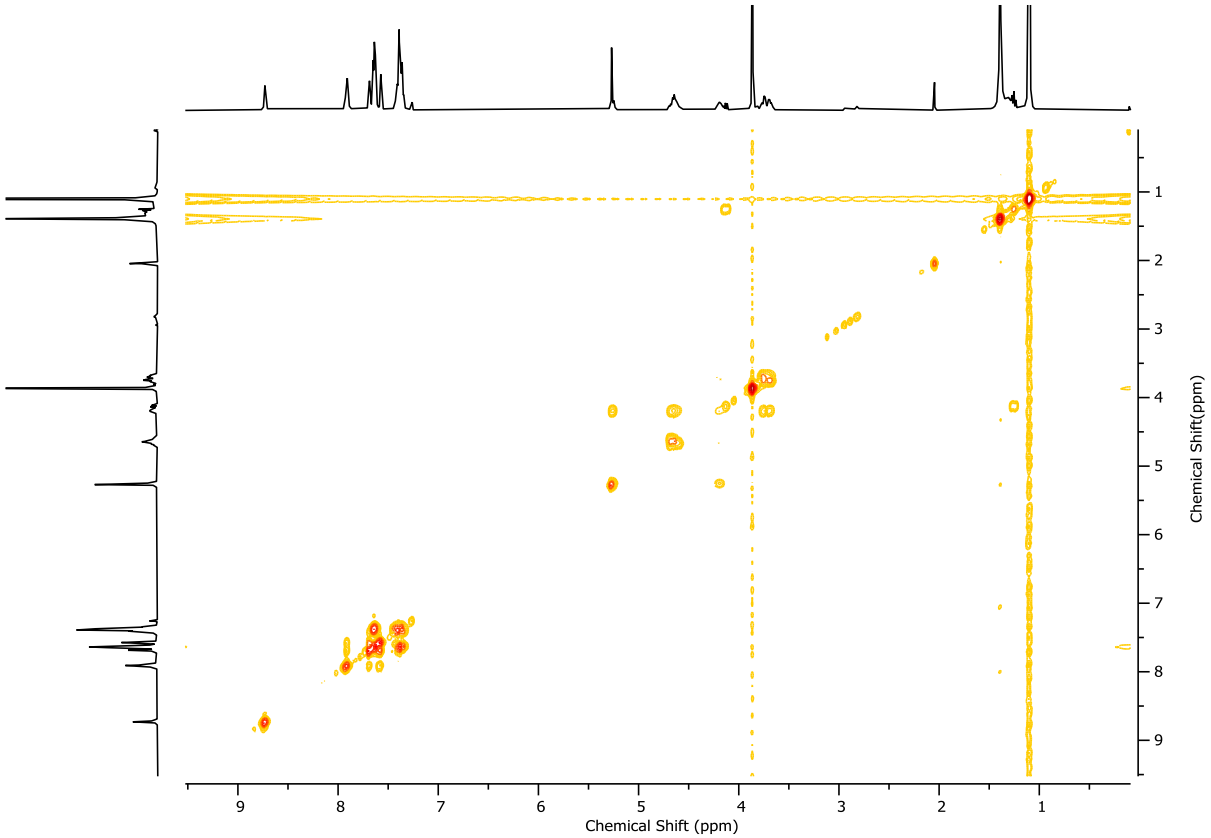

Figure 25: ^1H COSY NMR ($CDCl_3$, 400 MHz) (*R*)-**S7**.

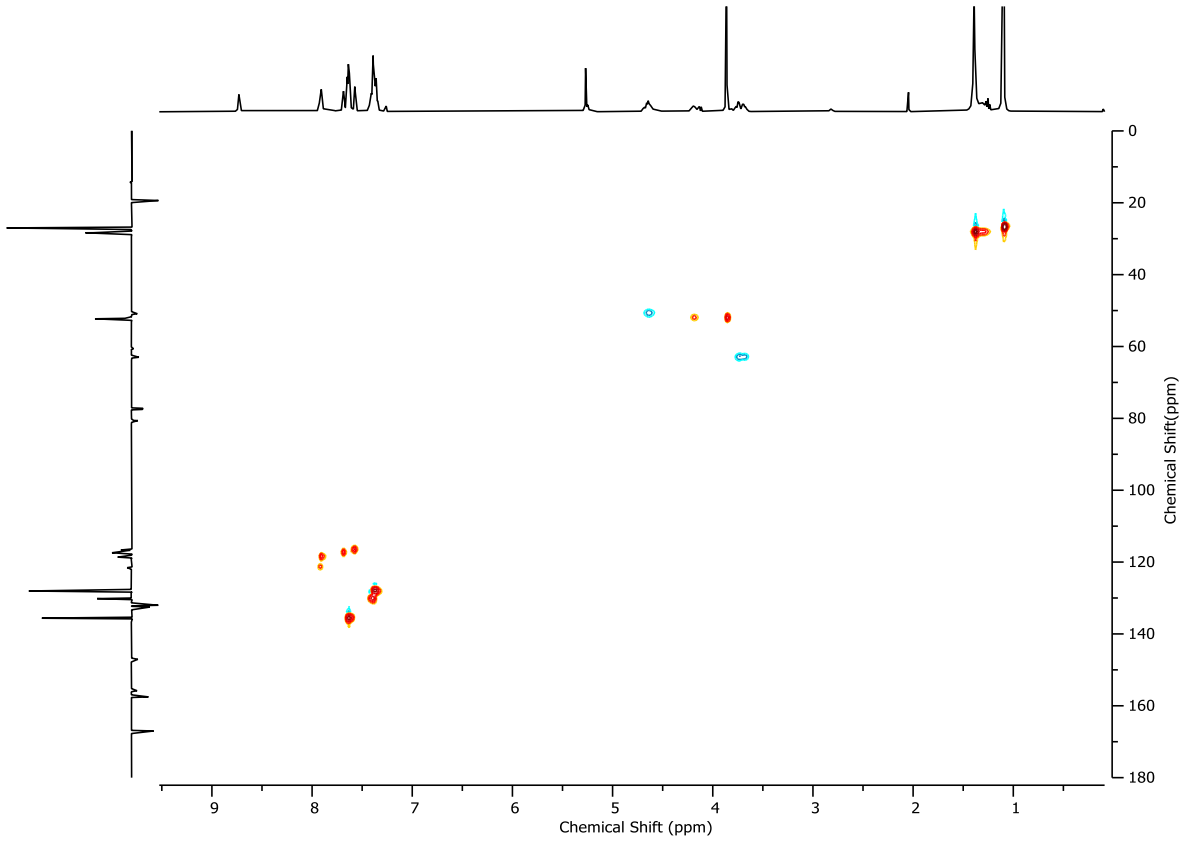

Figure 26: HSQC NMR ($CDCl_3$, 400 MHz) of (*R*)-**S7**.

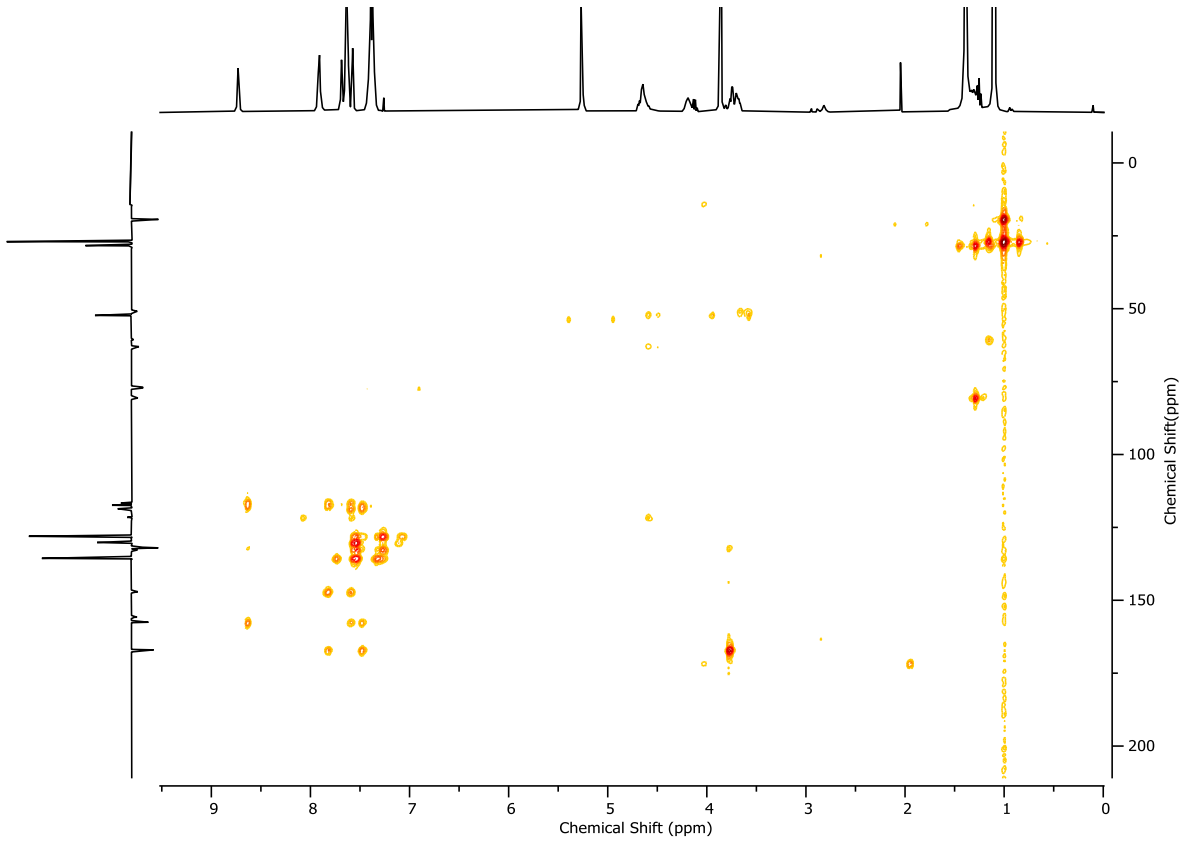

Figure 27: HMBC NMR ($CDCl_3$, 400 MHz) of (*R*)-**S7**.

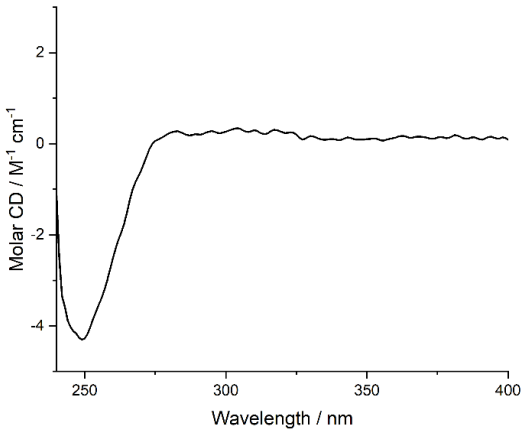

Figure 28: Circular Dichroism Spectra of (*R*)-**S7** (16 µM) at 293 K in $CHCl_3$.

2.6. Compound (*R*)-S8

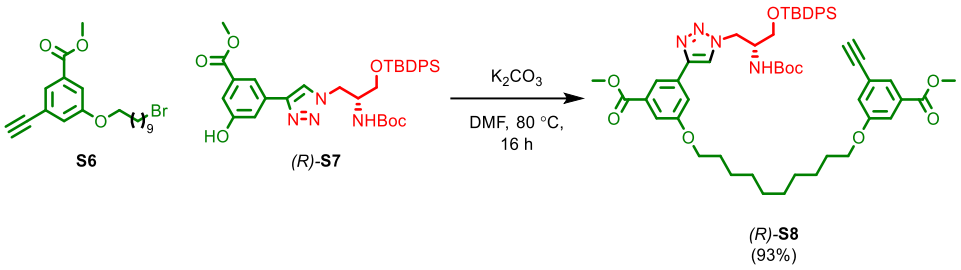

(*R*)-**S7** (425 mg, 0.67 mmol, 1.0 eq.), **S6** (399 mg, 1.01 mmol, 1.5 eq.), and K_2CO_3 (276 mg, 2.01 mmol, 3.0 eq.) were suspended in DMF (1.34 mL), and heated at 80 °C for 2 h. After cooling to ambient temperature, the crude mixture was diluted with EtOAc (10 mL) and washed with H_2O (5 mL), 5% LiCl (2 x 5 mL), and brine (5 mL). All aqueous phases were extracted with EtOAc (5 mL), and the combined organics were dried over $MgSO_4$, filtered, and concentrated *in vacuo*. The residue was purified by column chromatography (SiO_2, petrol-EtOAc 0→20%) to yield (*R*)-**S8** (591.1 mg, 0.63 mmol, 93%) as a yellow oil.

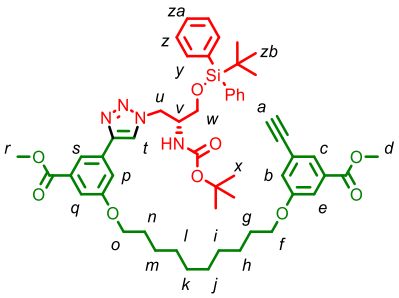

δ_H ($CDCl_3$, 400 MHz) 7.93 (t, *J* = 1.5, 1H, H_s), 7.79 – 7.76 (m, 1H, H_t), 7.73 (t, *J* = 1.4, 1H, H_c), 7.66 – 7.59 (m, 6H, H_p, H_y), 7.55 – 7.52 (m, 2H, H_e, H_q), 7.46 – 7.33 (m, 6H, H_z, H_{za}), 7.18 (dd, *J* = 2.6, 1.4, 1H, H_b), 5.00 (d, *J* = 8.6, 1H, H_{NHBoc}), 4.62 (d, *J* = 5.8, 2H, H_u), 4.23 – 4.12 (m, 1H, H_v), 4.06 (t, *J* = 6.5, 2H, H_o), 3.98 (t, *J* = 6.5, 2H, H_f), 3.93 (s, 3H, H_r), 3.90 (s, 3H, H_d), 3.72 (dd, *J* = 10.8, 4.0, 1H, H_w), 3.61 (m, 1H, H_w), 3.08 (s, 1H, H_a), 1.87 – 1.74 (m, 4H, H_g, H_n), 1.53 – 1.30 (m, 21H, H_h, H_i, H_j, H_k, H_l, H_m, H_x), 1.11 (s, 9H, H_{zb}); δ_C ($CDCl_3$, 101 MHz) 166.9, 166.4, 159.8, 159.1, 155.4, 147.0, 135.7, 135.7, 132.6, 132.2, 132.0, 131.8, 130.3, 130.3, 128.1, 125.7, 123.5, 122.8, 121.3, 119.2, 116.4, 116.2, 115.3, 82.8, 77.9, 68.6, 63.0, 52.5, 52.4, 52.0, 50.8, 29.6, 29.6, 29.5, 29.5, 29.4, 29.3, 28.4, 27.1, 26.2, 26.1, 19.5; HR-ESI-MS (+ve) m/z = 945.4830 $[M+H]^+$ (calc. m/z for $C_{54}H_{69}N_4O_9Si$ 945.4828).

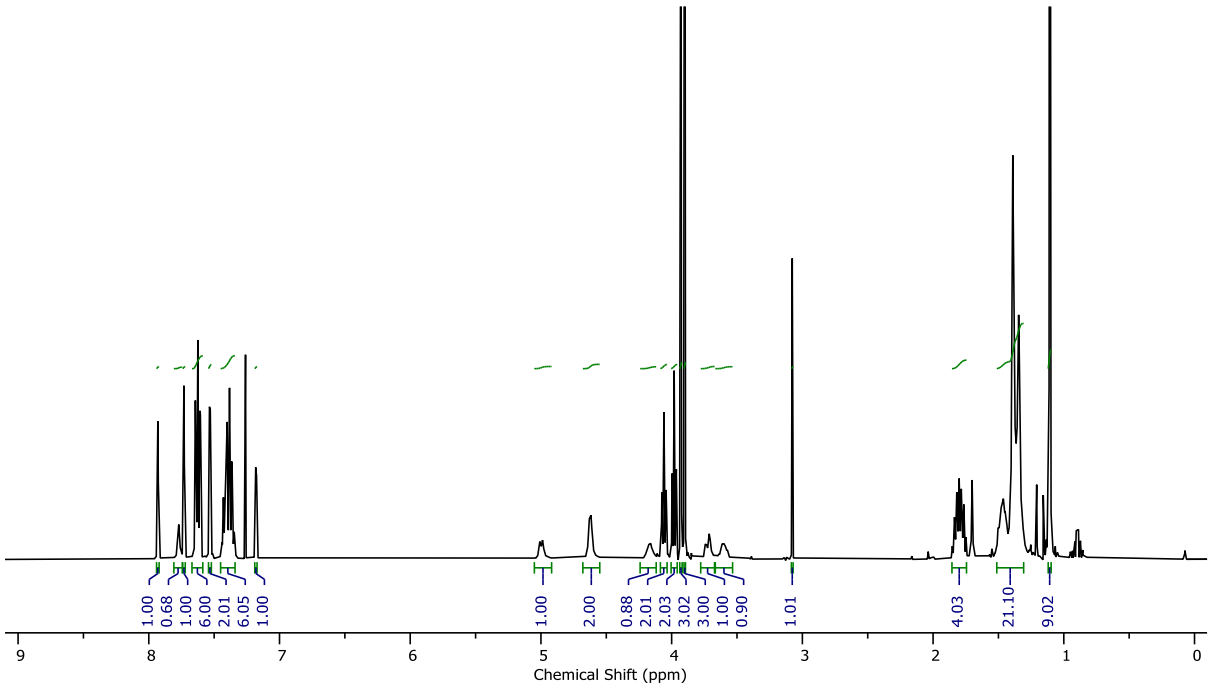

Figure 29: ^{1}H NMR ($CDCl_3$, 400 MHz) of (*R*)-**S8**.

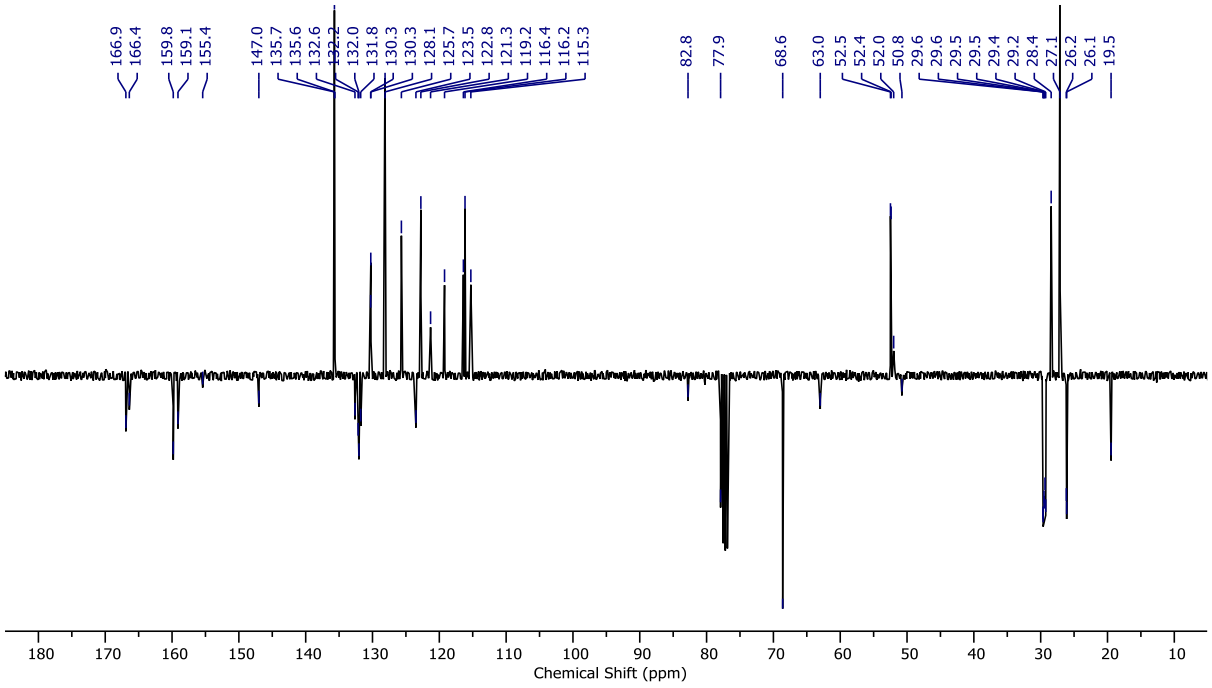

Figure 30: JMOD NMR ($CDCl_3$, 101 MHz) (*R*)-**S8**.

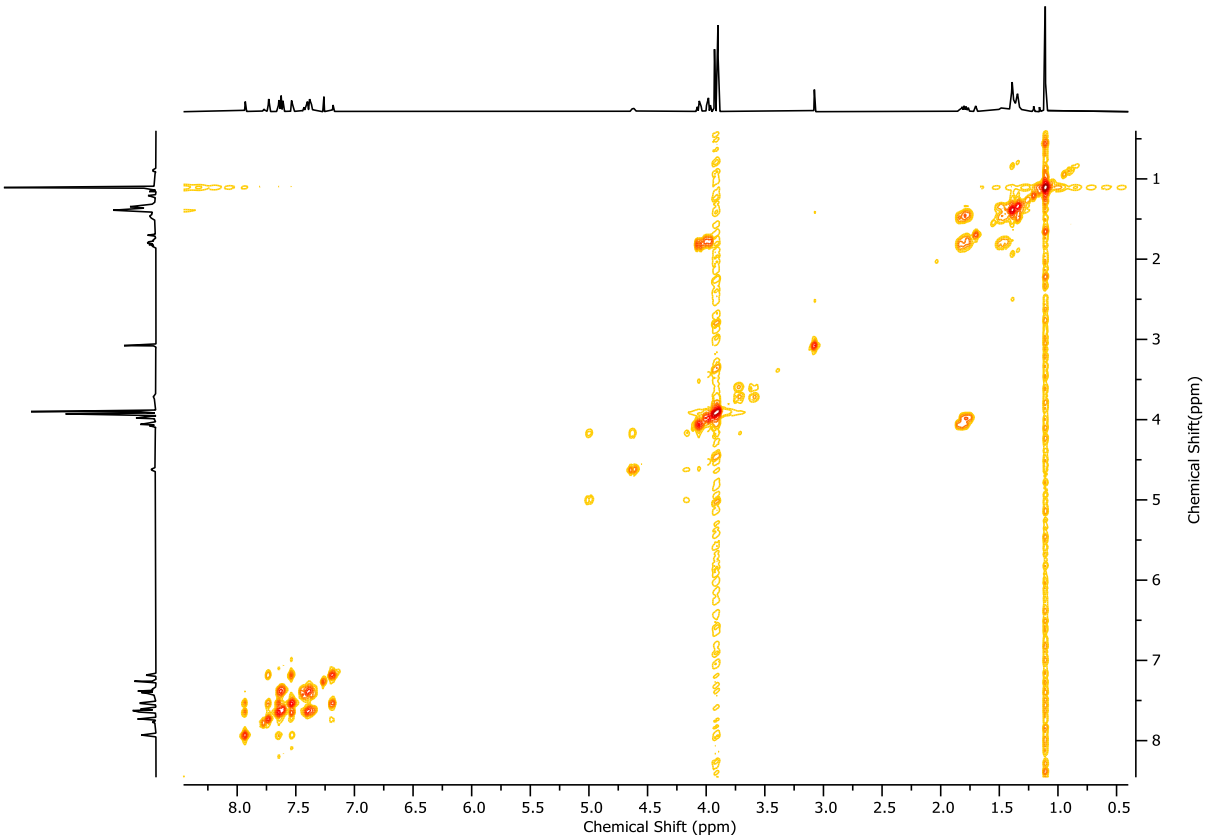

Figure 31: ^{1}H COSY NMR ($CDCl_3$, 400 MHz) (*R*)-**S8**.

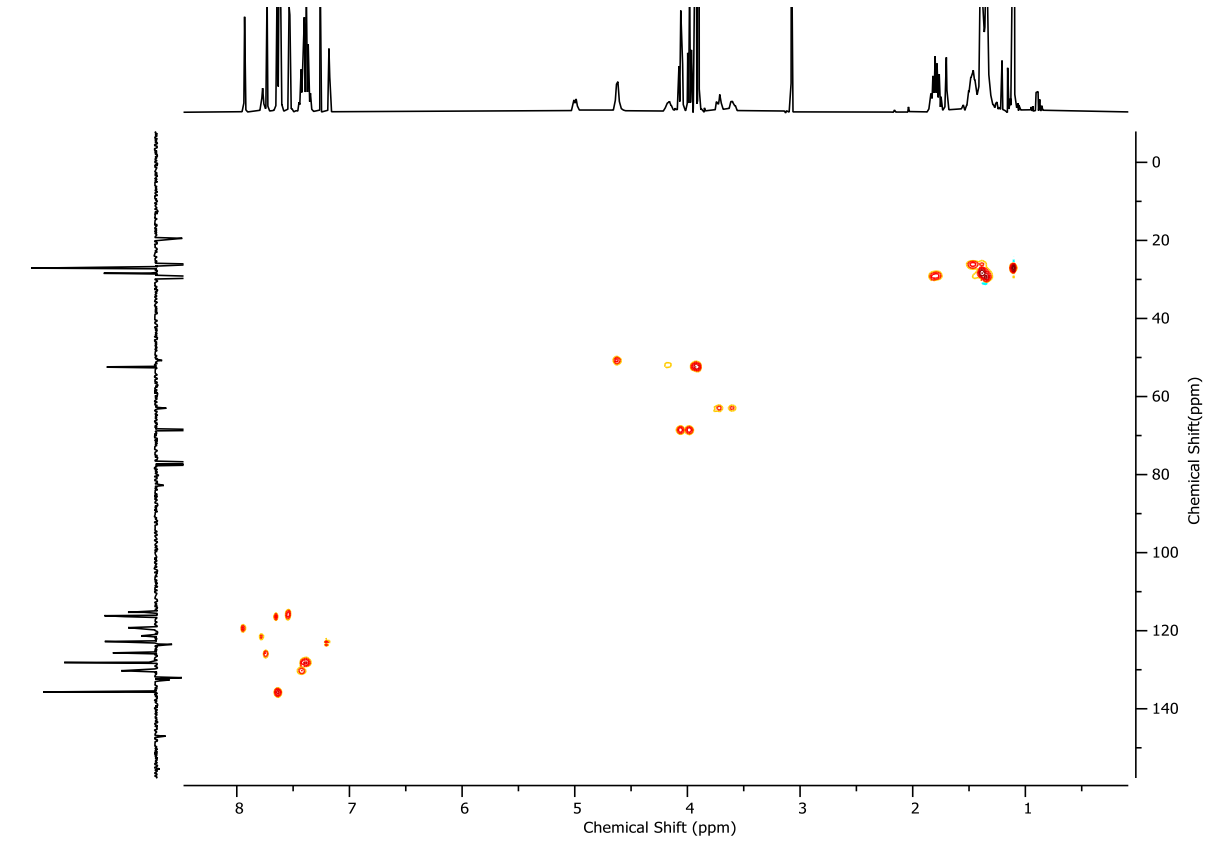

Figure 32: HSQC NMR ($CDCl_3$, 400 MHz) of (*R*)-**S8**.

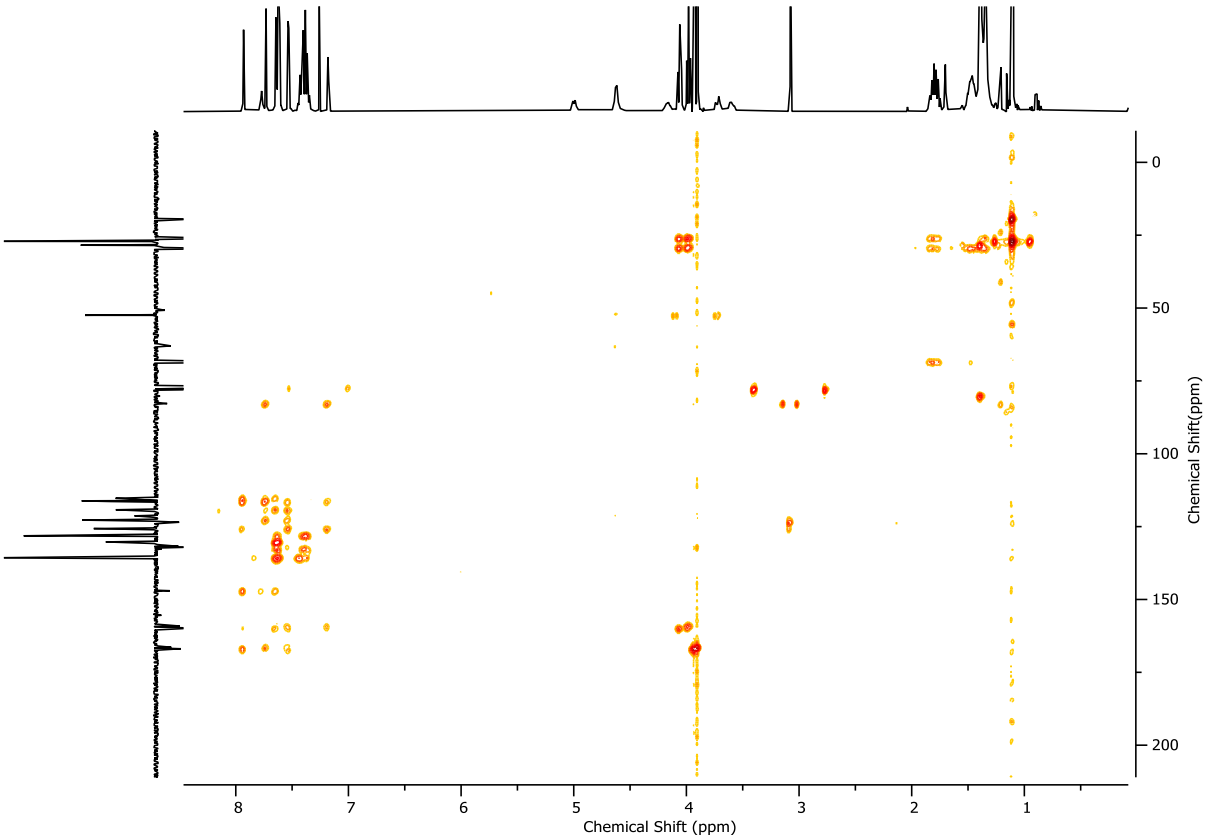

Figure 33: HMBC NMR ($CDCl_3$, 400 MHz) of (*R*)-**S8**.

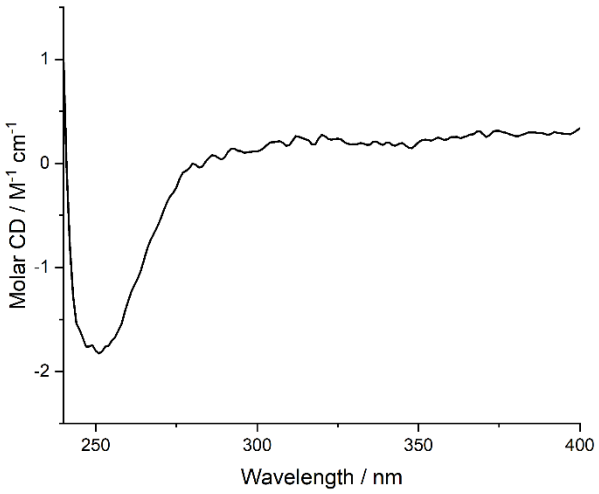

Figure 34: Circular Dichroism Spectra of (*R*)-**S8** (20 μM) at 293 K in $CHCl_3$.

2.7. Compound (*R*)-S9

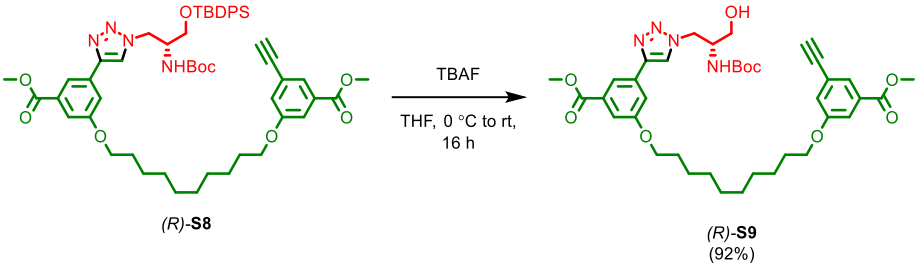

To a stirred solution of (*R*)-**S8** (591 mg, 0.63 mmol, 1.0 eq.) in THF (6.3 mL) at 0 °C was added dropwise a 1.0 M solution of TBAF in THF (690 µL, 0.69 mmol, 1.1 eq.), and the mixture was allowed to warm to ambient temperature. After 16 h, the crude mixture was concentrated *in vacuo*, the resulting residue dissolved in EtOAc (20 mL), and washed with H_2O (10 mL), and brine (10 mL). The combined aqueous layers were extracted with EtOAc (10 mL), and the combined organics were dried over $MgSO_4$, filtered and concentrated *in vacuo*. The residue was purified by column chromatography (SiO_2, CH_2Cl_2- CH_3CN 0→40%) to yield (*R*)-**S9** (409 mg, 0.579 mmol, 92%) as a white foam.

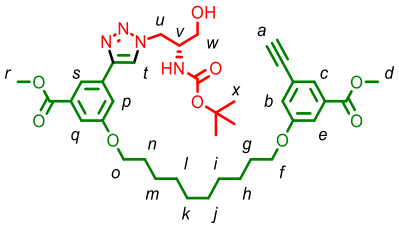

δ_H ($CDCl_3$, 400 MHz) 7.97 – 7.92 (m, 2H, H_s, H_t), 7.72 (t, J = 1.4, 1H, H_c), 7.65 (t, J = 2.0, 1H, H_p), 7.53 – 7.51 (m, 2H, H_q, H_e), 7.17 (dd, J = 2.6, 1.4, 1H, H_b), 5.28 (d, J = 8.4, 1H, H_{NHBoc}), 4.73 – 4.59 (m, 2H, H_u), 4.12 – 4.01 (m, 3H, H_v, H_o), 3.97 (t, J = 6.5, 2H, H_f), 3.92 (s, 3H, H_r), 3.90 (s, 3H, H_d), 3.73 (dd, J = 11.5, 3.9, 1H, H_w), 3.64 – 3.55 (m, 1H, H_w), 3.08 (s, 1H, H_a), 1.85 – 1.73 (m, 4H, H_g, H_n), 1.51 – 1.30 (m, 21H, H_h, H_i, H_j, H_k, H_l, H_m, H_x); δ_C ($CDCl_3$, 101 MHz) 166.9, 166.4, 159.9, 159.1, 147.2, 132.1, 131.9, 131.8, 125.7, 123.5, 122.8, 121.8, 119.2, 116.4, 116.2, 115.4, 82.8, 80.5, 77.9, 68.6, 61.8, 52.5, 52.4, 52.1, 29.6, 29.6, 29.5, 29.5, 29.3, 29.2, 28.5, 26.2, 26.1; HR-ESI-MS (+ve) m/z = 707.3651 (calc. m/z for $C_{38}H_{51}N_4O_9$ 707.3651).

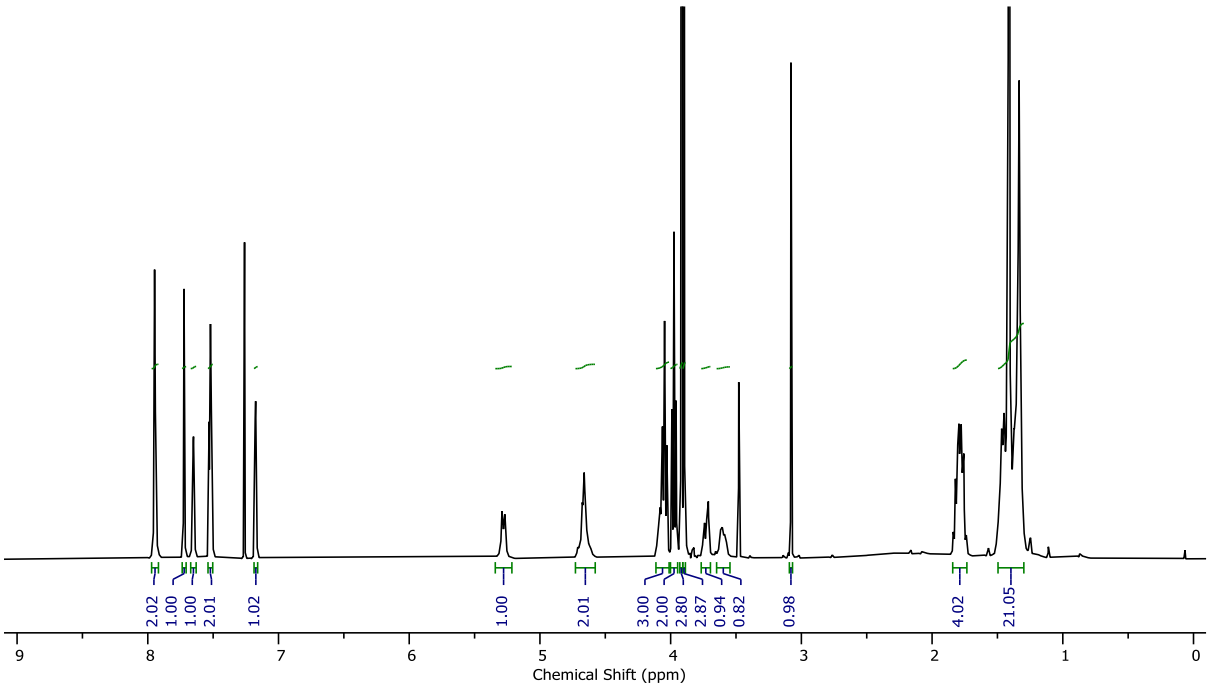

Figure 35: ^{1}H NMR ($CDCl_3$, 400 MHz) of (*R*)-***S9***.

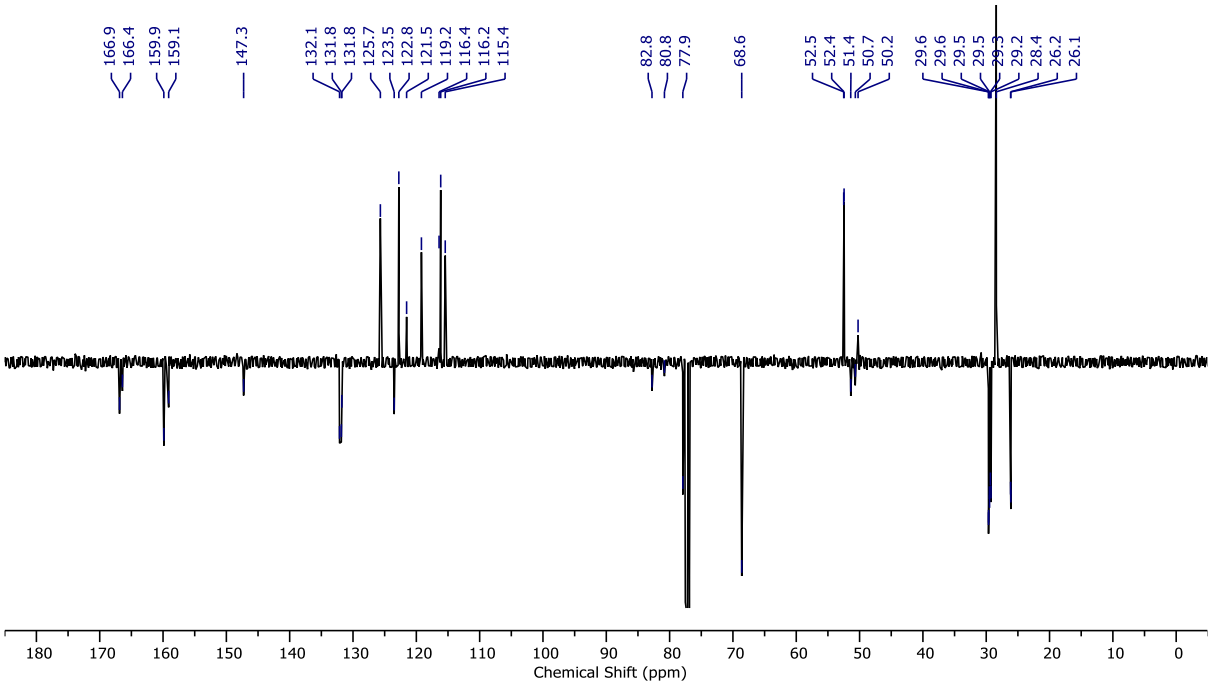

Figure 36: JMOD NMR ($CDCl_3$, 101 MHz) (*R*)-***S9***.

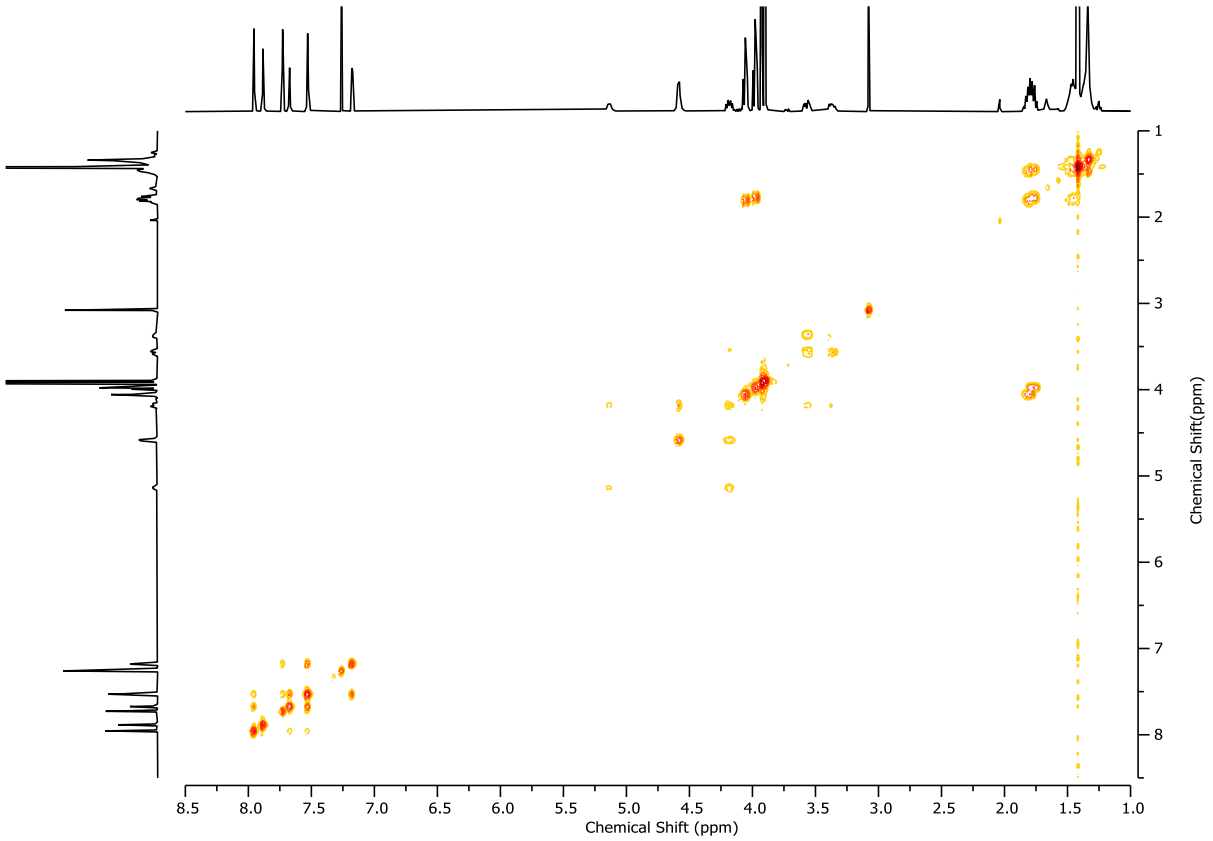

Figure 37: ^{1}H COSY NMR ($CDCl_3$, 400 MHz) (*R*)-**S9**.

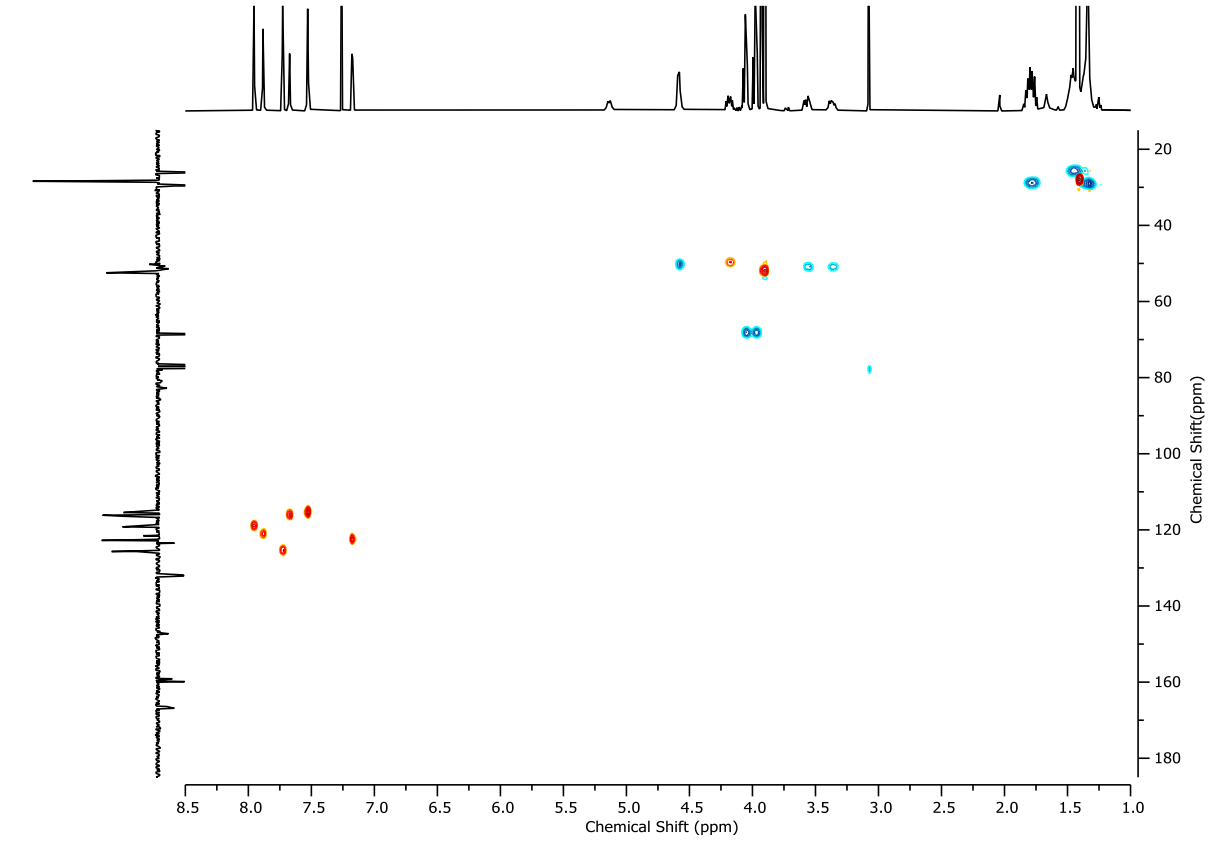

Figure 38: HSQC NMR ($CDCl_3$, 400 MHz) of (*R*)-**S9**.

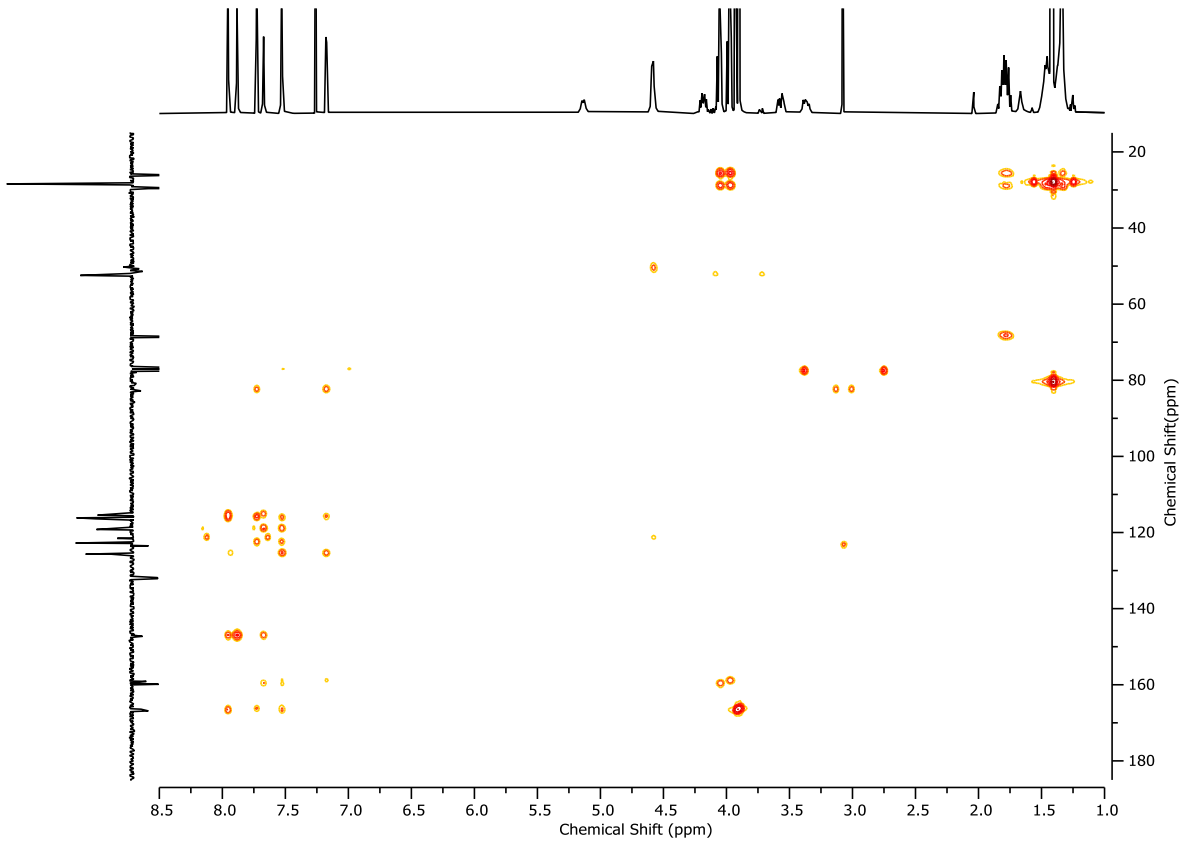

Figure 39: HMBC NMR ($CDCl_3$, 400 MHz) of (*R*)-**S9**.

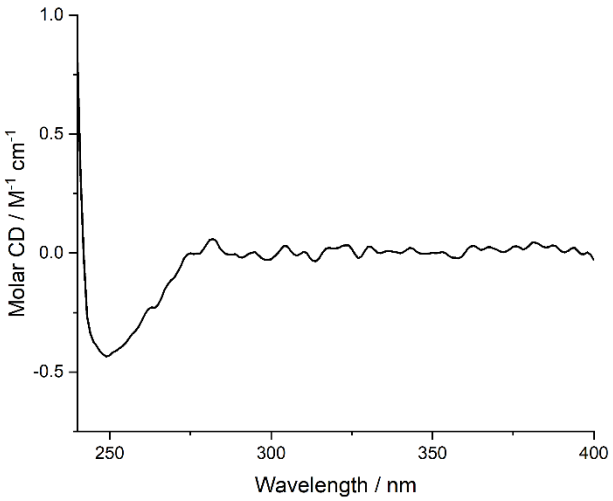

Figure 40: Circular Dichroism Spectra of (*R*)-**S9** (30 μM) at 293 K in $CHCl_3$.

2.8. Pre-macrocycle (*R*)-1

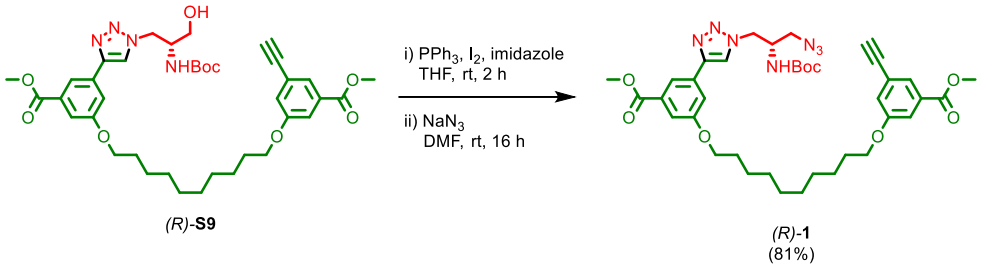

(*R*)-**S9** (*R*)-**1** (81%)

To a stirred solution of PPh_3 (467.7 mg, 0.59 mmol, 3.0 eq.) and imidazole (207.3 mg, 3.04 mmol, 5.0 eq.) in THF (4.5 mL) at 0 °C was added I_2 (451.9 mg, 1.78 mmol, 3.0 eq.) in 1 portion. After stirring for 10 min, a concentrated solution of (*R*)-**S9** (416.7 mg, 0.59 mmol, 1.0 eq.) in THF (1.4 mL) was added dropwise, the reaction mixture was allowed to warm to ambient temperature and stirred for 2 h. The crude mixture was filtered through Celite®, washing with CH_2Cl_2, and concentrated *in vacuo*. The residue was purified by column chromatography (SiO_2, petrol-EtOAc 0→40%). The resultant oil was immediately dissolved in DMF (2.9 mL) and NaN_3 (192.4 mg, 2.96 mmol, 5.0 eq.) was added. After stirring for 16 h at ambient temperature, the reaction mixture was diluted with EtOAc (10 mL), washed with H_2O (10 mL). The aqueous layer was extracted with EtOAc (3 x 10 mL). The combined organic fractions were washed with 5% LiCl (3 x 10 mL), and brine (10 mL) then dried over $MgSO_4$, filtered, and concentrated *in vacuo*. The residue was purified by column chromatography (SiO_2, CH_2Cl_2-EtOAc 0→20%) to yield (*R*)-**1** (353.1 mg, 0.48 mmol, 81%) as a white foam.

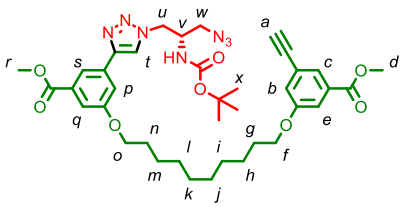

δ_H ($CDCl_3$, 400 MHz) 7.96 (t, *J* = 1.5, 1H, H_s), 7.88 (s, 1H, H_t), 7.73 (t, *J* = 1.4, 1H, H_c), 7.67 (dd, *J* = 2.6, 1.5, 1H, H_p), 7.56 – 7.50 (m, 2H, H_e, H_q), 7.18 (dd, *J* = 2.6, 1.4, 1H, H_b), 5.14 (d, *J* = 8.3, 1H, H_{NHBoc}), 4.59 (d, *J* = 5.7, 2H, H_u), 4.25 – 4.12 (m, 1H, H_v), 4.06 (t, *J* = 6.5, 2H, H_o), 3.98 (t, *J* = 6.5, 2H, H_f), 3.93 (s, 3H, H_r), 3.90 (s, 3H, H_d), 3.57 (dd, *J* = 12.4, 5.0, 1H, H_w), 3.37 (dd, *J* = 12.6, 6.4, 1H, H_w), 3.08 (s, 1H, H_a), 1.87 – 1.72 (m, 4H, H_g, H_n), 1.51 – 1.30 (m, 21H, H_h, H_i, H_j, H_k, H_l, H_m, H_x); δ_C ($CDCl_3$, 101 MHz) 166.9, 166.4, 159.9, 159.1, 147.3, 132.1, 131.8, 131.8, 125.7, 123.5, 122.8, 121.5, 119.2, 116.4, 116.2, 115.4, 82.8, 80.8, 77.9, 68.6, 52.5, 52.5, 51.4, 50.7, 50.2, 29.6, 29.6, 29.5, 29.5, 29.3, 29.3, 28.4, 26.2, 26.1; HR-ESI-MS (+ve) m/z = 732.3706 $[M+H]^+$ (calc. m/a for $C_{38}H_{50}N_7O_8$ 732.3715)

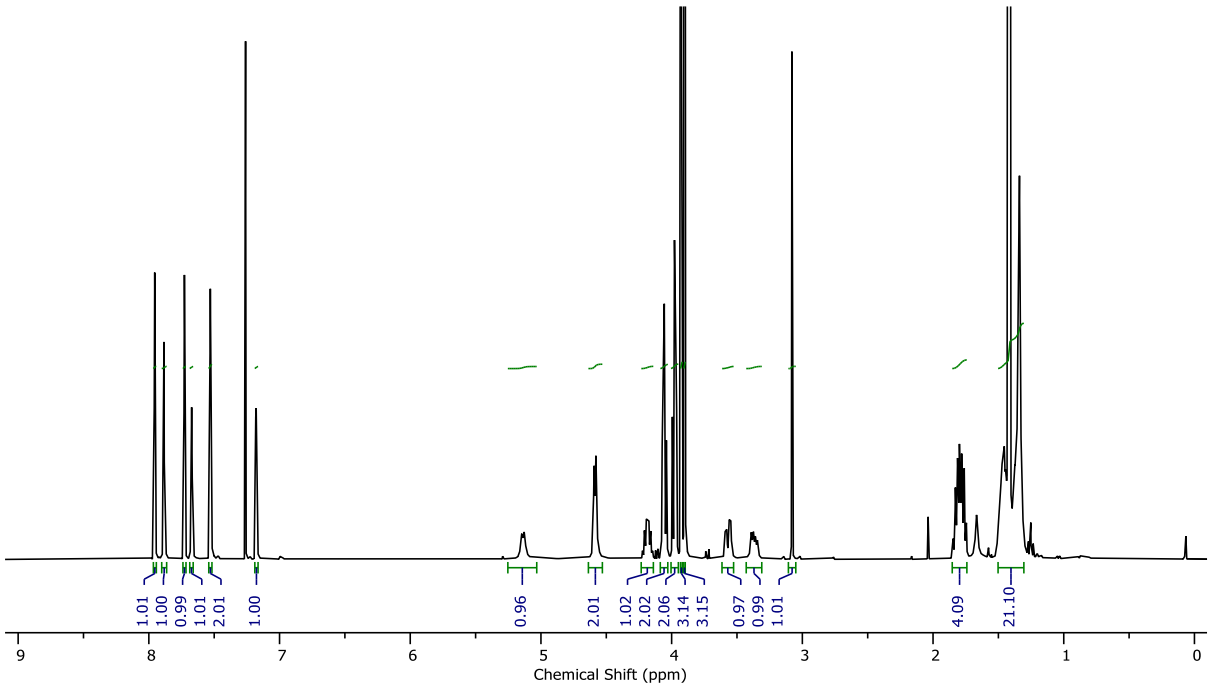

Figure 41: ^{1}H NMR ($CDCl_3$, 400 MHz) of (*R*)-**1**.

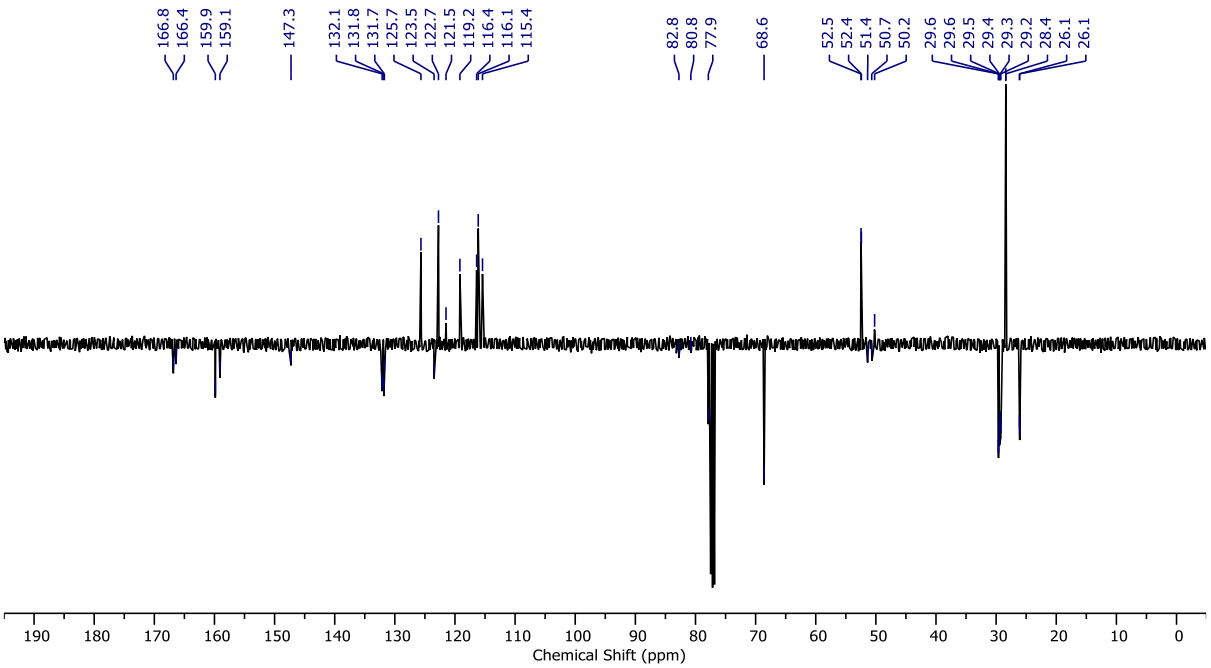

Figure 42: JMOD NMR ($CDCl_3$, 101 MHz) (*R*)-**1**.

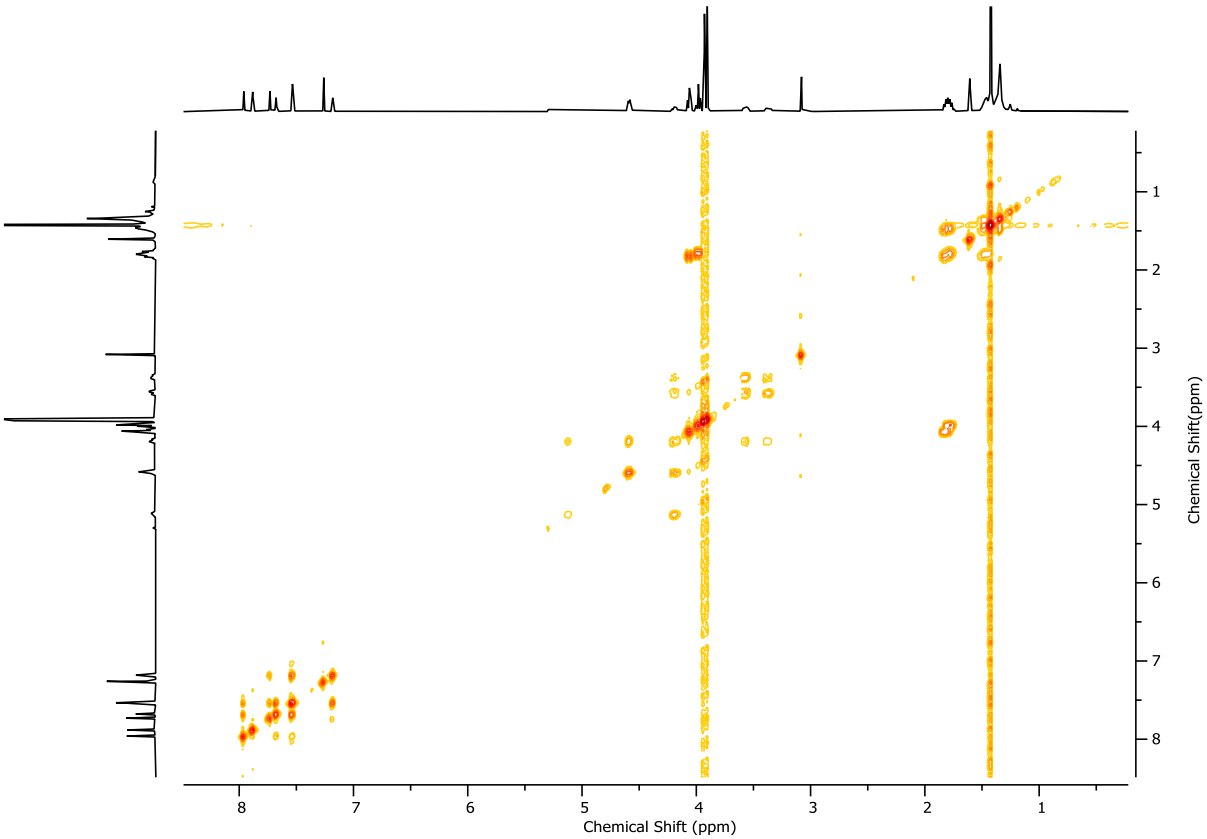

Figure 43: ^{1}H COSY NMR ($CDCl_3$, 400 MHz) (*R*)-**1**.

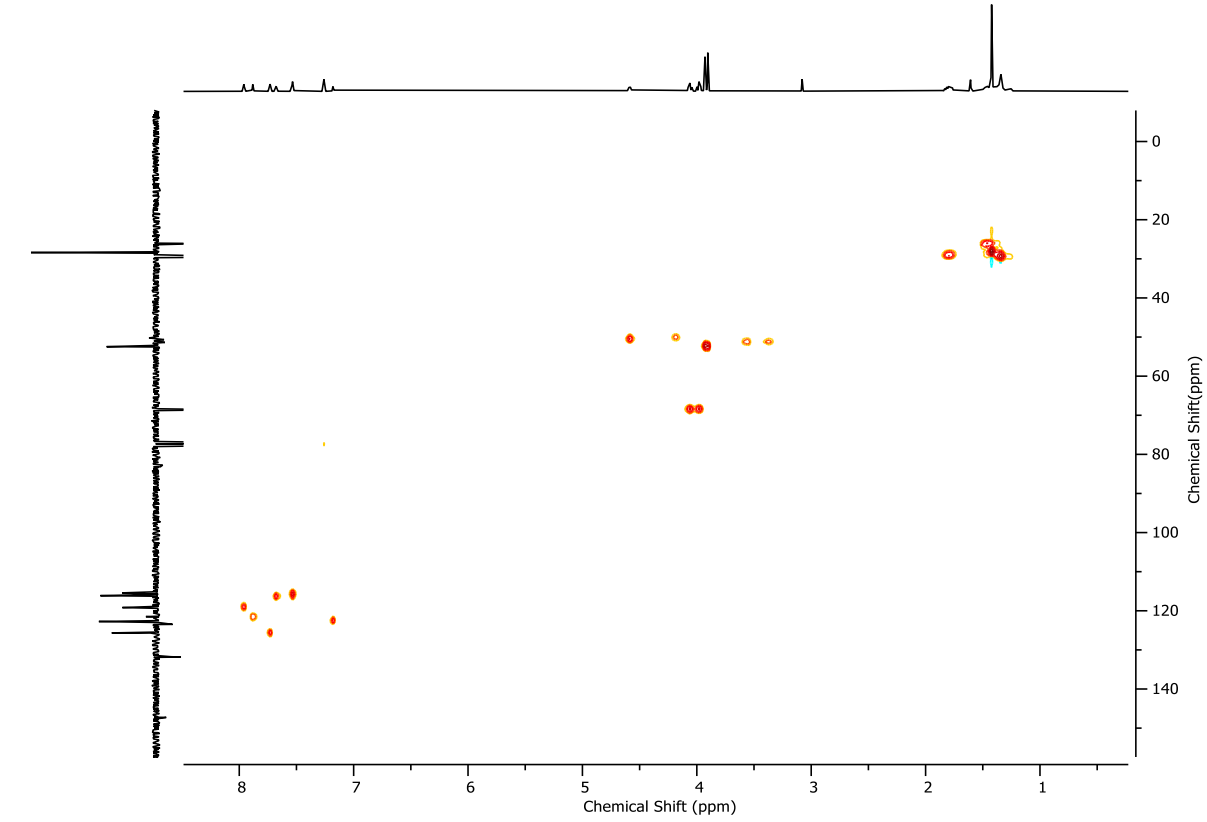

Figure 44: HSQC NMR ($CDCl_3$, 400 MHz) of (*R*)-**1**.

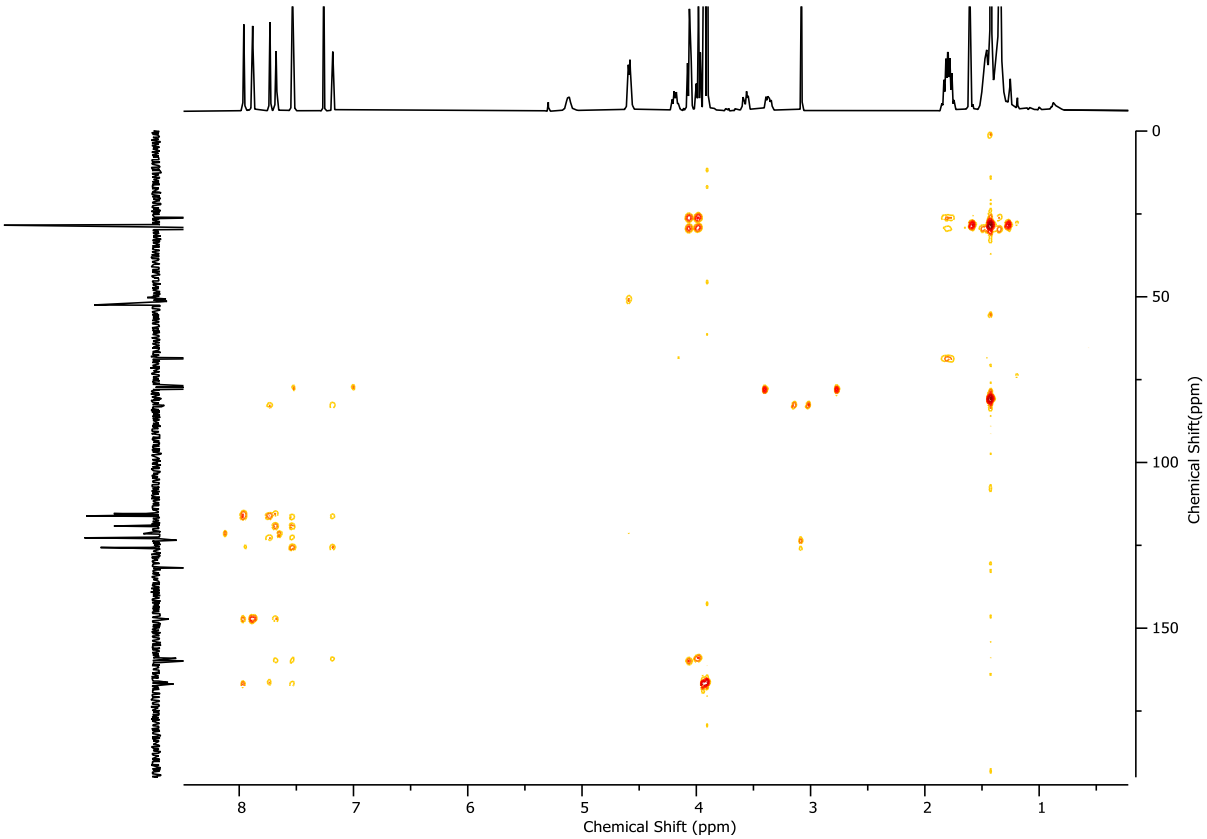

Figure 45: HMBC NMR ($CDCl_3$, 400 MHz) of (*R*)-**1**.

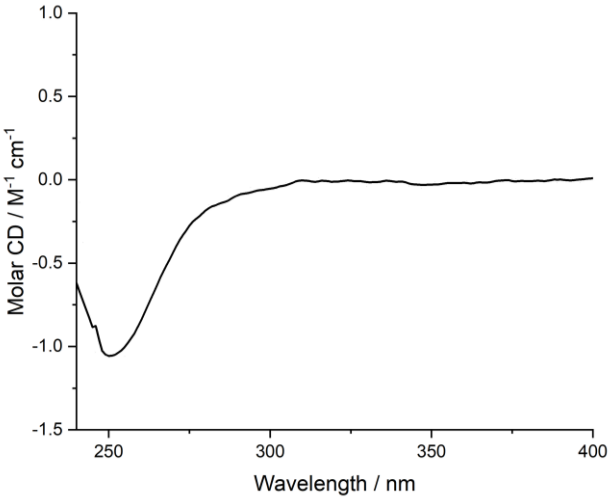

Figure 46: Circular Dichroism Spectra of (*R*)-**1** (27 μM) at 293 K in $CHCl_3$.

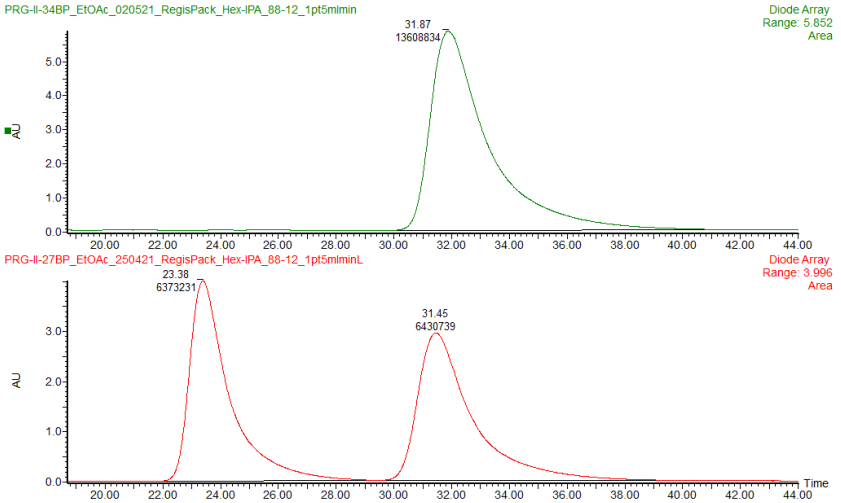

Figure 47: CSP-HPLC of (*R*)-**1** (loaded in EtOAc). RegisPack, *n*-hexane-IPA 88 : 12, flowrate 1.5 mLmin^{-1}. (top) (*S*)-**1** (not observed), (*R*)-**1** (31.87 min, 13608834, >99.9%). (bottom) *rac*-**1**, (*S*)-**1** (23,38 min, 6373231, 49.8%), (*R*)-**1** (31.45 min, 6430739, 50.2%).

3. Compounds leading to macrocycles 2 and 3

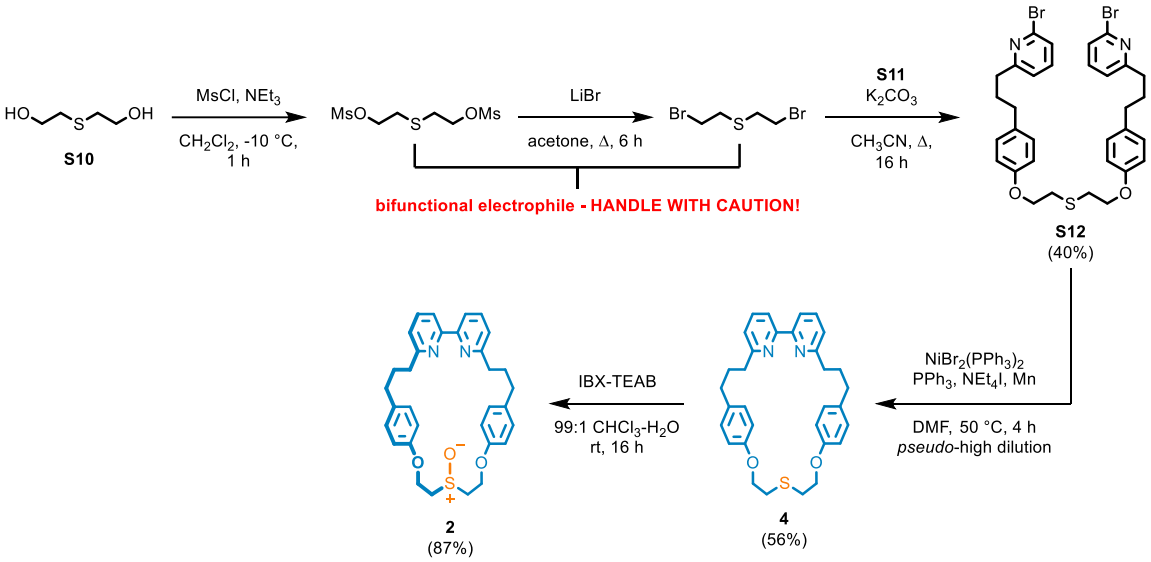

Scheme 2: Synthetic route to macrocycles **2** and **4**.

3.1. Compound S12

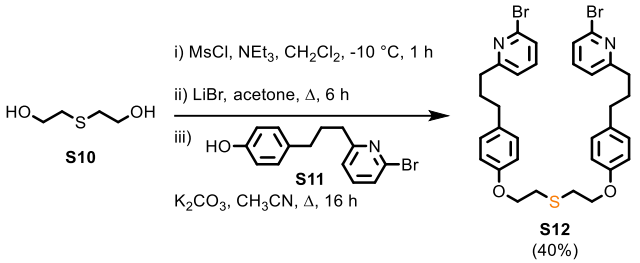

NOTE: the dimesylate and dibromo derivatives of S10 are bifunctional electrophiles, which should be handled with caution. To a stirred solution of **S10** (400 µL, 4.0 mmol, 1.0 eq.) in CH_2Cl_2 (20 mL), was added NEt_3 (3.9 mL, 27.7 mmol, 7.0 eq.), and the solution was cooled to -10°C. MsCl (950 µL, 12.3 mmol, 3.1 eq.) was added over 5 min, and the reaction mixture was stirred for 1 h. H_2O (5 mL) was added, the mixture was allowed to warm to ambient temperature, and the aqueous and organic layers separated. The aqueous was extracted with CH_2Cl_2 (2 x 5 mL), and the combined organics were washed with brine, dried over $MgSO_4$, filtered and concentrated *in vacuo*. The crude materials were dissolved in acetone (40 mL), and LiBr (3.55 g, 40.9 mmol, 10.2 eq.) was added. The reaction mixture was refluxed under an inert atmosphere for 6 h. After cooling to ambient temperature, the insoluble materials were filtered off, and the filtrate concentrated *in vacuo*. The crude materials were dissolved in CH_3CN (20 mL), and **S11** (2.39 g, 8.2 mmol, 2.1 eq.) and K_2CO_3 (2.81 g, 20.4 mmol, 5.1 eq.) were added. The reaction mixture was heated at reflux under an inert atmosphere for 16 h. After cooling to ambient temperatures, the crude mixture was filtered through Celite®, washing with CH_2Cl_2, and concentrated *in vacuo*. The residue was purified by column chromatography (SiO_2, 1:1 petrol/CH_2Cl_2-Et_2O 5→10%) to yield **S12** as a white solid (1.08 g, 1.61 mmol, 40% over 3 steps).

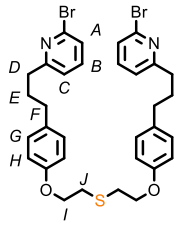

δ_H ($CDCl_3$, 400 MHz) 7.42 (t, J = 7.7, 2H, H_B), 7.28 (d, J = 7.8, 2H, H_A), 7.14 – 7.03 (m, 6H, H_C, H_G), 6.88 – 6.78 (m, 4H, H_H), 4.16 (t, J = 6.6, 4H, H_I), 3.00 (t, J = 6.6, 4H, H_J), 2.81 – 2.73 (m, 4H, H_D), 2.65 – 2.57 (m, 4H, H_F), 2.07 – 1.94 (m, 4H, H_E); δ_C ($CDCl_3$, 101 MHz) 163.9, 156.8, 141.7, 138.7, 134.5, 129.6, 125.4, 121.7, 114.7, 68.2, 36.9, 34.7, 31.9, 31.6. HR-ESI-MS (+ve) m/z = 669.0774 $[M+H]^+$ (calc. m/z for $C_{32}H_{35}Br_2N_2O_2S$ 669.0781); Melting point 63-65 °C.

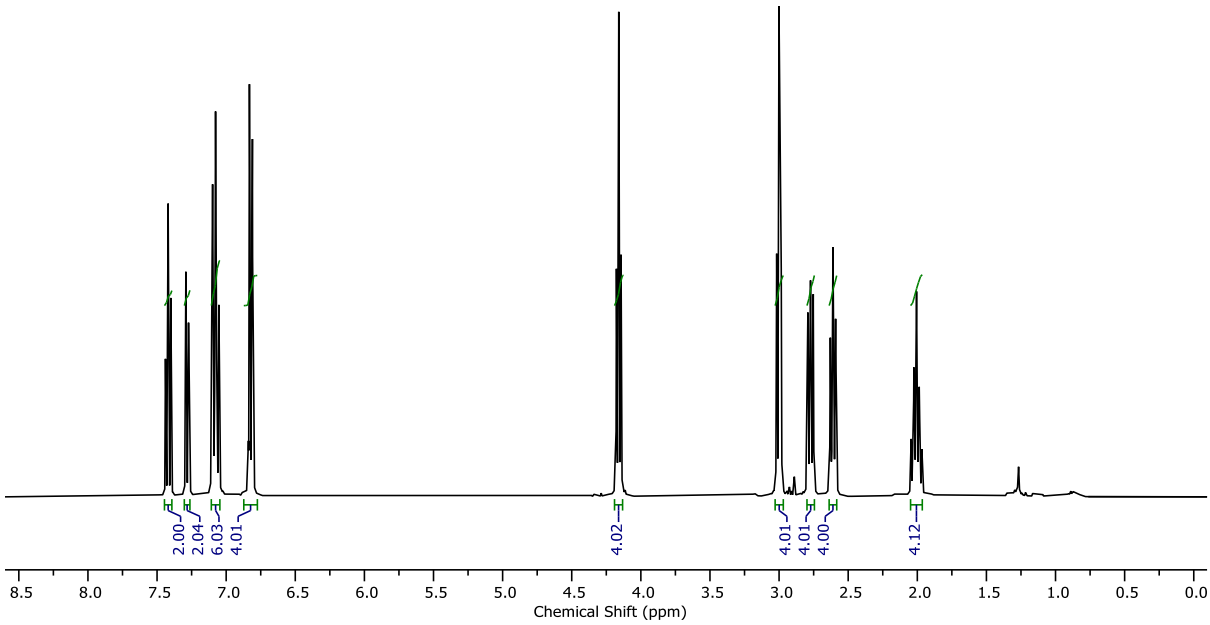

Figure 48: ^{1}H NMR ($CDCl_3$, 400 MHz) of **S12**.

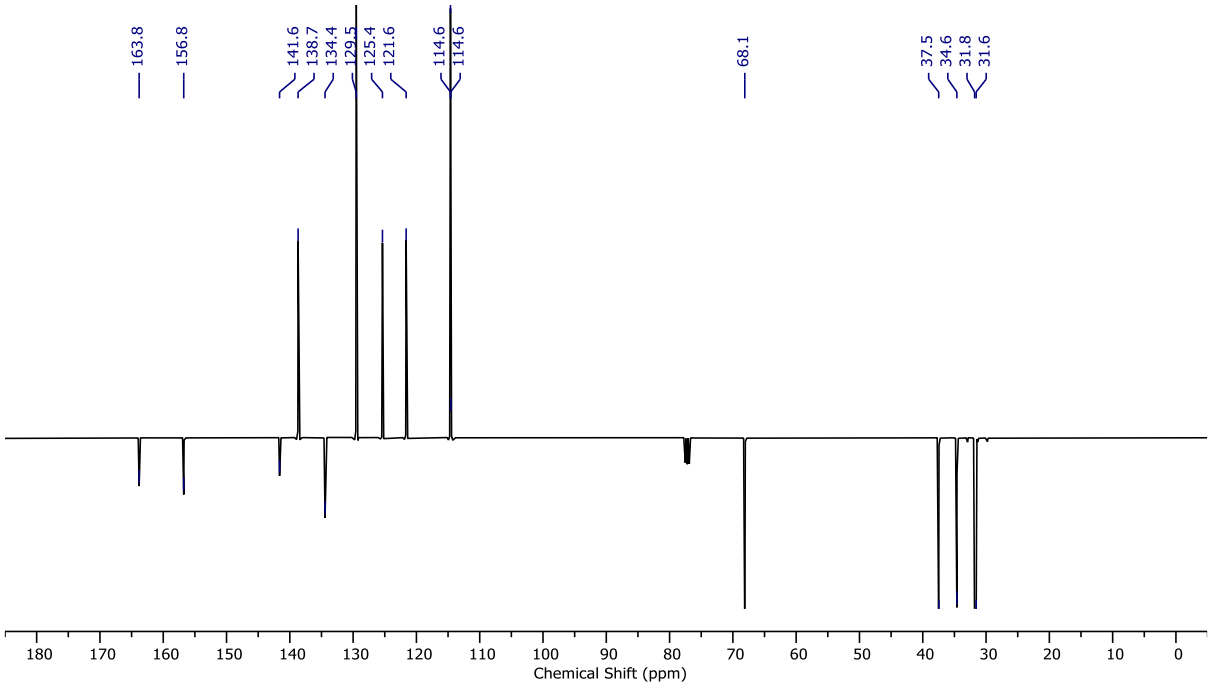

Figure 49: JMOD NMR ($CDCl_3$, 101 MHz) of **S12**.

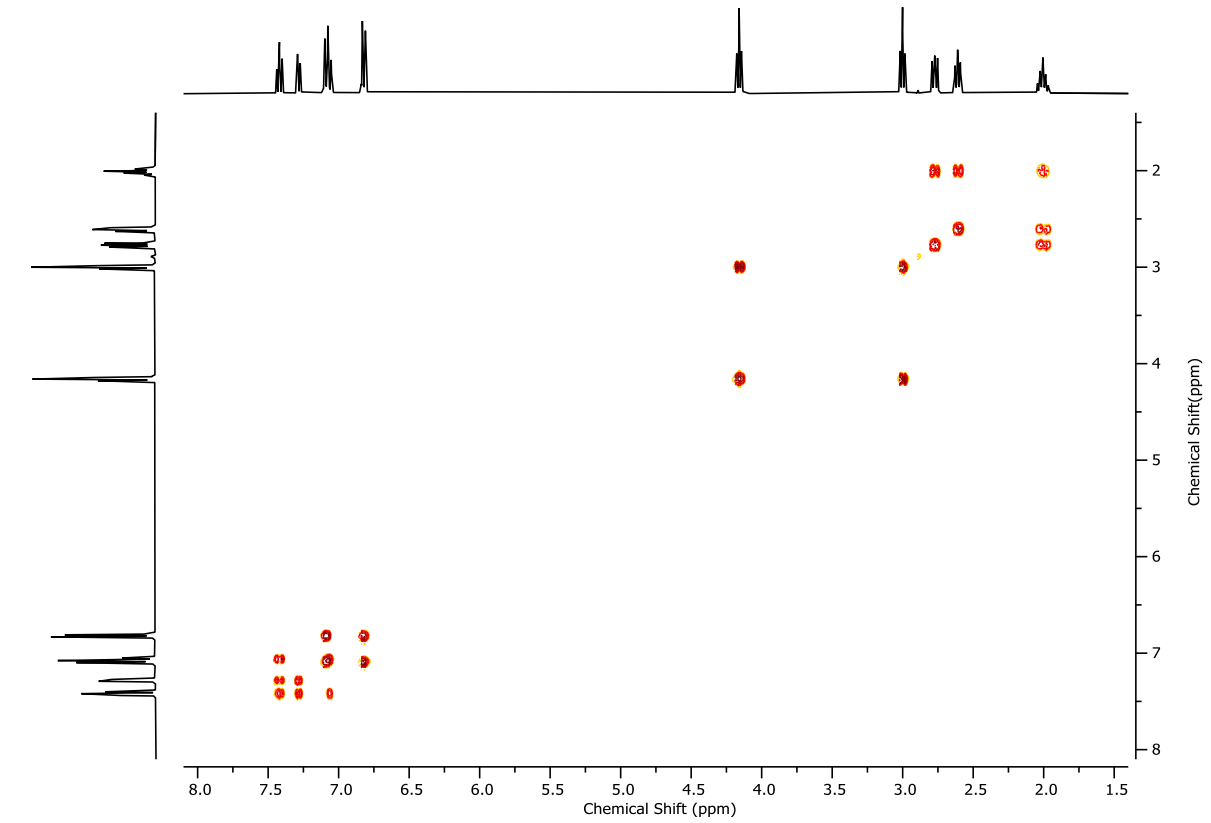

Figure 50: ^{1}H COSY NMR ($CDCl_3$, 400 MHz) of **S12**.

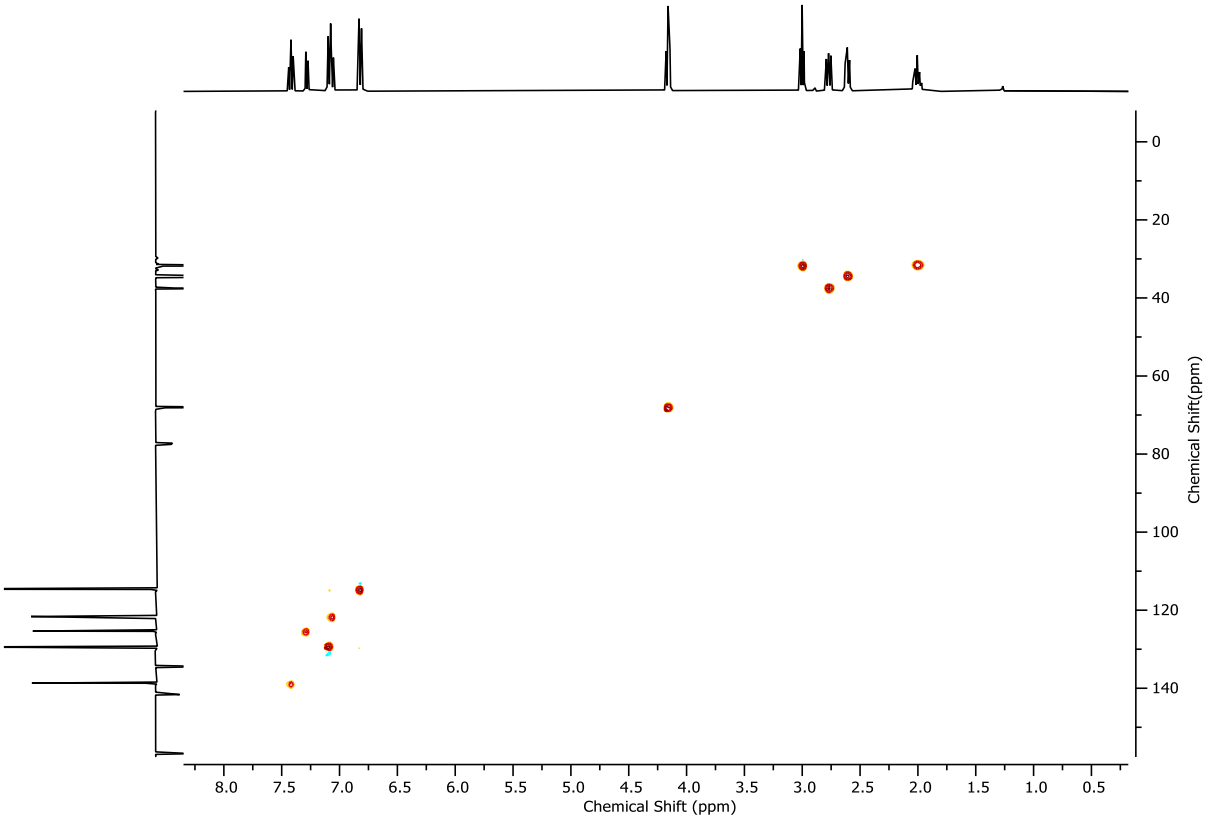

Figure 51: HSQC NMR ($CDCl_3$, 400 MHz) of **S12**.

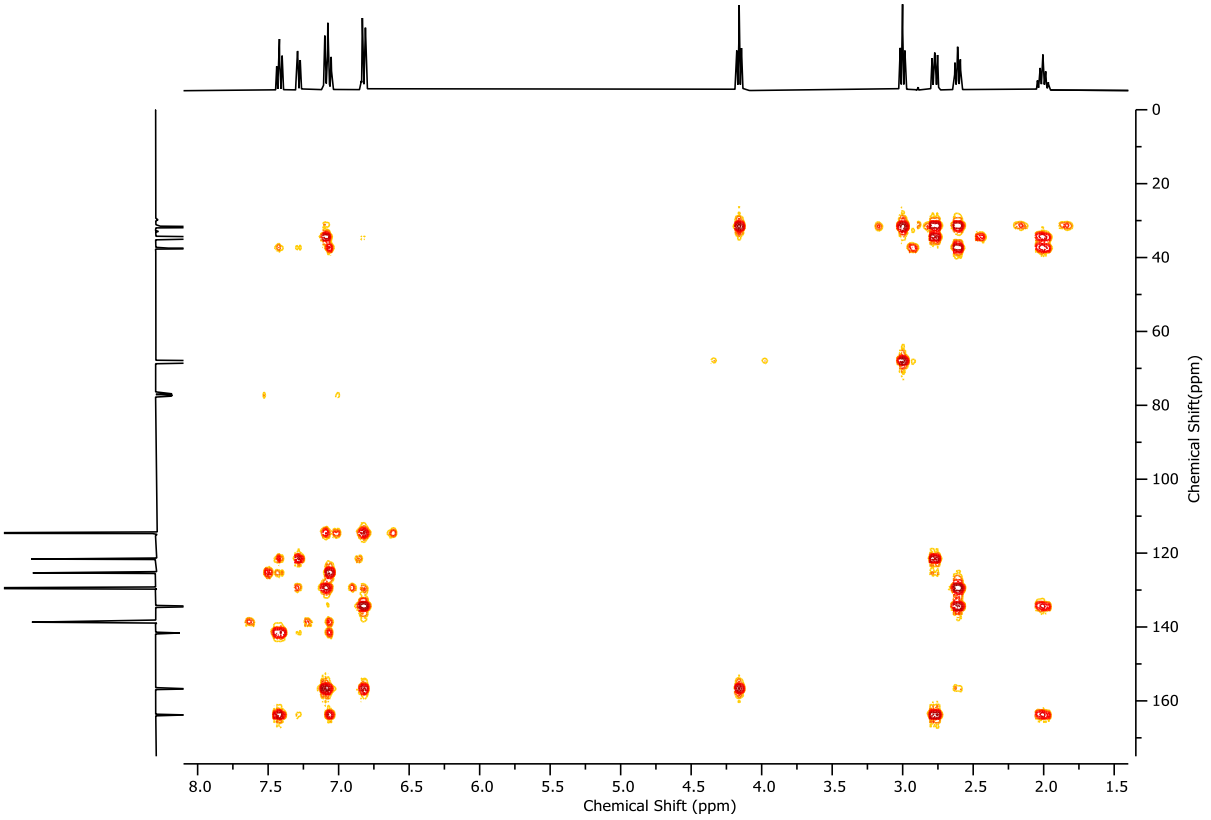

Figure 52: HMBC NMR ($CDCl_3$, 400 MHz) of **S12**.

3.2. Sulfide macrocycle 4

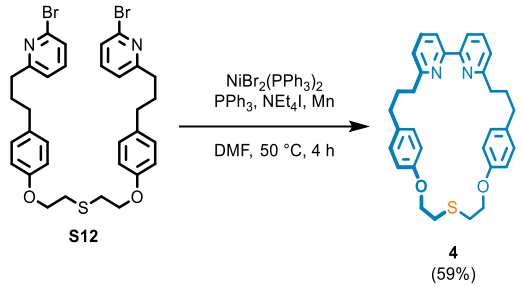

$NiBr_2(PPh_3)_2$ (1.09 g, 1.47 mmol, 1.0 eq.), PPh_3 (766.5 mg, 2.92 mmol, 2.0 eq.), Mn (802.1 g, 14.6 mmol, 10.0 eq.), and NEt_4I (376.5 mg, 1.46 mmol, 1.0 eq.) dissolved in DMF (15 mL) and sonicated for 15 min, until a deep red colour developed. The activated catalyst mixture was then stirred at 50 °C for 10 min, before a solution of **S12** (979.6g, 1.46 mmol, 1.0 eq.) in DMF (15 mL) was added *via* syringe pump over a 4 h period. After the addition was completed, the crude mixture was stirred at 50 °C for an additional 30 min, before cooling to ambient temperature. The reaction mixture was diluted with EtOAc (100 mL), and washed with a sat. EDTA/0.1 M NH_3 solution (30 mL), 5% LiCl (3 x 20 mL), and brine (30 mL). All aqueous phases were extracted with EtOAc (20 mL), and the combined organics were dried over $MgSO_4$, filtered and concentrated *in vacuo*. The residue was purified by column chromatography (SiO_2, CH_2Cl_2-petrol (1:1) with EtOAc 0→5%) to yield **4** (438.9 mg, 0.86 mmol, 59%) as a beige solid.

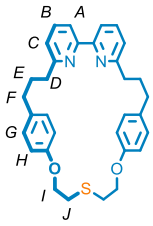

δ_H ($CDCl_3$, 400 MHz) 7.70 – 7.60 (m, 4H, H_A, H_B), 7.13 (p, J = 4.2, 2H, H_C), 7.06 – 6.99 (m, 4H, H_G), 6.74 – 6.66 (m, 4H, H_H), 4.15 (t, J = 6.6, 4H, H_I), 3.02 – 2.90 (m, 8H, H_J, H_D), 2.68 – 2.60 (m, 4H, H_F), 2.15 (t, 4H, H_E); δ_C ($CDCl_3$, 101 MHz) 162.3, 157.1, 156.5, 136.9, 135.1, 129.7, 122.6, 119.7, 114.7, 69.0, 37.9, 34.6, 32.1, 31.4; HR-ESI-MS (+ve) m/z = 511.2425 $[M+H]^+$ (calc. m/z for $C_{32}H_{35}N_2O_2S$ 511.2414); Melting point 79-81 °C.

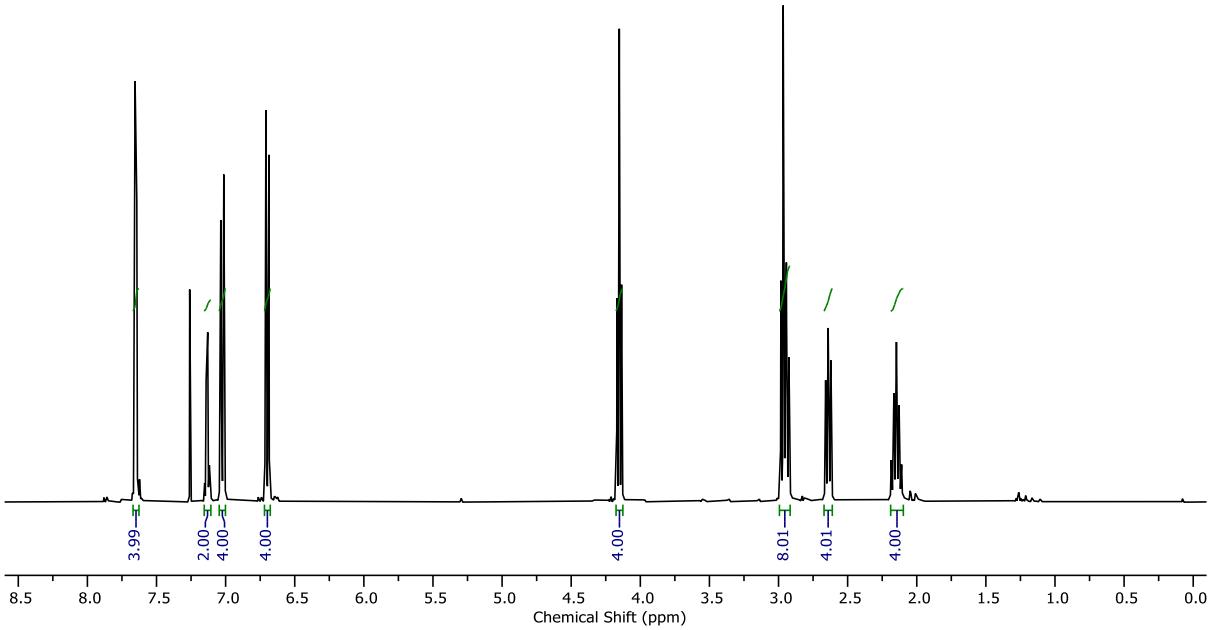

Figure 53: ^1H NMR ($CDCl_3$, 400 MHz) of **4**.

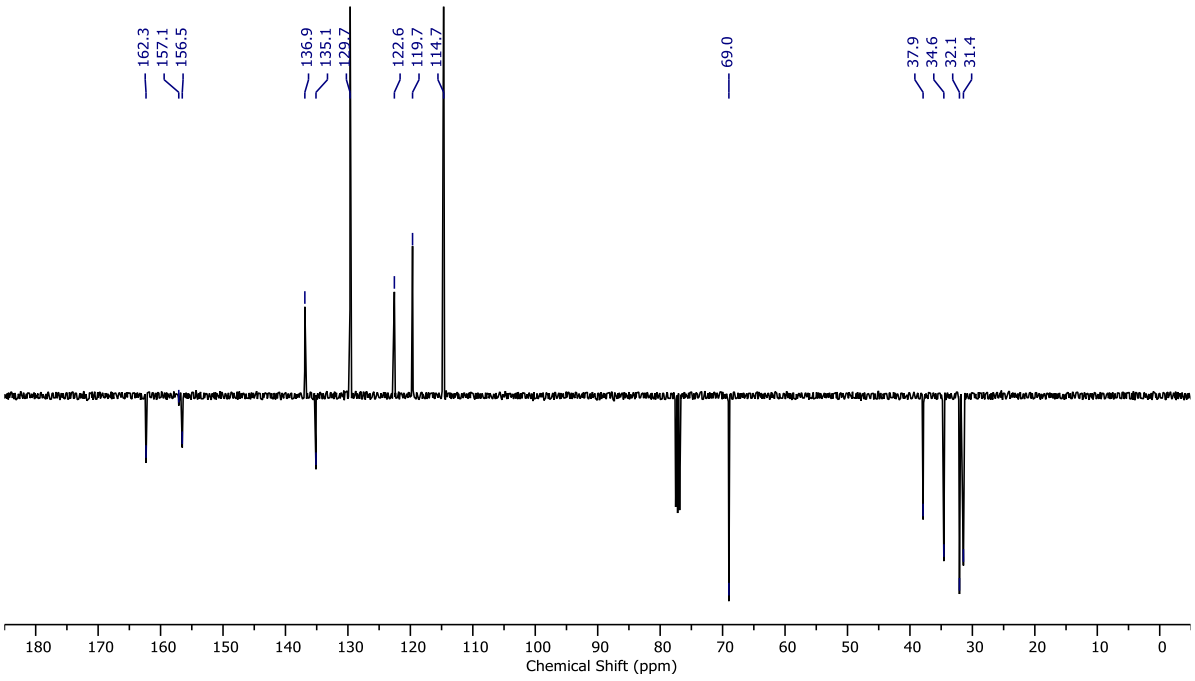

Figure 54: JMOD NMR ($CDCl_3$, 101 MHz) of **4**.

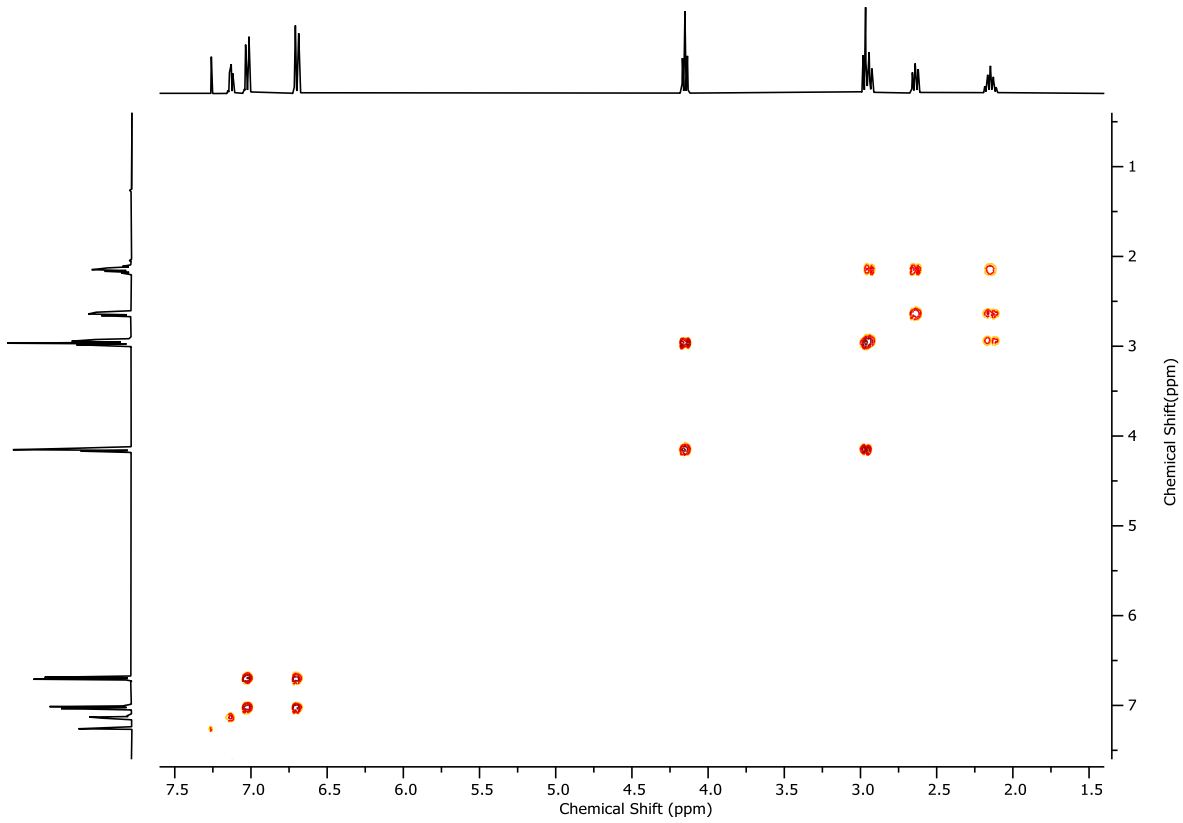

Figure 55: ^{1}H COSY NMR ($CDCl_3$, 400 MHz) of **4**.

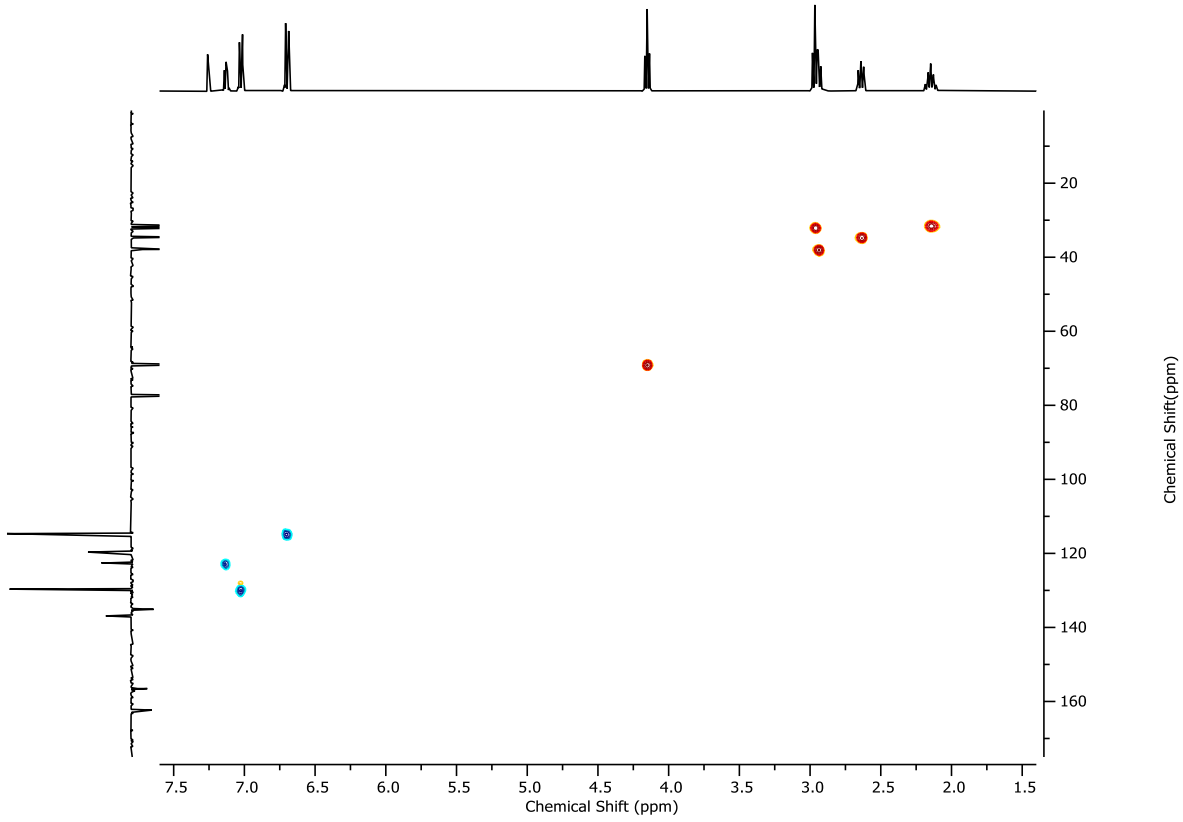

Figure 56: HSQC NMR ($CDCl_3$, 400 MHz) of **4**.

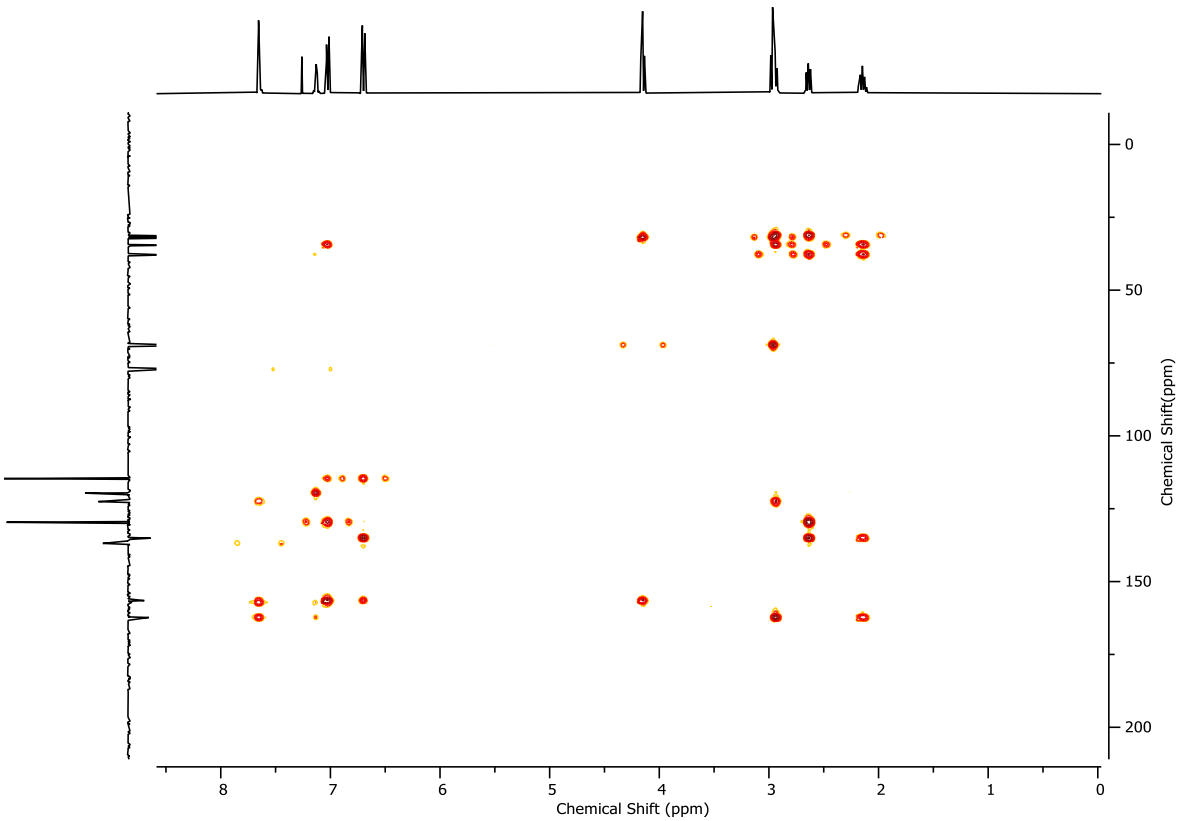

Figure 57: HMBC NMR ($CDCl_3$, 400 MHz) of **4**.

3.3. Sulfoxide macrocyle 2

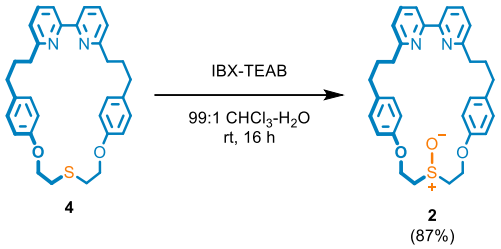

To a solution of **4** (85.5 mg, 0.168 mmol, 1.0 eq.) in 99:1 $CHCl_3/H_2O$ (1.68 mL), was added IBX (52 mg, 0.184 mmol, 1.1 eq) and tetraethylammonium bromide (39 mg, 0.184 mmol, 1.1 eq), and the resulting suspension was stirred for 16 h. The reaction mixture was then diluted with CH_2Cl_2 (10 mL), washed with 10% $NaHSO_3$ (5 mL), saturated $NaHCO_3$ (5 mL) and brine (5 mL), extracting all aqueous layers with CH_2Cl_2 (5 mL). The combined organics were dried over $MgSO_4$, filtered, and concentrated *in vacuo*. The residue was purified by column chromatography (SiO_2, CH_2Cl_2-MeOH 0→10%) to yield **2** (77.2 mg, 0.146 mmol, 87%) as an off-white foam.

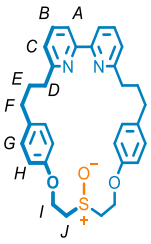

δ_H ($CDCl_3$, 400 MHz) 7.71 – 7.56 (m, 4H, H_A, H_B), 7.11 (dd, J = 5.9, 2.8, 2H, H_C), 7.02 (d, J = 8.8, 4H, H_G), 6.63 (d, J = 8.7, 4H, H_H), 4.50 – 4.31 (m, 4H, H_I), 3.42 (ddd, J = 13.2, 8.3, 4.7, 2H, H_J), 3.11 (ddd, J = 13.7, 5.4, 4.0, 2H, H_J), 2.92 (t, J = 7.3, 4H, H_D), 2.72 – 2.58 (m, 4H, H_F), 2.20 – 2.08 (m, 4H, H_E); δ_C ($CDCl_3$, 101 MHz) 162.1, 156.9, 155.5, 136.8, 135.7, 129.7, 122.5, 119.5, 114.8, 60.7, 52.1, 37.7, 34.4, 31.3; HR-ESI-MS (+ve) m/z = 527.2374 $[M+H]^+$ (calc. m/z for $C_{32}H_{35}N_2O_3S$ 527.2363).

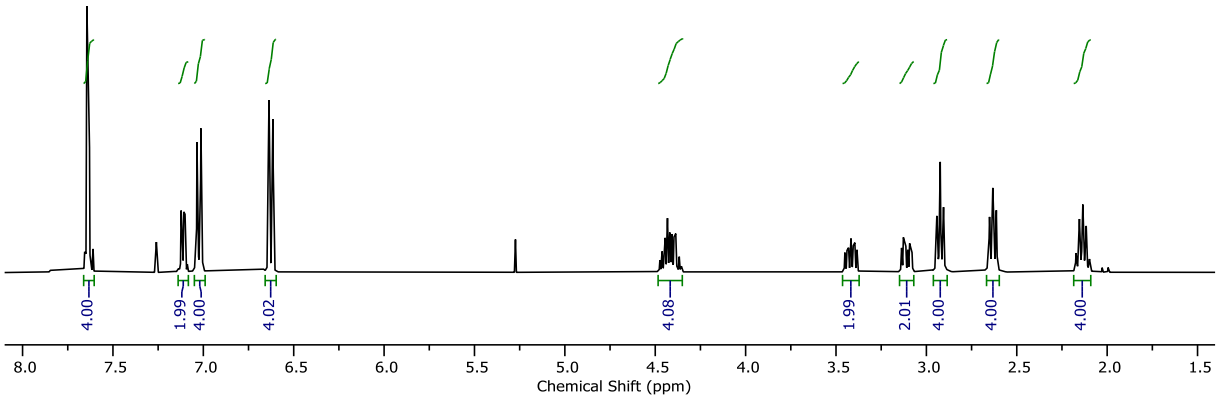

Figure 58: ^1H NMR ($CDCl_3$, 400 MHz) of **2**.

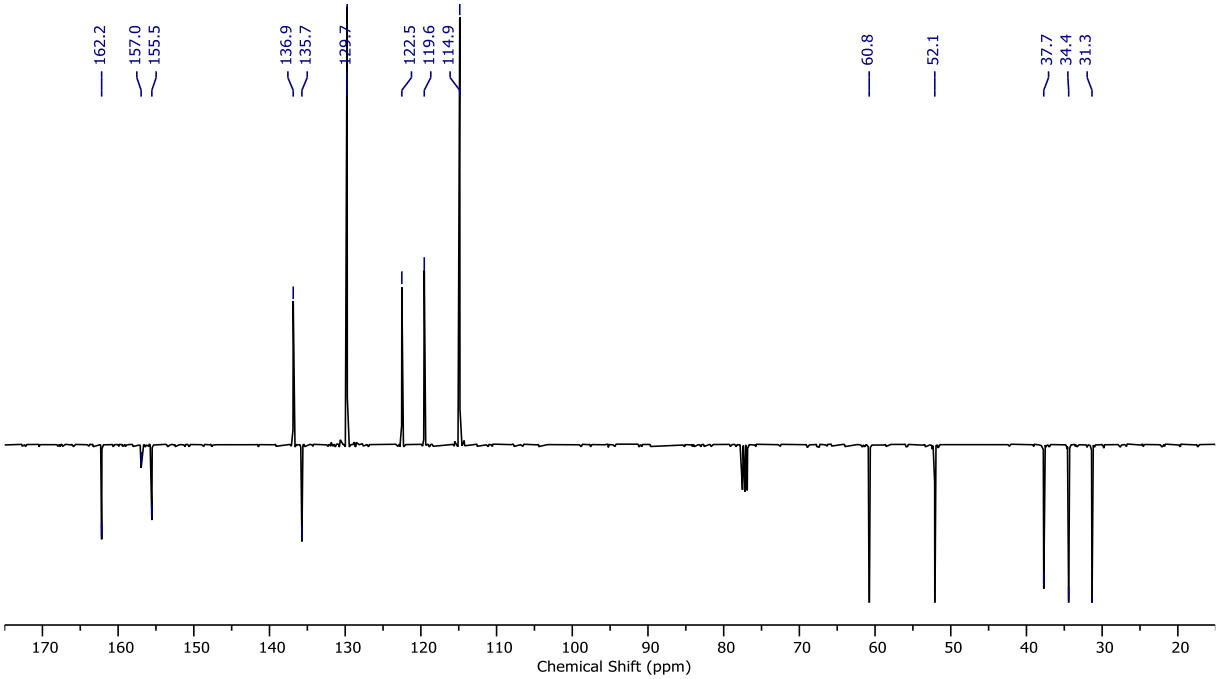

Figure 59: JMOD NMR ($CDCl_3$, 101 MHz) of **2**.

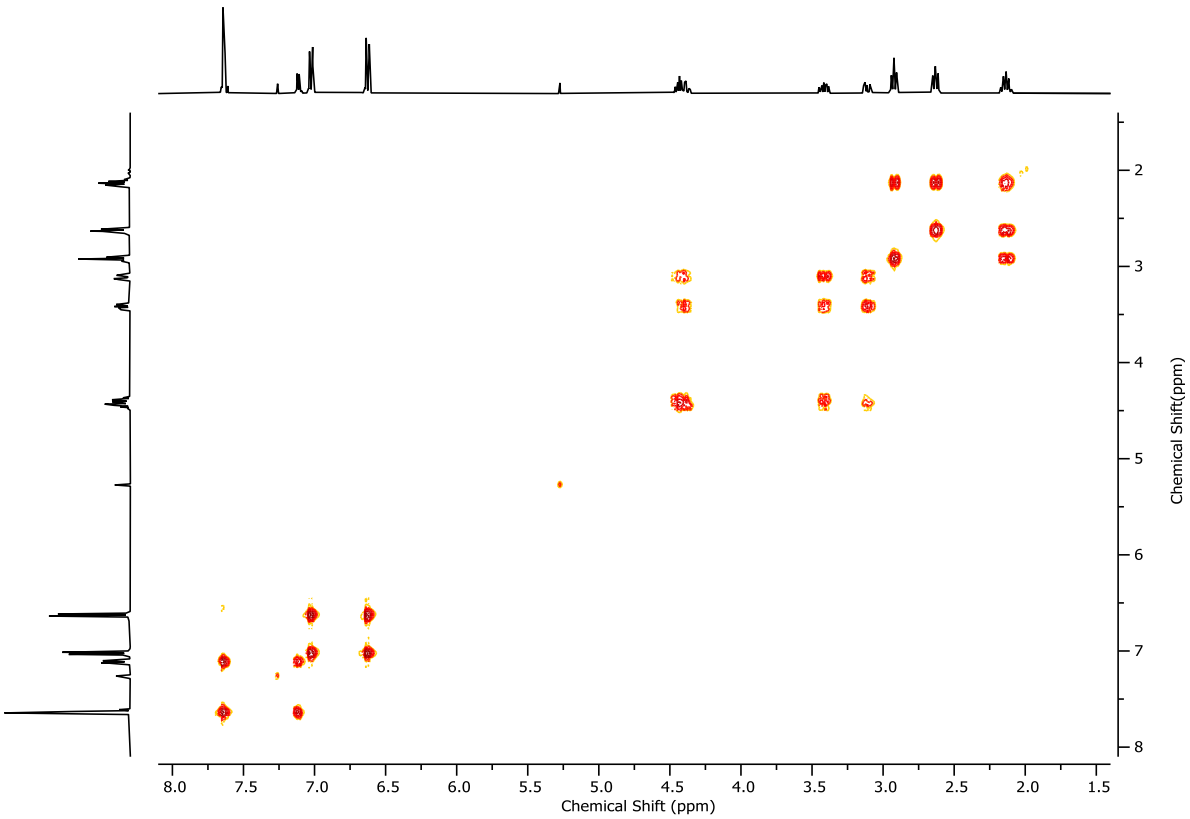

Figure 60: ^{1}H COSY NMR ($CDCl_3$, 400 MHz) of **2**.

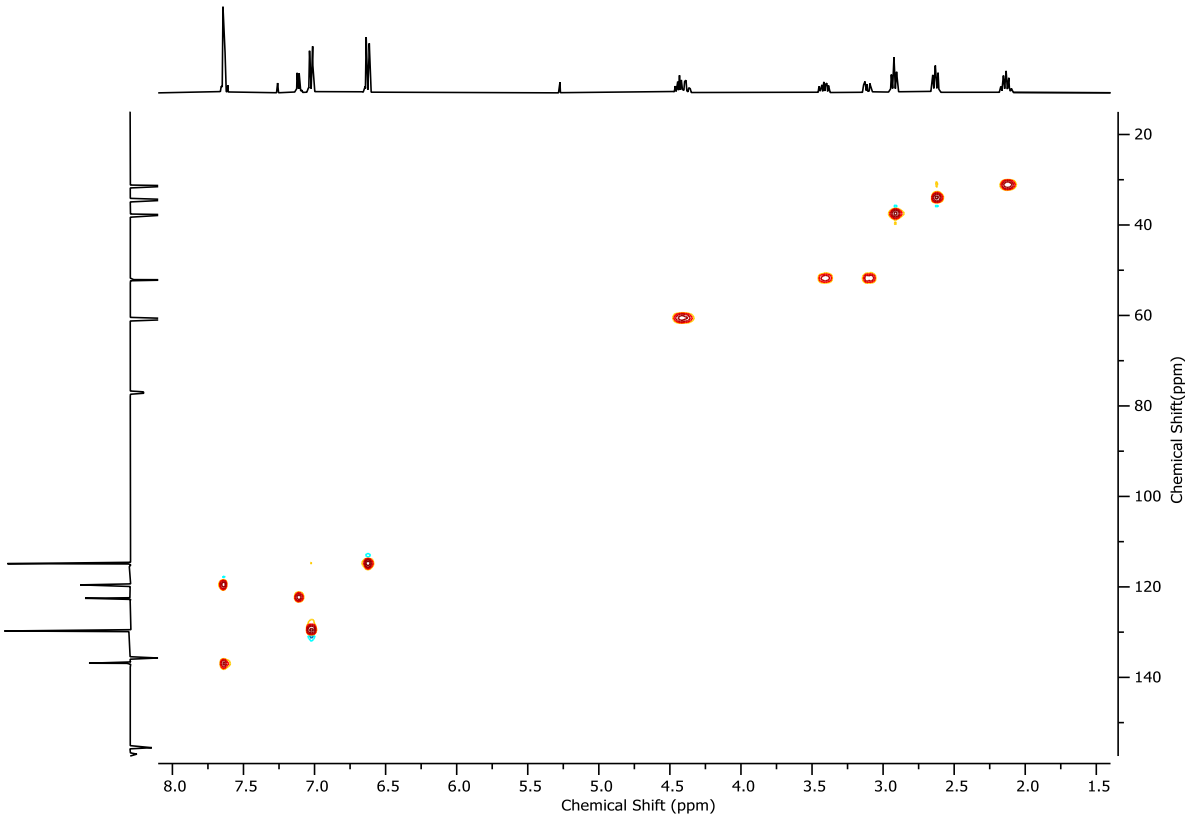

Figure 61: HSQC NMR ($CDCl_3$, 400 MHz) of **2**.

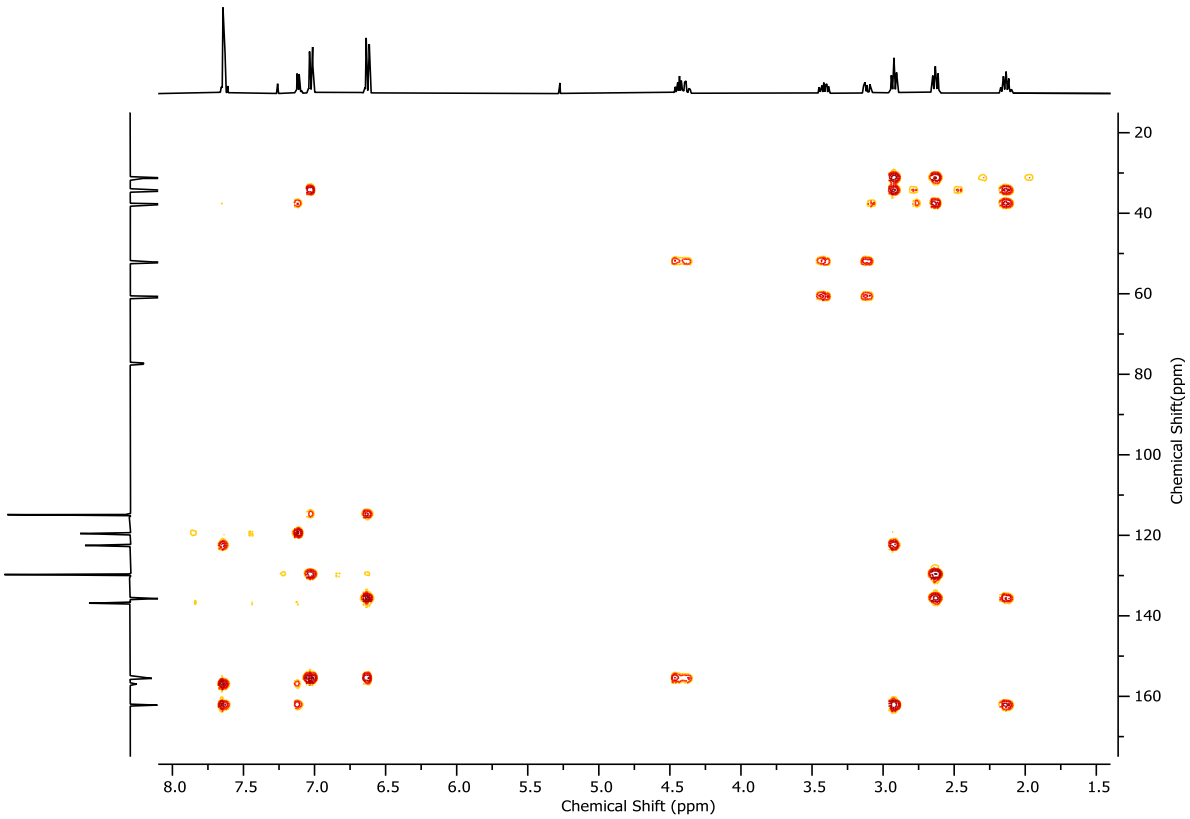

Figure 62: HMBC NMR ($CDCl_3$, 400 MHz) of **2**.

4. Synthesis of catananes (S_{ma},$R_{co\text{-}c}$)-3 and (R_{ma},$R_{co\text{-}c}$)-3

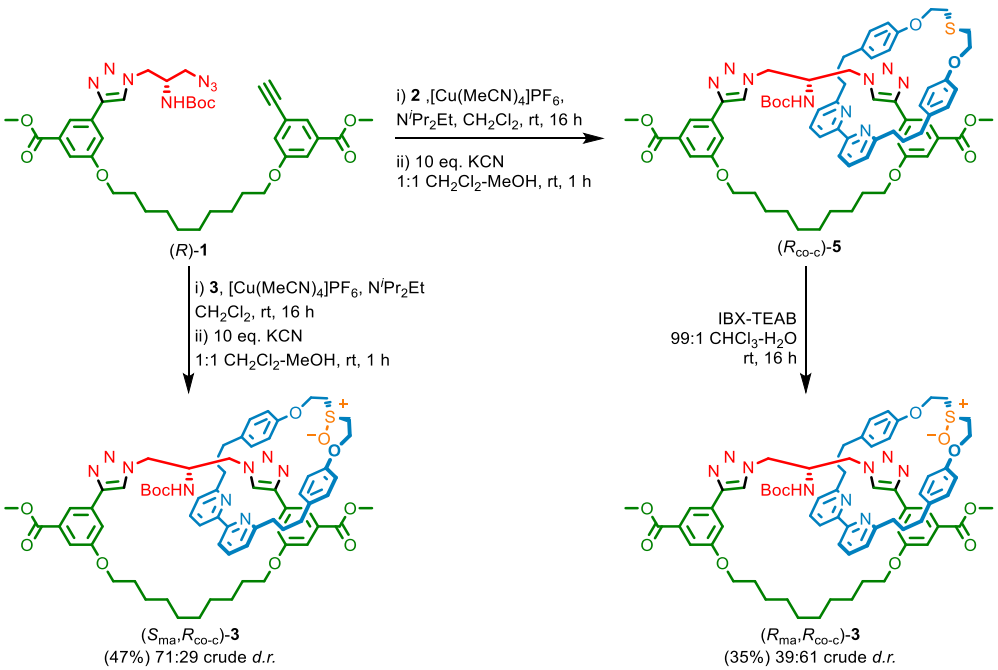

Scheme 3: Synthetic route to mechanically axially chiral epimeric catenanes (S_{ma},$R_{co\text{-}c}$)-**3** and (R_{ma},$R_{co\text{-}c}$)-**3**.

4.1. Catenane (S_{ma},$R_{co\text{-}c}$)-3

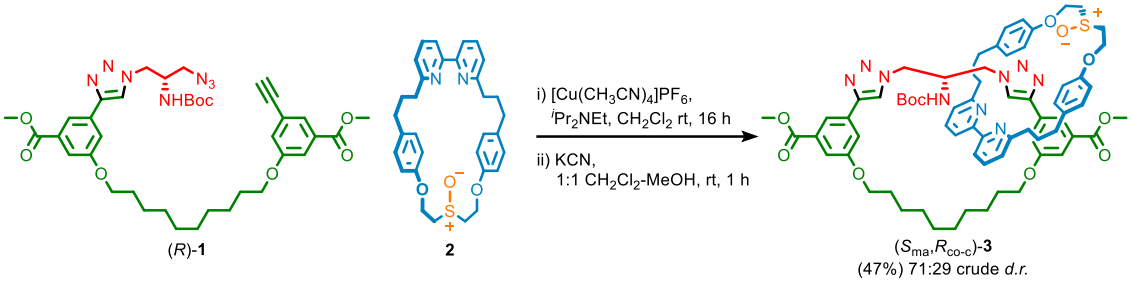

A CEM MW vial was charged with macrocycle **2** (43.1 mg, 0.082 mmol, 1.0 eq.) and $[Cu(CH_3CN)_4]PF_6$ (29.9 mg, 0.080 mmol, 0.98 eq.) and purged with N_2. CH_2Cl_2 (5.95 mL) and $^iPr_2NEt$ (28 µL, 0.164 mmol, 2.0 eq.) were added followed by a solution of pre-macrocycle (*R*)-**1** (65.9 mg, 0.090 mmol, 1.1 eq.) in CH_2Cl_2 (2.0 mL) at ambient temperature over 16 h. Then, MeOH (2.9 mL) and KCN as a solid (53 mg, 0.82 mmol, 10.0 eq.) were added and the resulting mixture was stirred vigorously for 1 h. The crude mixture was diluted with CH_2Cl_2 (8 mL) and washed with H_2O in two portions (10 mL and 5 mL), with separation of aqueous and organic phases. The combined aqueous phase was then extracted with CH_2Cl_2 (3 x 5 mL) and the combined organics were washed with brine (10 mL), dried over $MgSO_4$ and concentrated *in vacuo*. The residue was purified by column chromatography (SiO_2, CH_2Cl_2-CH_3CN 0→100%; CH_3CN-MeOH 0→5%) to yield (S_{ma},$R_{co\text{-}c}$)-**3** (48.3 mg, 0.0384 mmol, 47%, first eluting isomer) as an off-white foam and (R_{ma},$R_{co\text{-}c}$)-**3** (22.6 mg, 0.018 mmol, 22%, second eluting isomer) as a colorless oil. The absolute stereochemistry of the major diatereomer was assigned crystallographically using a sample of rac-(S_{ma},$R_{co\text{-}c}$)-**3** produced by reaction of *rac*-**1** (see 11.1). The mechanical stereochemistry of the minor diastereomer was assigned as opposite to that of the major diastereomer. The co-conformational stereochemistry of both is fixed by the absolute sterechemistry of (*R*)-**1**.

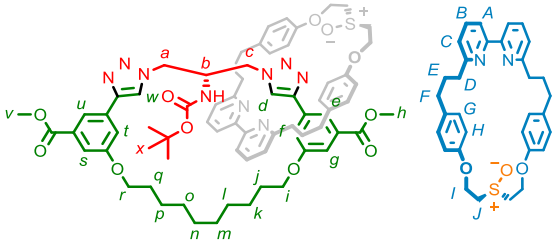

δ_H (400 MHz, $CDCl_3$) 10.34 (1H, s, $\boldsymbol{H}_d$), 8.32 (1H, s, $\boldsymbol{H}_e$), 8.10 (1H, s, $\boldsymbol{H}_u$), 7.79 – 7.60 (2H, m, $\boldsymbol{H}_{B/B'}$), 7.55 (1H, s, $\boldsymbol{H}_w$), 7.52 – 7.44 (2H, m, $\boldsymbol{H}_{A/A'}$), 7.39 (1H, s, $\boldsymbol{H}_s$), 7.29 (1H, s, $\boldsymbol{H}_g$), 7.16 (1H, m, $\boldsymbol{H}_{C'}$), 7.02 (1H, s, $\boldsymbol{H}_f$), 6.88 (3H, m, $\boldsymbol{H}_G$, $\boldsymbol{H}_C$), 6.80 – 6.63 (6H, m, $\boldsymbol{H}_H$, $\boldsymbol{H}_{H'}$, $\boldsymbol{H}_{G'}$), 6.52 (1H, s, $\boldsymbol{H}_t$), 5.69 (1H, m, $\boldsymbol{H}_{NHBoc}$), 4.80 – 4.35 (5H, m, $\boldsymbol{H}_{I/I'}$, $\boldsymbol{H}_a$), 4.21 – 4.02 (3H, m, $\boldsymbol{H}_i$, $\boldsymbol{H}_b$), 4.00 – 3.79 (7H, m, $\boldsymbol{H}_h$, $\boldsymbol{H}_v$, $\boldsymbol{H}_c$), 3.78 – 3.56 (3H, m, $\boldsymbol{H}_a$, $\boldsymbol{H}_J$, $\boldsymbol{H}_c$), 3.53 – 3.22 (3H, m, $\boldsymbol{H}_r$, $\boldsymbol{H}_J$), 3.16 (2H, m, $\boldsymbol{H}_{J'}$), 2.66 – 2.23 (8H, m, $\boldsymbol{H}_{D/D'}$, $\boldsymbol{H}_{F/F'}$), 2.15 – 1.67 (4H, m, $\boldsymbol{H}_j$, $\boldsymbol{H}_{E/E'}$), 1.64 – 1.02 (25H, m, $\boldsymbol{H}_q$, $\boldsymbol{H}_p$, $\boldsymbol{H}_o$, $\boldsymbol{H}_n$, $\boldsymbol{H}_m$, $\boldsymbol{H}_l$, $\boldsymbol{H}_k$, $\boldsymbol{H}_{E/E'}$, $\boldsymbol{H}_x$). $\boldsymbol{\delta}_C$ (101 MHz, $CDCl_3$) 167.1, 166.9, 163.4, 162.5, 158.9, 156.5, 156.4, 156.3, 156.2, 146.2, 145.9, 137.4, 136.8, 135.6, 133.40, 133.35, 132.8, 132.0, 131.7, 131.3, 129.7, 129.4, 122.1, 121.2, 120.8, 120.4, 119.1, 118.8, 118.2, 116.6, 114.8, 114.6, 114.0, 111.2, 67.8, 67.7, 60.3, 60.2, 52.7, 52.5, 52.1, 50.6, 50.3, 49.8, 36.5, 34.7, 29.8, 29.7, 29.4, 29.3, 29.25, 29.2, 29.0, 28.2, 26.7, 25.9. LR-ESI-MS (+ve) = 1258.6 $[M+H]^+$.

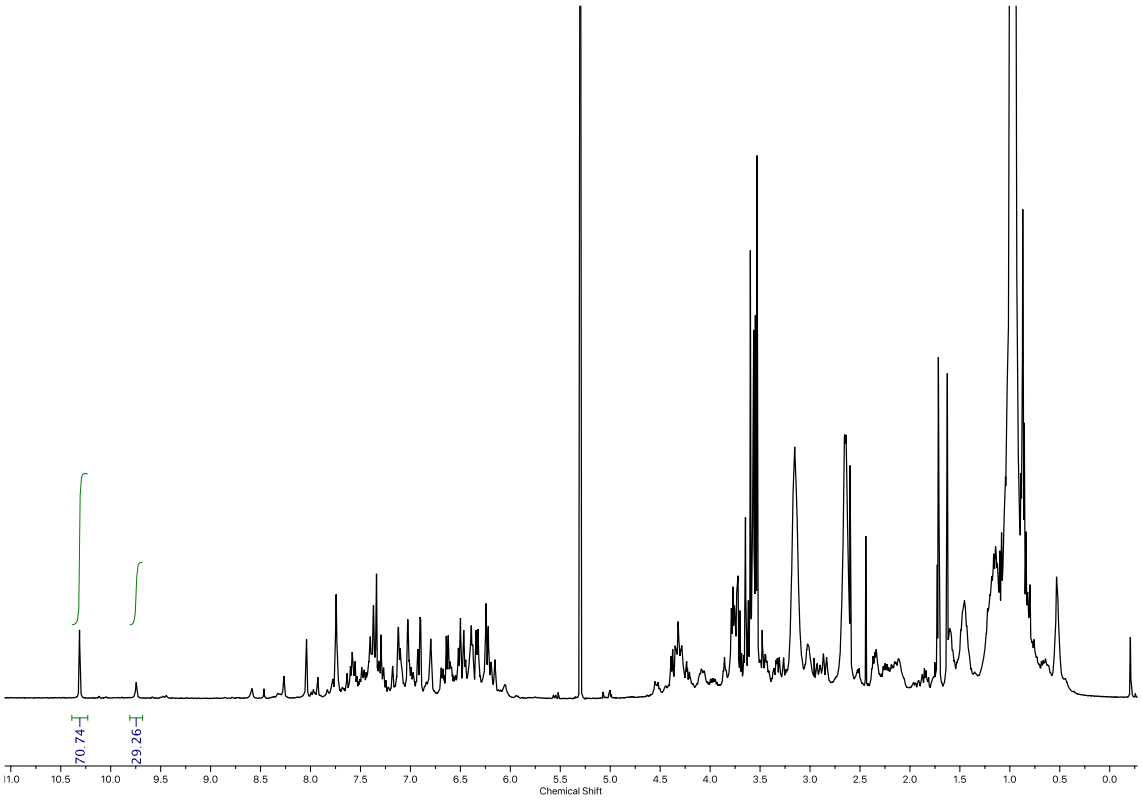

Figure 63: ^{1}H NMR ($CDCl_3$, 400 MHz) of AT-CuAAC crude leading to major isomer (S_{ma},$R_{co\text{-}c}$)-**3**. Integration of (S_{ma},$R_{co\text{-}c}$)-**3** (10.34 ppm, $\boldsymbol{H}_d$, 70.74H) and (R_{ma},$R_{co\text{-}c}$)-**3** (9.95 ppm, $\boldsymbol{H}_d$, 29.26H).

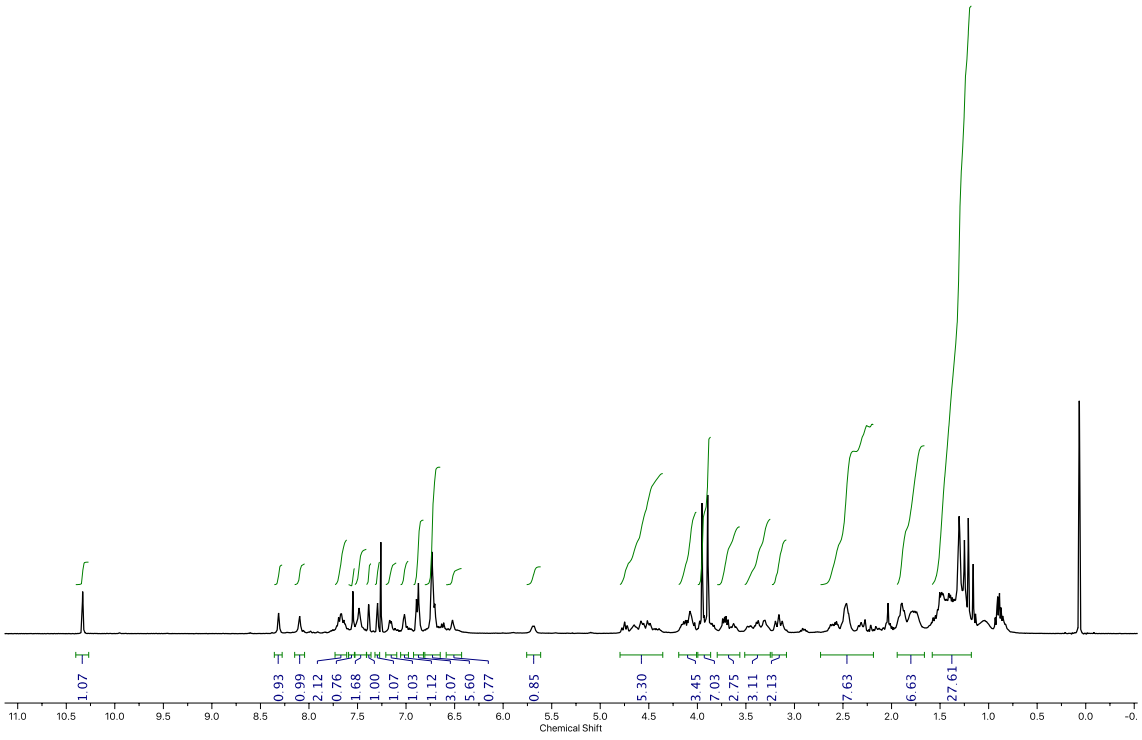

Figure 64: ^{1}H NMR ($CDCl_3$, 400 MHz) of (S_{ma},$R_{co\text{-}c}$)-**3**.

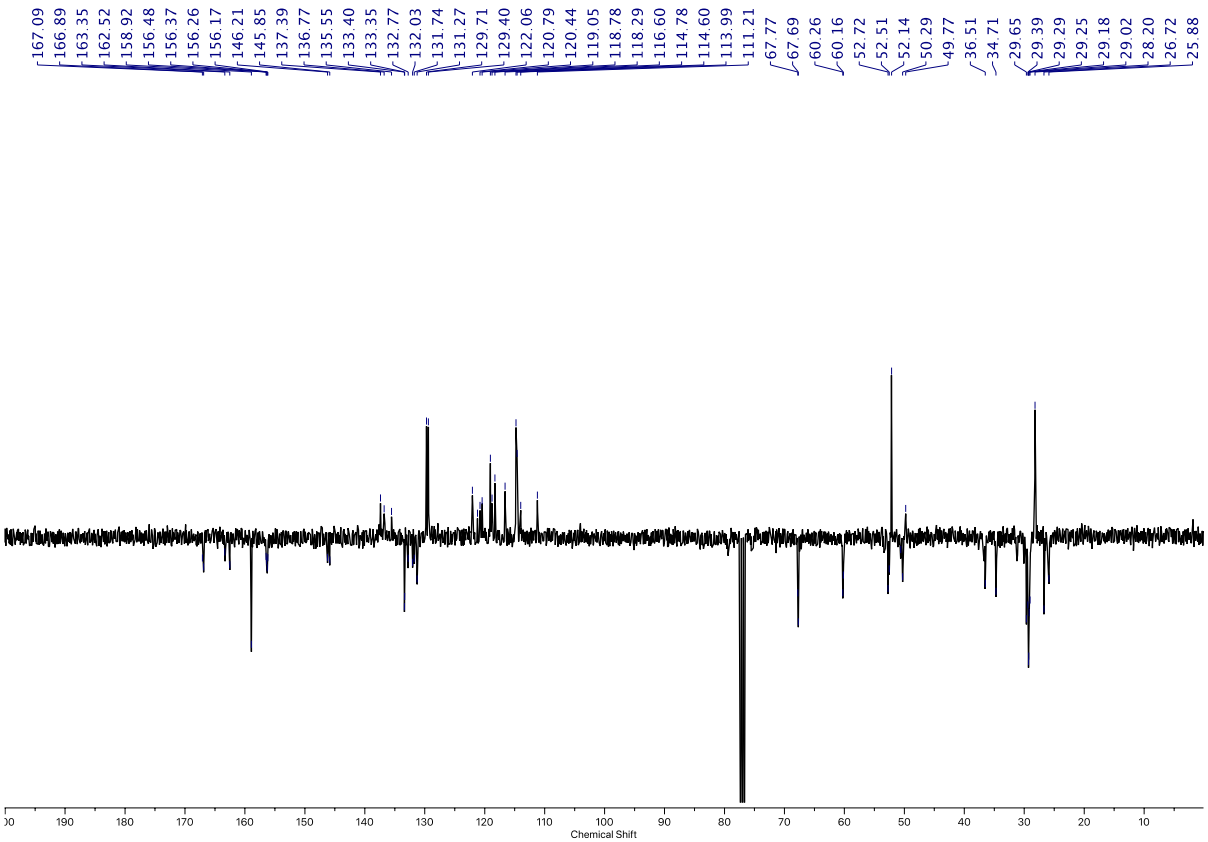

Figure 65: JMOD NMR ($CDCl_3$, 101 MHz) of (S_{ma},$R_{co\text{-}c}$)-**3**.

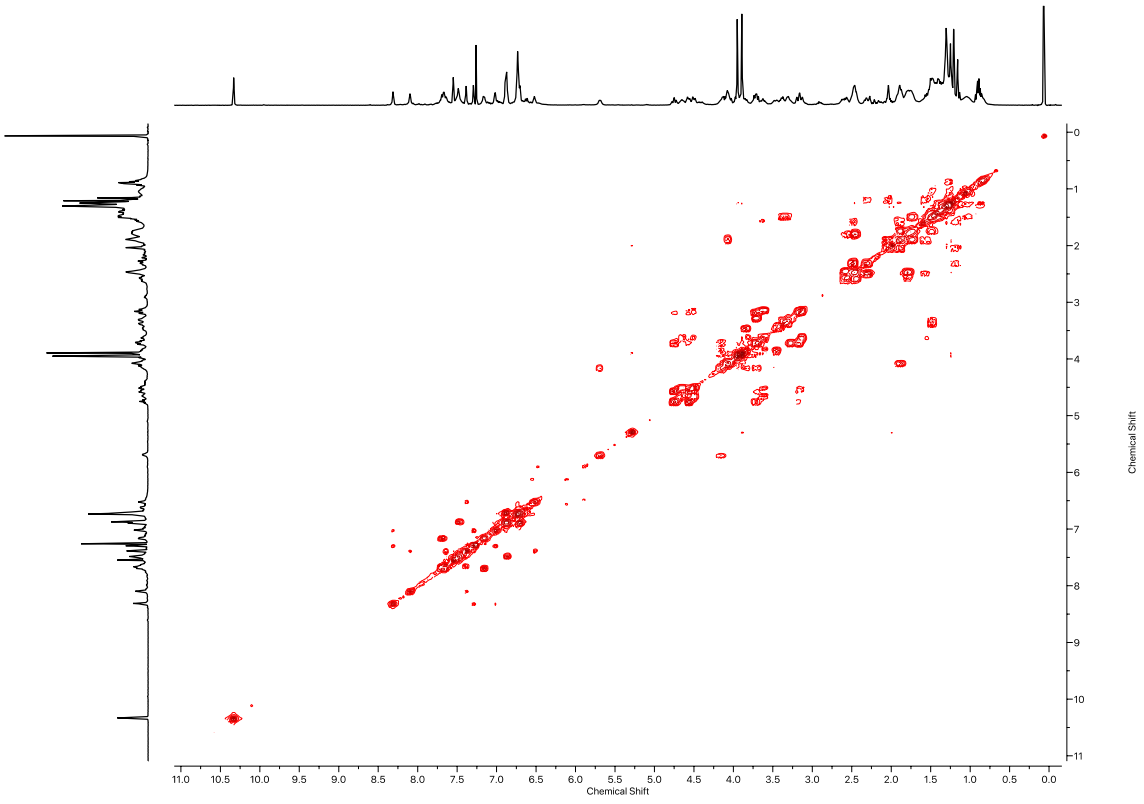

Figure 66: ^1H COSY NMR ($CDCl_3$, 400 MHz) of (S_{ma},$R_{co\text{-}c}$)-**3**.

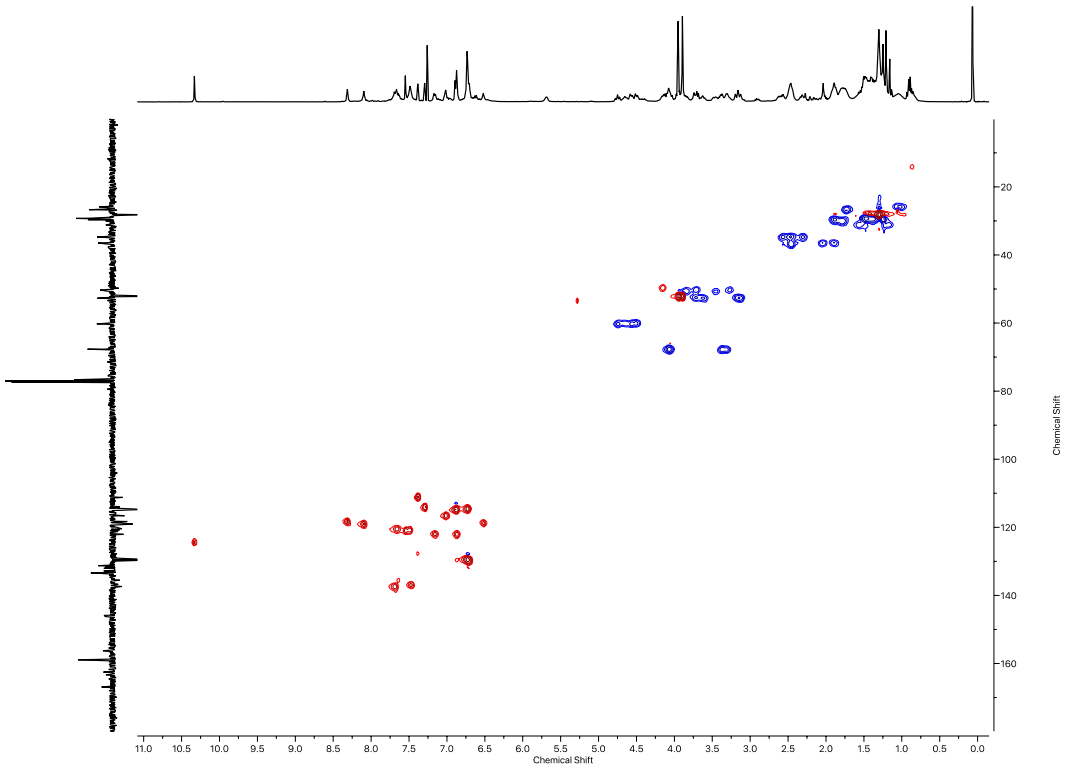

Figure 67: HSQC NMR ($CDCl_3$, 400 MHz) of (S_{ma},$R_{co\text{-}c}$)-**3**.

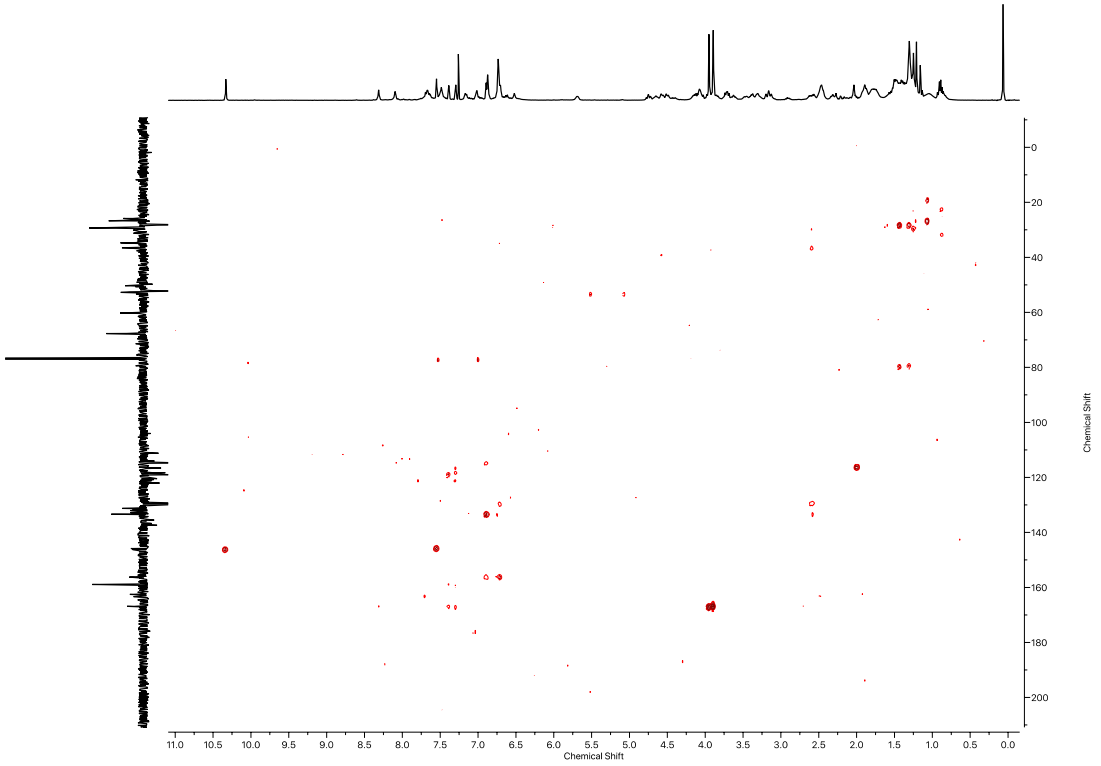

Figure 68: HMBC NMR ($CDCl_3$, 400 MHz) of (S_{ma},$R_{co\text{-}c}$)-**3**.

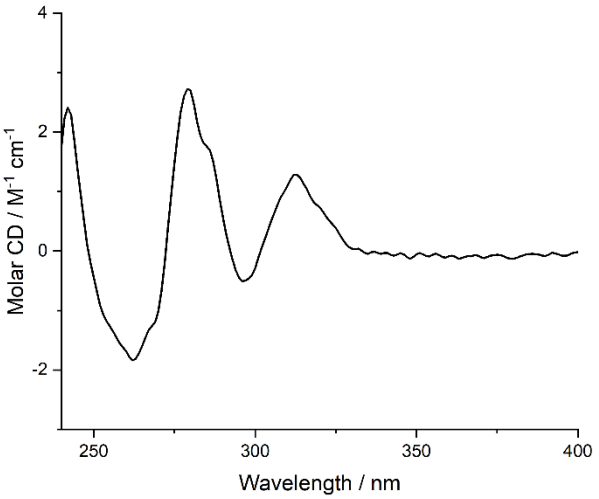

Figure 69: Circular Dichroism Spectra of (S_{ma},$R_{co\text{-}c}$)-**3** (19 µM) at 293 K in $CHCl_3$.

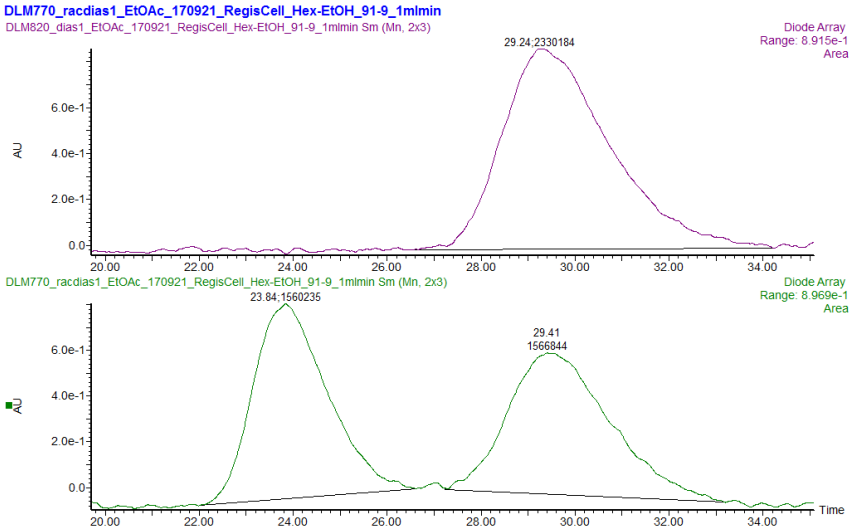

Figure 70: CSP-HPLC of (S_{ma},$R_{co\text{-}c}$)-**3** (loaded in EtOAc). RegisCell, *n*-hexane-EtOH 91 : 9, flowrate 1 mLmin^{-1}. (top) (S_{ma},$R_{co\text{-}c}$)-**3** (29.24 min, 2330184, >99.9%), (R_{ma},$S_{co\text{-}c}$)-**3** (not observed). (bottom) *rac*-**3**, (R_{ma},$S_{co\text{-}c}$)-**3** (23.84 min, 1560235, 49.9%), (S_{ma},$R_{co\text{-}c}$)-**3** (29.41 min, 1566844, 50.1%).

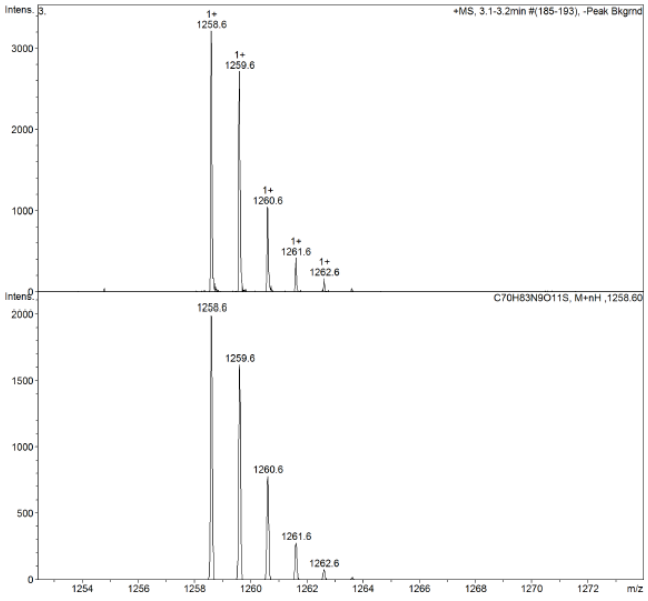

Figure 71: Observed (top) and calculated (bottom) isotopic patterns for (S_{ma},$R_{co\text{-}c}$)-**3**.

4.2. Catenane ($R_{co\text{-}c}$)-5

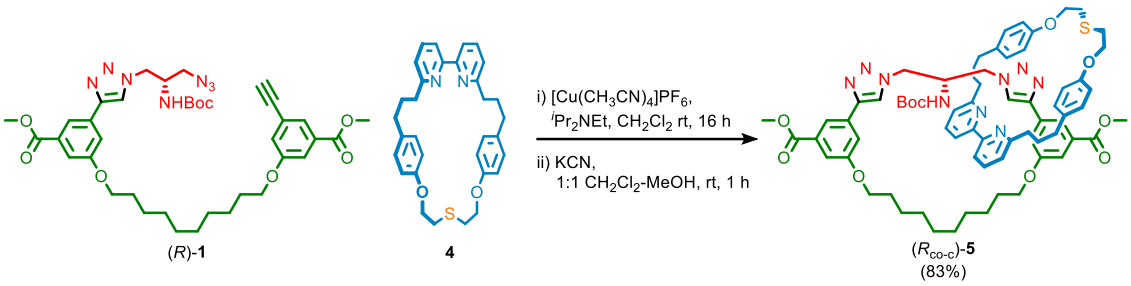

To a stirred solution of **4** (20.0 mg, 0.039 mmol, 1.00 eq.), $[Cu(CH_3CN)_4]PF_6$ (14.3 mg, 0.039 mmol, 0.98 eq.), and DIPEA (14 µL, 0.78 mmol, 2.00 eq.) in CH_2Cl_2 (4.1 mL) was added a solution of (*R*)-**1** (31.6 mg, 0.043 mmol, 1.1 eq.) in CH_2Cl_2 (1.60 mL) via syringe pump over a 16 h period. MeOH (3 mL) was then added, followed by KCN (25.0 mg, 0.39 mmol, 10.0 eq.). After stirring for 1 h, and the loss of deep orange colour, the mixture was diluted with CH_2Cl_2 (15 mL) and H_2O (10 mL). The aqueous and organic phases were separated, and the aqueous was extracted with CH_2Cl_2 (2 x 15 mL). The combined organics were washed with brine (10 mL), dried over $MgSO_4$ and concentrated *in vacuo*. The residue was purified by column chromatography (SiO_2, DCM-EtOAc 0→20%) to yield ($R_{co\text{-}c}$)-**5** (40.0 mg, 0.032 mmol, 83%) as an off-white foam. See 4.1 for a discussion of stereochemical assignment.

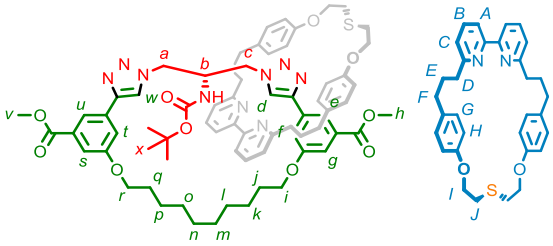

δ_H (400 MHz, $CDCl_3$) 10.07 (1H, s, $\boldsymbol{H}_d$), 8.33 (1H, s, $\boldsymbol{H}_e$), 8.09 (1H, s, $\boldsymbol{H}_u$), 7.92 (1H, s, $\boldsymbol{H}_w$), 7.65 – 7.54 (2H, m, $\boldsymbol{H}_B$, $\boldsymbol{H}_{B'}$), 7.53 – 7.46 (2H, m, $\boldsymbol{H}_A$, $\boldsymbol{H}_{A'}$), 7.41 (1H, dd, J = 2.5, 1.4, $\boldsymbol{H}_s$), 7.33 (1H, dd, J = 2.5, 1.4, $\boldsymbol{H}_g$), 7.09 (1H, d, J = 7.4, $\boldsymbol{H}_C$), 7.06 (1H, dd, J = 2.6, 1.5, $\boldsymbol{H}_f$), 6.99 (1H, dd, J = 6.3, 2.3, $\boldsymbol{H}_{C'}$), 6.75 – 6.70 (2H, m, $\boldsymbol{H}_G$), 6.68 – 6.59 (6H, m, $\boldsymbol{H}_{G'}$, $\boldsymbol{H}_H$, $\boldsymbol{H}_{H'}$), 6.52 (1H, t, J = 2.0, $\boldsymbol{H}_t$), 5.39 (1H, s, $\boldsymbol{H}_{NHBoc}$), 4.65 – 4.45 (2H, m, $\boldsymbol{H}_I$, $\boldsymbol{H}_{I'}$), 4.40 – 4.22 (2H,m, $\boldsymbol{H}_I$, $\boldsymbol{H}_{I'}$), 4.08 (2H, t, J = 5.4, $\boldsymbol{H}_r$), 4.00 – 3.75 (9H, m, $\boldsymbol{H}_a$, $\boldsymbol{H}_b$, $\boldsymbol{H}_h$, $\boldsymbol{H}_v$), 3.63 – 3.53 (2H, m, $\boldsymbol{H}_c$), 3.50 – 3.42 (2H, m, $\boldsymbol{H}_i$), 3.38 – 3.11 (4H, m, $\boldsymbol{H}_J$, $\boldsymbol{H}_{J'}$), 2.57 – 2.10 (8H, m, $\boldsymbol{H}_D$, $\boldsymbol{H}_{D'}$, $\boldsymbol{H}_F$, $\boldsymbol{H}_{F'}$), 1.95 – 1.82 (2H, m, $\boldsymbol{H}_q$), 1.82 – 1.62 (4H, m, $\boldsymbol{H}_E$, $\boldsymbol{H}_{E'}$), 1.61 – 1.22 (23H, m, $\boldsymbol{H}_x$, $\boldsymbol{H}_{j\text{-}p}$). δ_C (101 MHz, $CDCl_3$) 167.1, 166.8, 162.6, 162.5, 158.9, 158.88, 156.7, 156.5, 156.4, 156.2, 154.4, 146.3, 146.0, 137.1, 136.9, 132.7, 132.6, 132.3, 131.8, 131.6, 131.3, 129.0, 128.9, 125.0, 122.0, 121.9, 120.8, 120.6, 119.3, 118.9, 118.6, 117.1, 115.0, 114.7, 113.8, 111.6, 68.1, 67.9, 67.82, 67.80, 52.25, 52.21, 50.8, 49.4, 49.1, 36.6, 34.6, 34.56, 31.8, 31.6, 30.8, 30.4, 29.7, 29.5, 29.4, 29.3, 29.24, 29.21, 29.1, 28.3, 26.7, 26.0. LR-ESI-MS (+ve) m/z = 1242.6 $[M+H]^+$.

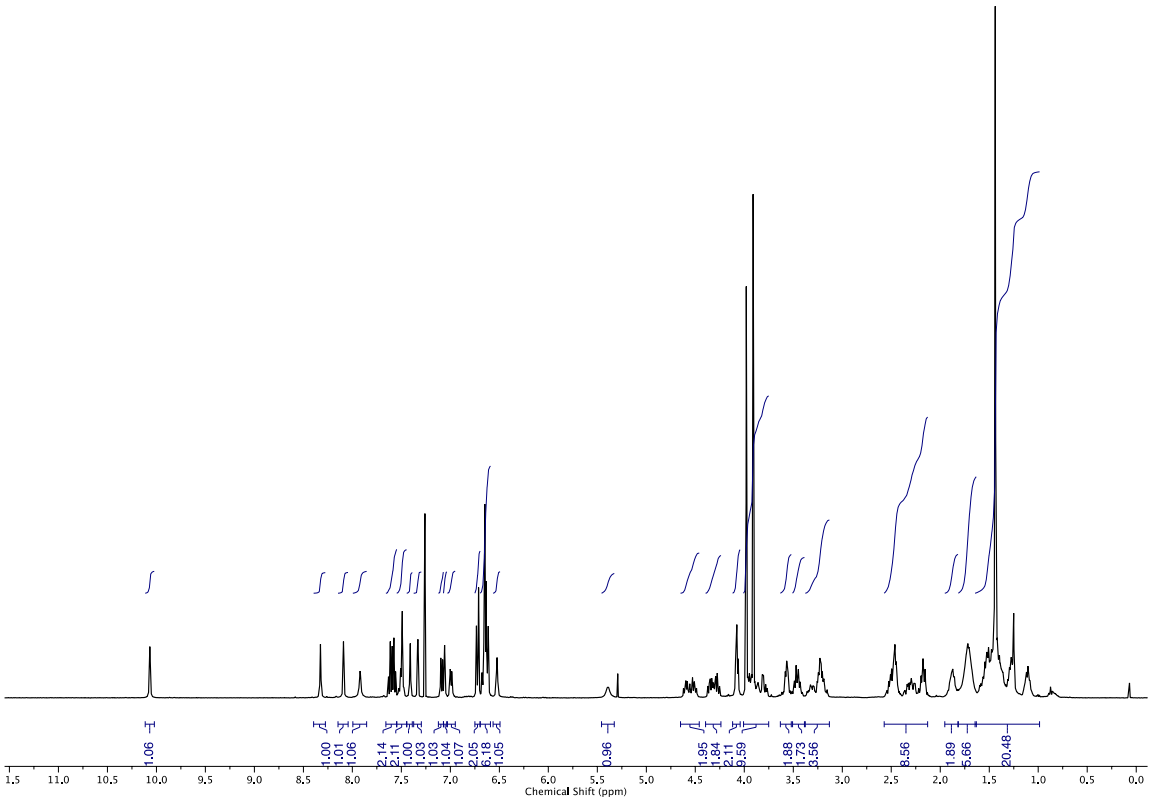

Figure 72: ^{1}H NMR ($CDCl_3$, 400 MHz) of ($R_{co\text{-}c}$)-**5**.

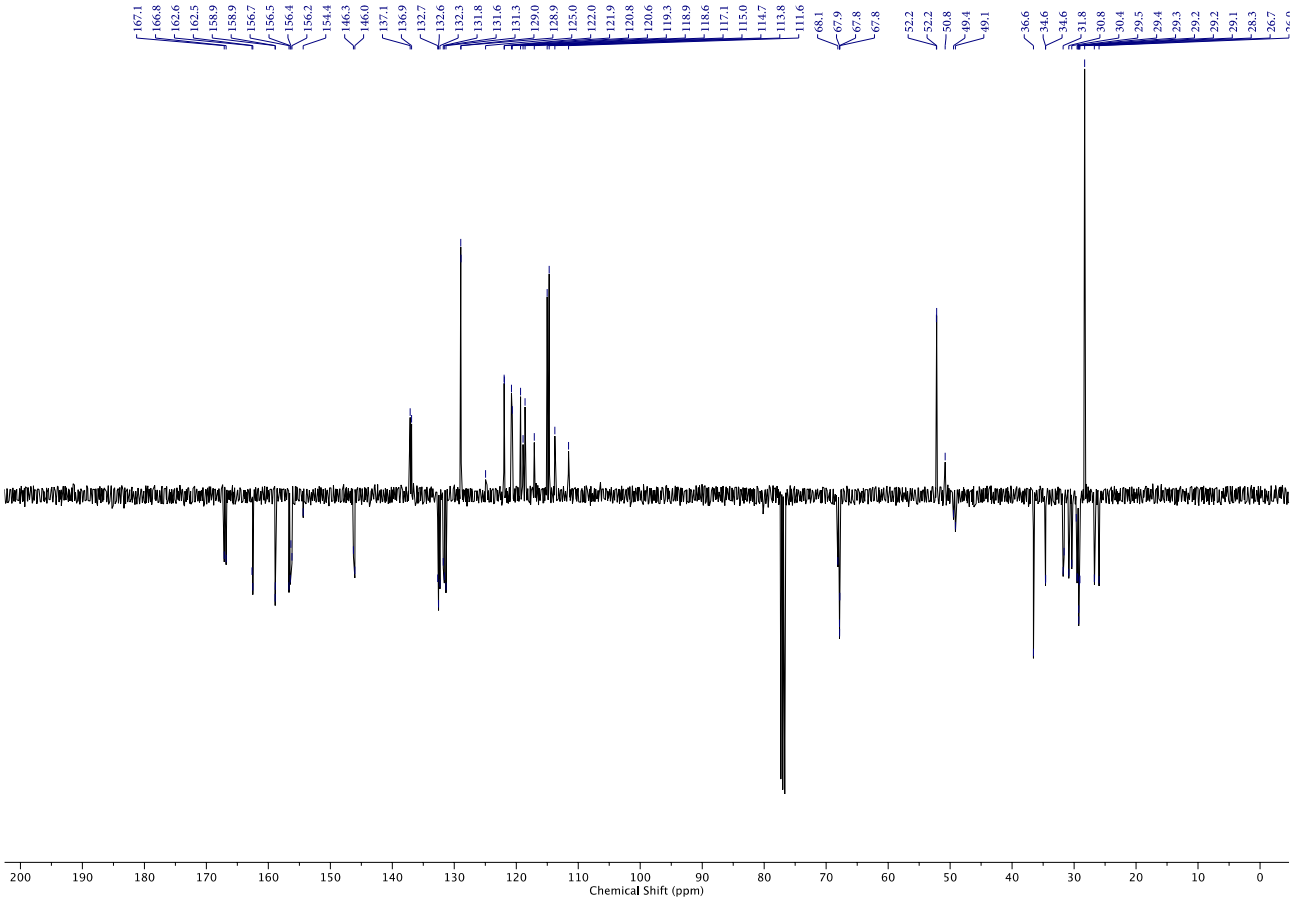

Figure 73: JMOD NMR ($CDCl_3$, 101 MHz) of ($R_{co\text{-}c}$)-**5**.

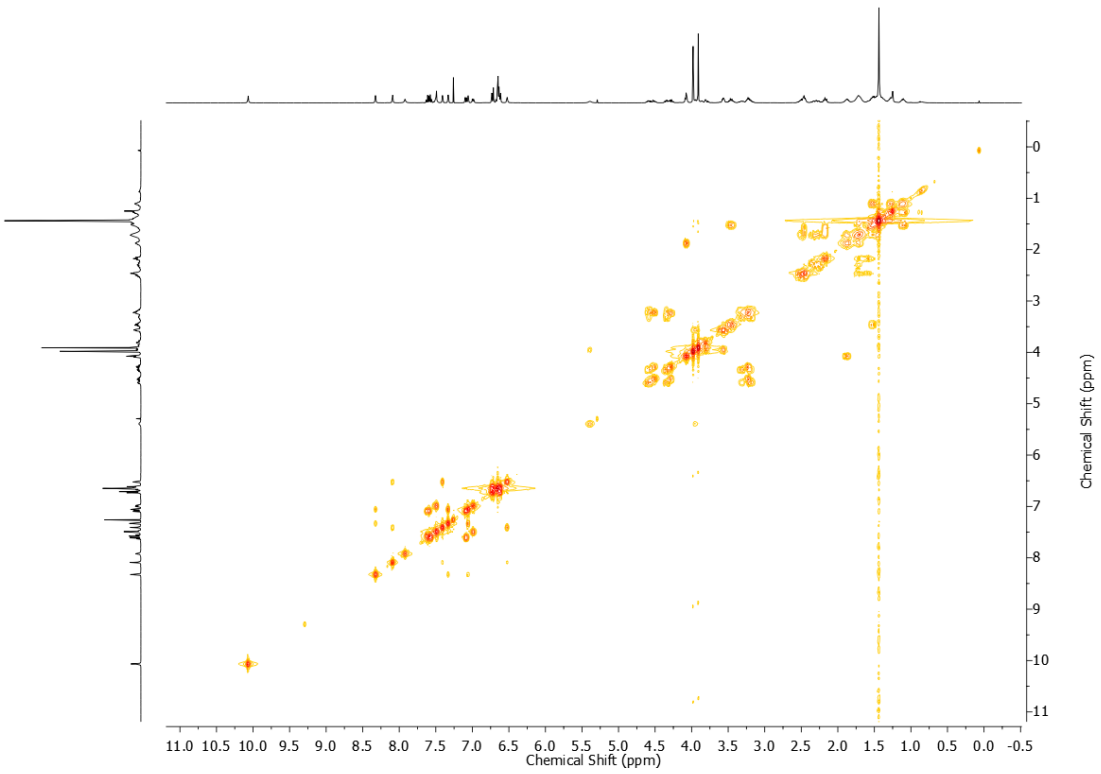

Figure 74: ^{1}H COSY NMR ($CDCl_3$, 400 MHz) of ($R_{co\text{-}c}$)-**5**.

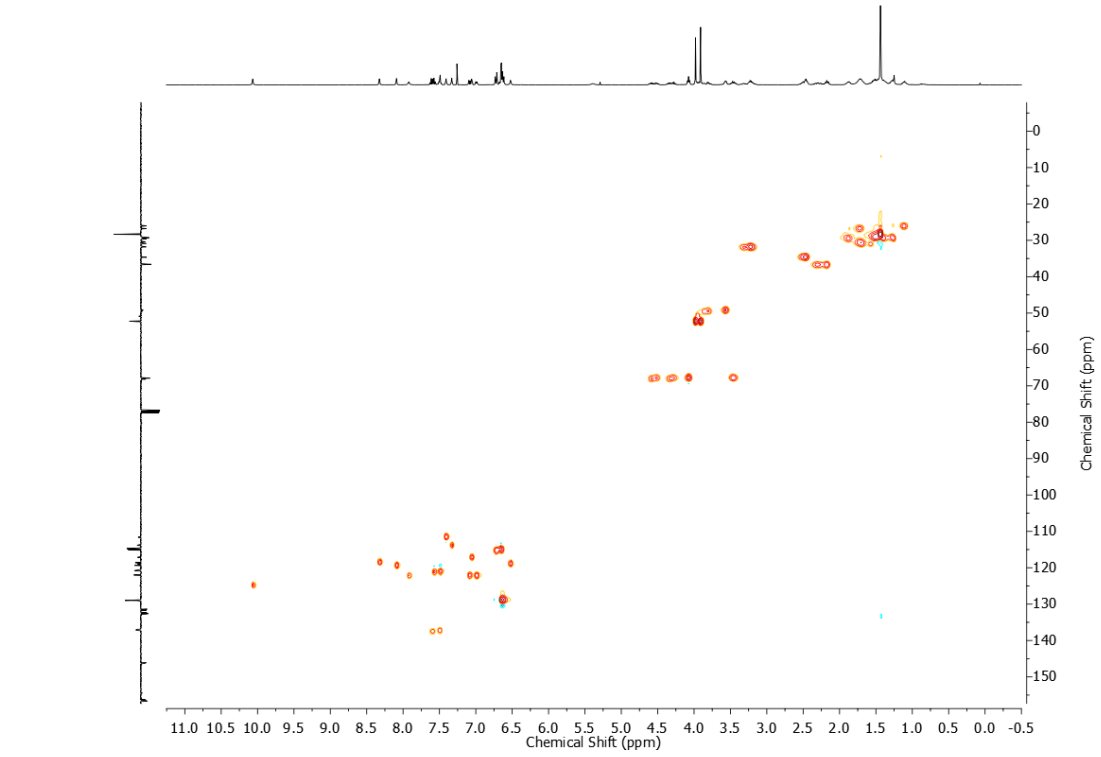

Figure 75: HSQC NMR ($CDCl_3$, 400 MHz) of ($R_{co\text{-}c}$)-**5**.

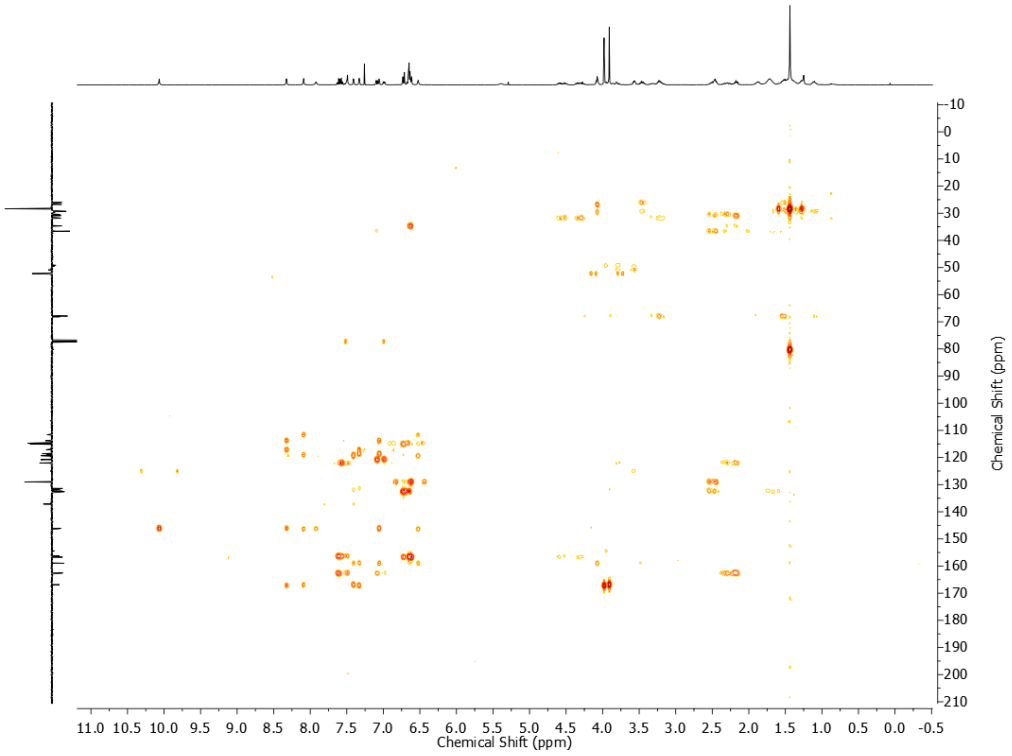

Figure 76: HMBC NMR ($CDCl_3$, 400 MHz) of ($R_{co\text{-}c}$)-**5**.

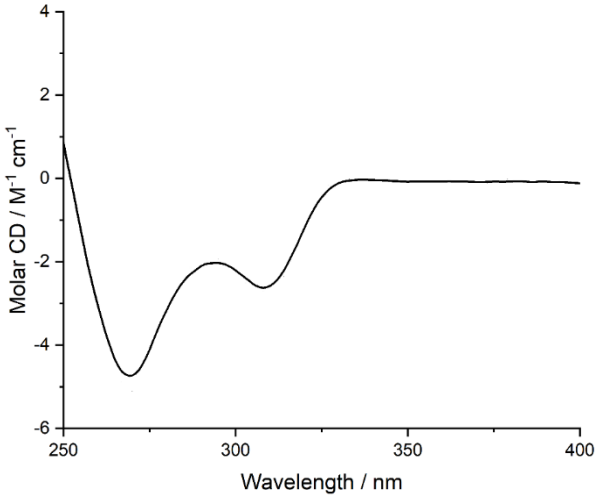

Figure 77: Circular Dichroism Spectrum of ($R_{co\text{-}c}$)-**5** (29 µM) at 293 K in $CHCl_3$.

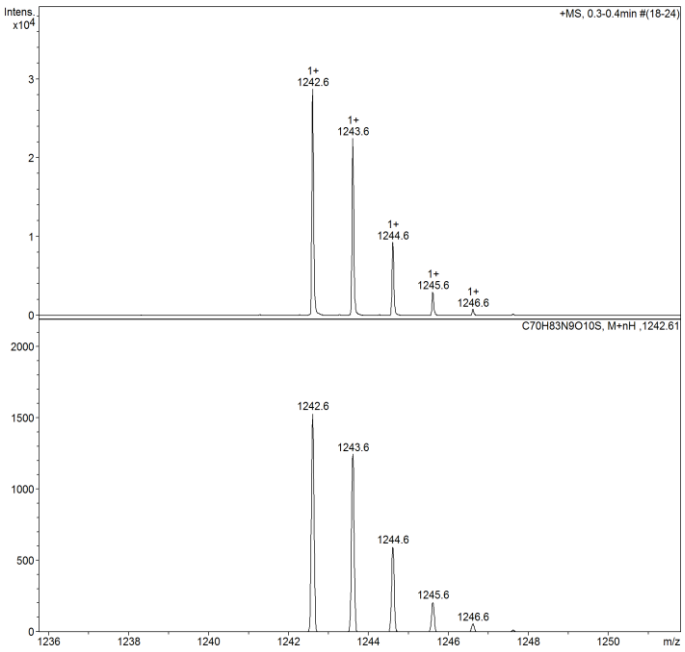

Figure 78: Observed (top) and calculated (bottom) isotopic patterns for ($R_{co\text{-}c}$)-**5**.

4.3. Catenane (R_{ma},$R_{co\text{-}c}$)-3

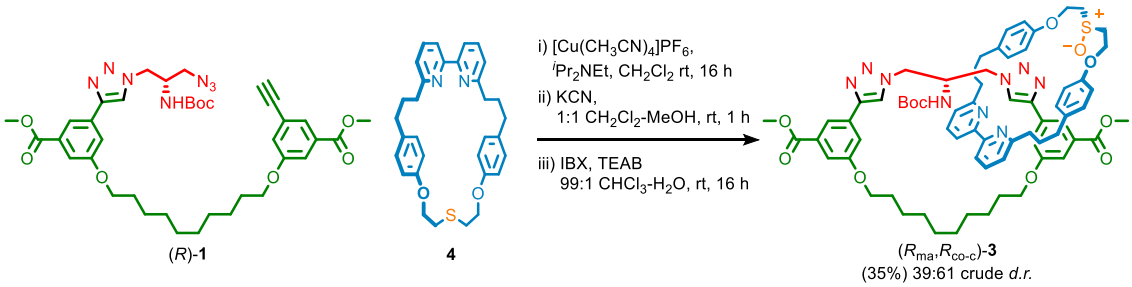

A CEM MW vial was charged with macrocycle **4** (27.3 mg, 0.053 mmol, 1.0 eq.) and $[Cu(CH_3CN)_4]PF_6$ (19.5 mg, 0.052 mmol, 0.98 eq.) and purged with N_2. CH_2Cl_2 (5.5 mL) and $^iPr_2NEt$ (19 µL, 0.11 mmol, 2.0 eq.) were added followed by a solution of pre-macrocycle (*R*)-**1** (43.0 mg, 0.059 mmol, 1.0 eq.) in CH_2Cl_2 (2.2 mL) at ambient temperature over 16 h. Then, MeOH (2.9 mL) and KCN as a solid (35 mg, 0.53 mmol, 10.0 eq.) were added and the resulting mixture was stirred vigorously for 1 h. The crude mixture was diluted with CH_2Cl_2 (5 mL) and washed with H_2O in two portions (10 mL and 5 mL), with separation of aqueous and organic phases. The combined aqueous phase was then extracted with CH_2Cl_2 (3 x 5 mL) and the combined organics were washed with brine (10 mL), dried over $MgSO_4$ and concentrated *in vacuo*. The residue corresponding to ($R_{co\text{-}c}$)-**5** was re-dissolved in 99:1 $CHCl_3/H_2O$ (0.67 µL), then tetraethylammonium bromide (12.3 mg, 0.058 mmol, 1.1 eq.) and IBX (30% of stabilizer, 23.3 mg, 0.058 mmol, 1.1 eq.) were added. The resulting suspension was stirred for 16 h at ambient temperature. The reaction mixture was then diluted with CH_2Cl_2 (5 mL), washed with 10% $NaHSO_3$ (5 mL), saturated $NaHCO_3$ (5 mL) and brine (5 mL), extracting all aqueous layers with CH_2Cl_2 (2 x 5 mL). The combined organics were dried over $MgSO_4$, filtered, and concentrated *in vacuo*. The residue was purified by column chromatography (SiO_2, CH_2Cl_2-CH_3CN 0→100%; CH_3CN-MeOH 0→5%) to yield (R_{ma},$R_{co\text{-}c}$)-**3** (23.0 mg, 0.0186 mmol, 35%, second eluting isomer) as an off-white foam and (S_{ma},$R_{co\text{-}c}$)-**3** (16.0 mg, 0.013 mmol, 24%, first eluting isomer) as a colorless oil.

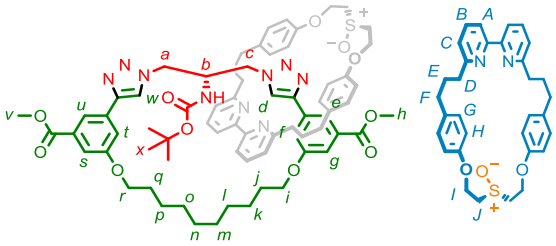

δ_H (400 MHz, $CDCl_3$) 9.96 (1H, s, $\boldsymbol{H}_d$), 8.06 (2H, s, $\boldsymbol{H}_e$, $\boldsymbol{H}_u$), 7.67 – 7.38 (6H, m, $\boldsymbol{H}_{A/A'}$, $\boldsymbol{H}_{B/B'}$, $\boldsymbol{H}_w$, $\boldsymbol{H}_s$), 7.34 (1H, dd, J = 2.4, 1.5, $\boldsymbol{H}_g$), 7.16 – 7.06 (2H, m, $\boldsymbol{H}_{C/C'}$, $\boldsymbol{H}_f$), 6.98 (1H, d, J = 7.6, $\boldsymbol{H}_{C/C'}$), 6.79 – 6.45 (9H, m, $\boldsymbol{H}_{G/G'}$, $\boldsymbol{H}_{H/H'}$, $\boldsymbol{H}_t$), 5.45 (1H, d, J = 3.9, -N*H*Boc), 4.76 – 4.49 (4H, m, $\boldsymbol{H}_{I/I'}$), 4.30 (1H, m, $\boldsymbol{H}_c$), 4.13 (2H, t, J = 5.4, $\boldsymbol{H}_r$), 4.03 (3H, s, $\boldsymbol{H}_h$), 3.99 – 3.65 (9H, m, $\boldsymbol{H}_v$, $\boldsymbol{H}_{J/J'}$, $\boldsymbol{H}_a$, $\boldsymbol{H}_b$, $\boldsymbol{H}_{c'}$), 3.53 – 3.25 (4H, m, $\boldsymbol{H}_i$, $\boldsymbol{H}_{J/J'}$), 2.52 – 2.10 (12H, m, $\boldsymbol{H}_D$, $\boldsymbol{H}_E$, $\boldsymbol{H}_F$, $\boldsymbol{H}_{D'}$, $\boldsymbol{H}_{E'}$, $\boldsymbol{H}_{F'}$), 1.97 – 1.81 (2H, m, $\boldsymbol{H}_q$), 1.58 – 1.13 (23H, m, $\boldsymbol{H}_{j\text{-}p}$, $\boldsymbol{H}_x$). δ_C (101 MHz, $CDCl_3$) 167.3, 167.0, 163.0, 162.7, 159.1, 159.0, 156.5, 156.2, 155.9, 155.9, 146.6, 146.3, 138.0, 137.3, 137.0, 133.3, 133.0, 132.5, 132.0, 131.8, 131.4, 122.3, 122.1, 120.6, 119.4, 119.1, 118.9, 116.7, 115.1, 115.1, 114.7, 111.9, 80.6, 77.5, 77.2, 76.8, 68.2, 67.8, 61.2, 61.1, 52.4, 52.0, 49.3, 36.9, 36.8, 34.8, 34.7, 30.9, 30.8, 29.8, 29.8, 29.5, 29.4, 29.2, 28.5, 26.8, 26.1. LR-ESI-MS (+ve) = 1258.6 $[M+H]^+$.

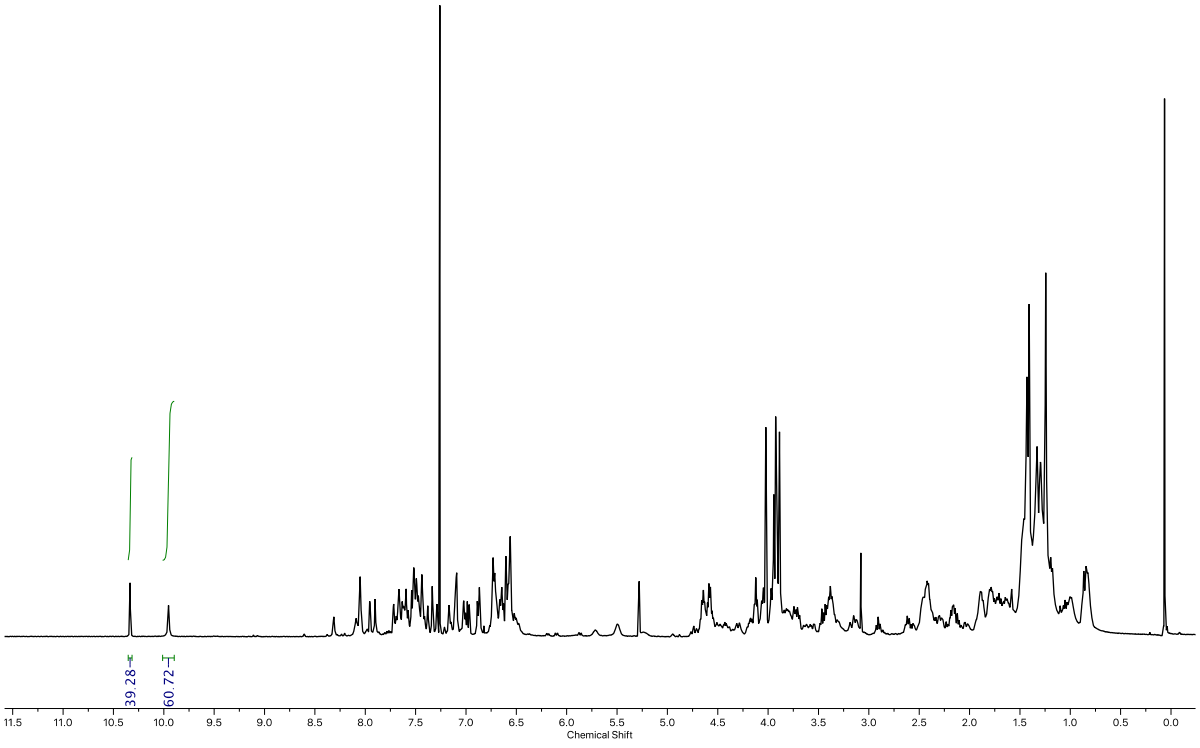

Figure 79: ^{1}H NMR ($CDCl_3$, 400 MHz) of crude oxidation leading to major (R_{ma},$R_{co\text{-}c}$)-**3**. Integration of (S_{ma},$R_{co\text{-}c}$)-**3** (10.34 ppm, $\boldsymbol{H}_d$, 39.28H) and (R_{ma},$R_{co\text{-}c}$)-**3** (9.95 ppm, $\boldsymbol{H}_d$, 60.72H).

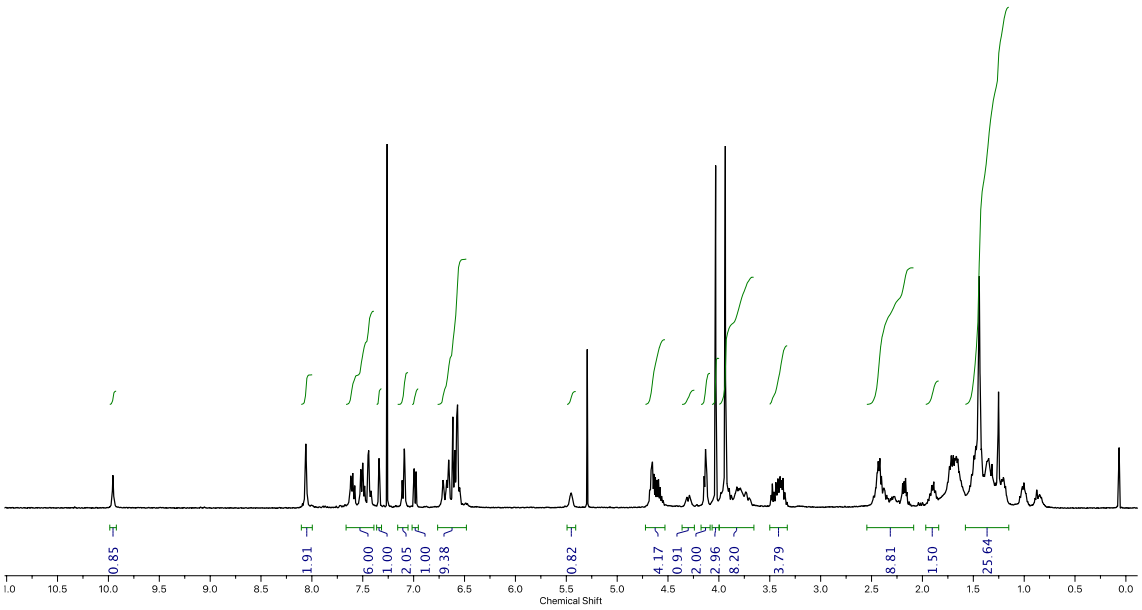

Figure 80: ^{1}H NMR ($CDCl_3$, 400 MHz) of (R_{ma},$R_{co\text{-}c}$)-**3**.

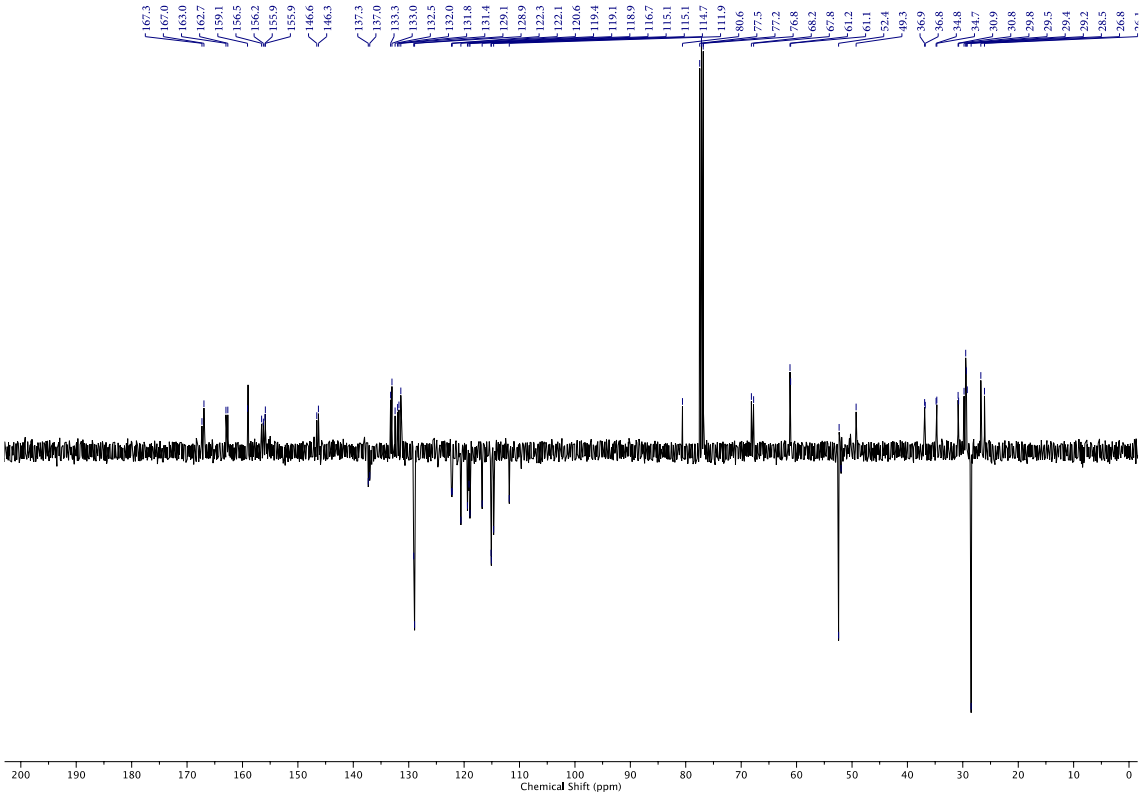

Figure 81: JMOD NMR ($CDCl_3$, 101 MHz) of (R_{ma},$R_{co\text{-}c}$)-**3**.

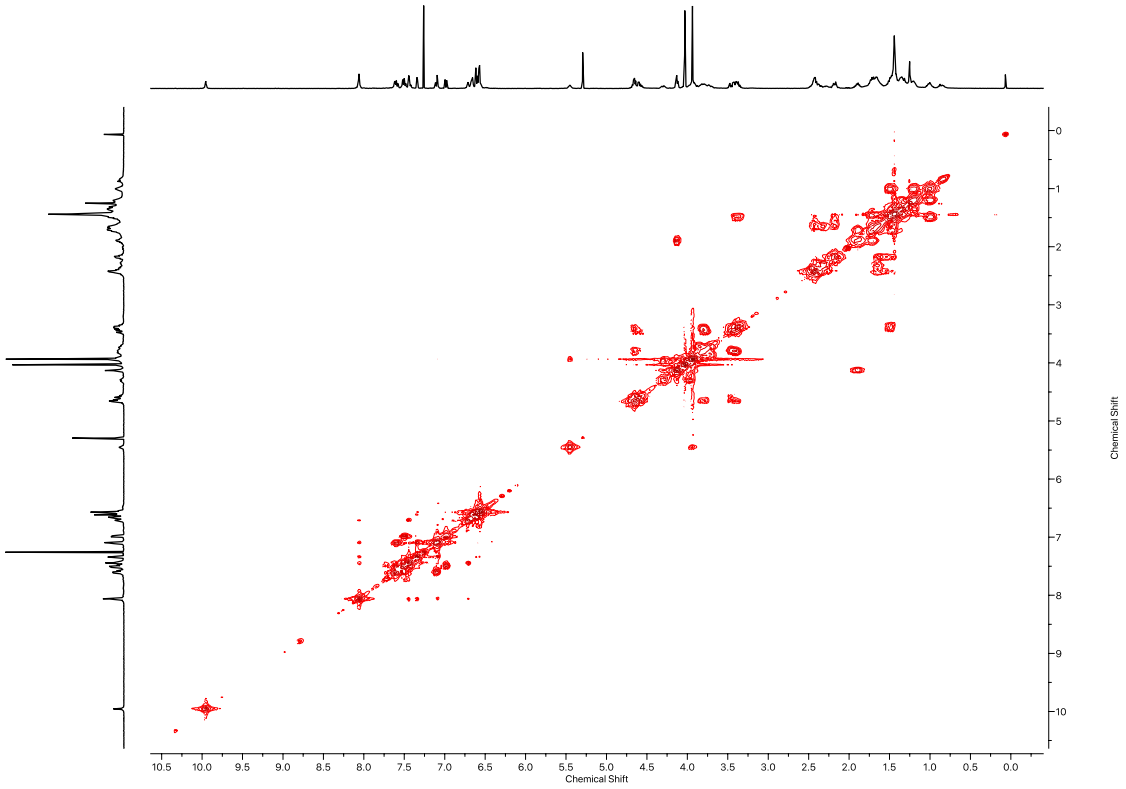

Figure 82: ^{1}H COSY NMR ($CDCl_3$, 400 MHz) of (R_{ma},$R_{co\text{-}c}$)-**3**.

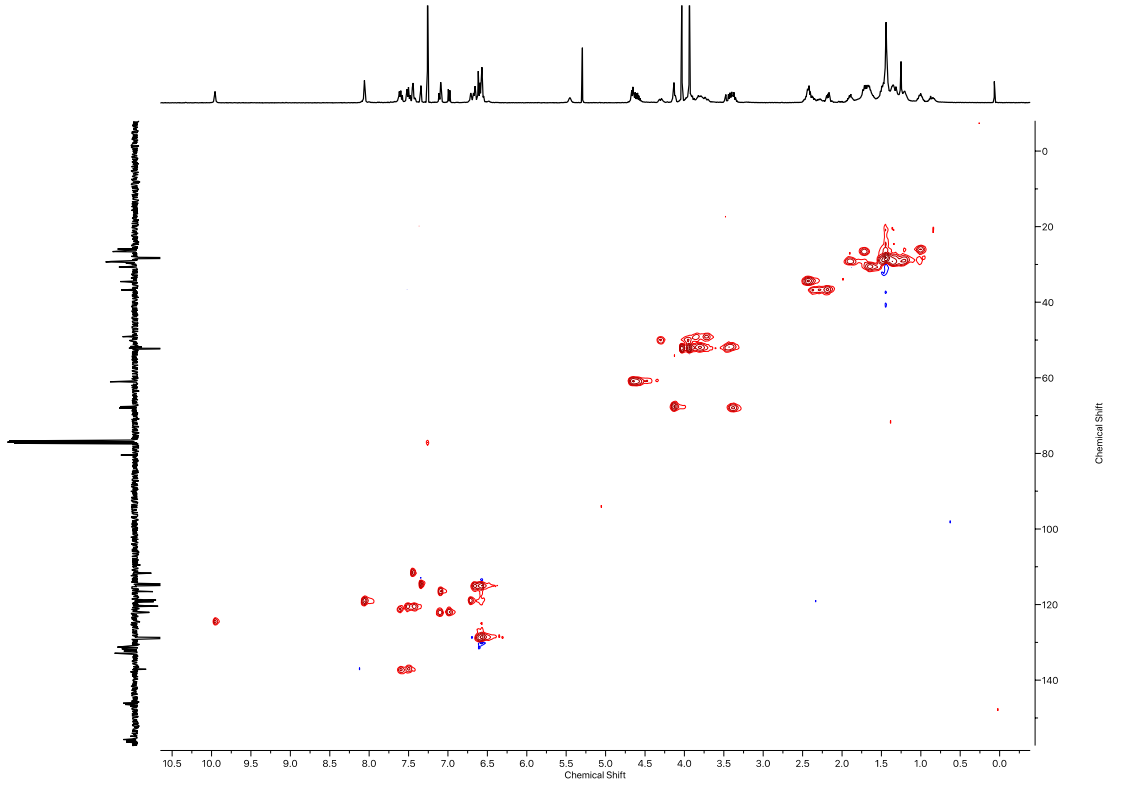

Figure 83: HSQC NMR ($CDCl_3$, 400 MHz) of (R_{ma},$R_{co\text{-}c}$)-**3**.

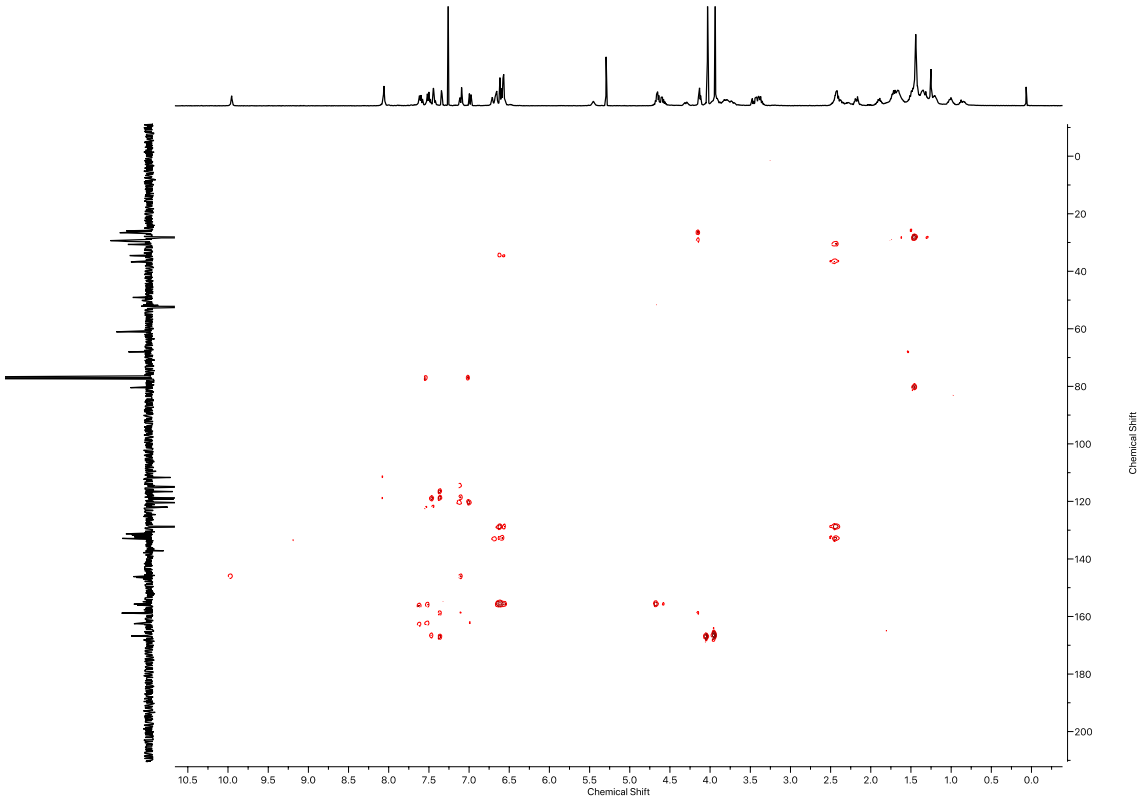

Figure 84: HMBC NMR ($CDCl_3$, 400 MHz) of (R_{ma},$R_{co\text{-}c}$)-**3**.

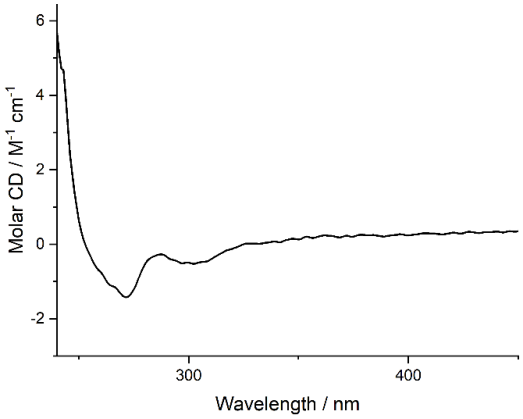

Figure 85: Circular Dichroism Spectra of (R_{ma},$R_{co\text{-}c}$)-**3** (31 µM) at 293 K in $CHCl_3$.

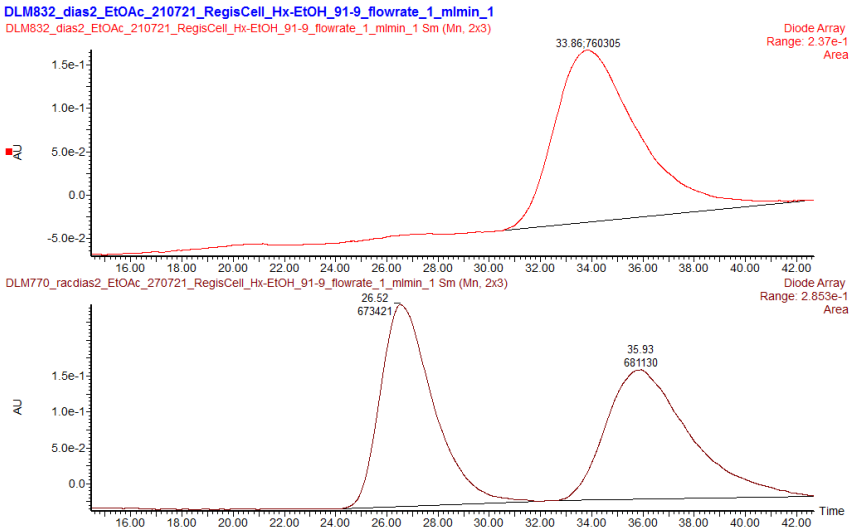

Figure 86: CSP-HPLC of (R_{ma},$R_{co\text{-}c}$)-**3** (loaded in EtOAc). RegisCell, *n*-hexane-EtOH 91 : 9, flowrate 1 mLmin^{-1}. (top) (R_{ma},$R_{co\text{-}c}$)-**3** (33.86 min, 760305, >99.9%), (S_{ma},$S_{co\text{-}c}$)-**3** (not observed). (bottom) *rac*-**3**, (S_{ma},$S_{co\text{-}c}$)-**3** (26.52 min, 673421, 49.7%), (R_{ma},$R_{co\text{-}c}$)-**3** (35.93 min, 681130, 50.3%).

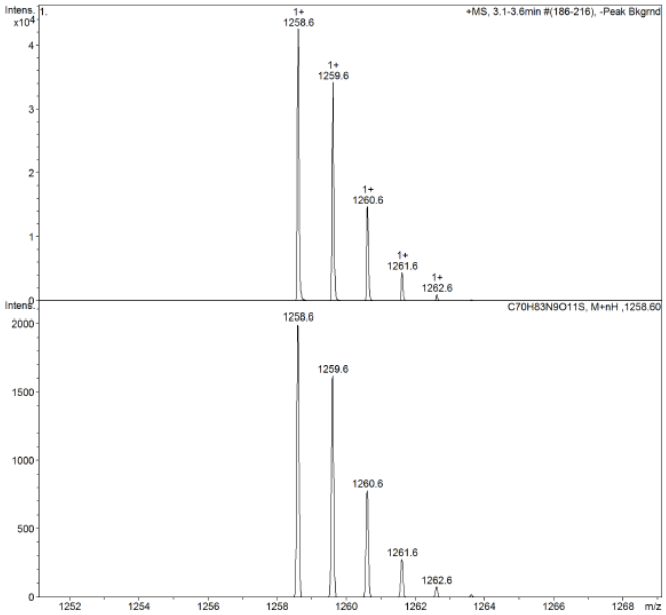

Figure 87: Observed (top) and calculated (bottom) isotopic patterns for (R_{ma},$R_{co\text{-}c}$)-**3**.

4.4. Macrocycle S13

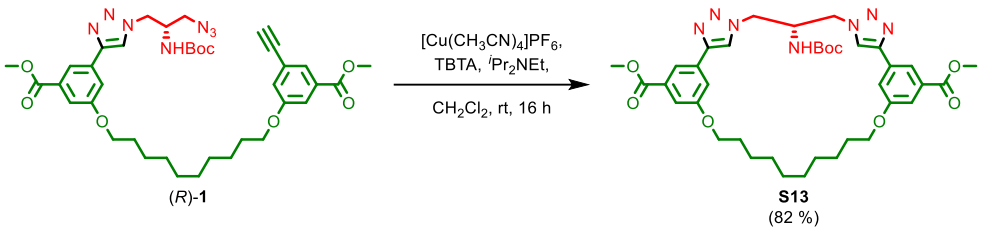

(*R*)-**1** **S13** (82 %)

A CEM MW vial was charged with TBTA (3.60 mg, 0.007 mmol, 0.2 eq.), $[Cu(CH_3CN)_4]PF_6$ (2.5 mg, 0.007 mmol, 0.2 eq.), $^{i}Pr_2NEt$ (12 µL, 0.068 mmol, 2.0 eq.), and CH_2Cl_2 (0.5 mL) and was purged with N_2. A solution of pre-macrocycle (*R*)-**1** (25 mg, 0.034 mmol, 1.0 eq.) in CH_2Cl_2 (0.2 mL) was added at ambient temperature over 16 h, and then stirred at ambient temperature for 1 h. The crude mixture was diluted with CH_2Cl_2 (5 mL) and washed with EDTA-NH_3 solution (2 x 10 mL), and the combined organics were washed with brine (10 mL), dried over $MgSO_4$ and concentrated *in vacuo*. The residue was purified by column chromatography (SiO_2, petrol-EtOAc 0→50) to yield macrocycle **S13** (20.3 mg, 0.0277 mmol, 82%) as a white foam.

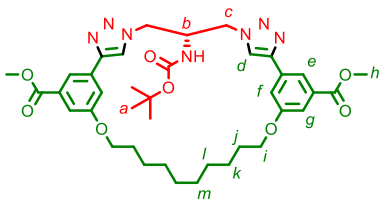

δ_H ($CDCl_3$, 400 MHz) 8.09 (2H, dd, *J* = 1.3, $\boldsymbol{H}_e$), 7.96 (2H, s, $\boldsymbol{H}_d$), 7.52 (2H, m, $\boldsymbol{H}_g$), 7.49 (2H, m, $\boldsymbol{H}_f$), 5.9 (1H, d, $\boldsymbol{H}_{NHBoc}$), 4.55 (3H, m, $\boldsymbol{H}_c$, $\boldsymbol{H}_b$), 4.45 (2H, dd, *J* = 16, 8, $\boldsymbol{H}_{c'}$), 4.06 (2H, m, $\boldsymbol{H}_i$), 3.93 (3H, s, $\boldsymbol{H}_h$), 1.81 (4H, quint, *J* = 8.0, $\boldsymbol{H}_j$), 1.48 (13H, m, $\boldsymbol{H}_a$, $\boldsymbol{H}_k$), 1.37 (8H, m, $\boldsymbol{H}_l$, $\boldsymbol{H}_m$); δ_C ($CDCl_3$, 101 MHz) 166.6, 159.5, 147.1, 132.2, 131.3,

121.9, 118.9, 116.5, 115.5, 68.5, 52.3, 50.8, 50.1, 29.1, 28.9, 28.3, 25.9. LR-ESI-MS (+ve) $[M+H]^+$ m/z (%) 732.7 (100); HR-EI-MS (+ve) $[M+Na]^+$ m/z 754.3534 (calc. for $C_{38}H_{49}N_7O_8Na$ m/z 754.3535).

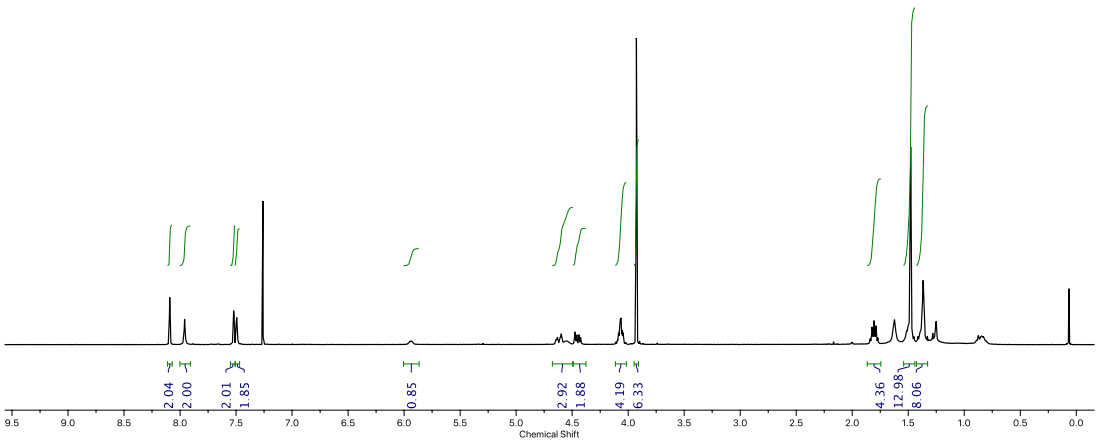

Figure 88: ^1H NMR ($CDCl_3$, 400 MHz) of **S13**.

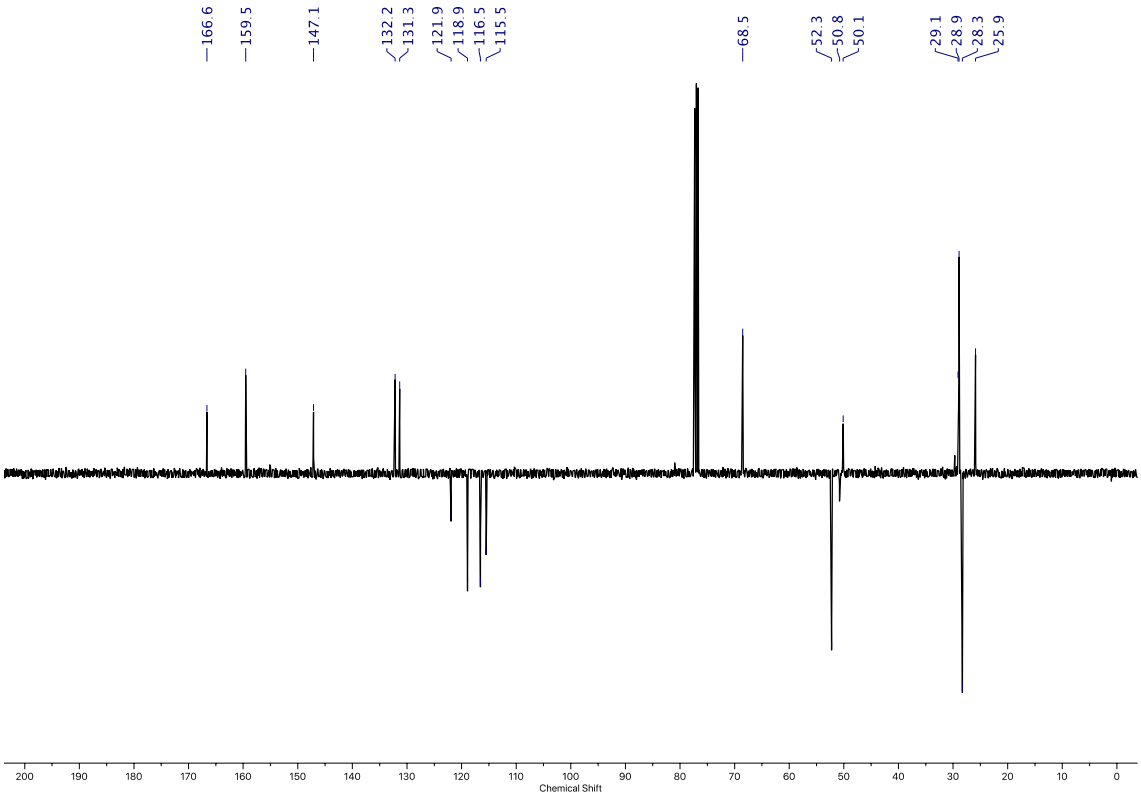

Figure 89: JMOD NMR ($CDCl_3$, 101 MHz) of **S13**.

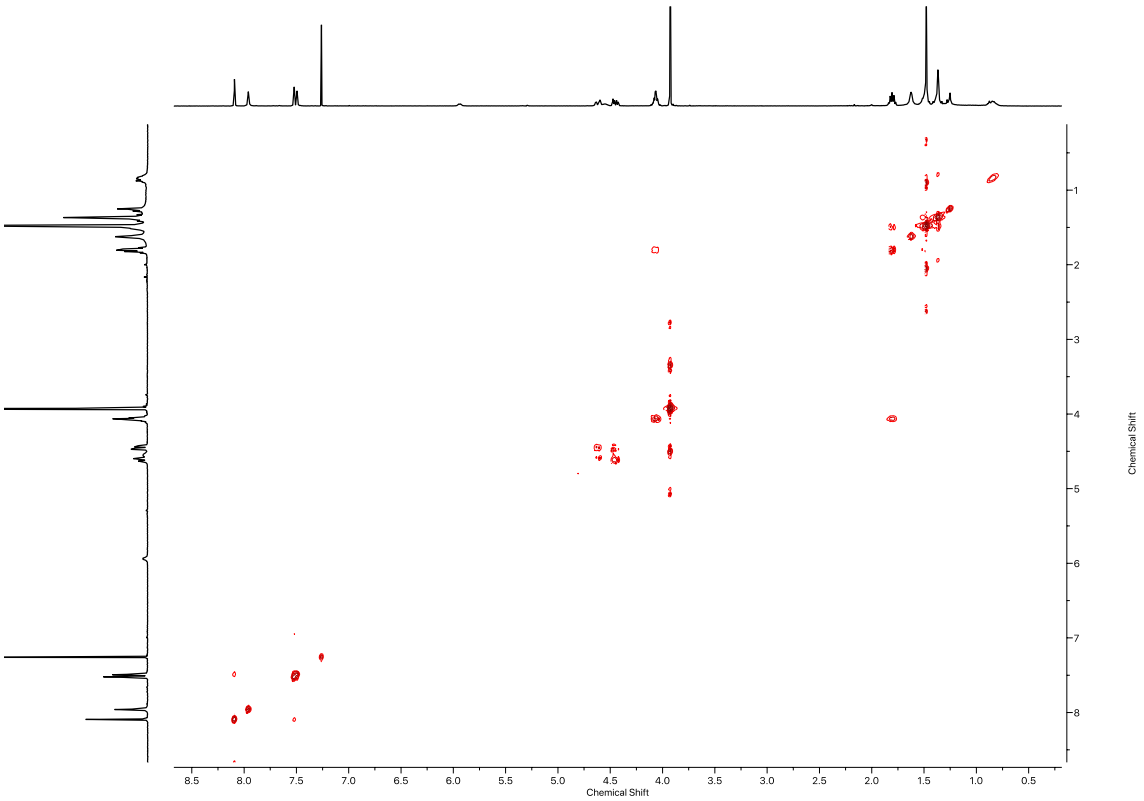

Figure 90: ^{1}H COSY NMR ($CDCl_3$, 400 MHz) of **S13**.

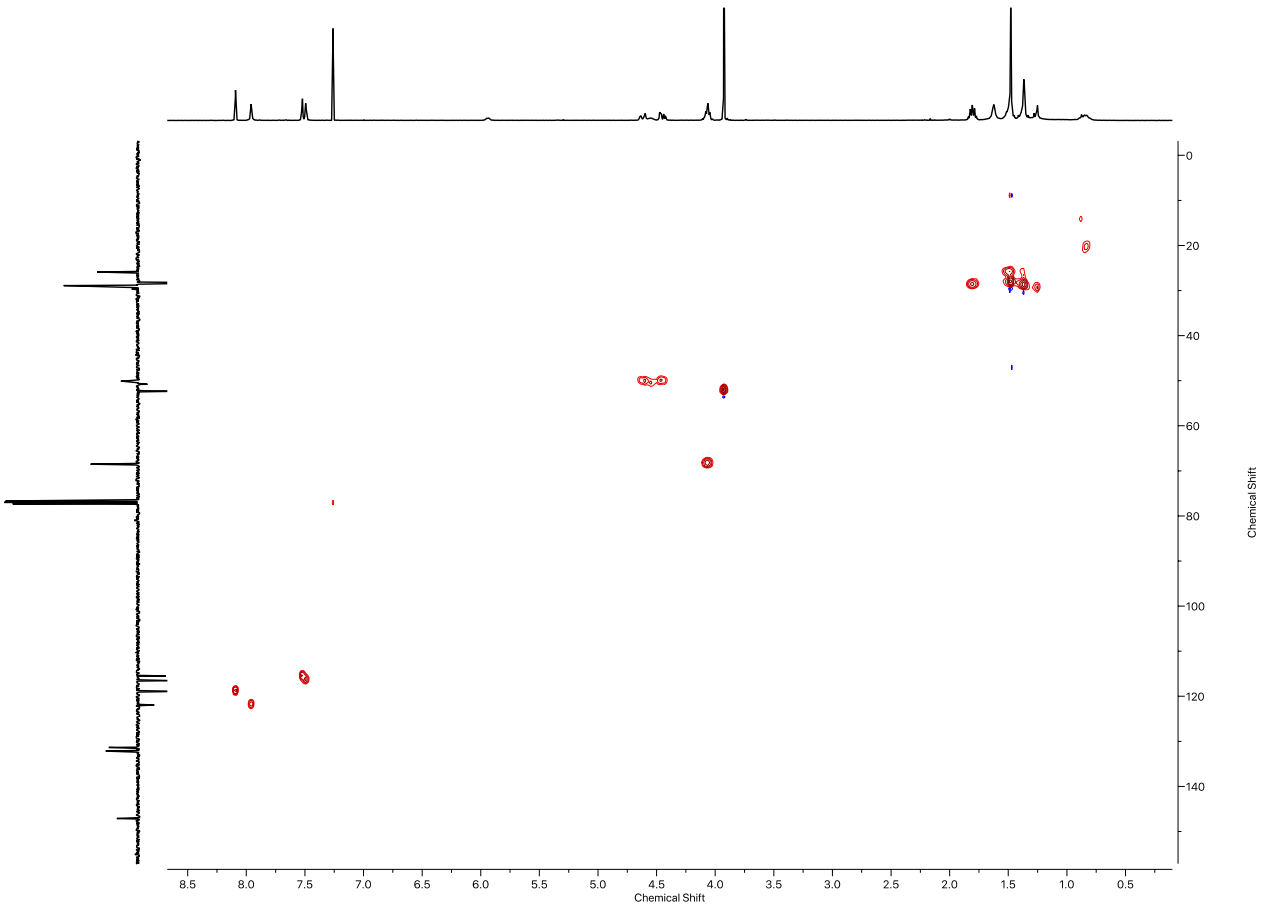

Figure 91: HSQC NMR ($CDCl_3$, 400 MHz) of **S13**.

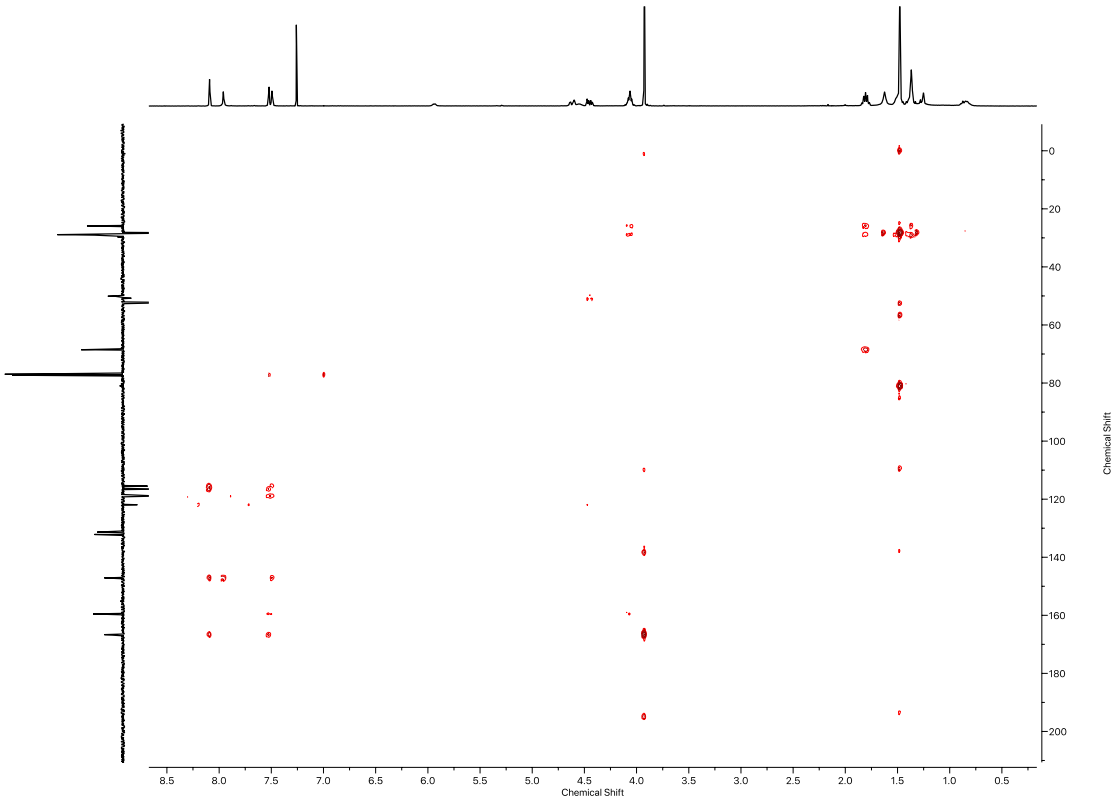

Figure 92: HMBC NMR ($CDCl_3$, 400 MHz) of **S13**.

5. Synthesis of enantiomeric catenanes (S_{ma})-6 and (R_{ma})-6

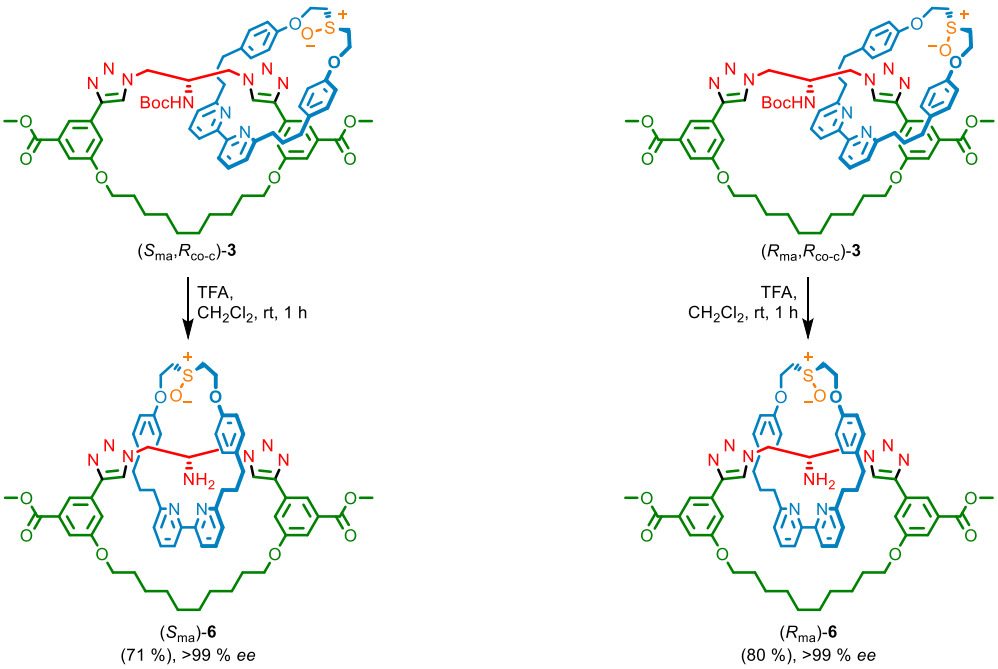

Scheme 4: Synthetic route to mechanically axially chiral enantiomeric catenanes (R_{ma})-**6** and (S_{ma})-**6**.

5.1. Catenane (S_{ma})-6

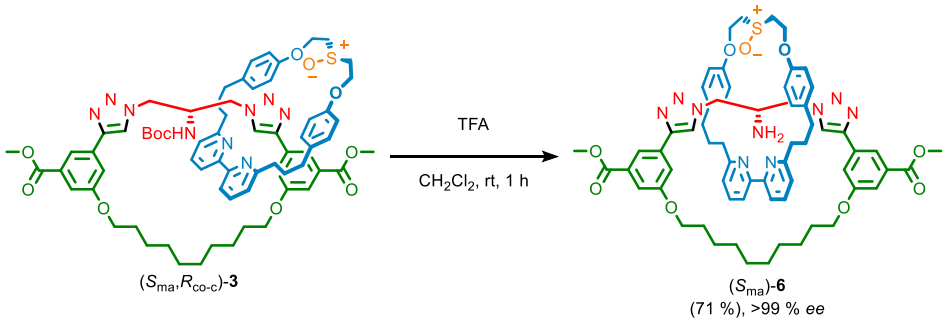

A solution of catenane (S_{ma},$R_{co\text{-}c}$)-**3** (35.7 mg, 0.028 mmol, 1.0 eq.) in CH_2Cl_2 (0.3 mL) was added TFA (65 µL, 0.85 mmol, 30 eq.) dropwise at 0 ºC, then stirred at ambient temperature for 1 h. The reaction mixture was then diluted with CH_2Cl_2 (5 mL) and poured into saturated $NaHCO_3$ (5 mL). The aqueous phase was extracted with CH_2Cl_2 (3 x 6 mL) and combined organics were washed with brine (5 mL), dried over $MgSO_4$, filtered and concentrated *in vacuo.* The residue was purified by column chromatography (SiO_2, CH_2Cl_2-MeOH 0→15%) to yield catenane (S_{ma})-**6** (23.4 mg, 0.020 mmol, 71%) as a white foam. The mechanical stereochemistry of the product was assigned by observing that this cannot change during the removal of the Boc group (or if it does, that the resulting product would be racemic, which was not observed).

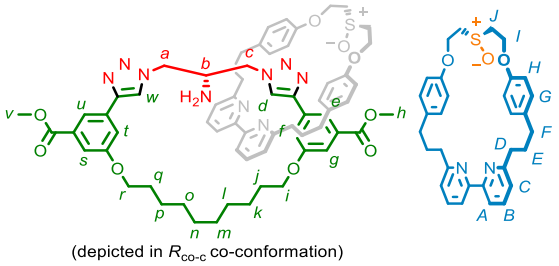

δ_H ($CDCl_3$, 400 MHz) 9.03 (s, 1H, $\boldsymbol{H}_d$), 8.31 (t, J = 1.4, 1H, $\boldsymbol{H}_e$), 8.18 (t, J = 1.4, 1H, $\boldsymbol{H}_u$), 7.97 (s, 1H, $\boldsymbol{H}_w$), 7.67 (t, J = 7.8, 1H, $\boldsymbol{H}_B$), 7.56 (dd, J = 7.8, 1.0, 1H, $\boldsymbol{H}_A$), 7.49 (t, J = 7.7, 1H, $\boldsymbol{H}_{B'}$), 7.43 (dd, J = 2.6, 1.4, 1H, $\boldsymbol{H}_s$), 7.40 – 7.36 (m, 2H, $\boldsymbol{H}_{A'}$, $\boldsymbol{H}_g$), 7.15 (dd, J = 7.7, 1.0, 1H, $\boldsymbol{H}_C$), 6.98 (dd, J = 7.7, 1.0, 1H, $\boldsymbol{H}_C$), 6.94 (dd, J = 2.6, 1.5, 1H, $\boldsymbol{H}_f$), 6.87 – 6.78 (m, 5H, $\boldsymbol{H}_G$, $\boldsymbol{H}_{G'}$, $\boldsymbol{H}_t$), 6.66 (dd, 4H, $\boldsymbol{H}_H$, $\boldsymbol{H}_{H'}$), 4.77 – 4.48 (m, 4H, $\boldsymbol{H}_I$), 3.96 – 3.88 (m, 8H, $\boldsymbol{H}_h$, $\boldsymbol{H}_r$, $\boldsymbol{H}_v$, $\boldsymbol{H}_a$), 3.80-3.64 (m, 3H, $\boldsymbol{H}_J$, $\boldsymbol{H}_a$), 3.55 (t, J = 6.5, 2H, $\boldsymbol{H}_i$), 3.46 (dd, J = 13.9, 4.7, 1H, $\boldsymbol{H}_c$), 3.30 (dd, J = 13.9, 8.3, 1H, $\boldsymbol{H}_c$), 3.25 – 3.15 (m, 2H, $\boldsymbol{H}_J$), 3.08 (m, 1H, $\boldsymbol{H}_b$), 2.59 – 2.39 (m, 4H, $\boldsymbol{H}_F$, $\boldsymbol{H}_{F'}$), 2.37 – 2.29 (m, 2H, $\boldsymbol{H}_D$), 2.22 (td, J = 13.3, 4.6, 1H, $\boldsymbol{H}_D$), 2.11 (td, J = 13.3, 5.0, 1H, $\boldsymbol{H}_D$), 1.84 – 1.47 (m, 8H, $\boldsymbol{H}_E$, $\boldsymbol{H}_{E'}$, $\boldsymbol{H}_j$, $\boldsymbol{H}_q$), 1.43 – 1.11 (m, 12H, $\boldsymbol{H}_k$, $\boldsymbol{H}_l$, $\boldsymbol{H}_m$, $\boldsymbol{H}_n$, $\boldsymbol{H}_o$, $\boldsymbol{H}_p$); δ_C ($CDCl_3$, 101 MHz) 167.1, 162.9, 162.8, 159.3, 159.2, 157.4, 156.7, 156.3, 156.3, 146.6, 146.6, 137.8, 137.1, 133.7, 133.4, 132.6, 132.3, 132.1, 132.0, 129.9, 129.6, 123.0, 122.6, 122.2, 121.4, 121.0, 120.8, 119.2, 118.4, 118.1, 116.7, 115.0, 114.9, 114.4, 112.8, 68.1, 68.0, 61.0, 60.5, 54.0, 53.9, 53.2, 53.0, 52.4, 52.4, 51.9, 37.1, 36.7, 35.0, 34.8, 31.9, 31.2, 29.8, 29.7, 29.6, 29.5, 29.5, 29.4, 26.7, 26.3; LR-ESI-MS (+ve) = 1158.6 $[M+H]^+$.

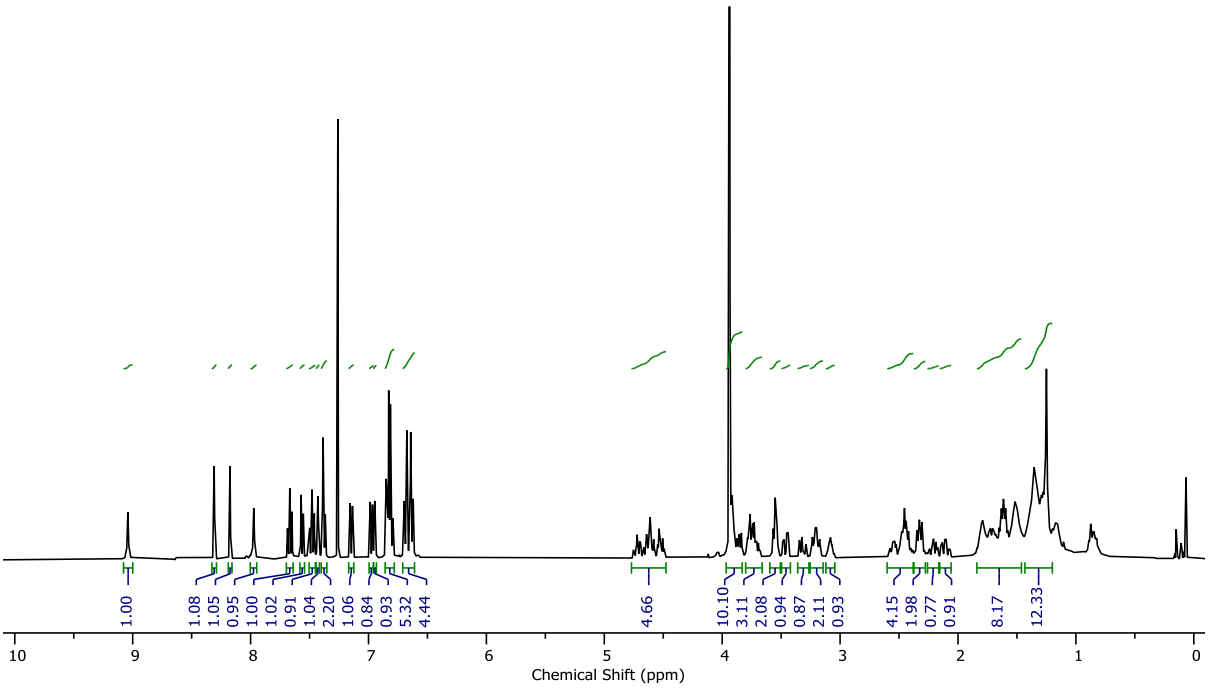

Figure 93: ^{1}H NMR ($CDCl_3$, 400 MHz) of (S_{ma})-**6**.

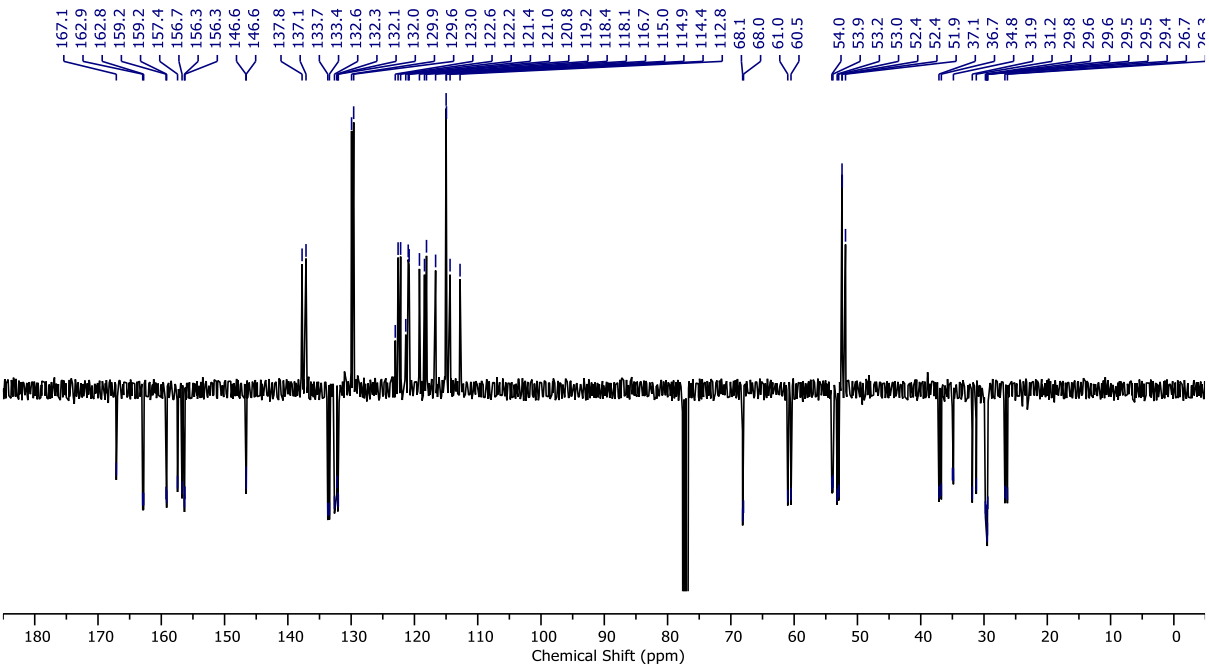

Figure 94: JMOD NMR ($CDCl_3$, 101 MHz) of (S_{ma})-**6**.

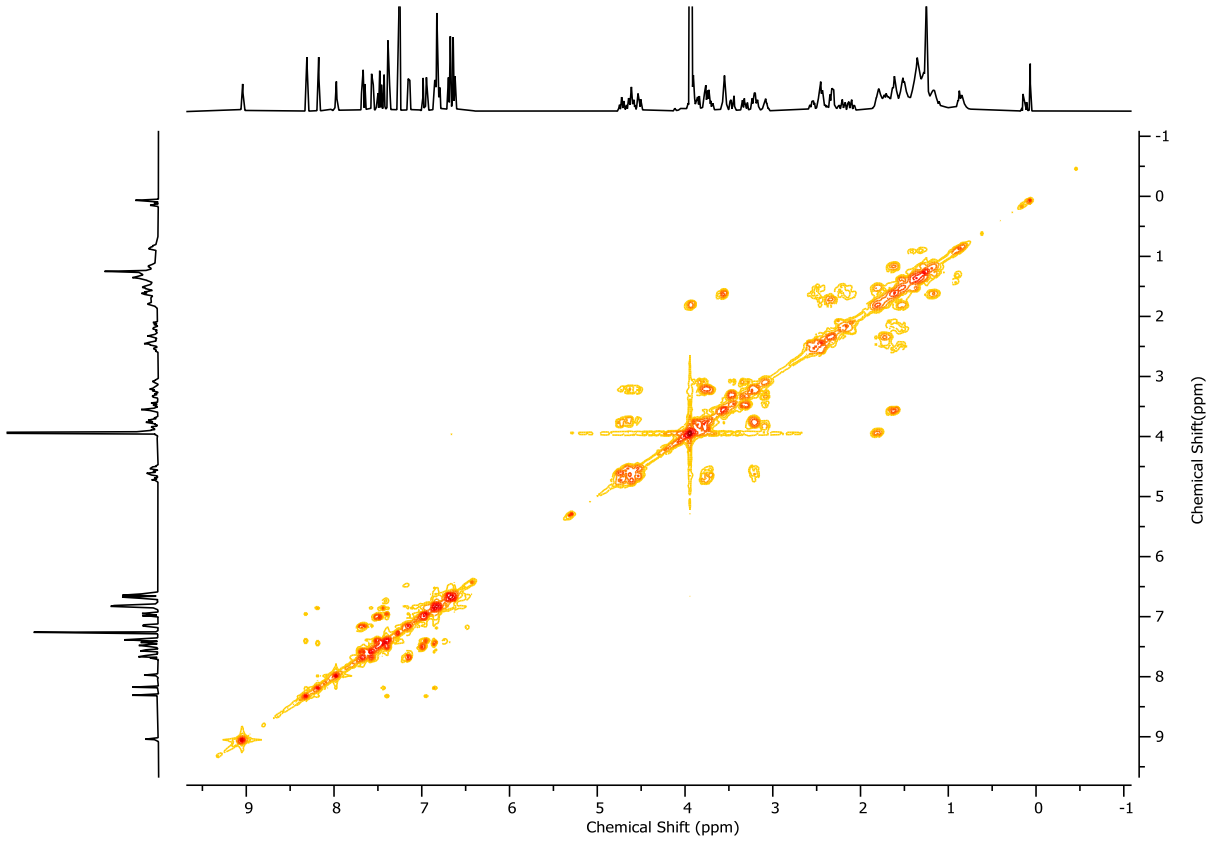

Figure 95: ^{1}H COSY NMR ($CDCl_3$, 400 MHz) of (S_{ma})-**6**.

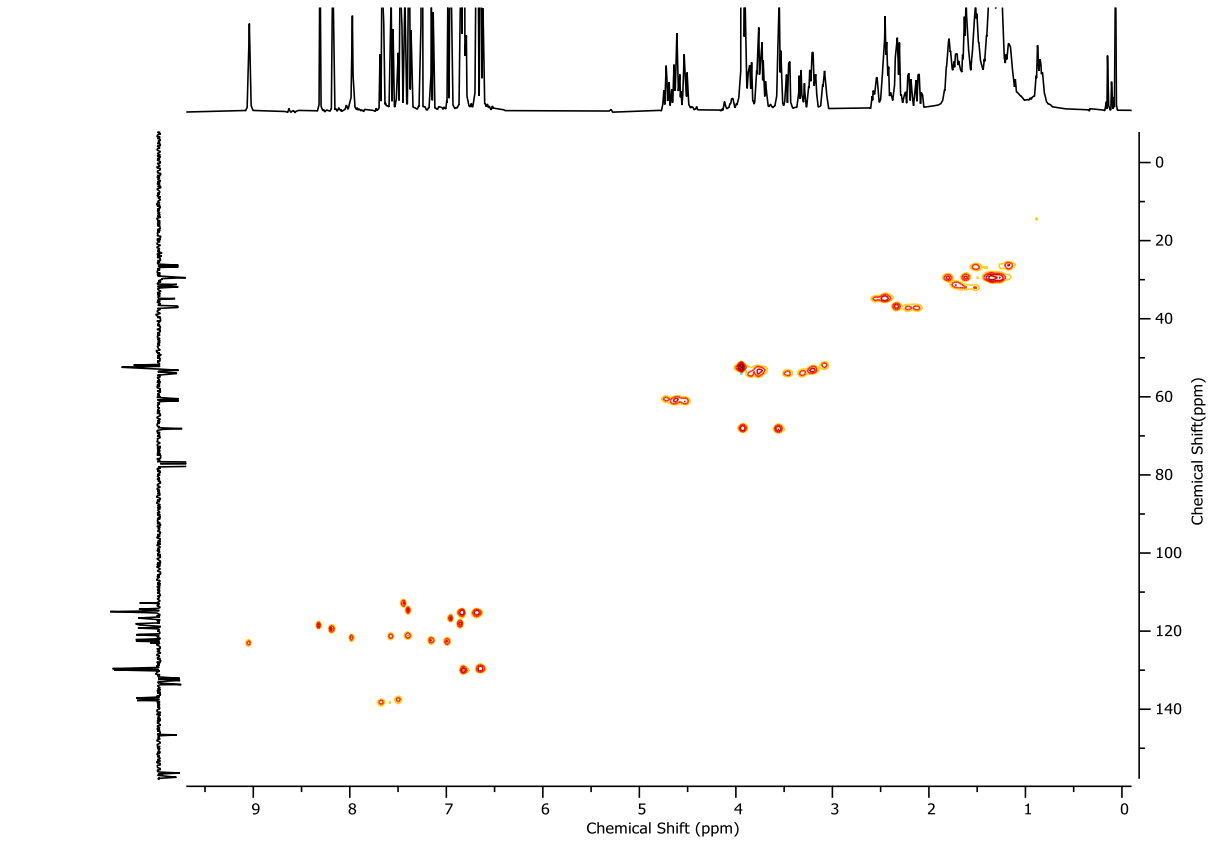

Figure 96: HSQC NMR ($CDCl_3$, 400 MHz) of (S_{ma})-**6**.

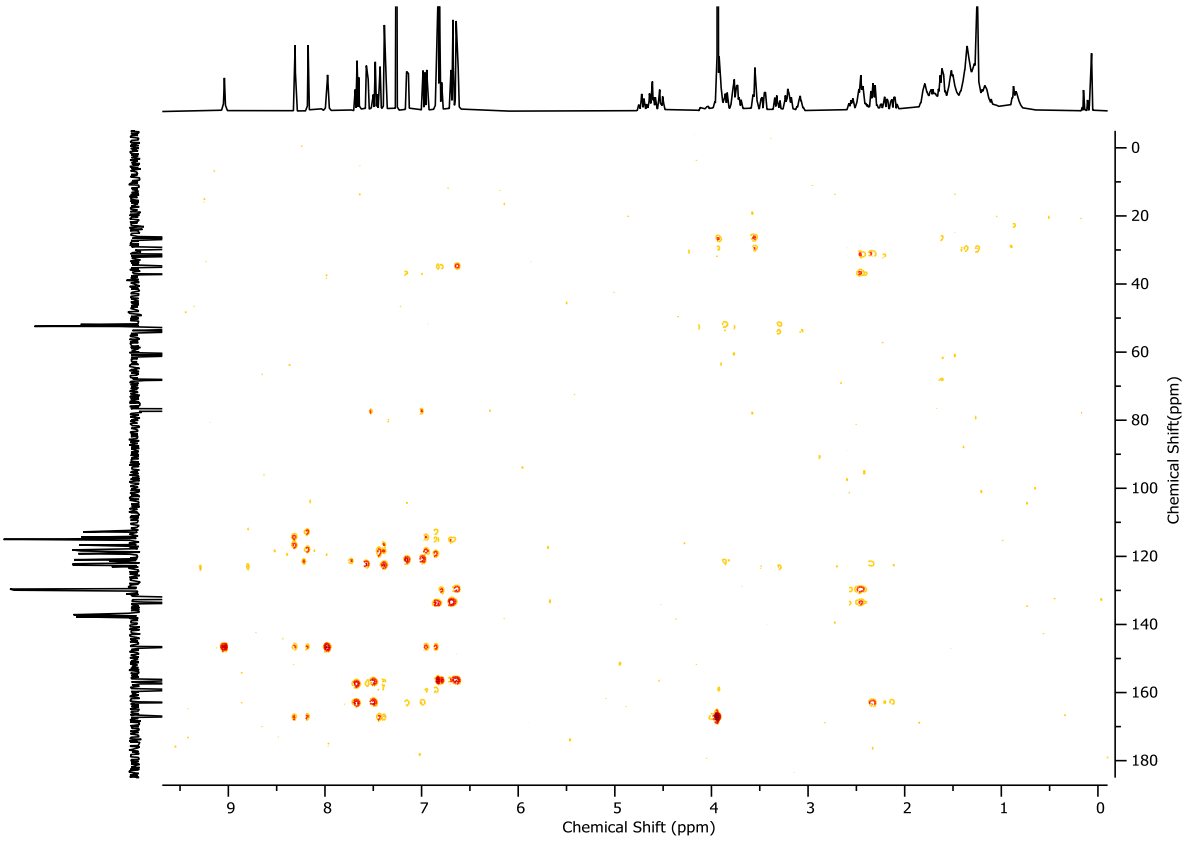

Figure 97: HMBC NMR ($CDCl_3$, 400 MHz) of (S_{ma})-**6**.

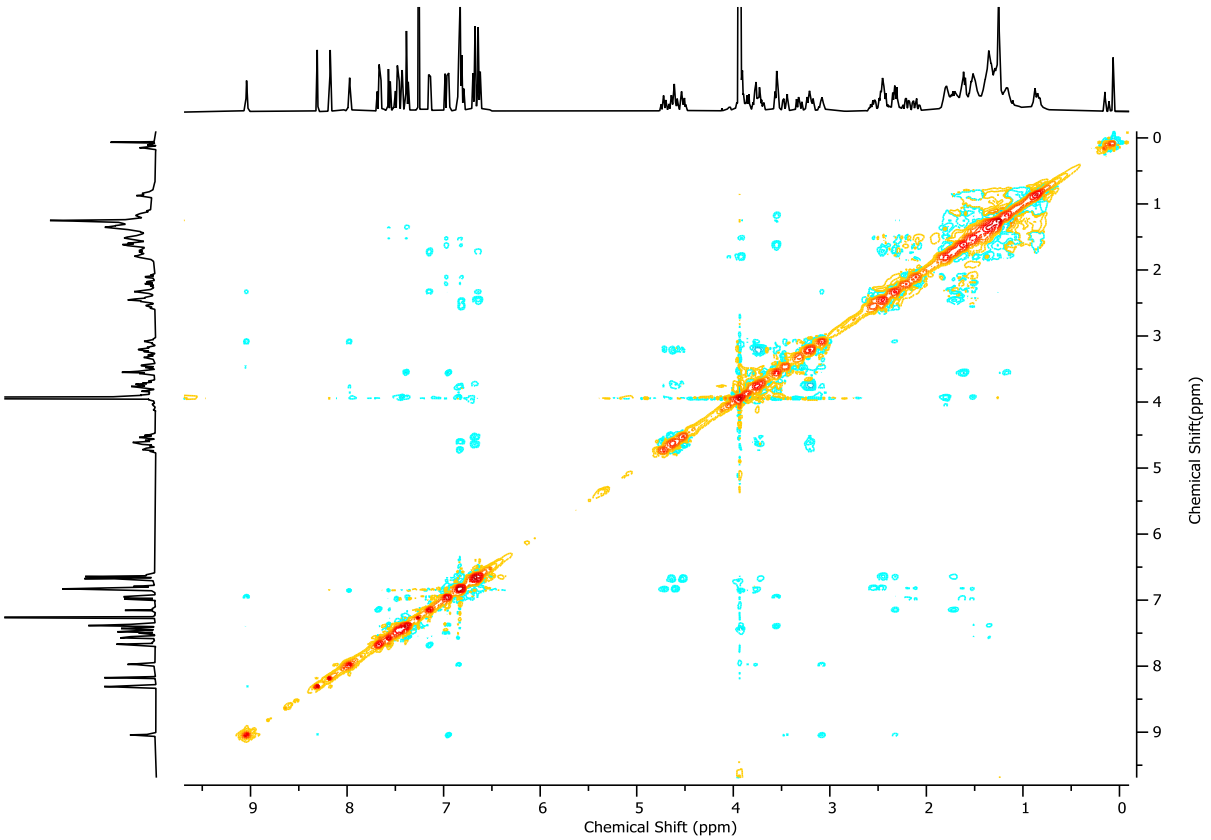

Figure 98: ^{1}H NOESY NMR ($CDCl_3$, 400 MHz) of (S_{ma})-**6**.

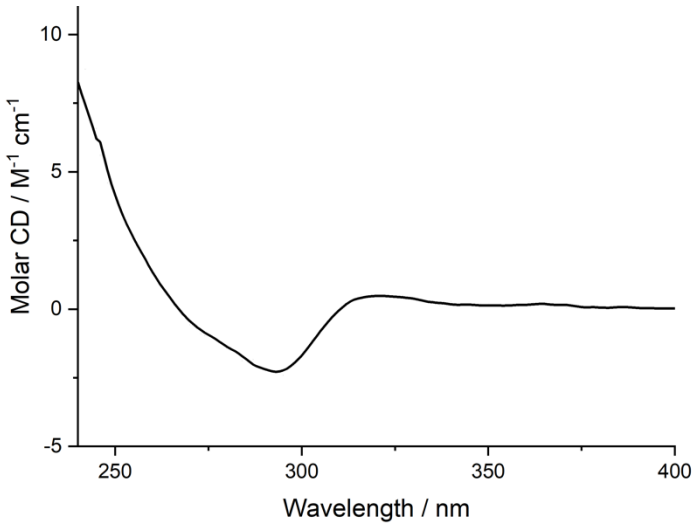

Figure 99: Circular Dichroism Spectra of (S_{ma})-**6** (15 µM) at 293 K in $CHCl_3$.

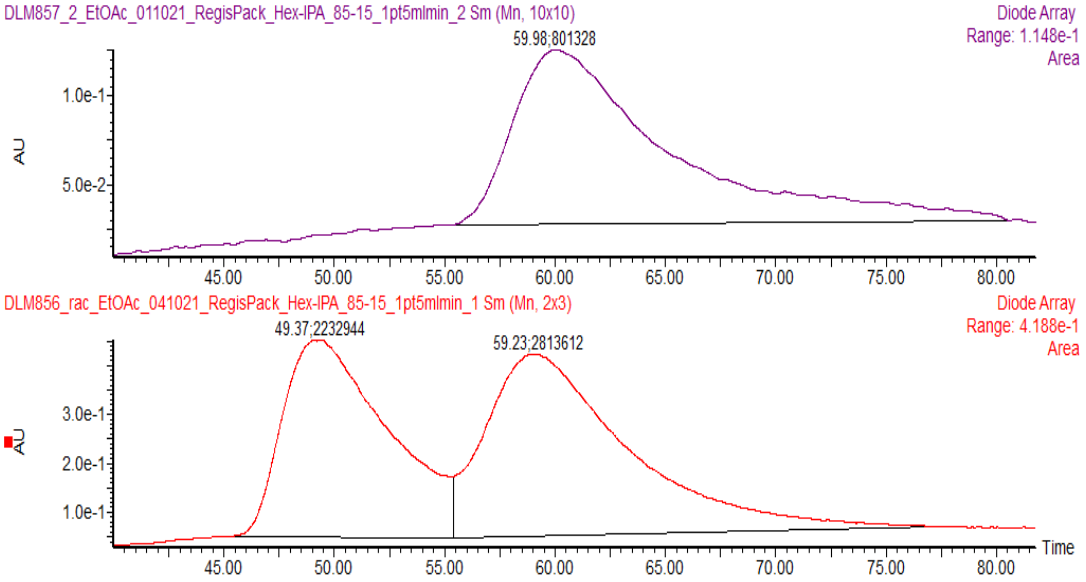

Figure 100: CSP-HPLC of (S_{ma})-**6** (loaded in EtOAc). RegisCell, *n*-hexane-EtOH 85 : 15, flowrate 1.5 $mLmin^{-1}$. (top) (S_{ma})-**6** (59.98 min, 801328, >99.9%), (R_{ma})-**6** (not observed). (bottom) *rac*-**6**, (R_{ma})-**6** (49.37 min, 2232944, 44.2%), (S_{ma})-**6** (59.23 min, 2813612, 55.8%).

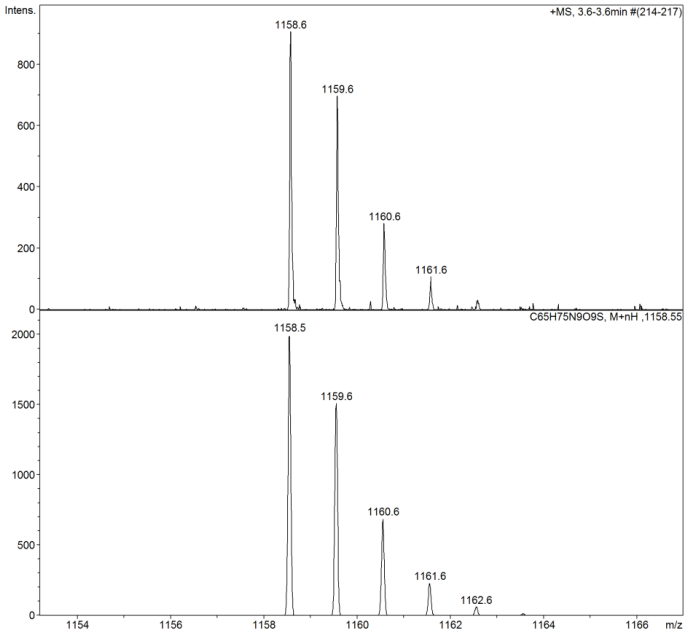

Figure 101: Observed (top) and calculated (bottom) isotopic patterns for *(S_{ma})*-**6**.

5.2. Catenane (R_{ma})-6

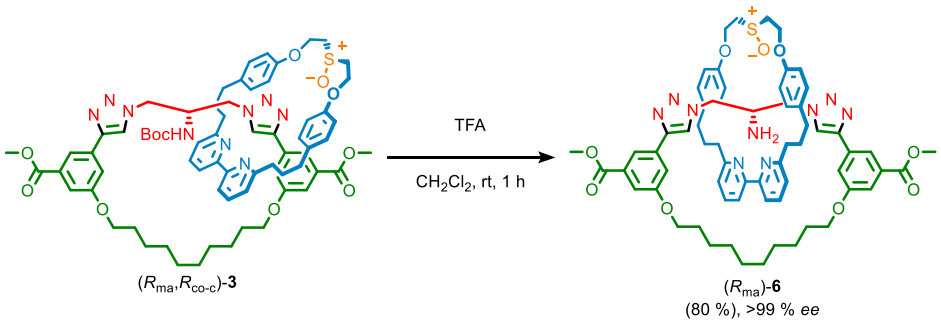

A solution of catenane (R_{ma},R_{co-c})-**6** (28.2 mg, 0.022 mmol, 1.0 eq.) in CH_2Cl_2 (0.3 mL) was added TFA (51 µL, 0.67 mmol, 30 eq.) dropwise at 0 ºC, then stirred atambient temperature for 1 h. The reaction mixture was then diluted with CH_2Cl_2 (5 mL) and poured into saturated $NaHCO_3$ (5 mL). The aqueous phase was extracted with CH_2Cl_2 (3 x 5 mL) and combined organics were washed with brine (5 mL), dried over $MgSO_4$, filtered and concentrated *in vacuo.* The residue was purified by column chromatography (SiO_2, CH_2Cl_2-MeOH 0→15%) to yield catenane (R_{ma})-**6** (20.8 mg, 0.018 mmol, 80%) as a white foam.

All spectroscopic data is consistent with those reported for (S_{ma})-**6**, with the exception of circular dichroism spectra.

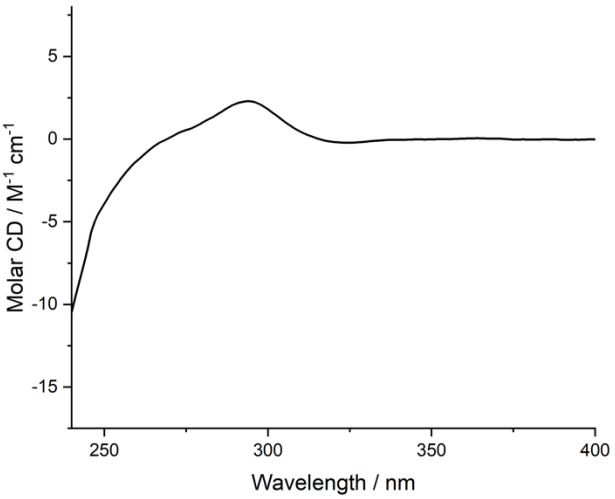

Figure 102: Circular Dichroism Spectra of (R_{ma})-**6** (21 µM) at 293 K in $CHCl_3$.

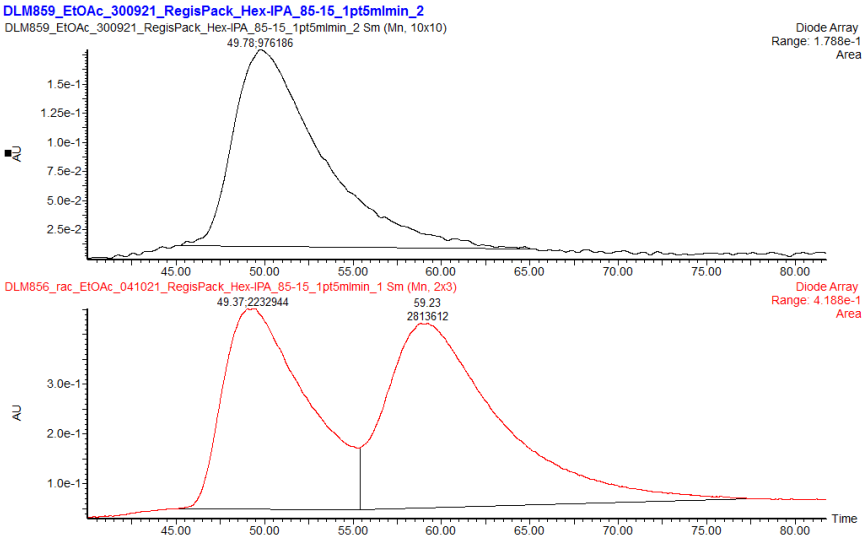

Figure 103: CSP-HPLC of (R_{ma})-**6** (loaded in EtOAc). RegisCell, *n*-hexane-EtOH 85:15, flowrate 1.5 mLmin^{-1}. (top) (R_{ma})-**6** (49.78 min, 976186, >99.9%), (S_{ma})-**6** (not observed); (bottom) *rac*-**6**, (R_{ma})-**6** (49.37 min, 2232944, 44.2%), (S_{ma})-**6** (59.23 min, 2813612, 55.8%).

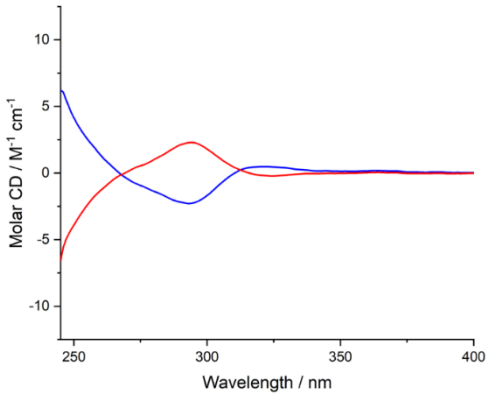

Figure 104: Circular Dichroism Spectra of (R_{ma})-**6** (red, 21 µM) and (S_{ma})-**6** (blue, 15 µM) at 293 K in $CHCl_3$.

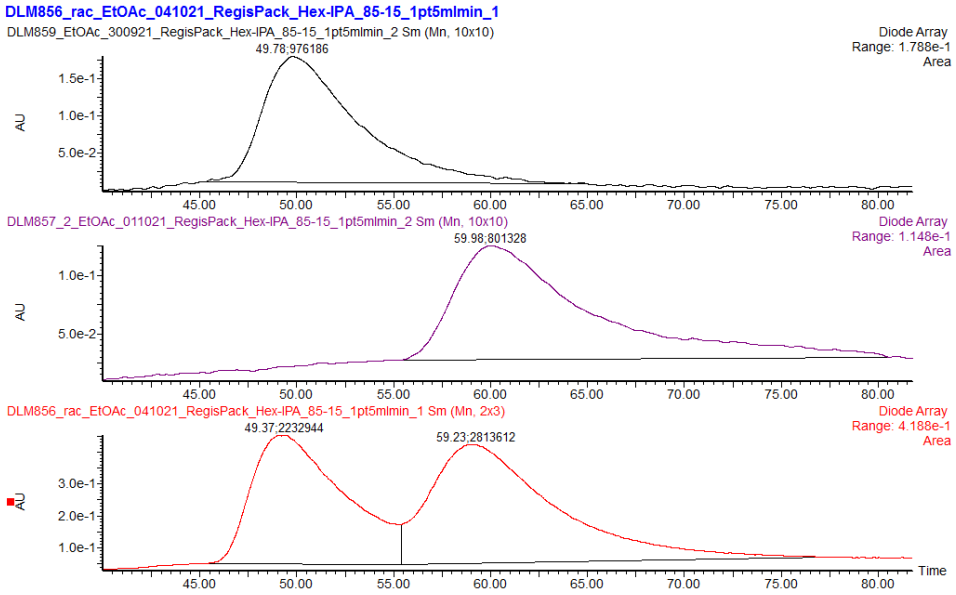

Figure 105: CSP-HPLC of (R_{ma})-**6** and (S_{ma})-**6** (loaded in EtOAc) 286 nm trace. RegisCell, *n*-hexane-EtOH 88:12, flowrate 1 mLmin^{-1}. (top) (R_{ma})-**6** (49.78 min, 976186, >99.9%), (S_{ma})-**6** (not observed); (middle) (S_{ma})-**6** (59.98 min, 801328, >99.9%), (R_{ma})-**6** (not observed).; (bottom) *rac*-**6**, (R_{ma})-**6** (49.37 min, 2232944, 44.2%), (S_{ma})-**6** (59.23 min, 2813612, 55.8%).

5.3. Macrocycle S14

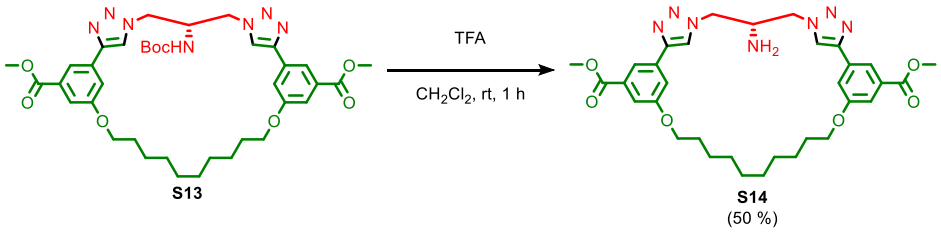

A solution of macrocycle **S13** (37.2 mg, 0.051 mmol, 1.0 eq.) in CH_2Cl_2 (0.5 mL) was added TFA (117 µL, 1.52 mmol, 30 eq.) dropwise then stirred at ambient temperature for 1 h. The reaction mixture was then diluted with CH_2Cl_2 (5 mL) and washed with 5M NaOH (2 x 5 mL). The aqueous phase was extracted with CH_2Cl_2 (3 x 8 mL) and combined organics were washed with brine (5 mL), dried over $MgSO_4$, filtered and concentrated *in vacuo.* The residue was purified by column chromatography (SiO_2, CH_2Cl_2 → EtOAc then CH_2Cl_2 → MeOH 0→15%) to yield **S14** (16.0 mg, 0.025 mmol, 50%) as a white foam.

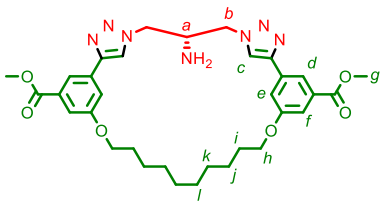

δ_H ($CDCl_3$, 400 MHz) 8.11 (t, J = 1.4, 2H, H_e), 7.90 (s, 2H, H_c), 7.51 (m, 2H, H_f), 7.47 (m, 2H, H_d), 4.44 (m, 4H, H_b), 4.06 (app t, J = 6.3, 4. H, H_h), 3.97 (t, J = 6.0, 1H, H_a), 3.92 (s, 6H, H_g), 1.80 (quint, J = 7.5, 4H, H_i), 1.50 (m, 2H, -NH_2), 1.31 (m, 12H, H_j, H_k, H_l); δ_C ($CDCl_3$, 101 MHz) 166.7, 159.5, 147.0, 132.2, 131.5, 121.8, 119.0, 116.8, 115.2, 68.5, 53.2, 52.3, 51.8, 29.7, 29.1, 28.9, 25.9; LR-ESI-MS (+ve) $[M+H]^+$ m/z (%) 632.5 (100); HR-EI-MS (+ve) $[M+H]^+$ m/z 632.3193 (calc. for $C_{33}H_{42}N_7O_6$ m/z 632.3191).

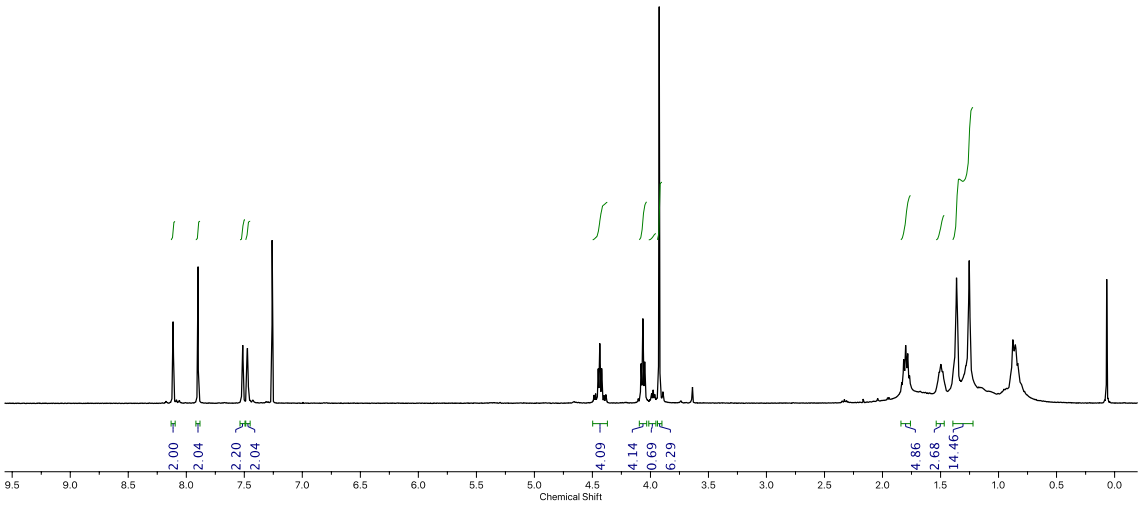

Figure 106: ^{1}H NMR ($CDCl_3$, 400 MHz) of **S14**.

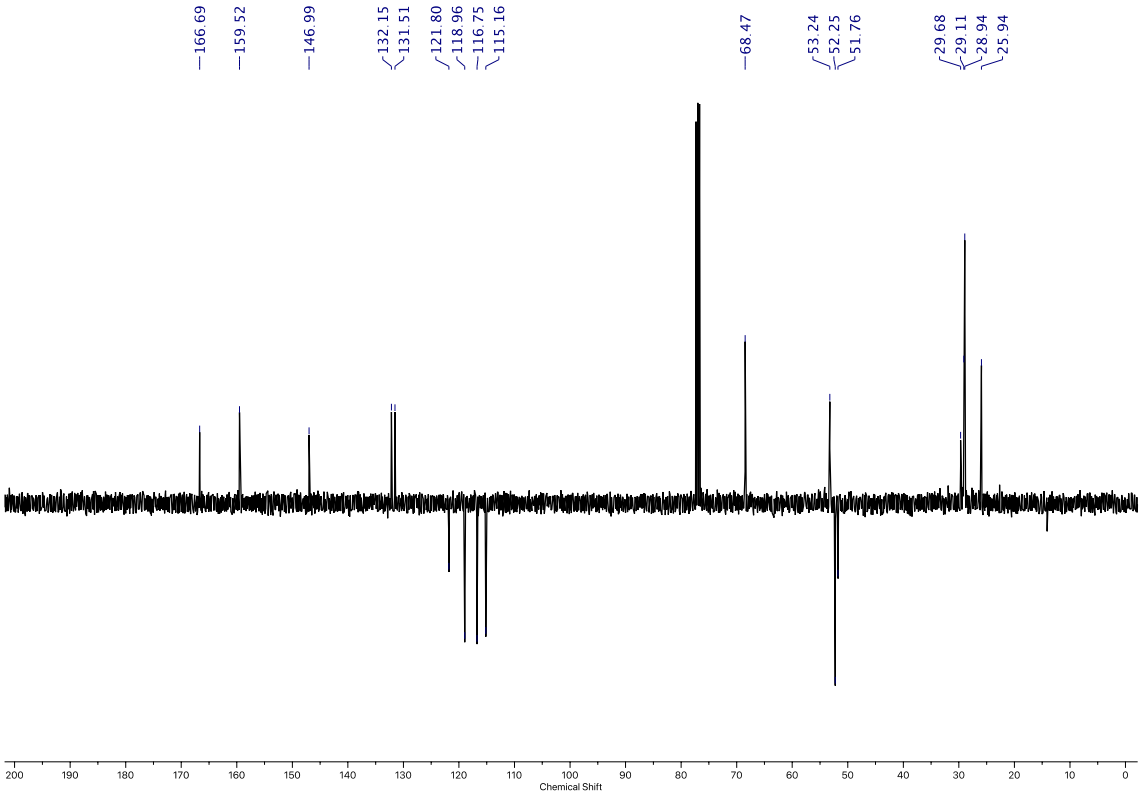

Figure 107: JMOD NMR ($CDCl_3$, 101 MHz) of **S14**.

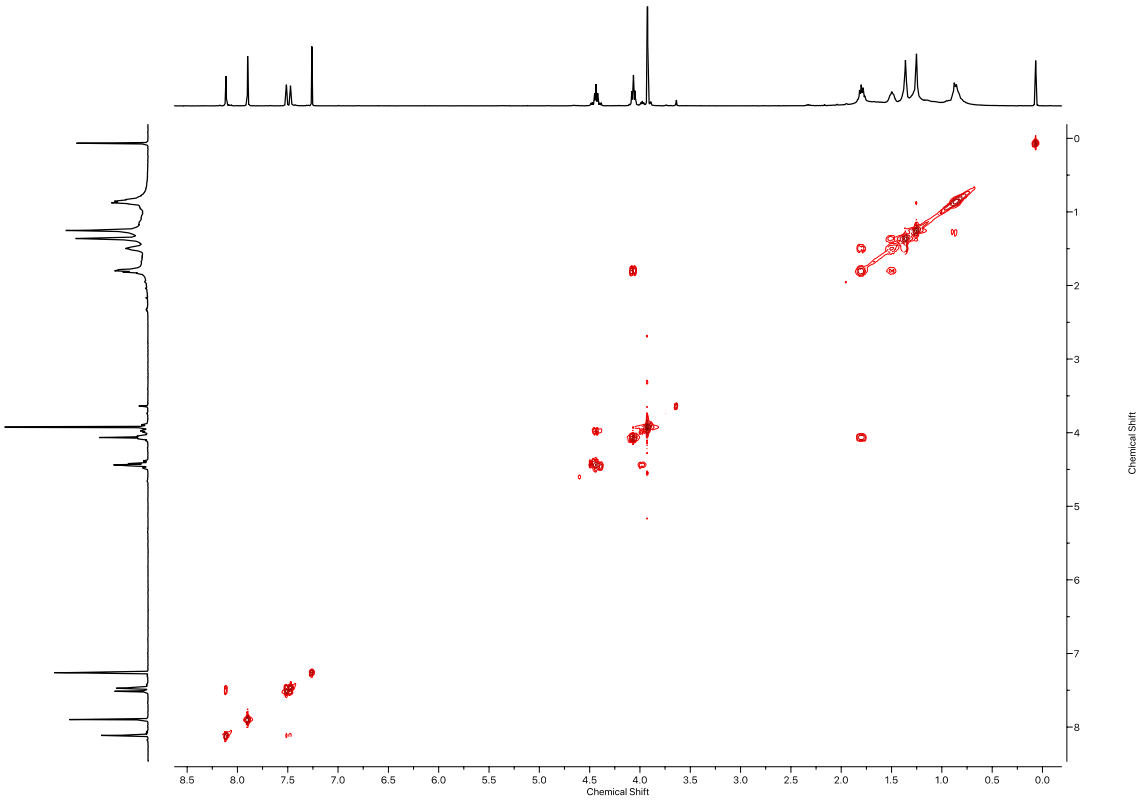

Figure 108: ^{1}H COSY NMR ($CDCl_3$, 400 MHz) of **S14**.

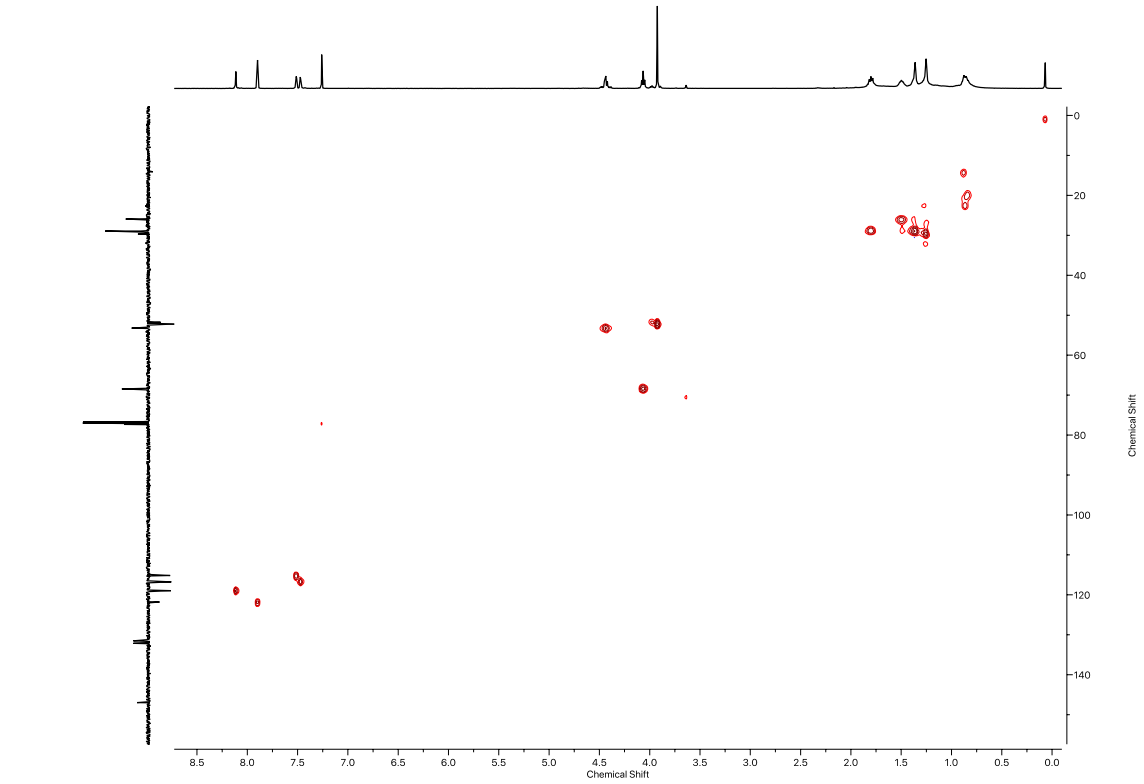

Figure 109: HSQC NMR ($CDCl_3$, 400 MHz) of **S14**.

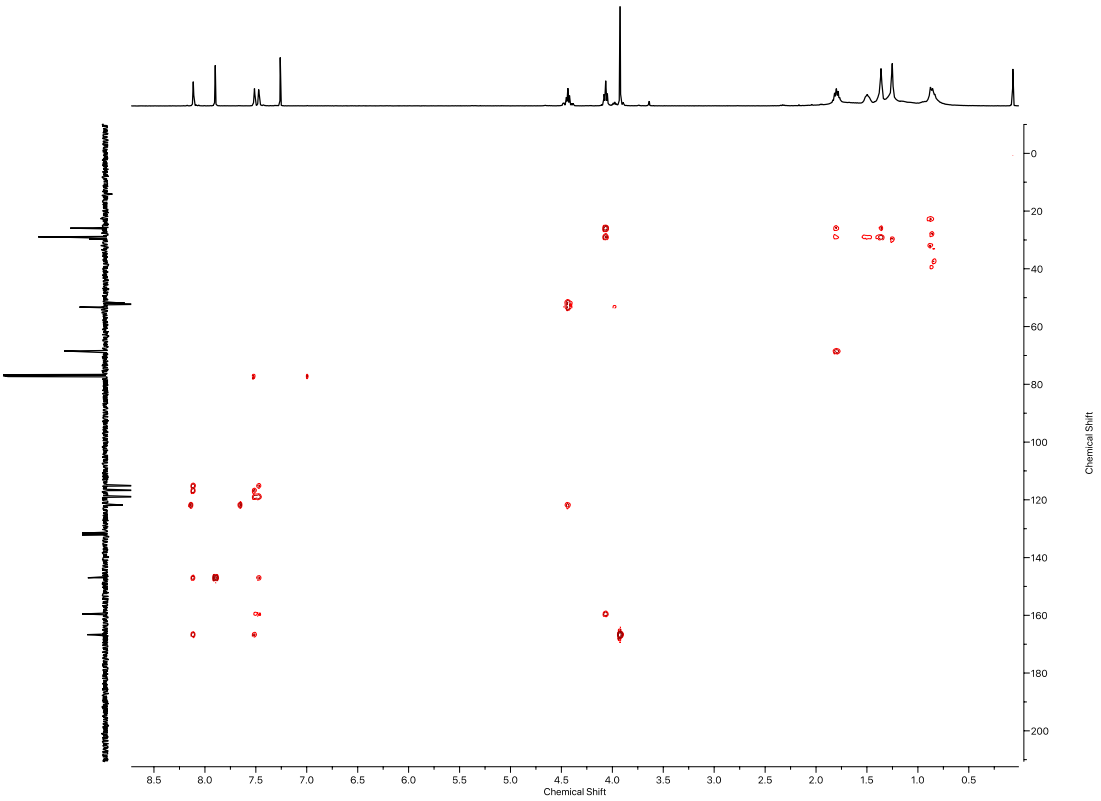

Figure 110: HMBC NMR ($CDCl_3$, 400 MHz) of **S14**.

6. Synthesis of enantiomeric catenanes (S_{ma})-S15 and (R_{ma})-S15

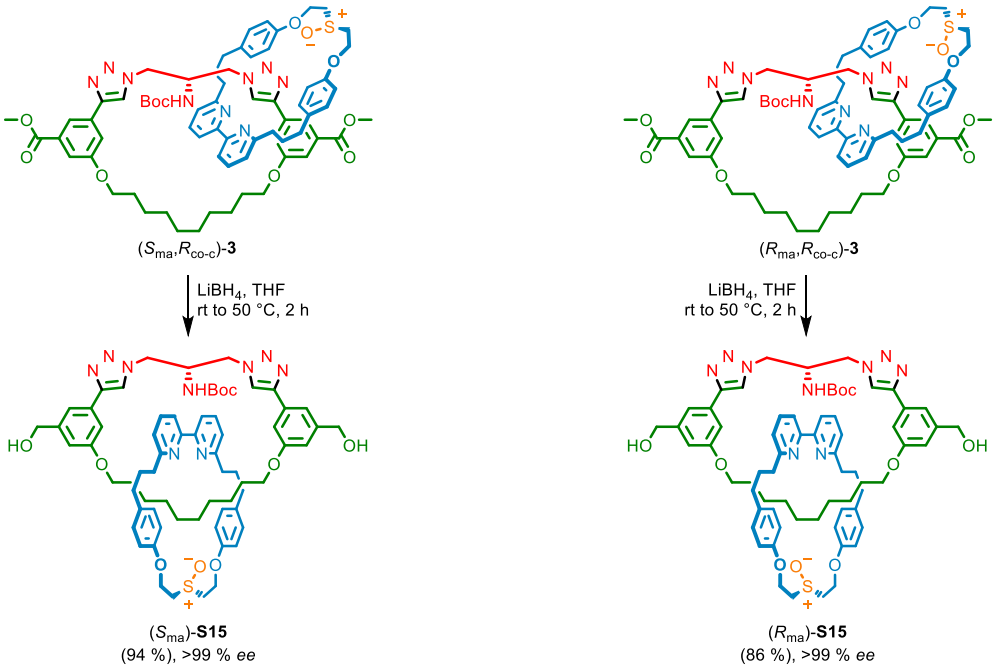

Scheme 5: Synthetic route to mechanically axially chiral enantiomeric catenanes (R_{ma})-**S15** and (S_{ma})-**S15**.

6.1. Catenane (S_{ma})-S15

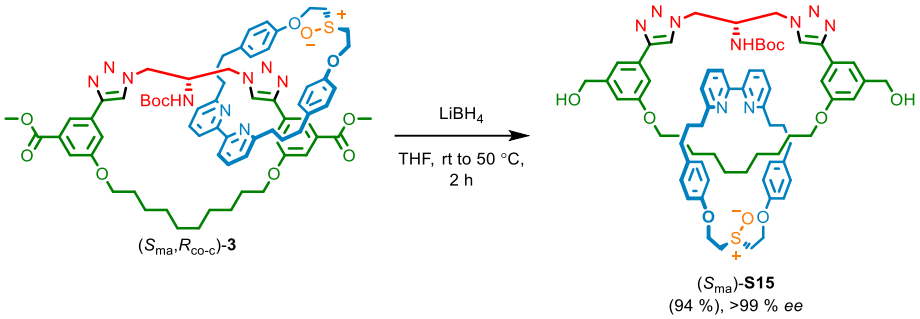

A dry CEM MW vial was charged with catenane (S_{ma},R_{co-c})-**3** (21.9 mg, 0.017 mmol, 1.0 eq.) and THF (0.5 mL). $LiBH_4$ (3.3 mg, 0.09 mmol, 5.0 eq.) was added at ambient temperature, and the solution was stirred for 2 h at 50 °C. The crude mixture was allowed to cool down, EtOAc (4 mL) was added and organics were washed with H_2O in two portions (2 mL and 4 mL), and the combined organics were washed with brine (8 mL), dried over $MgSO_4$ and concentrated *in vacuo*. The residue was purified by column chromatography (SiO_2, CH_2Cl_2-MeOH 0→10%) to yield catenane (S_{ma})-**S15** (19.0 mg, 0.016 mmol, 94%) as a white foam. The mechanical stereochemistry of the product was assigned by observing that this cannot change during the reduction step (or if it does, that the resulting product would be racemic, which was not observed).

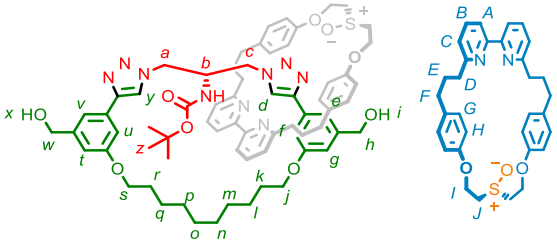

δ_H (DMSO-d_6, 500 MHz) 8.57 (s, 1H, $\boldsymbol{H}_d$), 8.40 (s, 1H, $\boldsymbol{H}_y$), 7.74 (t, J = 10, 1H, $\boldsymbol{H}_B$), 7.70-7.58 (m, 3H, $\boldsymbol{H}_A$, $\boldsymbol{H}_{A'}$, $\boldsymbol{H}_{B'}$), 7.51-7.47 (m, 2H, $\boldsymbol{H}_e$, $\boldsymbol{H}_v$), 7.30-7.12 (m, 4H, $\boldsymbol{H}_f$, $\boldsymbol{H}_C$, $\boldsymbol{H}_{C'}$, $\boldsymbol{H}_{\text{-NHBoc}}$), 7.01 (s, 1H, $\boldsymbol{H}_u$), 6.87-6.77 (m, 5H, $\boldsymbol{H}_G$, $\boldsymbol{H}_{G'}$, $\boldsymbol{H}_g$), 6.72-6.52 (m, 5H, $\boldsymbol{H}_t$, $\boldsymbol{H}_H$, $\boldsymbol{H}_{H'}$), 5.31 (t, J = 5.5, 1H, $\boldsymbol{H}_i$), 5.27 (t, J = 6, 1H, $\boldsymbol{H}_x$), 4.66-4.29 (m, 17H, $\boldsymbol{H}_a$, $\boldsymbol{H}_b$, $\boldsymbol{H}_c$, $\boldsymbol{H}_h$, $\boldsymbol{H}_w$, $\boldsymbol{H}_s$, $\boldsymbol{H}_j$, $\boldsymbol{H}_l$, $\boldsymbol{H}_{l'}$), 3.67-3.57 (m, 2H, $\boldsymbol{H}_J$), 3.51-3.45 (m, 2H, $\boldsymbol{H}_{J'}$), 2.80-2.69 (m, 4H, $\boldsymbol{H}_D$, $\boldsymbol{H}_F$), 2.49-2.44 (m, 4H, $\boldsymbol{H}_{D'}$, $\boldsymbol{H}_{F'}$) 1.76-1.61 (m, 4H, $\boldsymbol{H}_E$, $\boldsymbol{H}_{E'}$), 1.28-1.20 (m, 9H, $\boldsymbol{H}_k$, $\boldsymbol{H}_r$, $\boldsymbol{H}_l$, $\boldsymbol{H}_q$), 1.14 (m, 9H, $\boldsymbol{H}_z$), 0.52-0.31 (m, 8H, $\boldsymbol{H}_l$, $\boldsymbol{H}_m$); δ_C (DMSO-d_6, 126 MHz) 166.6, 159.5, 147.1, 132.2, 131.3, 121.9, 118.9, 116.5, 115.5, 68.5, 52.3, 50.8, 50.1, 29.1, 28.9, 28.3, 25.9. LR-ESI-MS (+ve) $[M+H]^+$ m/z (%) 1203.0 (100).

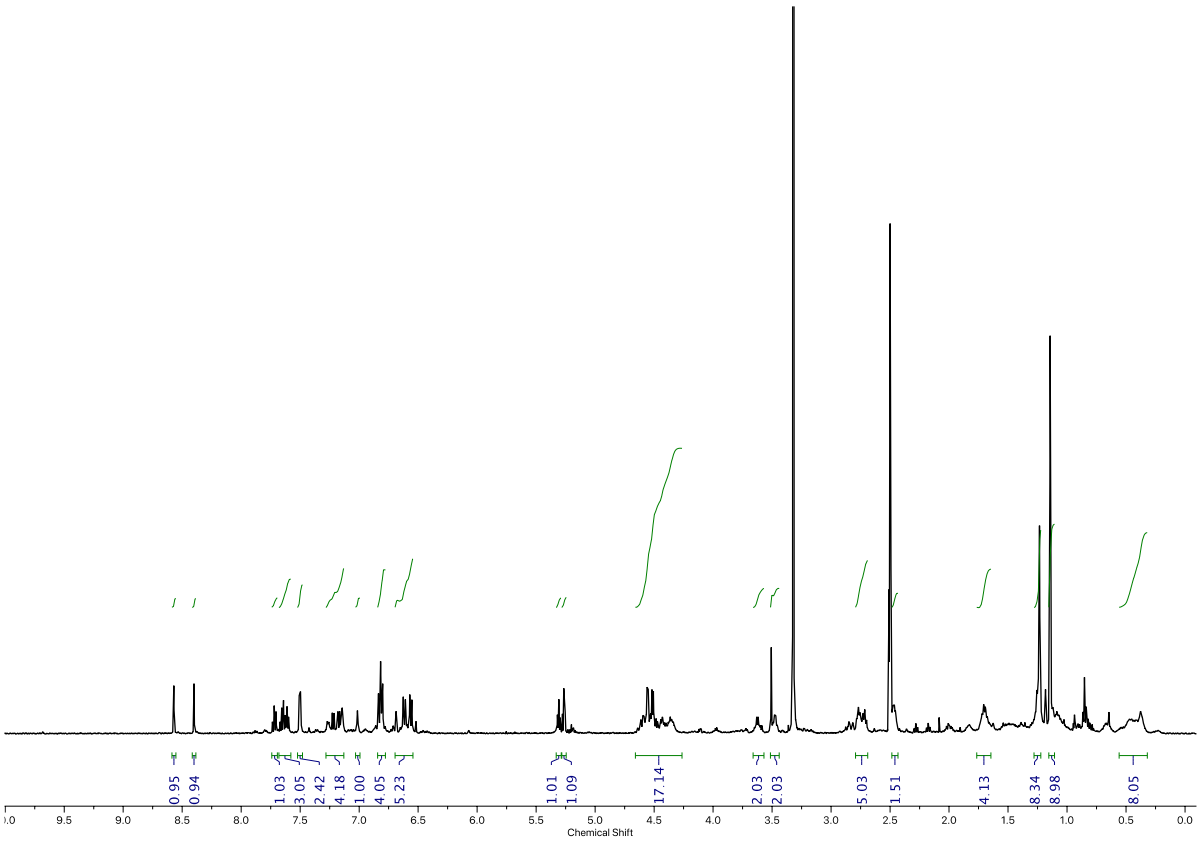

Figure 111: ^{1}H NMR ($CDCl_3$, 500 MHz) of (S_{ma})-**S15**.

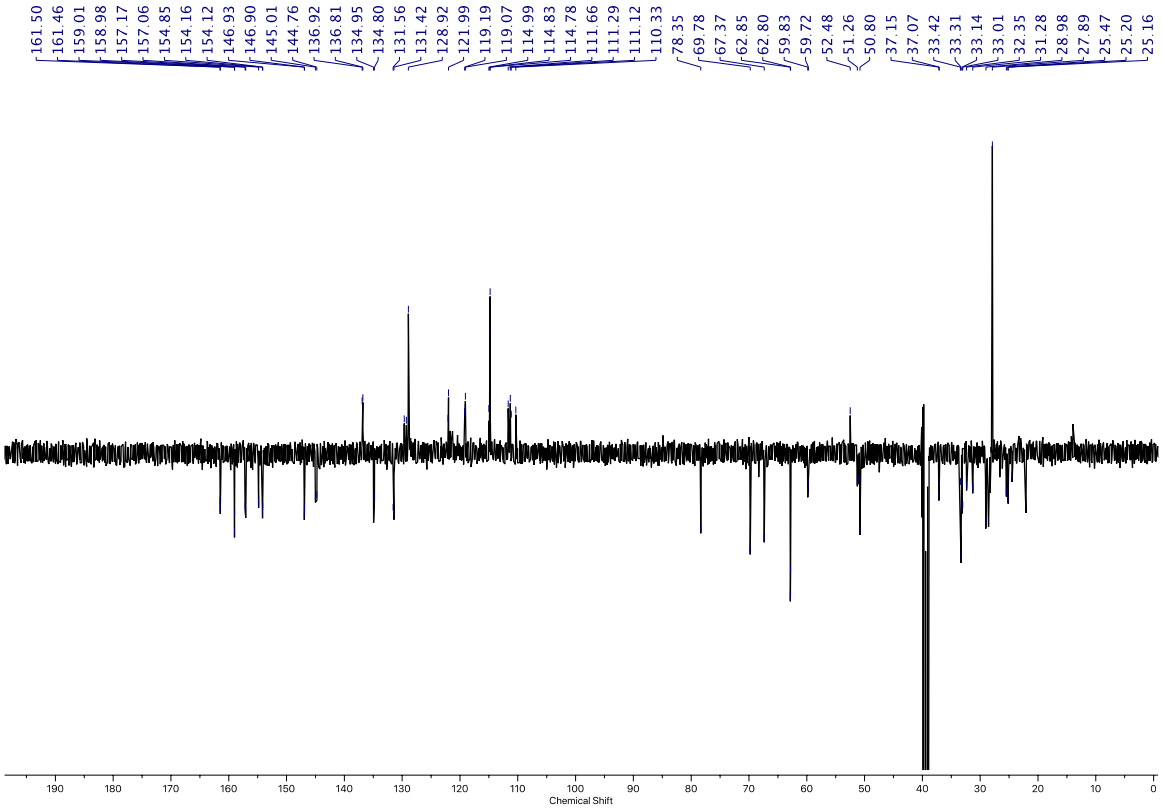

Figure 112: JMOD NMR ($CDCl_3$, 126 MHz) of (S_{ma})-**S15**.

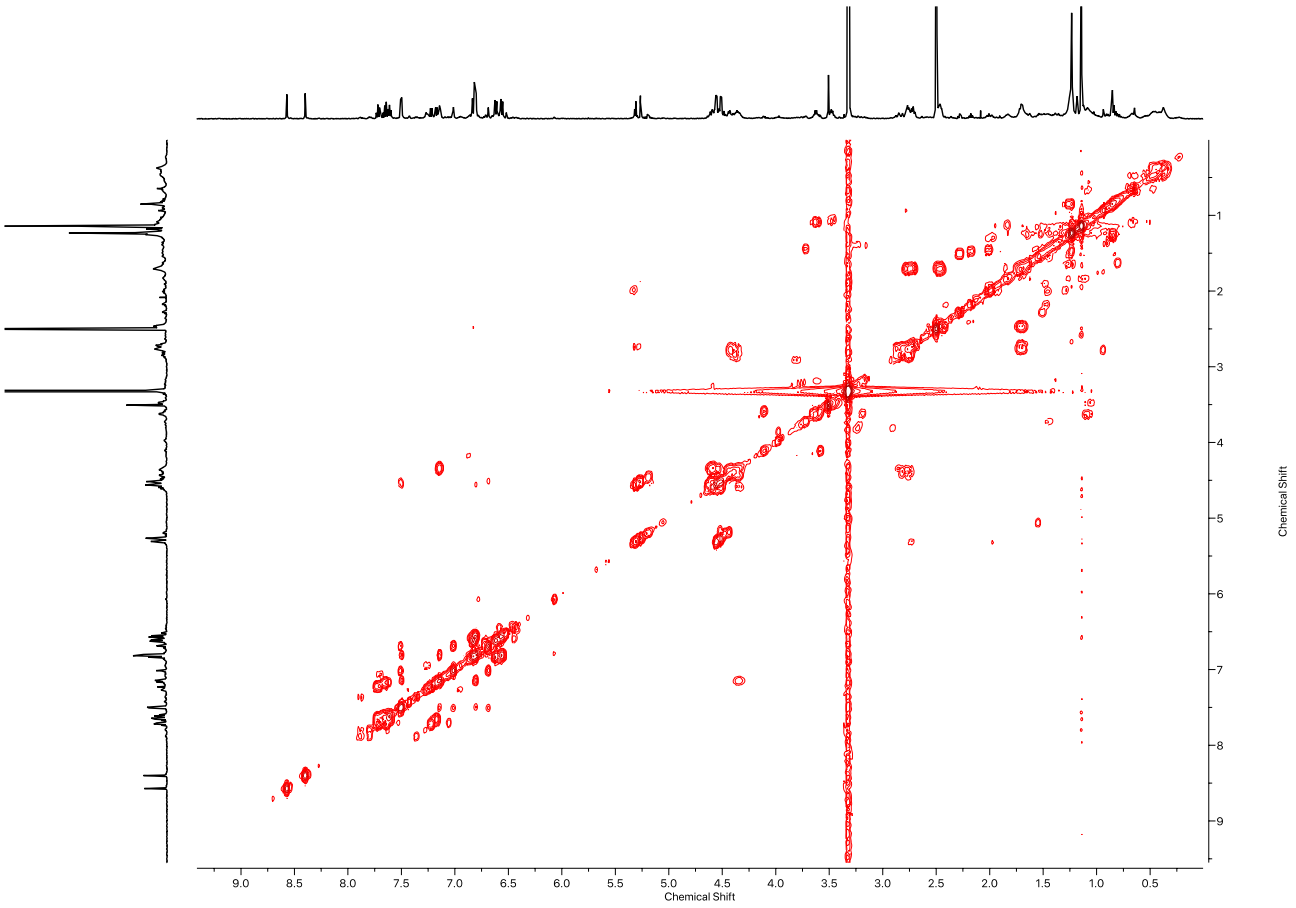

Figure 113: ^{1}H COSY NMR (DMSO, 500 MHz) of (S_{ma})-**S15**.

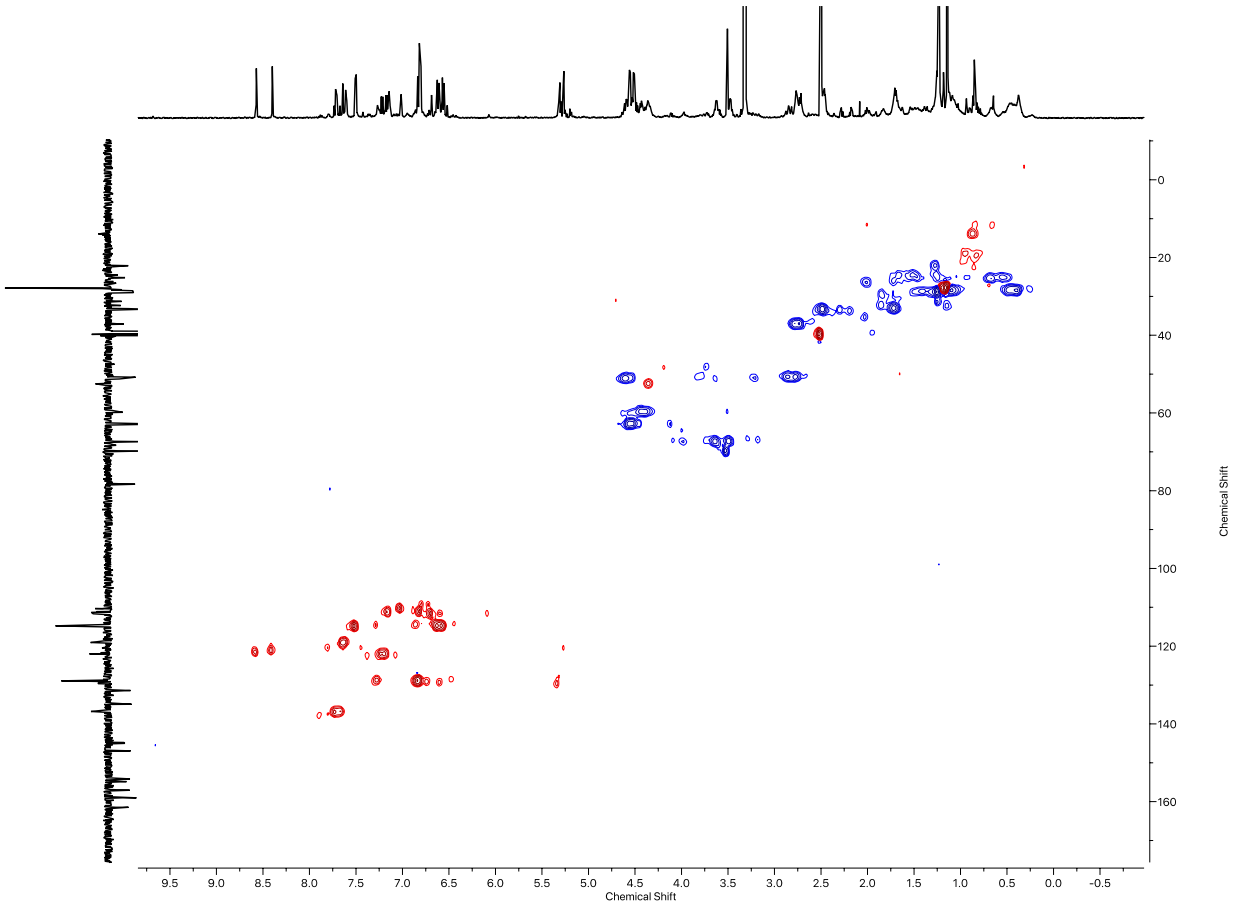

Figure 114: HSQC NMR (DMSO, 500 MHz) of (S_{ma})-**S15**.

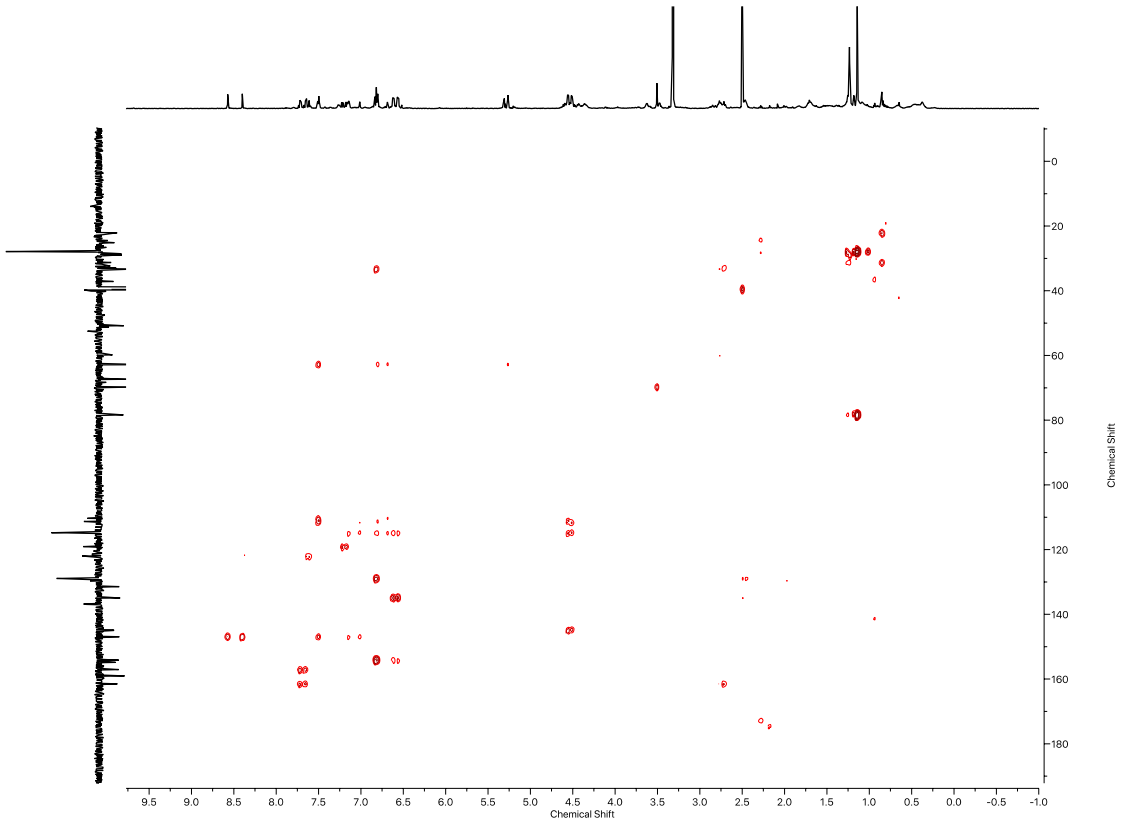

Figure 115: HMBC NMR (DMSO, 500 MHz) of (S_{ma})-**S15**.

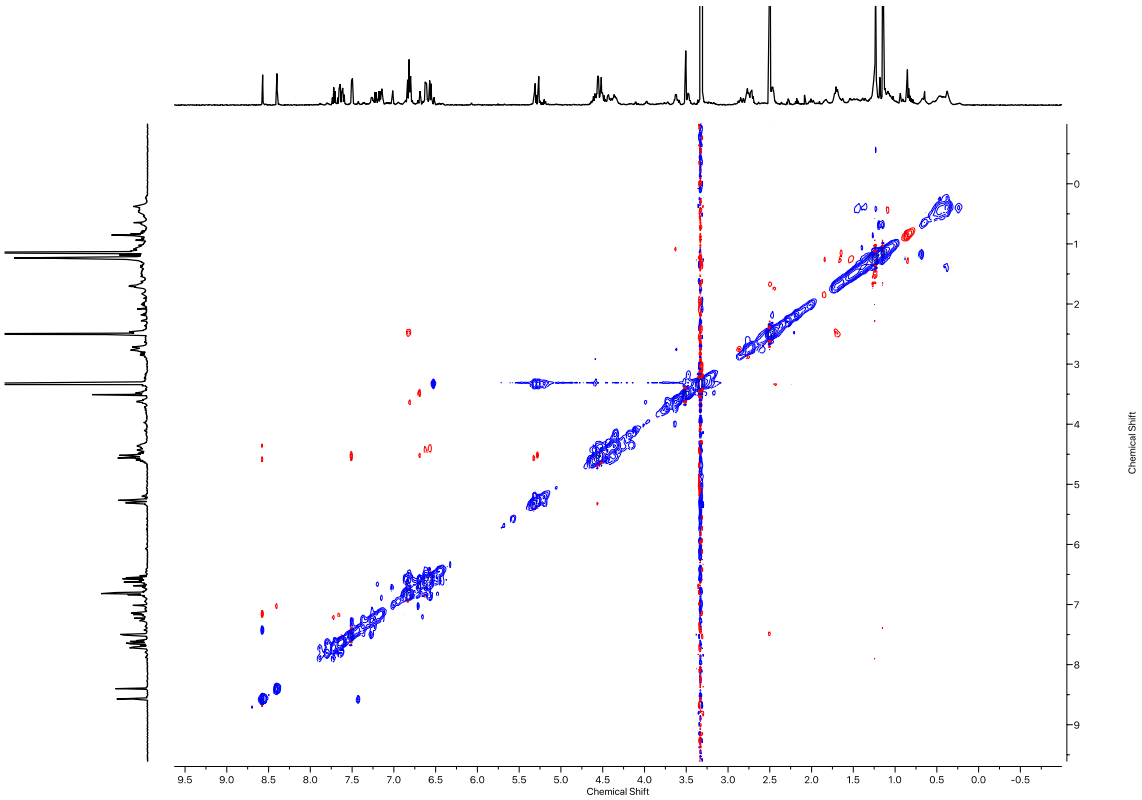

Figure 116: ^{1}H NOESY NMR (DMSO, 500 MHz) of (S_{ma})-**S15**.

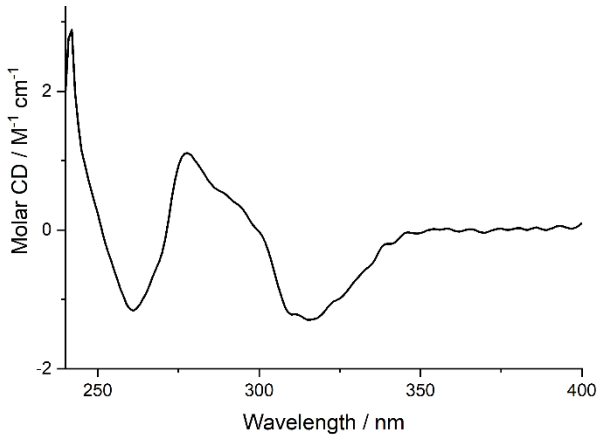

Figure 117: Circular Dichroism Spectra of (S_{ma})-**S15** (18 µM) at 293 K in $CHCl_3$.

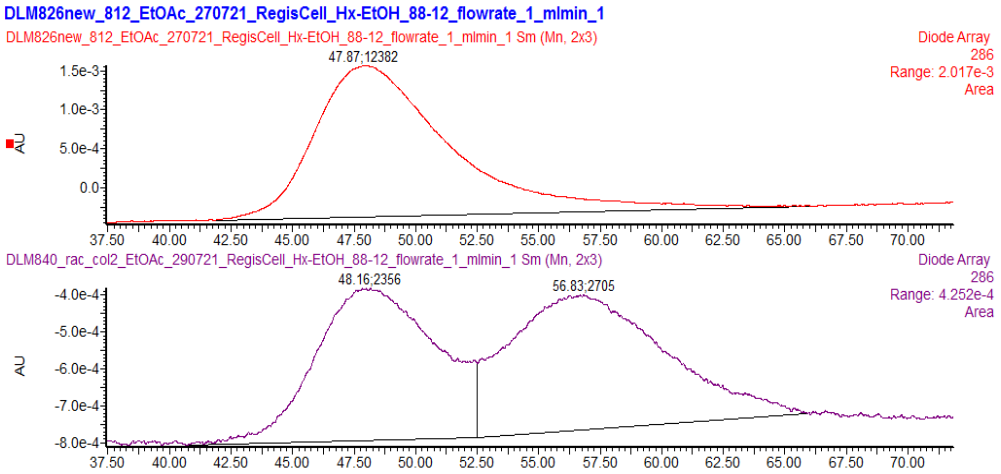

Figure 118: CSP-HPLC of (S_{ma})-**S15** (loaded in EtOAc) 286 nm trace. RegisCell, *n*-hexane-EtOH 88 : 12, flowrate 1 mLmin^{-1}. (top) (S_{ma})-**S15** (47.87 min, 12382, >99.9%), (R_{ma})-**S15** (not observed). (bottom) *rac*-**S15**, (S_{ma})-**S15** (48.16 min, 2356, 50.1%), (R_{ma})-**S15** (56.83 min, 2705, 49.9%).

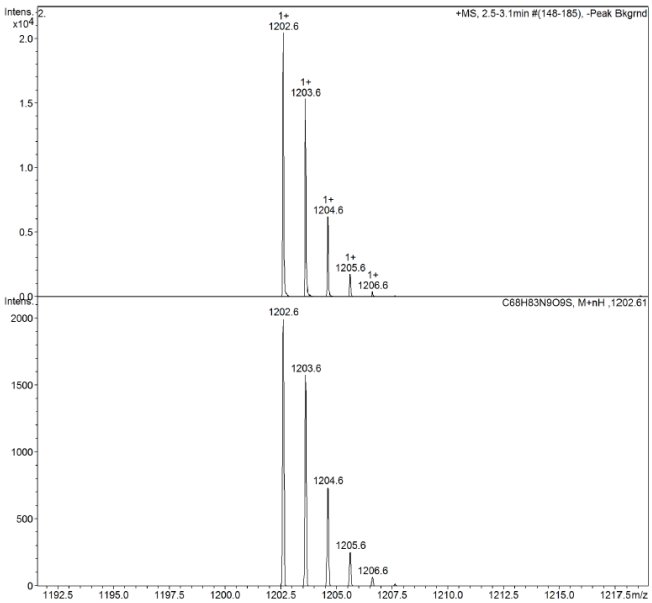

Figure 119: Observed (top) and calculated (bottom) isotopic patterns for *(S_{ma})*-**S15**.

6.2. Catenane (R_{ma})-S15

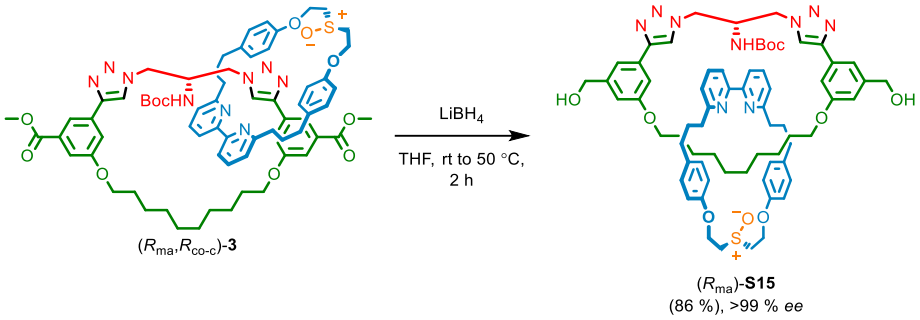

A dry CEM MW vial was charged with catenane (R_{ma},$R_{co\text{-}c}$)-**3** (23.5 mg, 0.019 mmol, 1.0 eq.) and THF (0.5 mL). $LiBH_4$ (3.5 mg, 0.09 mmol, 5.0 eq.) was added at ambient temperature, and the solution was stirred for 2 h at 50 °C. The crude mixture was allowed to cool down, EtOAc (4 mL) was added and organics were washed with H_2O in two portions (2 mL and 4 mL), and the combined organics were washed with brine (8 mL), dried over $MgSO_4$ and concentrated *in vacuo*. The residue was purified by column chromatography (SiO_2, CH_2Cl_2-MeOH 0→10%) to yield catenane (R_{ma})-**S15** (19.3 mg, 0.016 mmol, 85%) as a white foam.

All spectroscopic data is consistent with those reported for (S_{ma})-**S15**, with the exception of circular dichroism spectra.

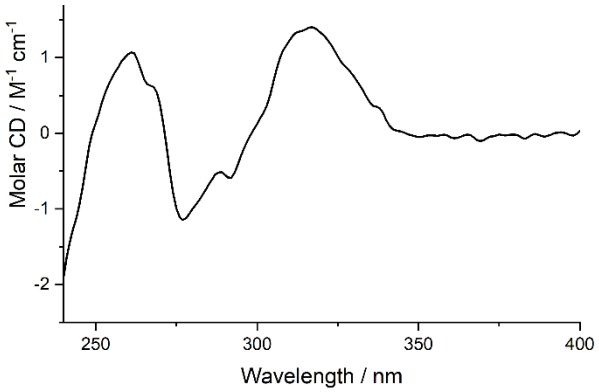

Figure 120: Circular Dichroism Spectra of (R_{ma})-**S15** (16 µM) at 293 K in $CHCl_3$.

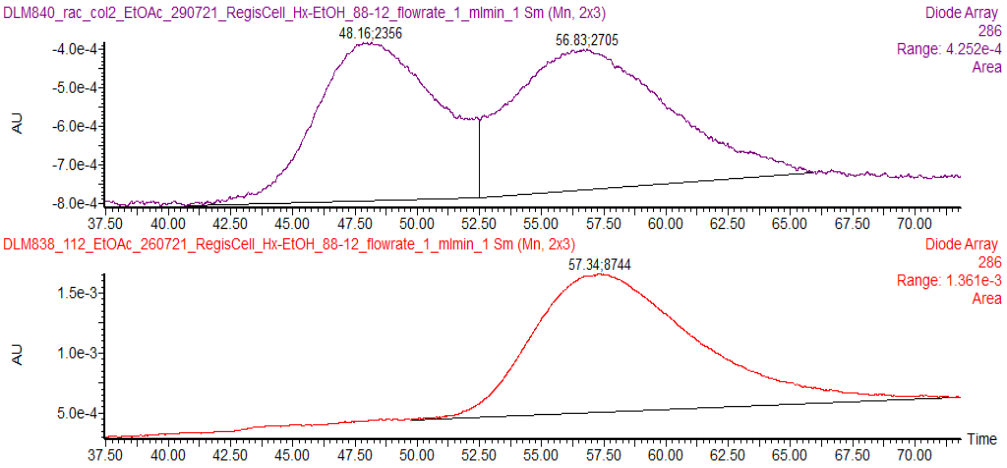

Figure 121: CSP-HPLC of (R_{ma})-**S15** (loaded in EtOAc) 286 nm trace. RegisCell, *n*-hexane-EtOH 88:12, flowrate 1 mLmin^{-1}. (top) *rac*-**S15**, (S_{ma})-**S15** (48.16 min, 2356, 50.1%), (R_{ma})-**S15** (56.83 min, 2705, 49.9%); (bottom) (S_{ma})-**S15** (not observed), (R_{ma})-**S15** (57.34 min, 8744, >99.9%).

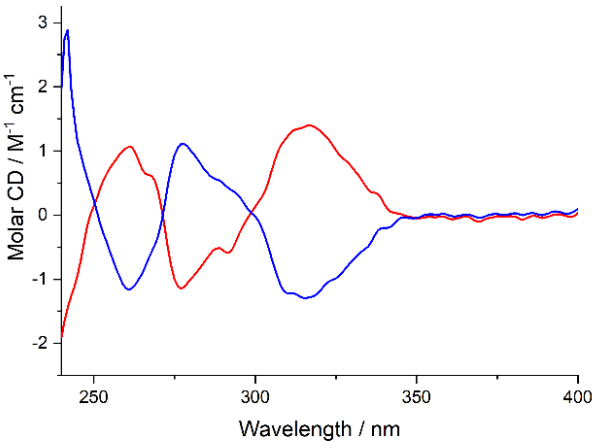

Figure 122: Circular Dichroism Spectra of (S_{ma})-**S15** (red, 16 µM) and (R_{ma})-**S15** (blue, 18.3 µM)at 293 K in $CHCl_3$.

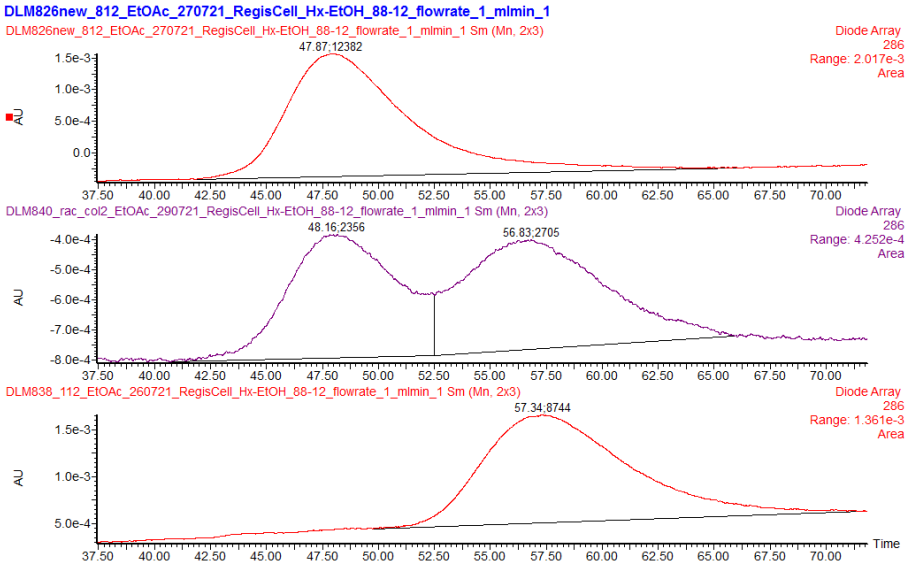

Figure 123: CSP-HPLC of (R_{ma})-**S15** and (S_{ma})-**S15** (loaded in EtOAc) 286 nm trace. RegisCell, *n*-hexane-EtOH 88:12, flowrate 1 mLmin^{-1}. (top) (S_{ma})-**S15** (47.87 min, 12382, >99.9%), (R_{ma})-**S15** (not observed); (middle) *rac*-**S15**, (S_{ma})-**S15** (48.16 min, 2356, 50.1%), (R_{ma})-**S15** (56.83 min, 2705, 49.9%); (bottom) (S_{ma})-**S15** (not observed), (R_{ma})-**S15** (57.34 min, 8744, >99.9%).

6.3. Macrocycle S16

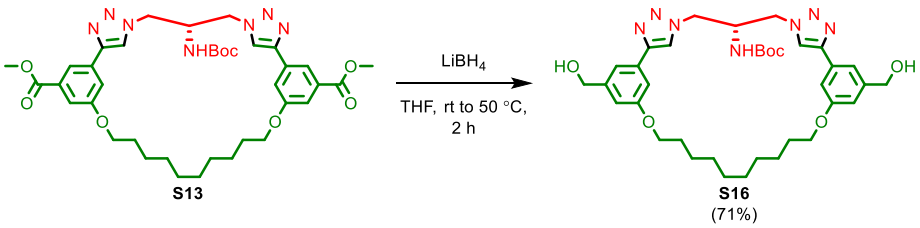

To a solution of macrocycle **S13** (17.7 mg, 0.024 mmol, 1.0 eq.) in THF (0.5 mL) at ambient temperature was added $LiBH_4$ (2.6 mg, 0.121 mmol, 5 eq.), and then the reaction mixture was stirred at 50 °C for 2 h. The reaction mixture was diluted with EtOAc (5 mL) and washed with H_2O (2 x 5 mL). The aqueous phase was extracted with EtOAc (2 x 8 mL) and combined organics were washed with brine (5 mL), dried over $MgSO_4$, filtered and concentrated *in vacuo.* The residue was purified by column chromatography (SiO_2, CH_2Cl_2 → EtOAc then CH_2Cl_2 → MeOH 0→15%) to yield **S16** (11.6 mg, 0.017 mmol, 71%) as a white foam. Two rotamers of **S16** are observed due to slow rotation of -NHBoc group at 298 K, which were equilibrated by VT-NMR (Fig. S125).

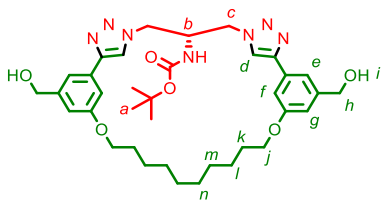

δ_H ($CDCl_3$, 500 MHz) 8.61 (s, 2H, $\boldsymbol{H}_d$), 7.50 (s, 2H, $\boldsymbol{H}_c$), 7.19 (d, J = 8.9, 1H, -N*H*Boc), 7.11 (br. s, 2H, $\boldsymbol{H}_f$), 6.84 (m, 2H, $\boldsymbol{H}_d$), 5.24 (t, J = 5.5, 2H, $\boldsymbol{H}_i$), 4.65-4.44 (m, 9H, $\boldsymbol{H}_b$, $\boldsymbol{H}_c$, $\boldsymbol{H}_h$), 4.00 (t, J = 6.5, 4H, $\boldsymbol{H}_j$), 1.72 (quint., 4H, $\boldsymbol{H}_k$), 1.45 (m, 4H, $\boldsymbol{H}_l$), 1.31 (m, 8H, $\boldsymbol{H}_m$, $\boldsymbol{H}_n$), 1.23 (s, 9H, $\boldsymbol{H}_a$); δ_C ($CDCl_3$, 101 MHz) 166.7, 159.5, 147.0, 132.2, 131.5, 121.8, 119.0, 116.8, 115.2, 68.5, 53.2, 52.3, 51.8, 29.7, 29.1, 28.9, 25.9; LR-ESI-MS (+ve) $[M+H]^+$ m/z (%) 632.5 (100); HR-EI-MS (+ve) $[M+H]^+$ m/z 676.3813 (calc. for $C_{36}H_{50}N_7O_6$ m/z 676.3817).

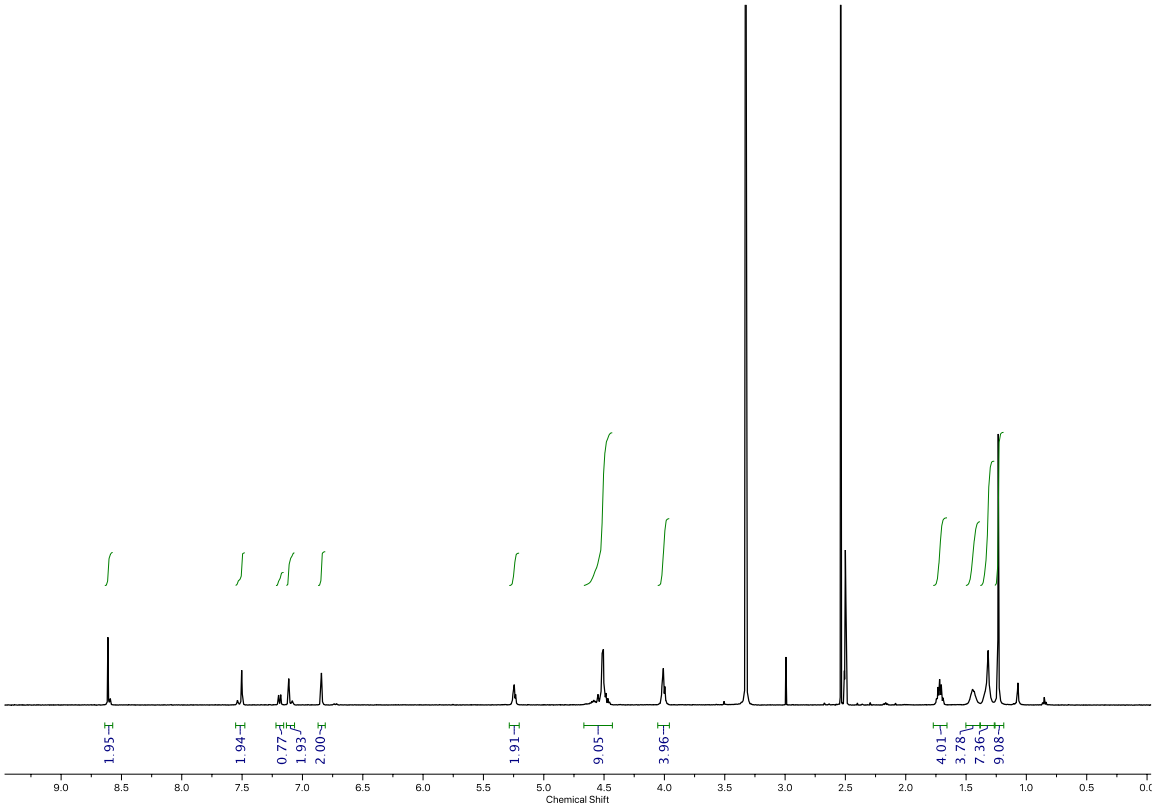

Figure 124: ^1H NMR ($CDCl_3$, 500 MHz) of **S16**.

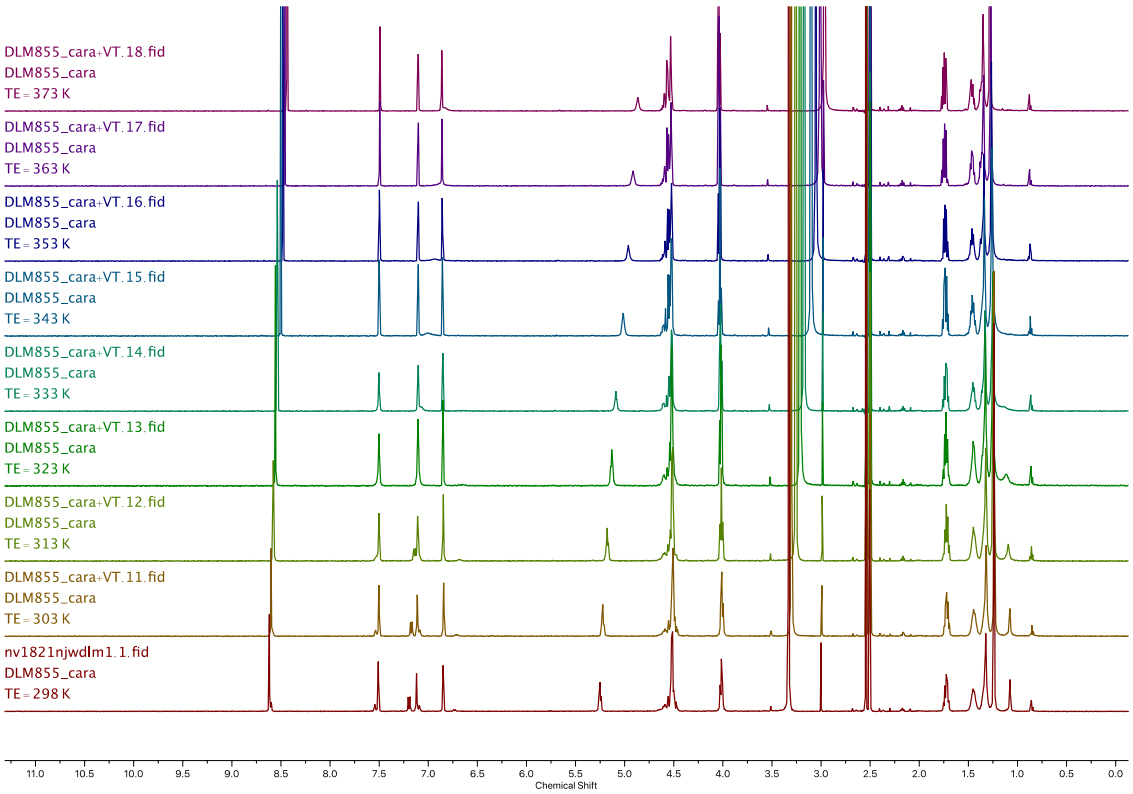

Figure 125: ^{1}H VT-NMR ($CDCl_3$, 500 MHz) of **S16**.

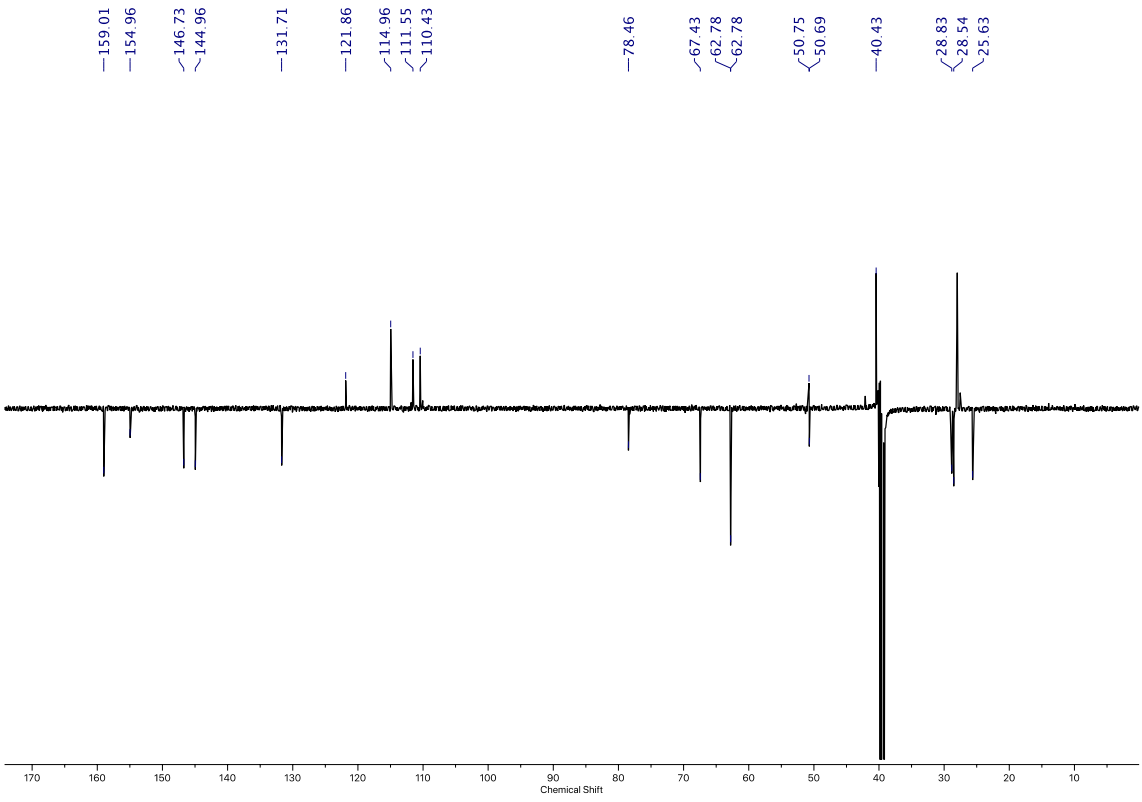

Figure 126: JMOD NMR ($CDCl_3$, 126 MHz) of **S16**.

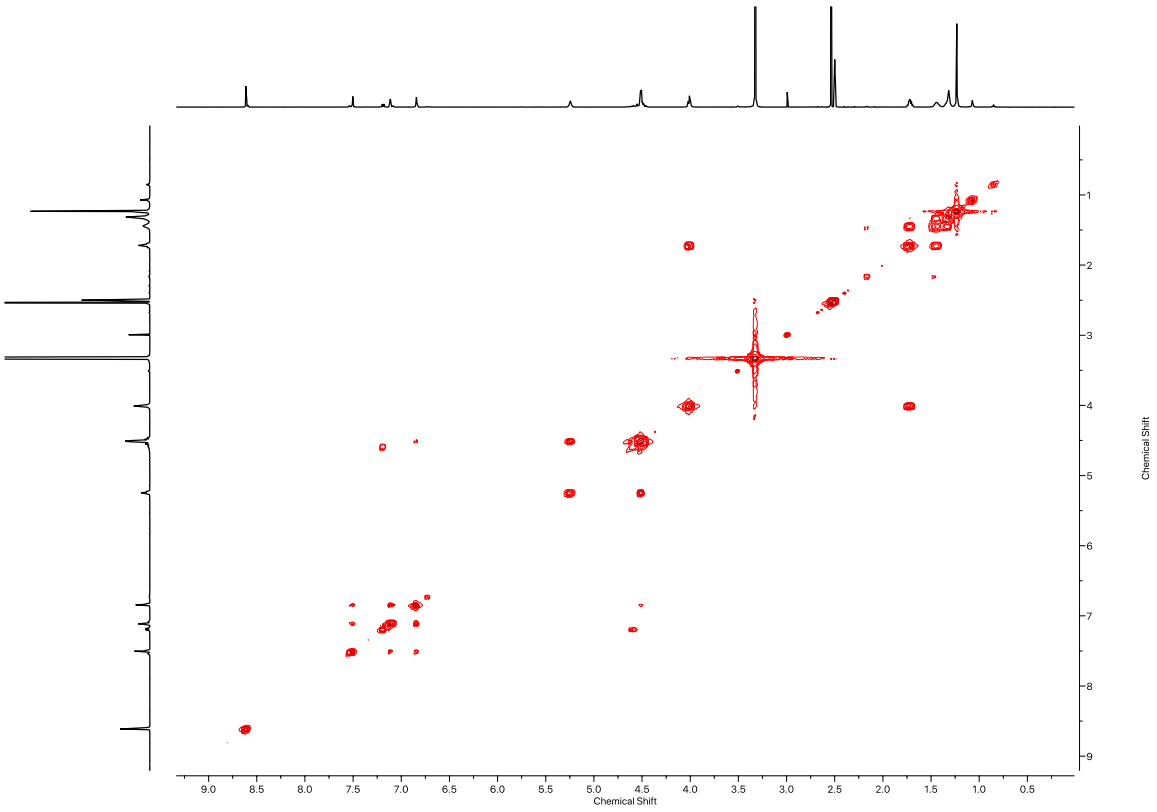

Figure 127: ^{1}H COSY NMR (DMSO, 500 MHz) of **S16**.

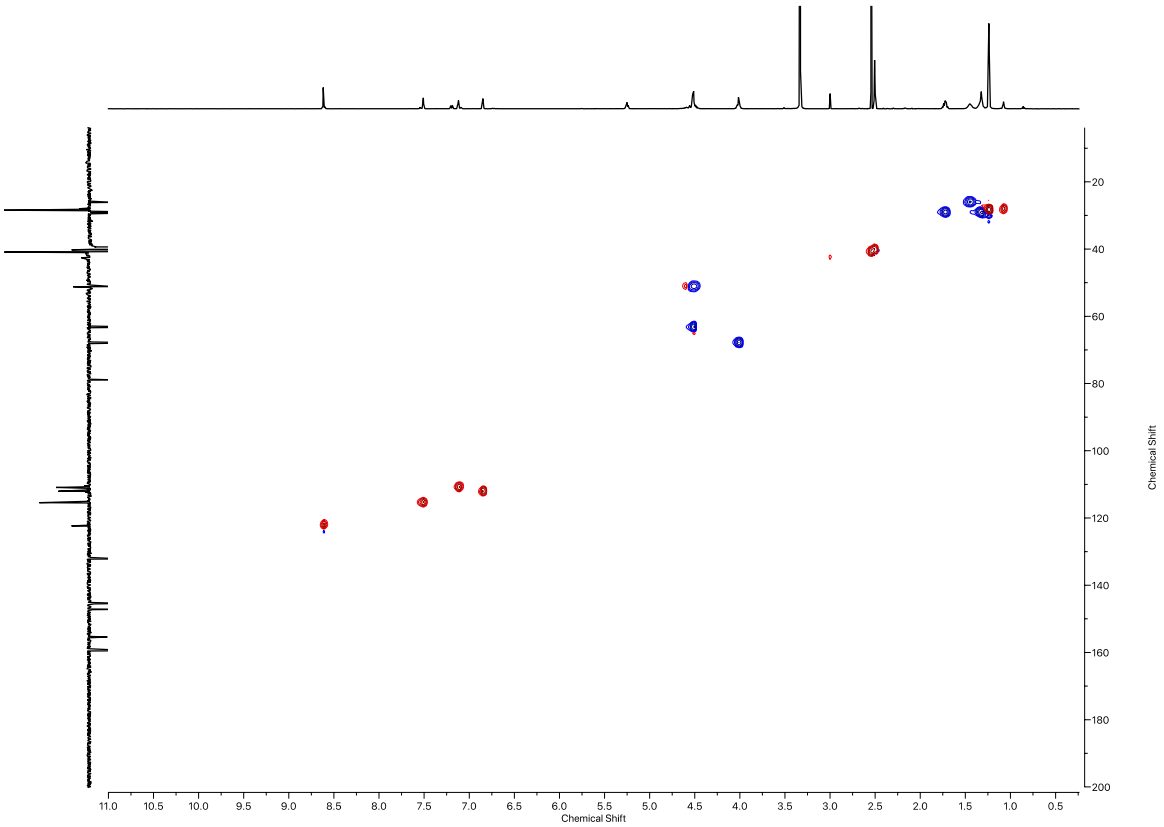

Figure 128: HSQC NMR (DMSO, 500 MHz) of **S16**.

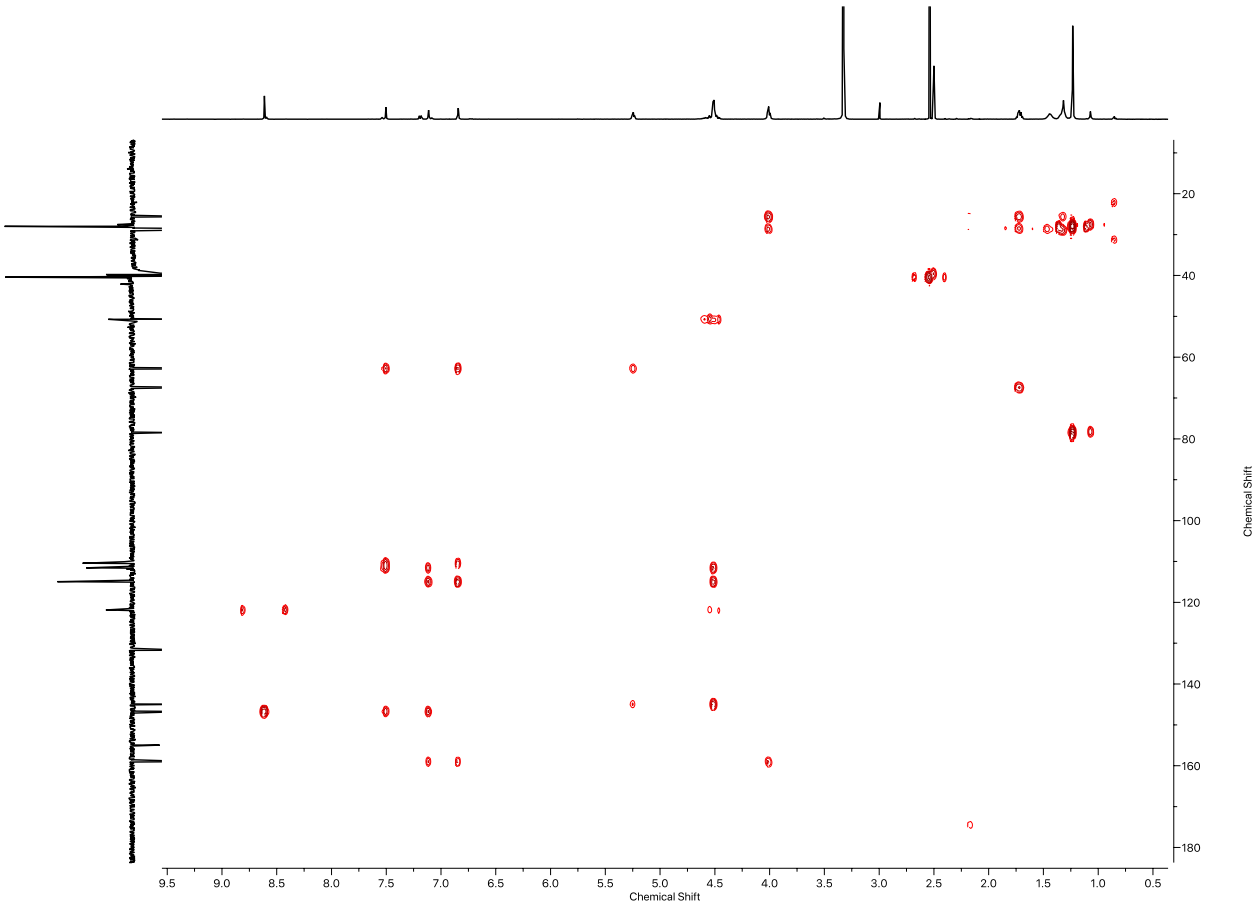

Figure 129: HMBC NMR (DMSO, 500 MHz) of **S16**.

7. Compounds leading to rotaxane half-axle (*R*)-8

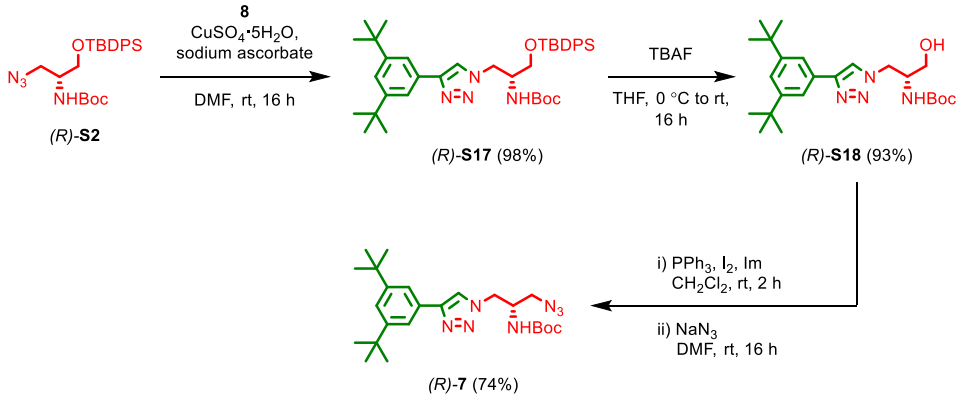

Scheme 6: Synthetic route to rotaxane half axle (*R*)-**7**.

7.1. Compound (*R*)-S17

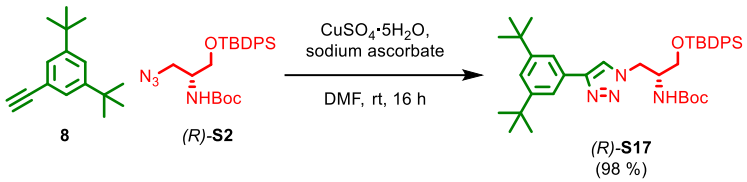

To a solution of *(R)*-**S2** (803.1 mg, 1.77 mmol, 1.0 eq.), alkyne **8** (417.6 mg, 1.95 mmol, 1.1 eq.) and sodium ascorbate (442.4 mg, 1.96 mmol,1.0 eq.) in DMF (7.4 mL) was added copper(II) sulfate pentahydrate (417.6 mg, 1.77 mmol, 1.0 eq.) and stirred at ambient temperature for 16h. The reaction mixture was diluted with EtOAc (10 mL) and washed with a saturated EDTA/NH_3 solution (10 mL). The aqueous layer was extracted with EtOAc (3 x 10 mL). The combined organic fractions were washed with 5% LiCl (3 x 5 mL), and brine (10 mL) then dried over $MgSO_4$, filtered, and concentrated *in vacuo*. The residue was purified by column chromatography (SiO_2, 1:1 petrol-Et_2O 0→20%) to yield (*R*)-**S17** as an off-white foam (1.16 g, 1.73 mmol, 98%).

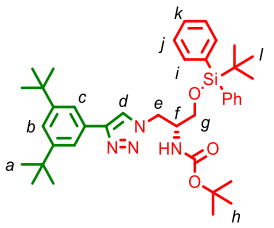

δ_H ($CDCl_3$, 400 MHz) 7.80 (s, 1H, H_d), 7.67 – 7.57 (m, 6H, H_c, H_i), 7.45 – 7.30 (m, 7H, H_b, H_j, H_k), 5.02 (d, J = 8.5, 1H, H_{NHBoc}), 4.65 (d, J = 5.6, 2H, H_e), 4.17 (br. s, 1H, H_f), 3.71 (dd, J = 10.6, 4.4, 1H, H_g), 3.52 (dd, J = 10.1, 6.0, 1H, H_g), 1.40 (s, 9H, H_h), 1.37 (s, 18H, H_a), 1.11 (s, 9H, H_l); δ_C ($CDCl_3$, 101 MHz) 151.5, 148.8, 135.7, 135.6, 132.7, 130.2, 130.2, 129.9, 128.1, 122.5, 120.9, 120.3, 62.9, 52.0, 50.4, 35.1, 31.6, 28.5, 27.1, 19.5; HR-ESI-MS (+ve) m/z = 669.4198 $[M+H]^+$ (calc. m/z for $C_{40}H_{57}N_4O_3Si$ 669.4194).

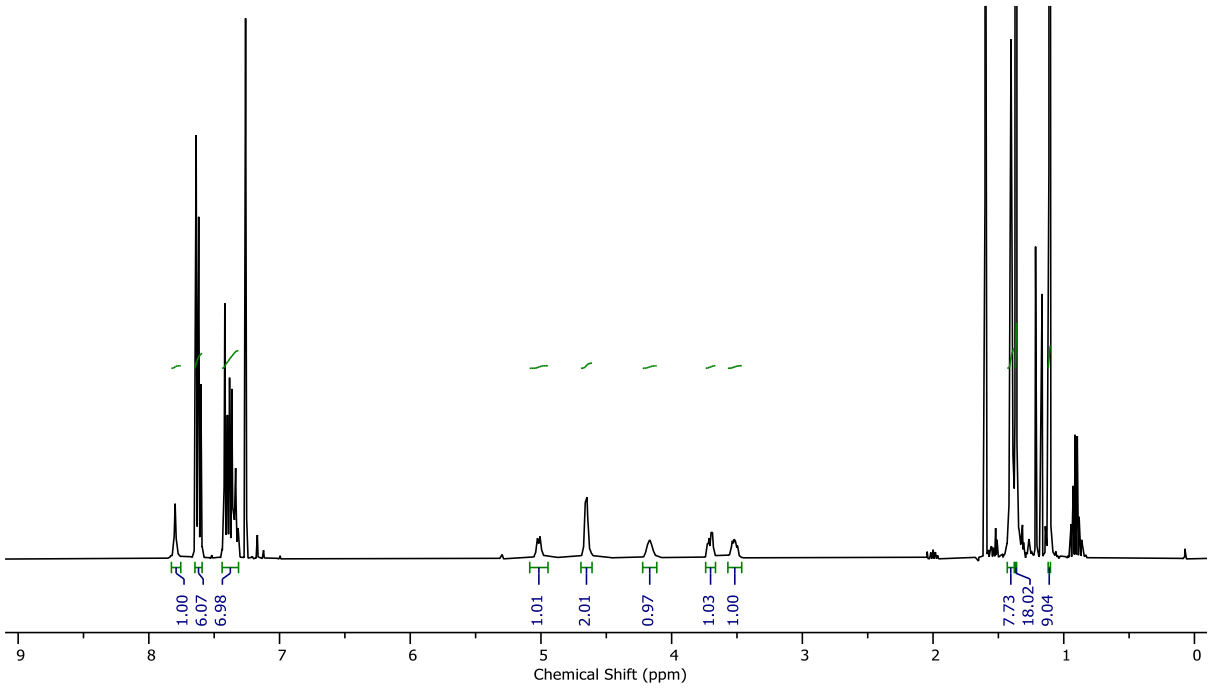

Figure 130: ^1H NMR ($CDCl_3$, 400 MHz) of (*R*)-**S17**.

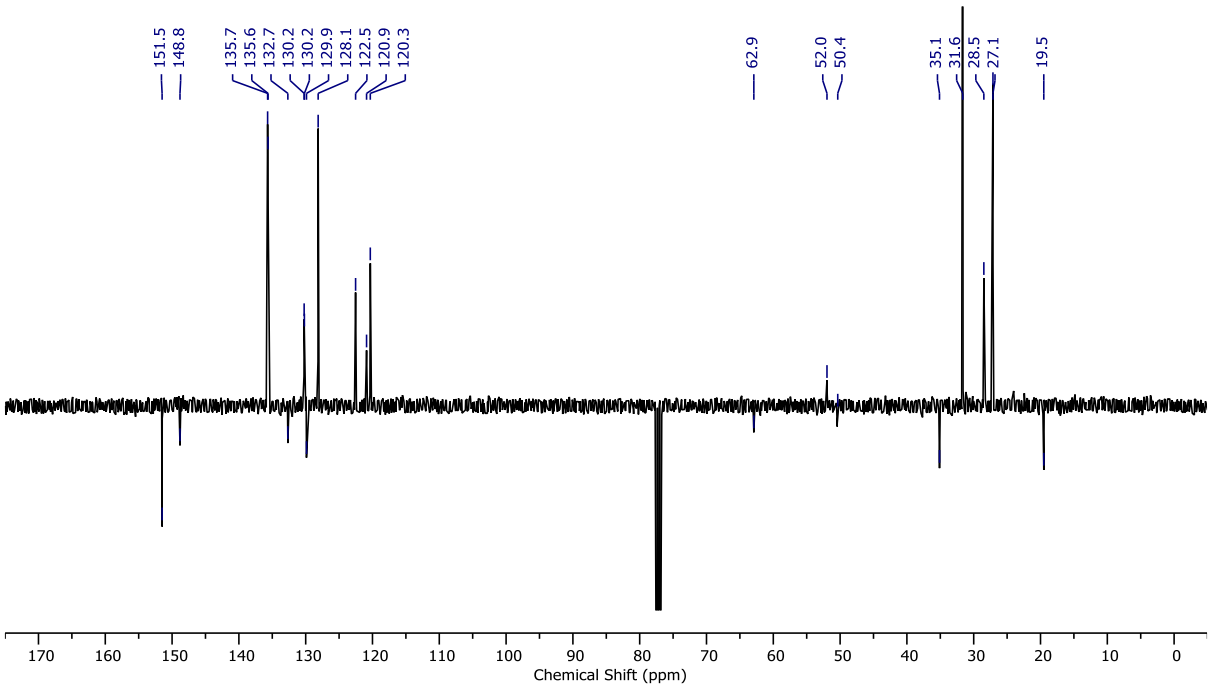

Figure 131: JMOD NMR ($CDCl_3$, 101 MHz) of (*R*)-**S17**.

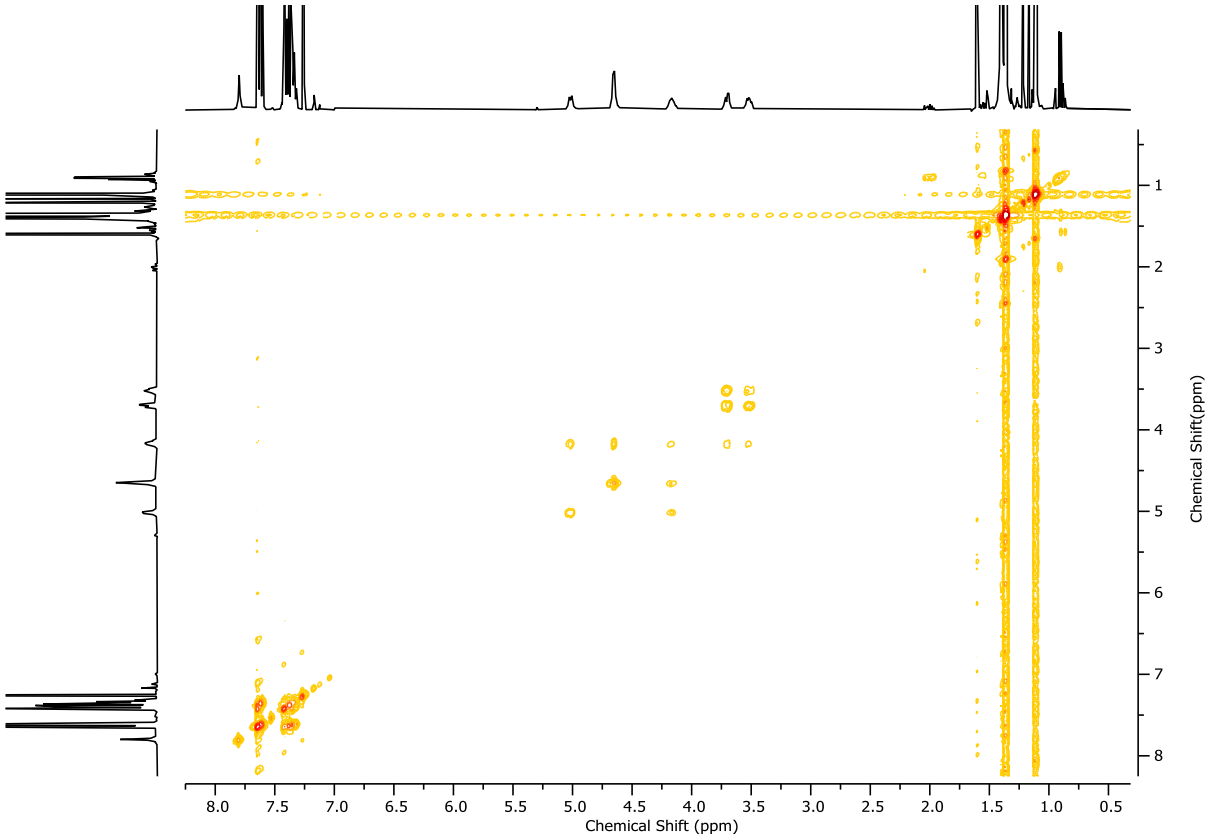

Figure 132: ^1H COSY NMR ($CDCl_3$, 400 MHz) of (*R*)-**S17**.

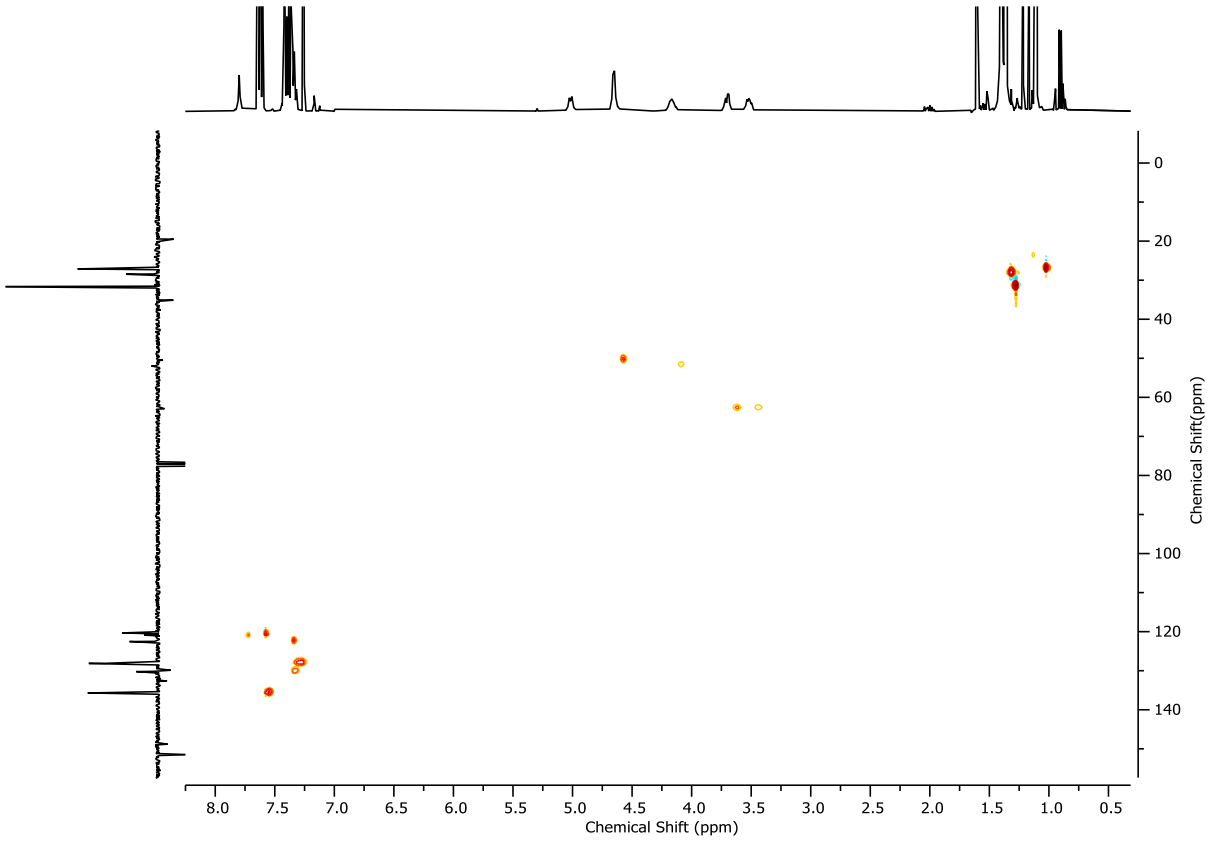

Figure 133: HSQC NMR ($CDCl_3$, 400 MHz) of (*R*)-**S17**

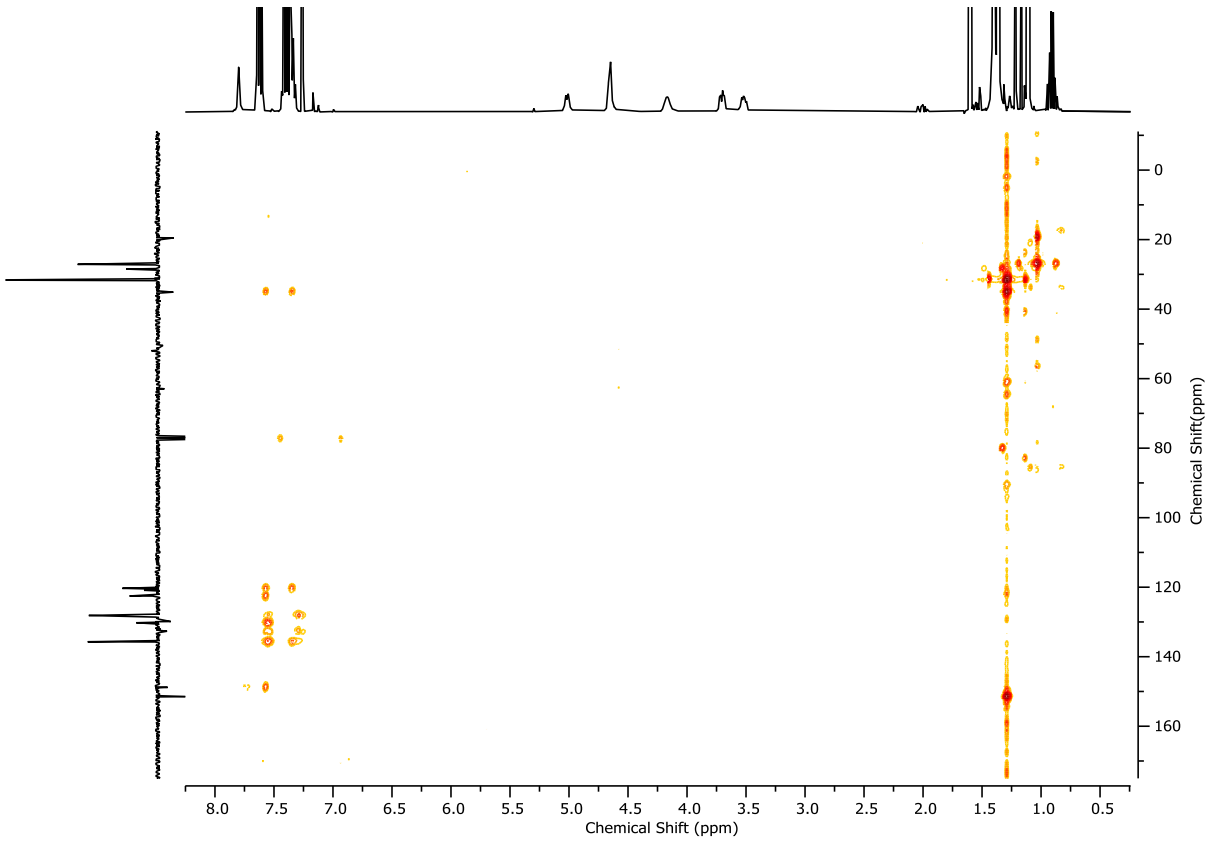

Figure 134: HMBC NMR ($CDCl_3$, 400 MHz) of (*R*)-**S17**.

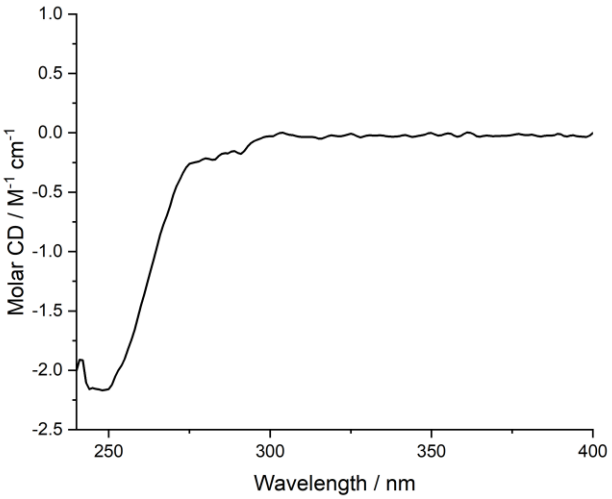

Figure 135: Circular Dichroism Spectra of (*R*)-**S17** (64 µM) at 293 K in $CHCl_3$.

7.2. Compound (*R*)-S18

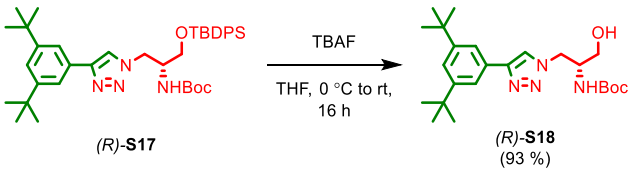

To a solution of (*R*)-**S17** (849.1 mg, 1.27 mmol, 1.0 eq.) in THF (6.3 mL) at 0 °C was added dropwise a 1.0 M solution of TBAF in THF (1.4 mL, 1.40 mmol, 1.1 eq.), and the mixture was allowed to warm to ambient temperature. After 16 h, the crude mixture was concentrated *in vacuo*, the resulting residue dissolved in EtOAc (15 mL) and washed with H_2O (10 mL). The aqueous layer was extracted with EtOAc (3 x 10 mL). The combined organic fractions were washed with brine (10 mL) then dried over $MgSO_4$, filtered, and concentrated *in vacuo*. The residue was purified by column chromatography (SiO_2, CH_2Cl_2- CH_3CN 0→20%) to yield (*R*)-**S18** (508.9 mg, 1.18 mmol, 93%) as a white solid.

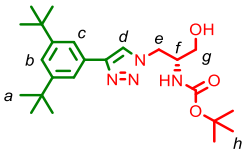

δ_H ($CDCl_3$, 400 MHz) 7.88 (s, 1H, H_d), 7.65 (d, J = 1.8, 2H, H_c), 7.42 (t, J = 1.8, 2H, H_b), 5.35 (d, J = 7.9, 1H, H_{NHBoc}), 4.70 (dd, J = 13.9, 6.4, 1H, H_e), 4.63 (dd, J = 13.9, 5.2, 1H, H_e), 4.09 – 4.00 (m, 1H, H_f), 3.75 – 3.68 (m, 1H, H_g), 3.60 – 3.53 (dd, 1H, H_g), 1.44 (s, 9H, H_h), 1.37 (s, 18H, H_a); δ_C ($CDCl_3$, 101 MHz) 155.9, 151.6, 149.0, 129.6, 123.9, 121.2, 120.3, 80.4, 61.5, 52.2, 50.0, 35.1, 31.6, 28.5; HR-ESI-MS (+ve) m/z = 431.3019 $[M+H]^+$ (calc. m/z for $C_{24}H_{39}N_4O_3$ 431.3017); Melting Point 130-133 °C.

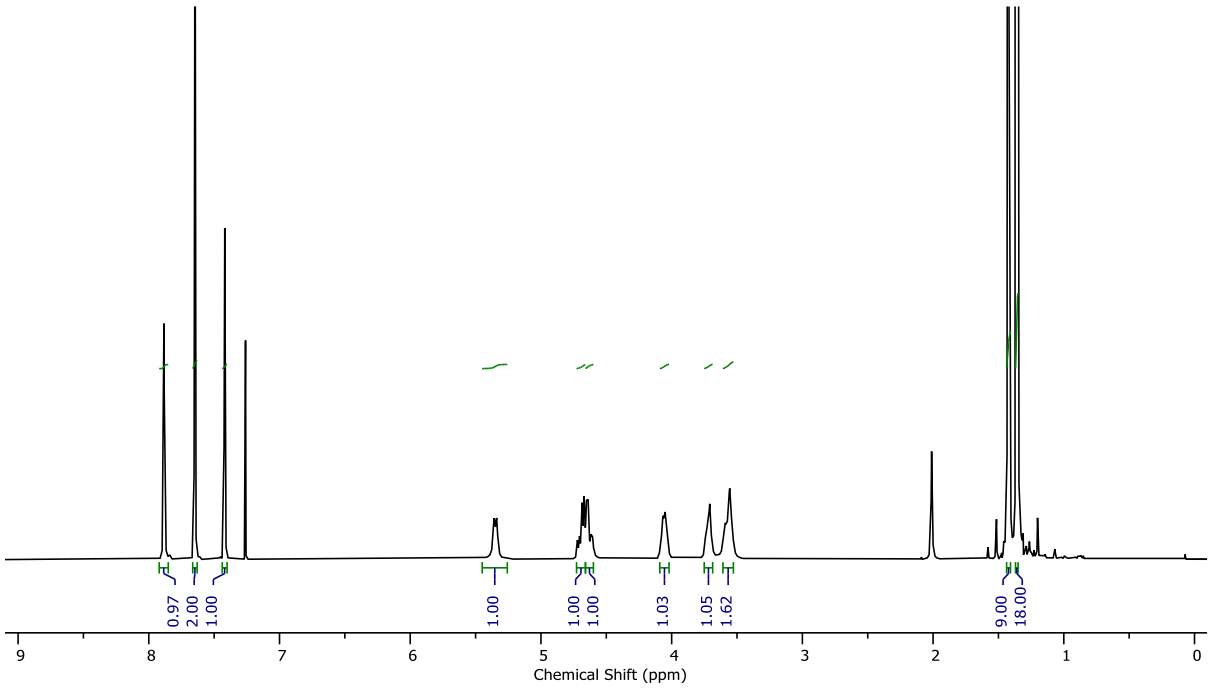

Figure 136: ^{1}H NMR ($CDCl_3$, 400 MHz) of (*R*)-**S18**.

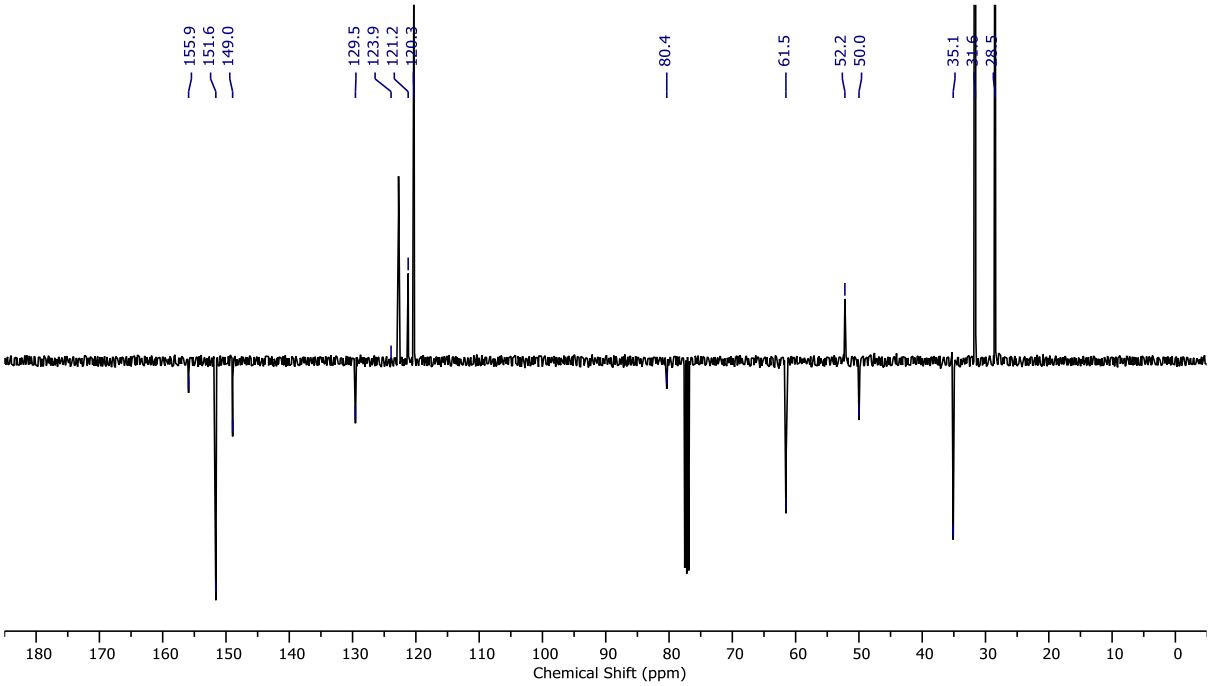

Figure 137: JMOD NMR ($CDCl_3$, 101 MHz) of (*R*)-**S18**.

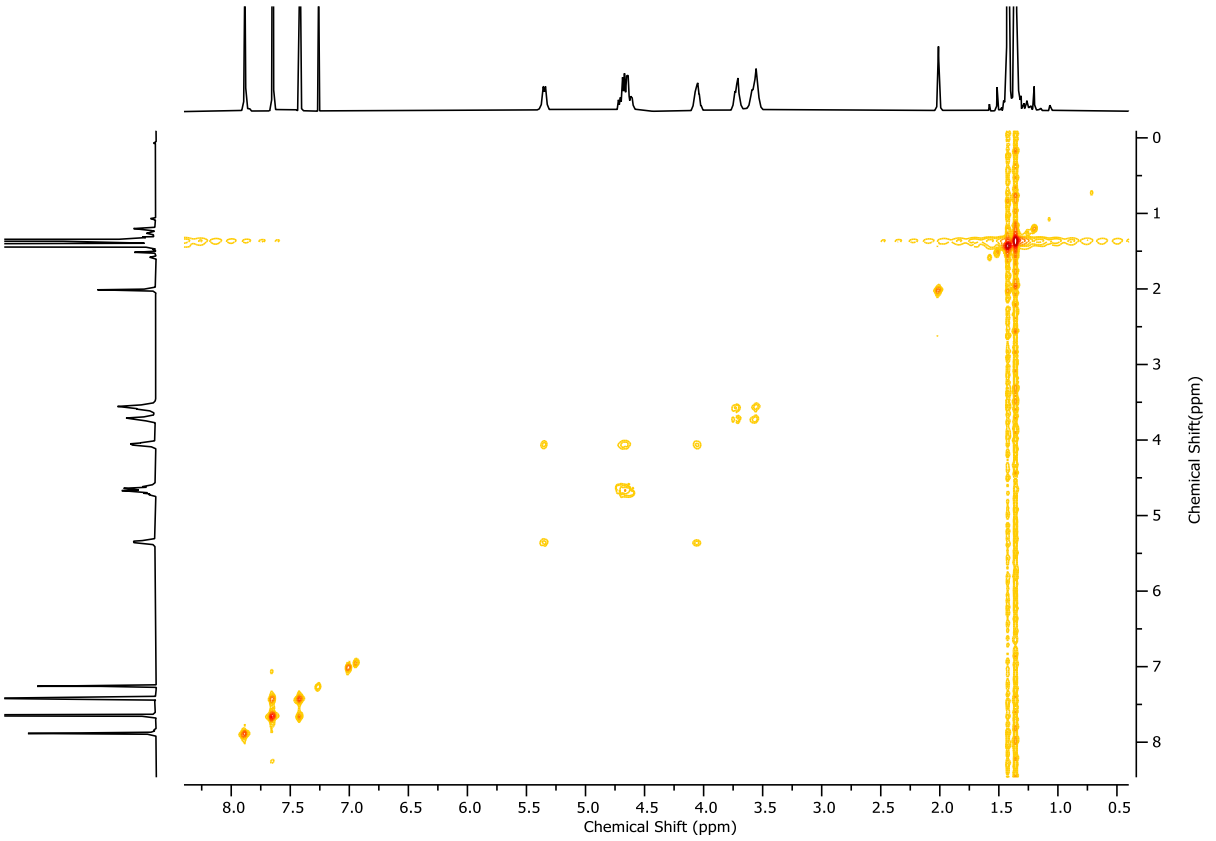

Figure 138: ^{1}H COSY NMR ($CDCl_3$, 400 MHz) of (*R*)-**S18**.

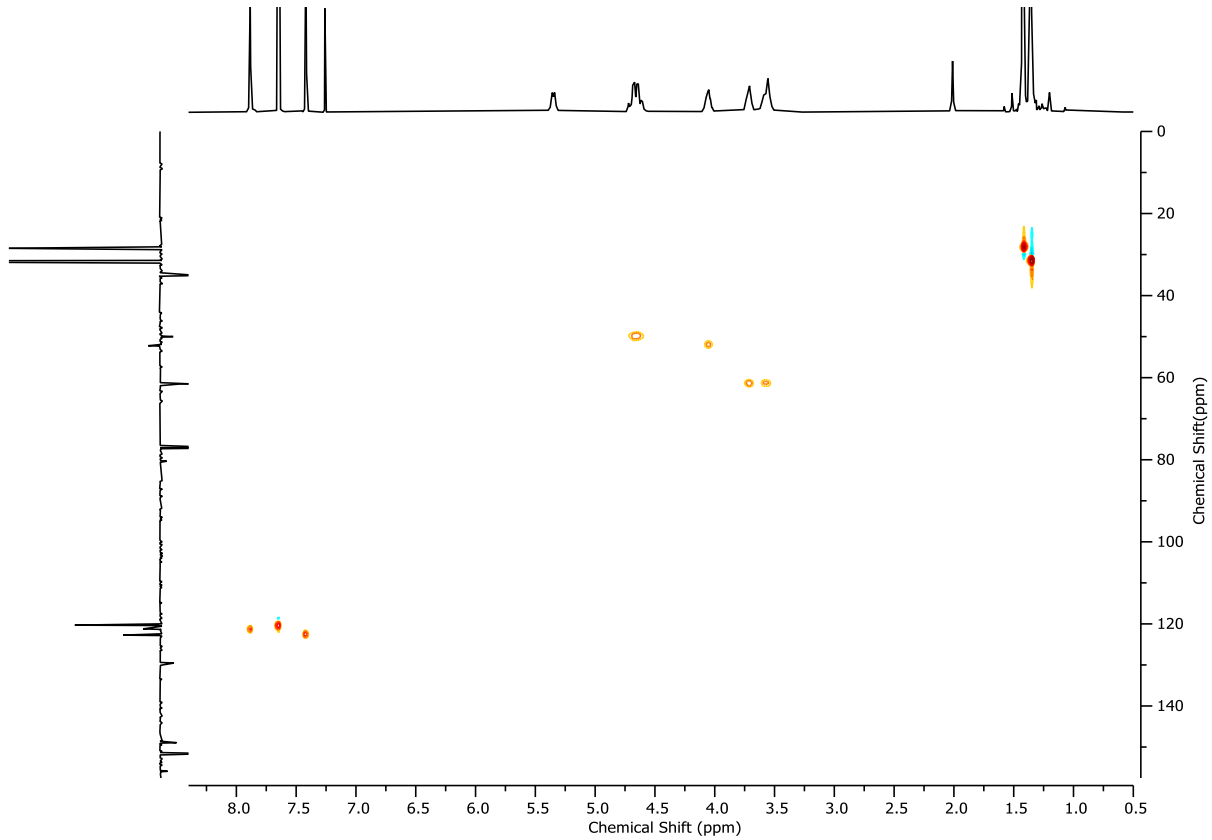

Figure 139: HSQC NMR ($CDCl_3$, 400 MHz) of (*R*)-**S18**.

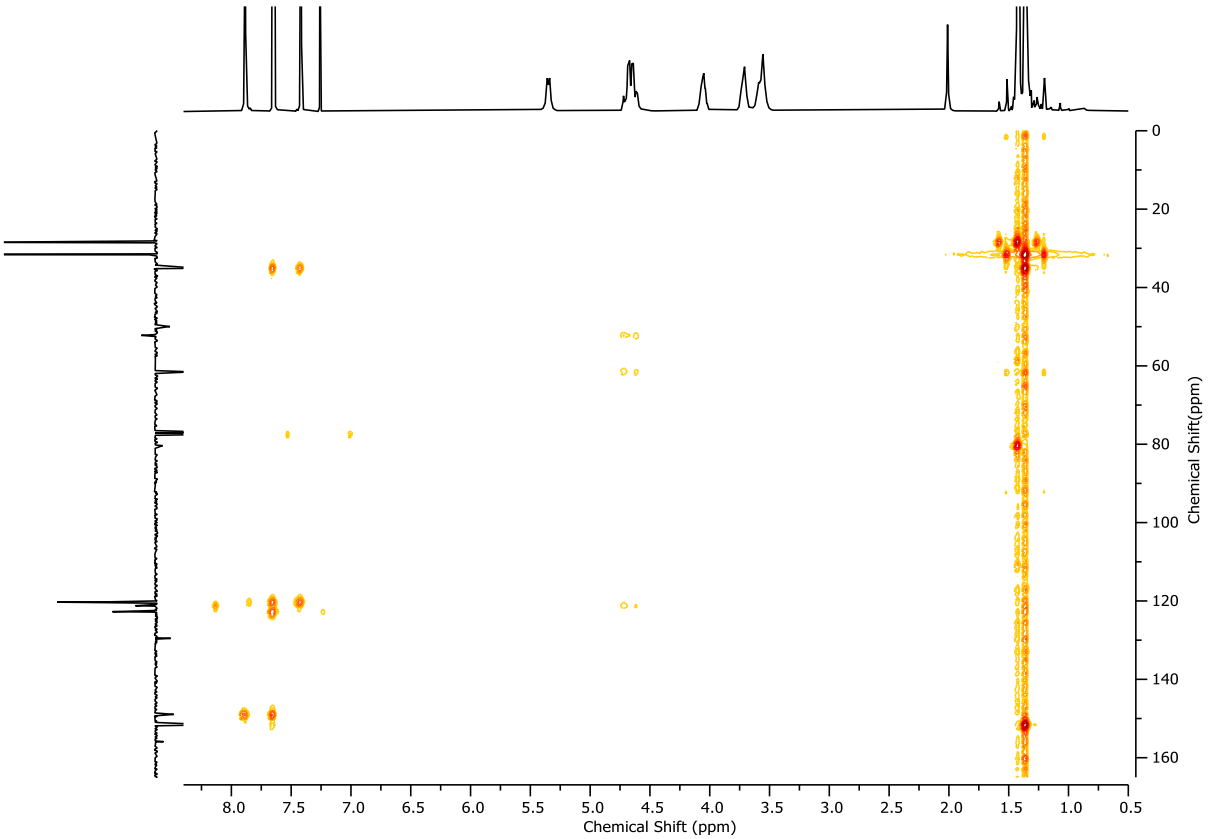

Figure 140: HMBC NMR ($CDCl_3$, 400 MHz) of (*R*)-**S18**.

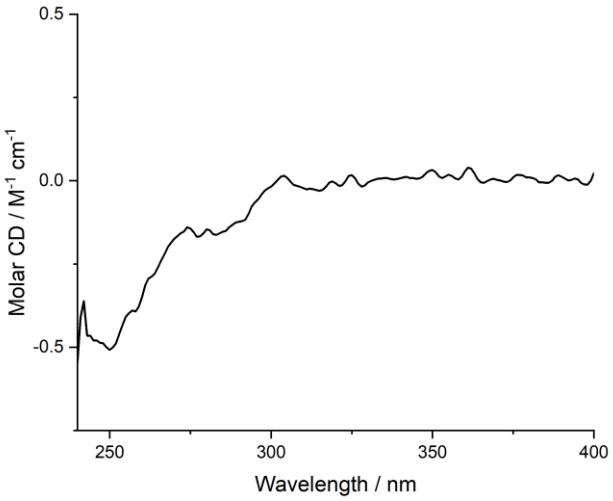

Figure 141: Circular Dichroism Spectra of (*R*)-**S18** (46 µM) at 293 K in $CHCl_3$.

7.3. Rotaxane half-axle (*R*)-7

(*R*)-**S18** (*R*)-**7** (74%) >99% *ee*

To a solution of PPh_3 (216.0 mg, 0.82 mmol, 3.0 eq.) and imidazole (99.4 mg, 1.46 mmol, 5.0 eq.) in CH_2Cl_2 (1.8 mL) was added I_2 (207.3 mg, 0.82 mmol, 3.0 eq.) in 1 portion at 0 °C. After stirring for 10 min, a solution of (*R*)-**S18** (118.1 mg, 0.27 mmol, 1.0 eq.) in CH_2Cl_2 (1.0 mL) was added dropwise. The reaction mixture was allowed to warm to ambient temperature and stirred for 2 h. The crude mixture was filtered through Celite®, washing with CH_2Cl_2, and concentrated *in vacuo*. The residue was purified by column chromatography (SiO_2, petrol-EtOAc 0→10%). The resultant oil was immediately dissolved in DMF (1.3 mL) and NaN_3 (155.3 mg, 2.39 mmol, 8.9 eq.) was added. After stirring for 16 h at ambient temperature, the reaction mixture was diluted with EtOAc (10 mL) and washed with H_2O (10 mL). The aqueous layer was extracted with EtOAc (3 x 10 mL). The combined organic fractions were washed with 5% LiCl (2 x 15 mL), and brine (15 mL) then dried over $MgSO_4$, filtered, and concentrated *in vacuo*. The residue was purified by column chromatography (SiO_2, petrol-EtOAc 0→20%) to yield (*R*)-**7** (93.1 mg, 0.20 mmol, 74%) as an off-white foam.

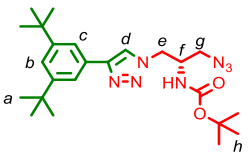

δ_H ($CDCl_3$, 400 MHz) 7.82 (s, 1H, H_d), 7.67 (d, J = 1.8, 2H, H_c), 7.42 (t, J = 1.8, 1H, H_b), 5.19 (d, J = 8.3, 1H, H_{NHBoc}), 4.59 (d, J = 5.6, 2H, H_e), 4.23 – 4.10 (m, 1H, H_f), 3.55 (dd, J = 12.4, 5.1, 1H, H_g), 3.33 (dd, J = 12.4, 6.4, 1H, H_g), 1.43 (s, 9H, H_h), 1.37 (s, 18H, H_a); δ_C ($CDCl_3$, 101 MHz) 155.2, 151.6, 149.0, 129.5, 122.8, 121.0, 120.3, 80.7, 51.3, 50.4, 50.3, 35.1, 31.6, 28.4; HR-ESI-MS (+ve) m/z = 456.3082 $[M+H]^+$ (calc. m/z for $C_{24}H_{38}N_7O_2$ 456.3081).

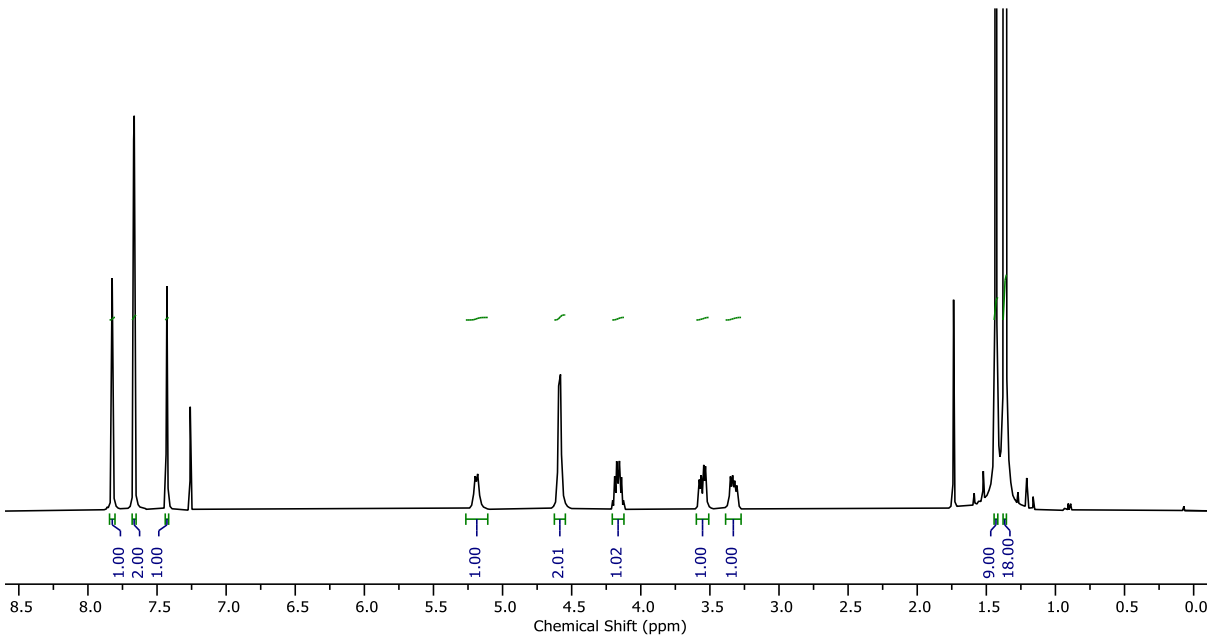

Figure 142: ^1H NMR ($CDCl_3$, 400 MHz) of (*R*)-**7**.

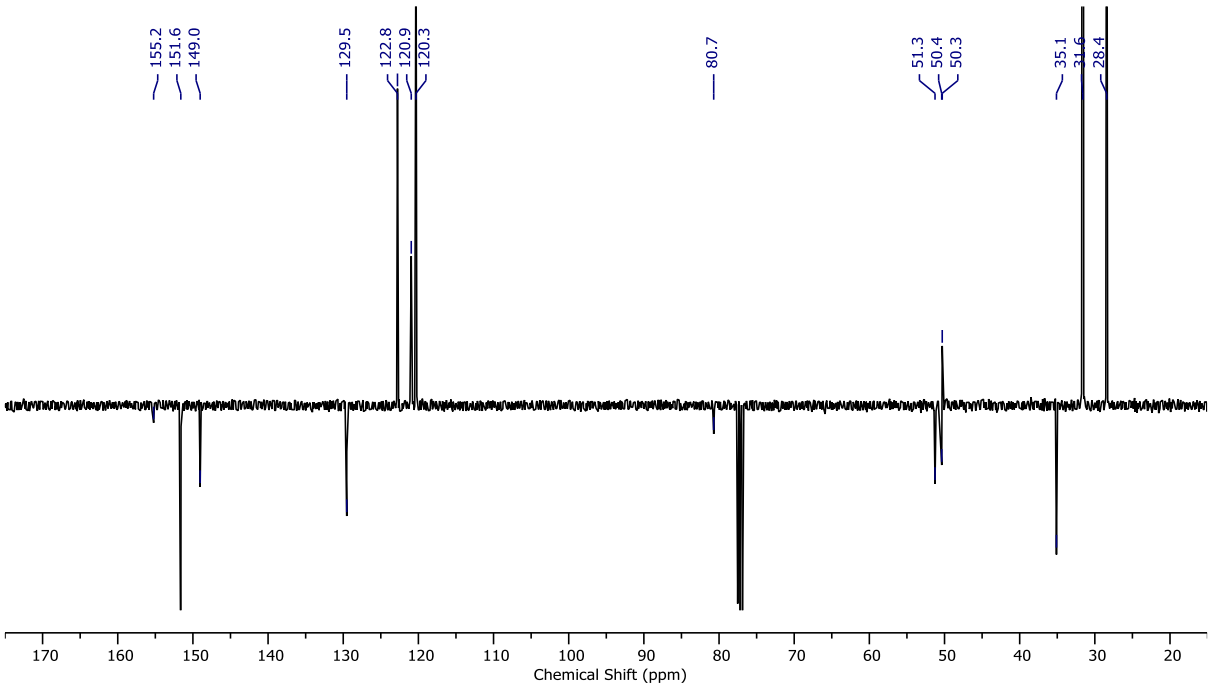

Figure 143: JMOD NMR ($CDCl_3$, 101 MHz) of (*R*)-**7**.

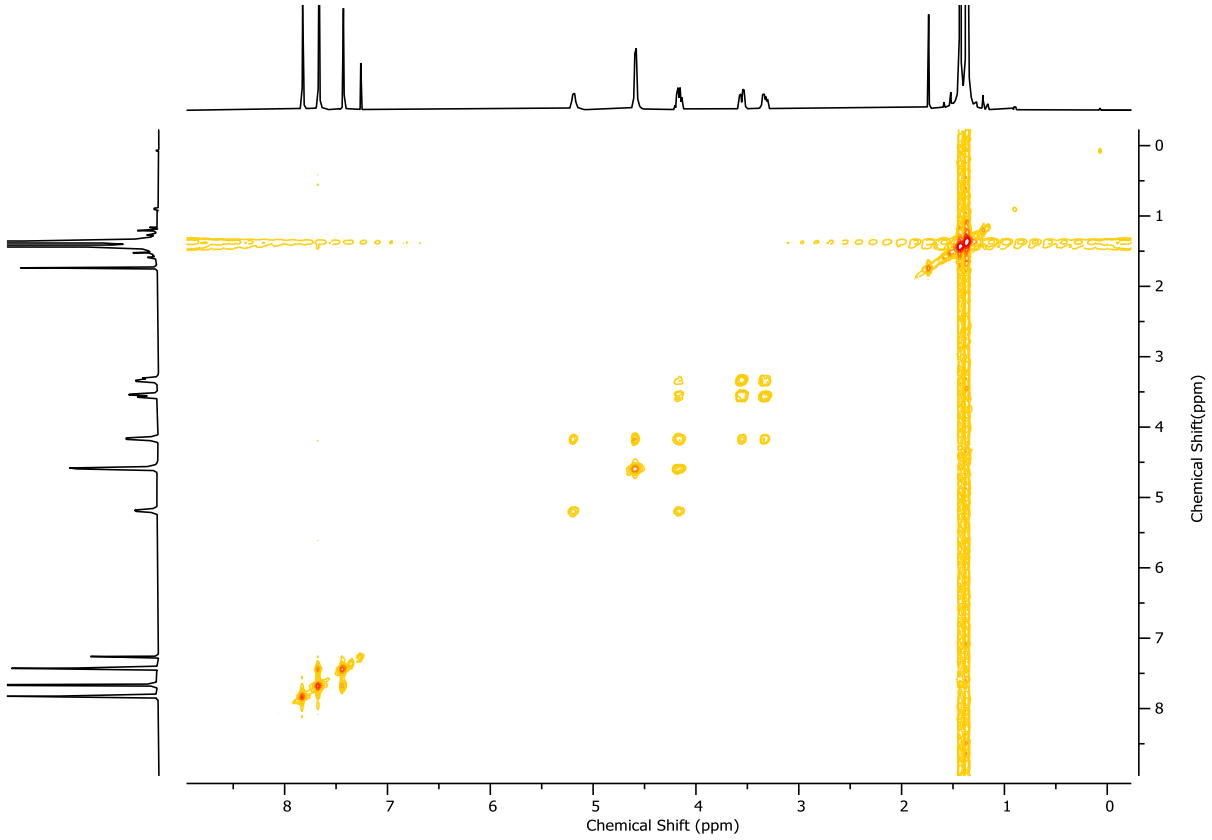

Figure 144: ^1H COSY NMR ($CDCl_3$, 400 MHz) of (*R*)-**7**.

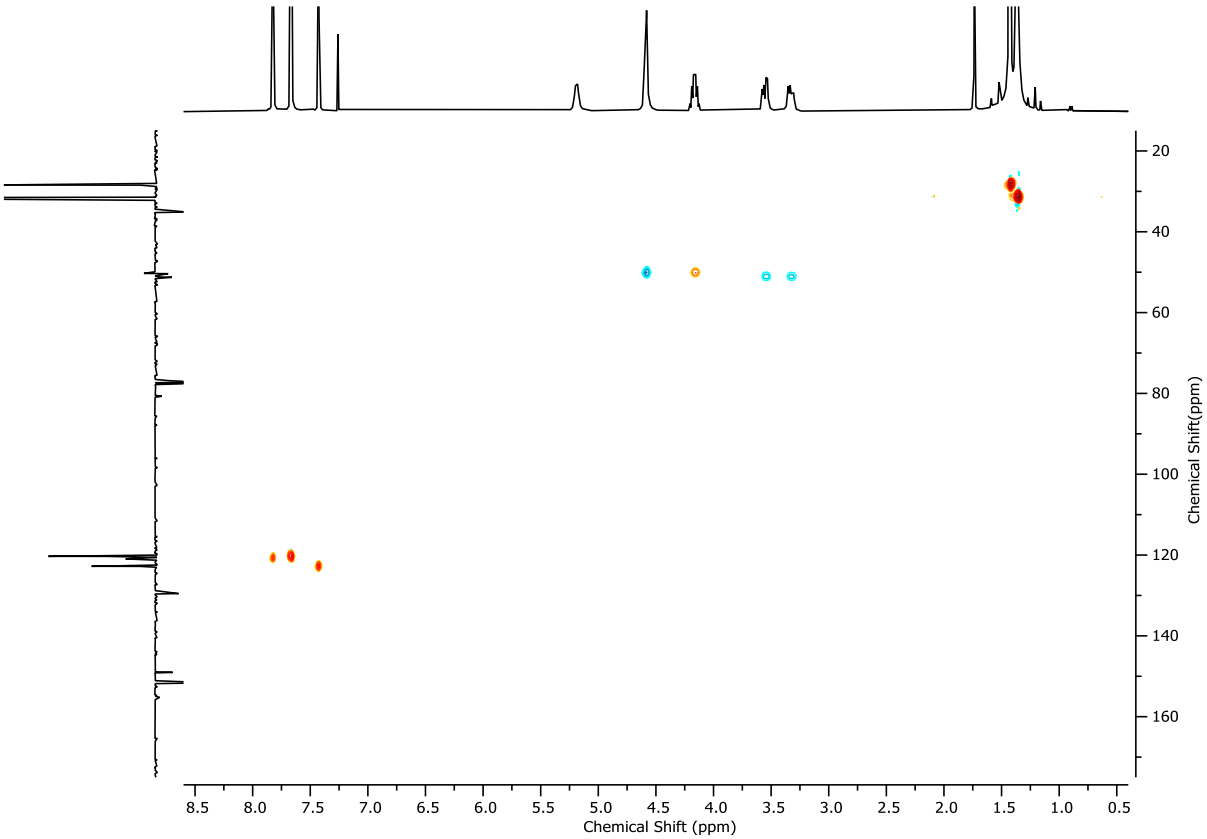

Figure 145: HSQC NMR ($CDCl_3$, 400 MHz) of (*R*)-**7**.

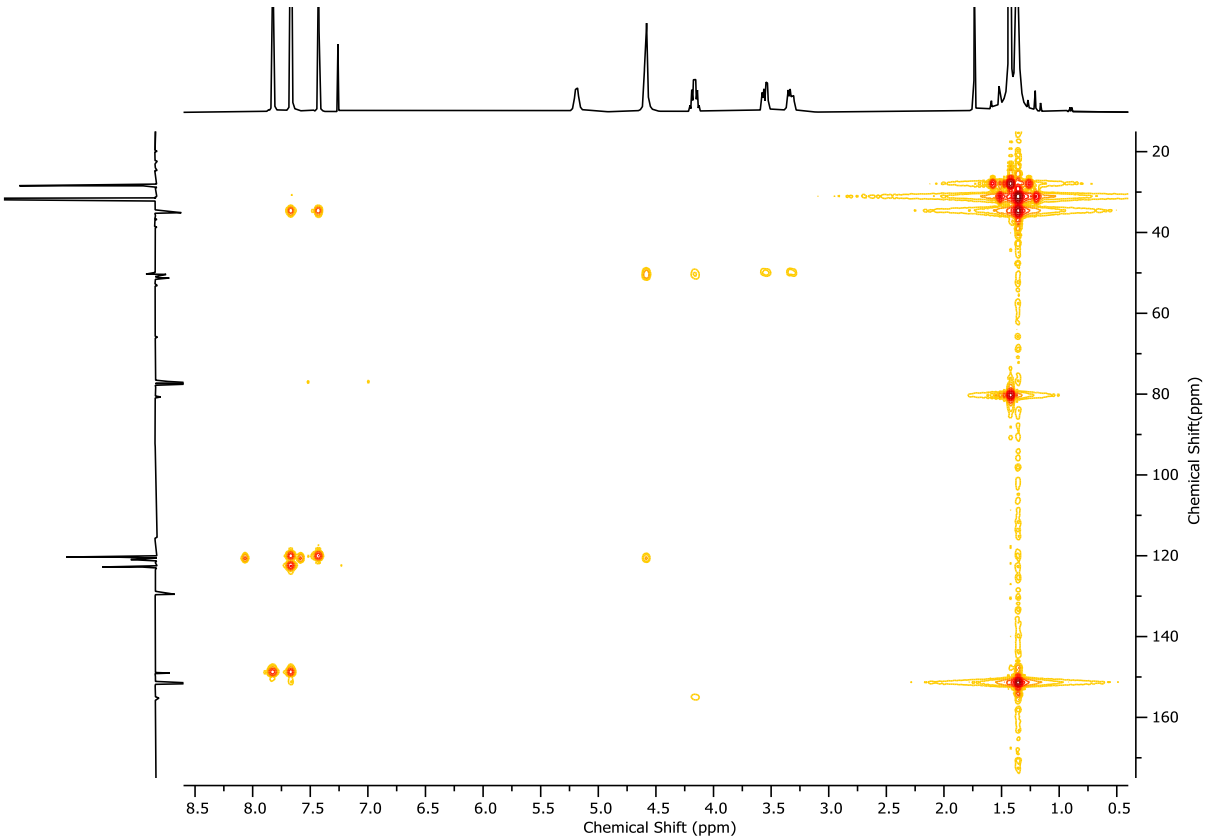

Figure 146: HMBC NMR ($CDCl_3$, 400 MHz) of (*R*)-**7**.

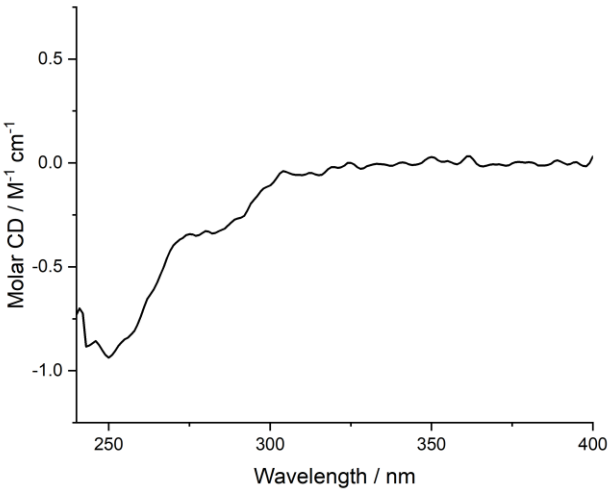

Figure 147: Circular Dichroism Spectra of (*R*)-**7** (41 μM) at 293 K in $CHCl_3$.

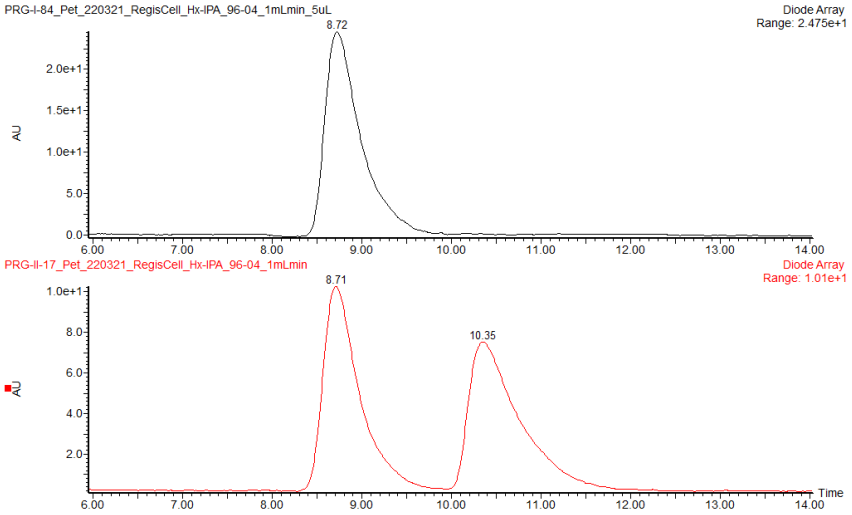

Figure 148: CSP-HPLC of (*R*)-**7** (loaded in Et_2O). RegisCell, *n*-hexane-EtOH 98 : 2, flowrate 1 $mLmin^{-1}$. (top) (*R*)-**7** (8.72 min, 11538817, >99.9%), (*S*)-**7** (not observed). (bottom) *rac*-**7**, (*R*)-**7** (8.71 min, 4729977, 50.1%), (*S*)-**7** (10.35 min, 4710027, 49.9%).

8. Synthesis of rotaxanes (S_{ma},$R_{co\text{-}c}$)-10 and (R_{ma},$R_{co\text{-}c}$)-10

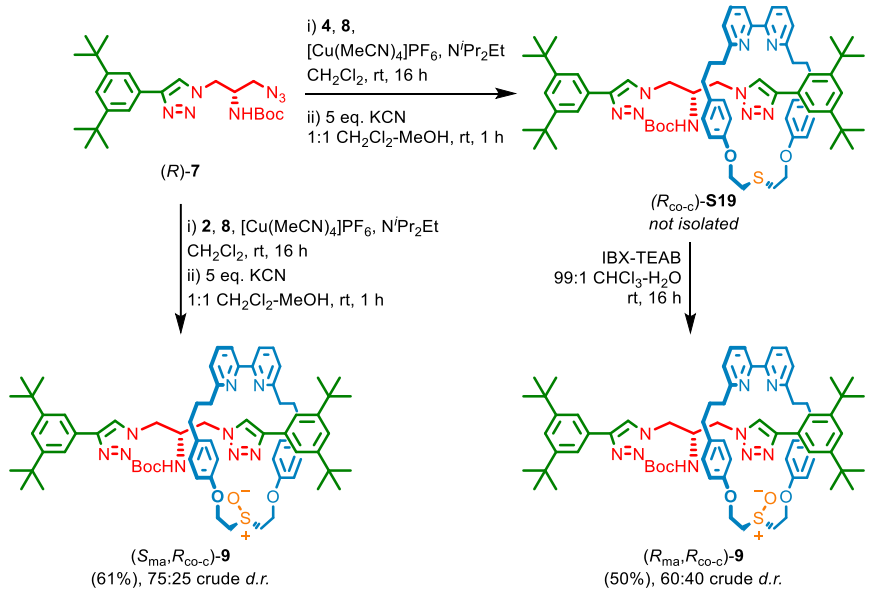

Scheme 7: Synthetic route to mechanically axially chiral epimeric catenanes (R_{ma},$R_{co\text{-}c}$)-**9** and (S_{ma},$R_{co\text{-}c}$)-**9**.

8.1. Rotaxane (S_{ma},$R_{co\text{-}c}$)-9

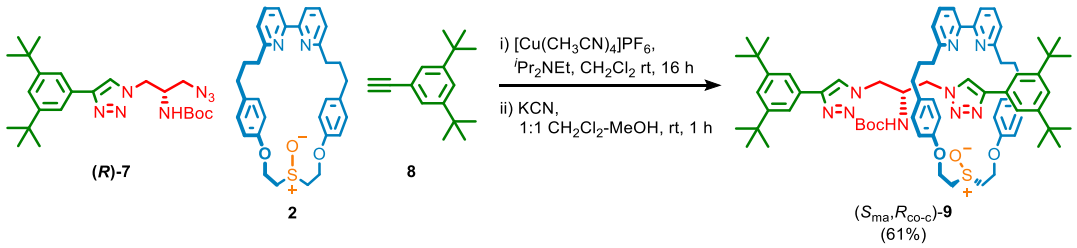

A CEM MW vial was charged with alkyne **8** (18.7 mg, 0.087 mmol, 1.1 eq.), azide (*R*)-**7** (38.3 mg, 0.084 mmol, 1.1 eq.), macrocycle **2** (40.2 mg, 0.076 mmol, 1.0 eq.) and $[Cu(CH_3CN)_4]PF_6$ (27.7 mg, 0.074 mmol, 0.97 eq.) and purged with N_2. CH_2Cl_2 (1.9 mL) and $^{i}Pr_2NEt$ (26 µL, 0.15 mmol, 2.0 eq.) were added and the resulting deep red solution was stirred at ambient temperature for 16 h. Then, MeOH (1.9 mL) and KCN as a solid (25 mg, 0.38 mmol, 5.0 eq.) were added and the resulting mixture was stirred vigorously for 1 h. The crude mixture was diluted with CH_2Cl_2 (5 mL) and washed with H_2O in two portions (10 mL and 5 mL). The combined aqueous phase was then extracted with CH_2Cl_2 (3 x 5 mL) and the combined organics were washed with brine (10 mL), dried over $MgSO_4$ and concentrated *in vacuo*. The residue was purified by column chromatography (SiO_2, petrol-EtOAc 0→50% then petrol-EtOAc (1:1) with MeOH 0→5%) to yield (S_{ma},$R_{co\text{-}c}$)-**9** (55.3 mg, 0.046 mmol, 61%) as a white foam. See 8.2 for a discussion of stereochemical assignment.

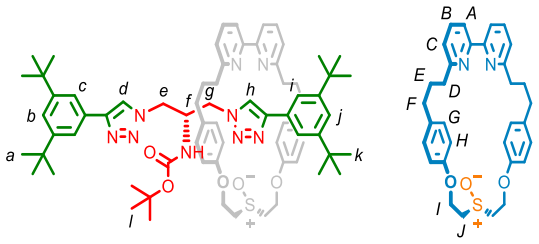

δ_H ($CDCl_3$, 400 MHz) 9.41 (s, 1H, H_h), 7.73 (s, 1H, H_d), 7.67 (d, J = 1.6, 2H, H_c), 7.63 (app. td, J = 8.3, 7.8, 2H, H_B), 7.55 (d, J = 1.8, 2H, H_i), 7.45 (dd, J = 7.7, 0.9, 2H, H_A), 7.40 (t, J = 1.8, 1H, H_b), 7.28 (t, J = 1.8, 1H, H_j), 7.16 – 7.09 (m, 2H, H_C), 6.69 – 6.61 (m, 8H, H_G, H_H), 5.35 (d, J = 6.6, 1H, H_{NHBoc}), 4.74 – 4.63 (m, 2H, H_I), 4.62 – 4.54 (m, 2H, H_I), 4.11 – 3.98 (m, 3H, H_J, H_e), 3.90 (app. q, J = 7.7, 1H, H_e), 3.76 – 3.67 (m, 2H, H_f, H_g), 3.64 – 3.54 (m, 1H, H_g), 3.27 – 3.14 (m, 2H, H_J), 2.60 – 2.50 (m, 2H, H_F), 2.49 – 2.33 (m, 6H, H_D, H_F), 1.83 – 1.65 (m, 4H, H_E), 1.37 (s, 18H, H_a), 1.25 (s, 9H, H_l), 1.22 (s, 18H, H_k); δ_C ($CDCl_3$, 101 MHz) 162.9, 162.9, 157.6, 157.6, 156.0, 155.9, 151.4, 150.9, 148.4, 147.4, 137.2, 133.8, 133.6, 132.3, 132.2, 132.1, 132.1, 130.6, 130.1, 129.5, 129.4, 128.8, 128.6, 122.3, 122.0, 121.6, 120.5, 120.3, 120.0, 79.9, 60.9, 60.9, 53.2, 53.1, 51.1, 50.5, 50.3, 37.2, 37.1, 35.1, 35.0, 34.9, 34.8, 31.7, 31.5, 31.4, 31.0, 30.4, 29.9, 28.4; LR-ESI-MS (+ve) m/z = 1196.7 $[M+H]^+$.

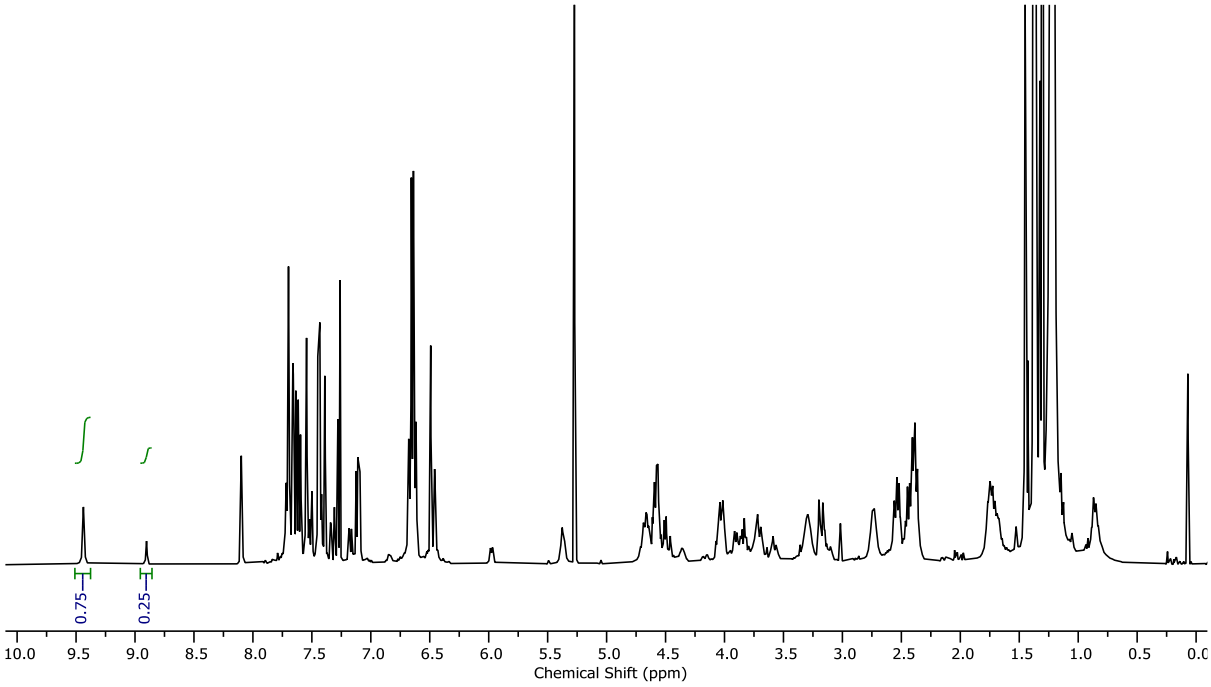

Figure 149: Crude ^{1}H NMR of **9** *via* AT-CuAAC reaction of macrocycle **3** ($CDCl_3$, 400 MHz). Diastereoisomer integration: $\boldsymbol{H}_h$ protons (major 9.44 ppm, 0.75, minor 8.89 ppm, 0.25).

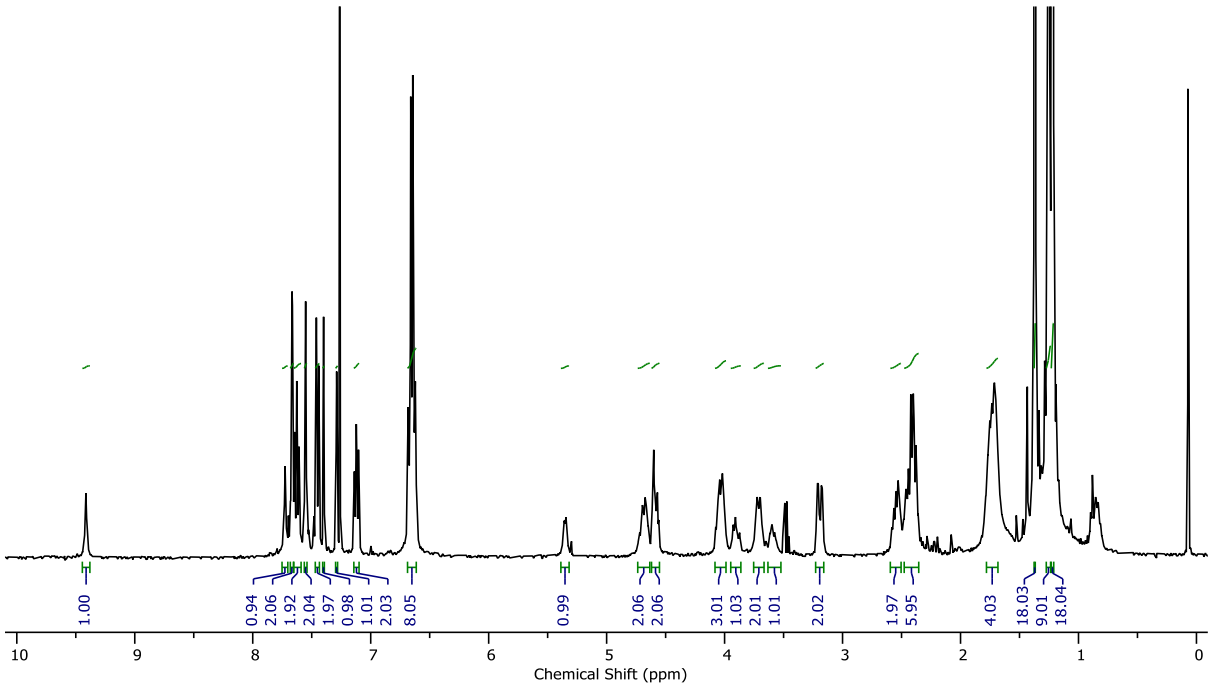

Figure 150: ^{1}H NMR ($CDCl_3$, 400 MHz) of (S_{ma},$R_{co\text{-}c}$)-**9**.

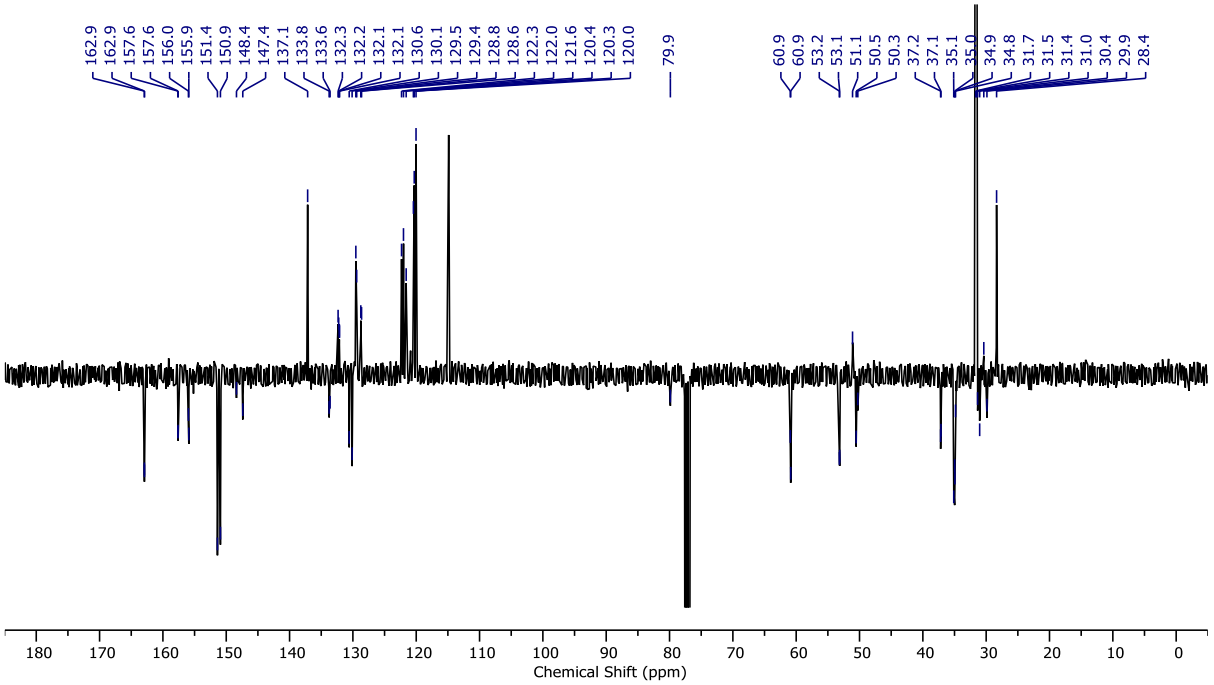

Figure 151: JMOD NMR ($CDCl_3$, 101 MHz) of (S_{ma},$R_{co\text{-}c}$)-**9**.

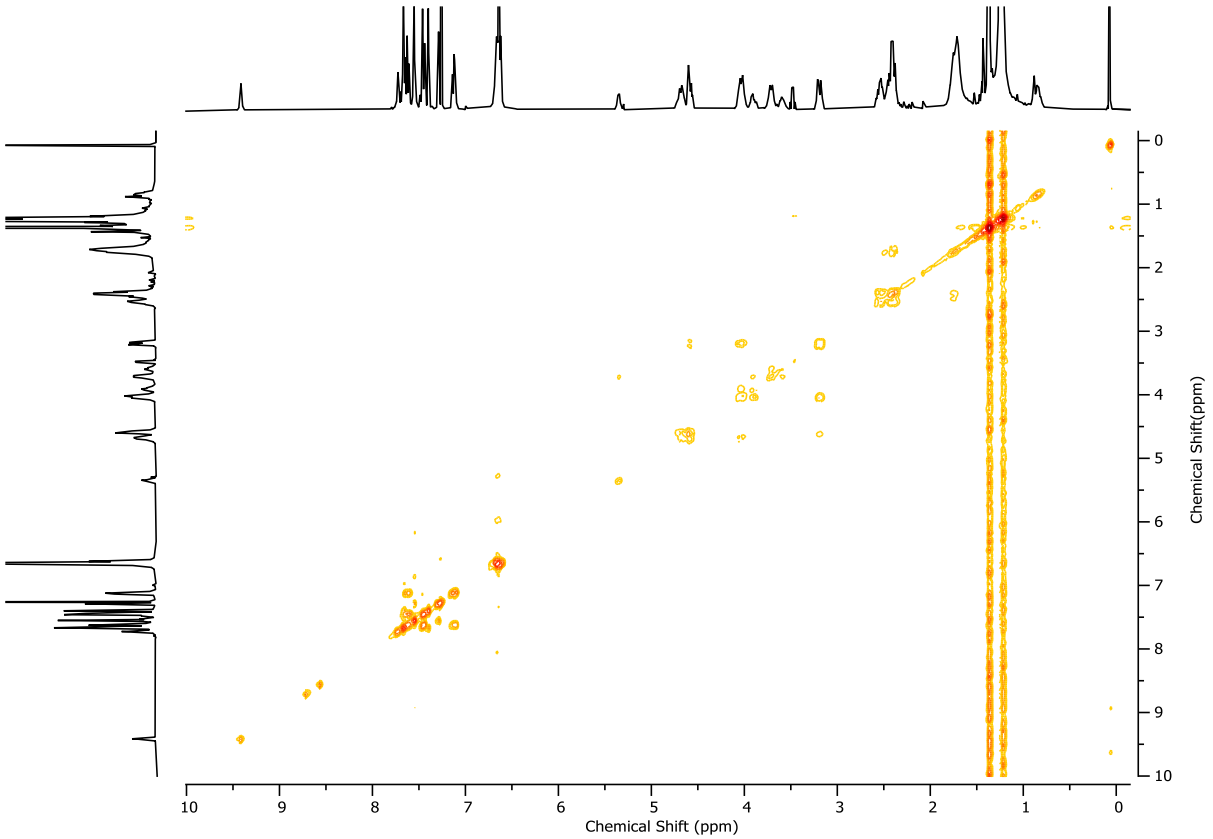

Figure 152: ^{1}H COSY NMR ($CDCl_3$, 400 MHz) of (S_{ma},$R_{co\text{-}c}$)-**9**.

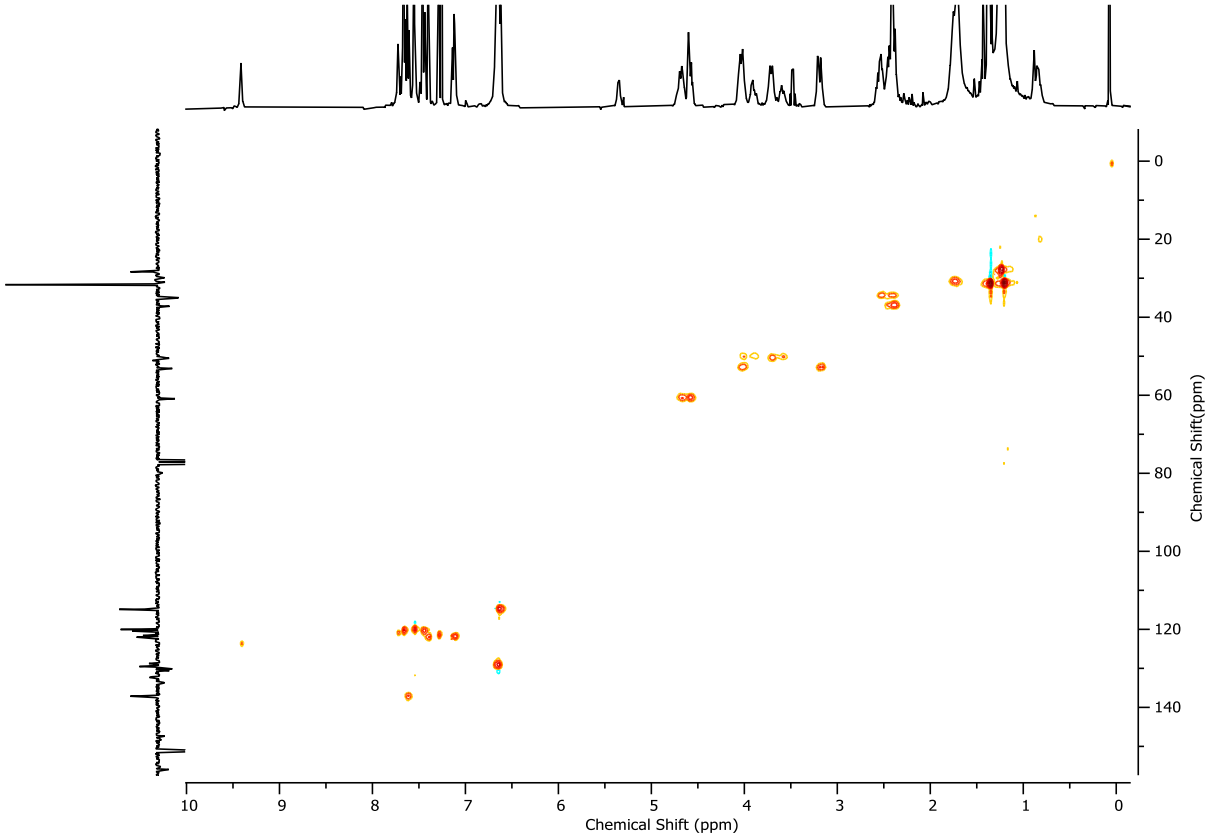

Figure 153: HSQC NMR ($CDCl_3$, 400 MHz) of (S_{ma},$R_{co\text{-}c}$)-**9**.

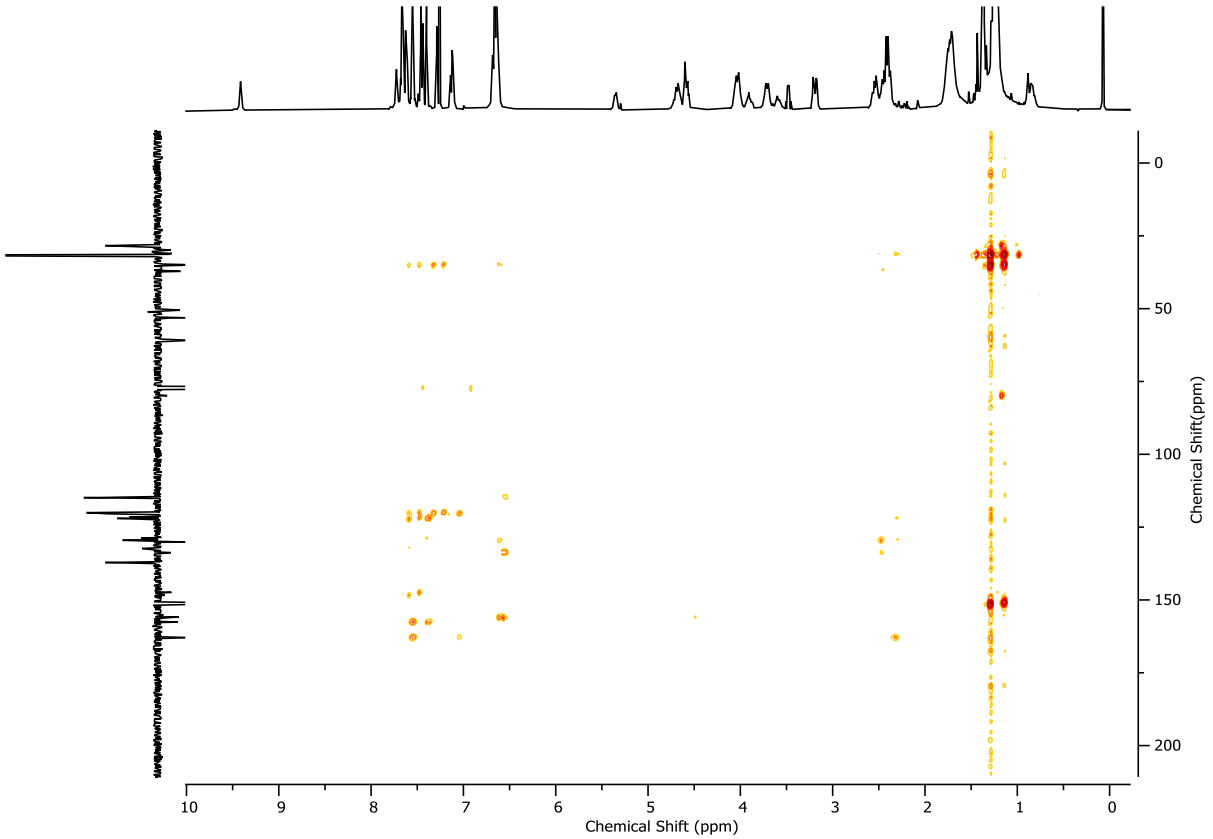

Figure 154: HMBC NMR ($CDCl_3$, 400 MHz) of (S_{ma},$R_{co\text{-}c}$)-**9**.

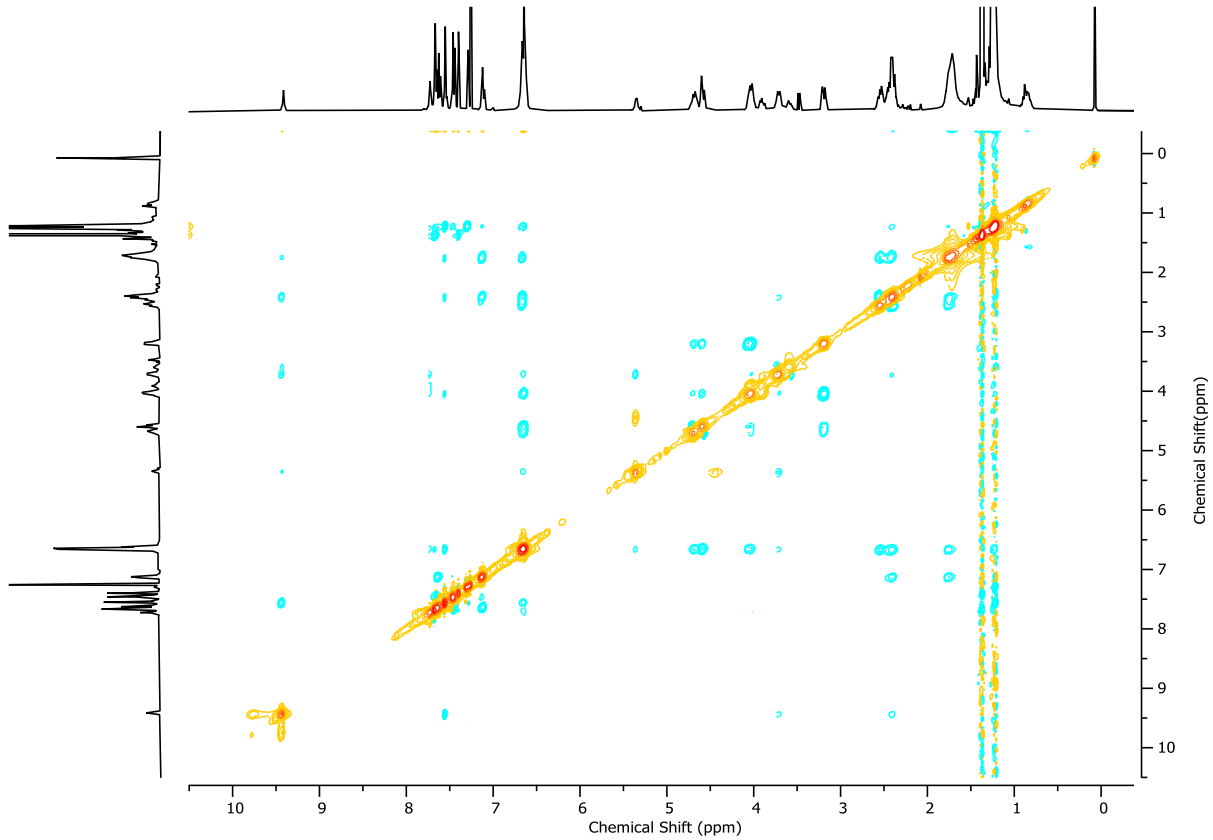

Figure 155: ^{1}H NOESY NMR ($CDCl_3$, 400 MHz) of (S_{ma},$R_{co\text{-}c}$)-**9**.

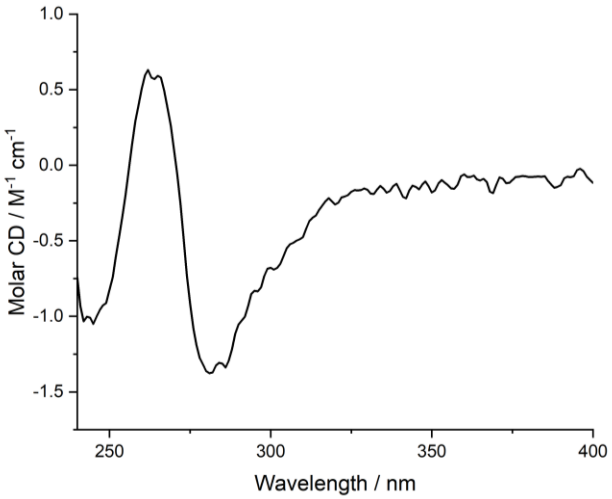

Figure 156: Circular Dichroism Spectra of (S_{ma},$R_{co\text{-}c}$)-**9** (21 μM) at 293 K in $CHCl_3$.

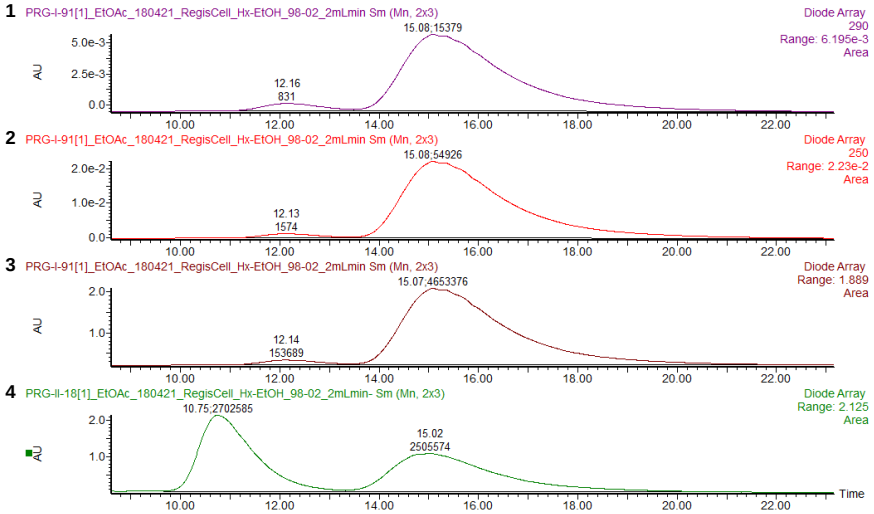

Figure 157: CSP-HPLC of (S_{ma},$R_{co\text{-}c}$)-**9** (loaded in EtOAc) with 290 nm and 250 nm traces. RegisCell, *n*-hexane-EtOH 98 : 2, flowrate 2 mLmin^{-1}. The minor signal observed at ~12.15 min is not consistent with the minor enantiomer (10.75 min); varying the wavelength of detection yielded different relative integrals vs the major enantiomer ((1) 290 nm = 5.1%), (2) 250 nm = 2.8%), (3) diode array = 3.2%). This impurity could not be detected by ^{1}H NMR and could not be completely removed from the sample. On this basis, the enantiopurity of (R_{ma},$S_{co\text{-}c}$)-**9** is estimated to be >99% *ee*. (4) *rac*-**9**, (R_{ma},$S_{co\text{-}c}$)-**9** (10.75 min, 2702585, 51.8%), (S_{ma},$R_{co\text{-}c}$)-**9** (15.02 min, 2505574, 48.2%).

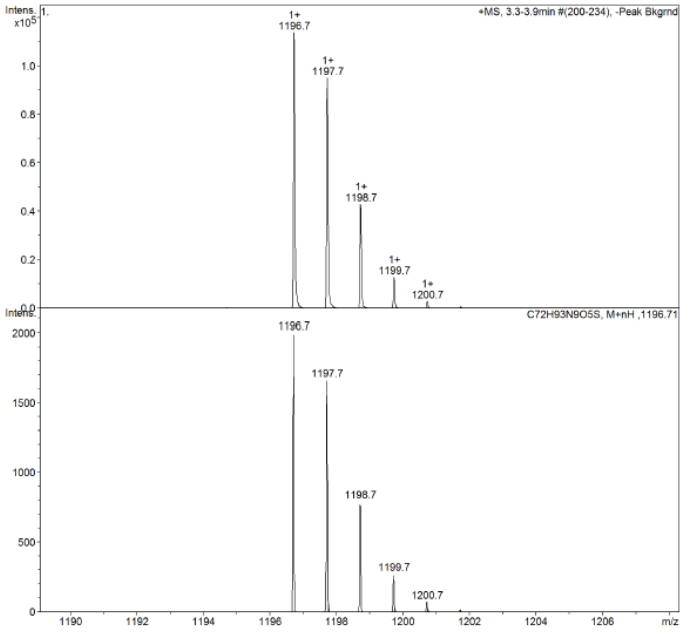

Figure 158: Observed (top) and calculated (bottom) isotopic patterns for (S_{ma},$R_{co\text{-}c}$)-**9**.

8.2. Rotaxane (R_{ma},$R_{co\text{-}c}$)-9

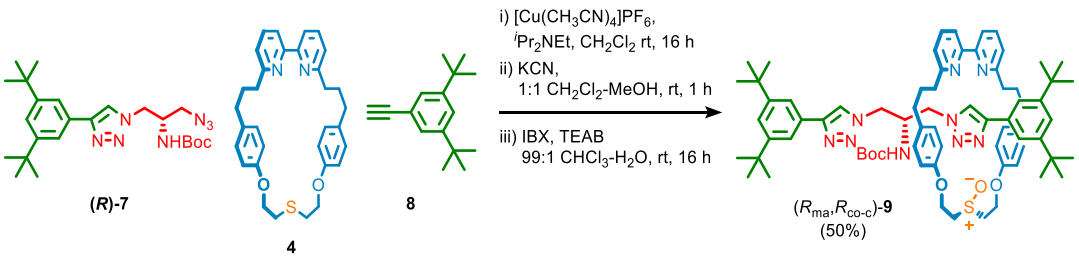

A CEM MW vial was charged with alkyne **8** (18.3 mg, 0.085 mmol, 1.1 eq.), azide (*R*)-**7** (38.2 mg, 0.083 mmol, 1.1 eq.), macrocycle **4** (38.7 mg, 0.076 mmol, 1.0 eq.), and $[Cu(CH_3CN)_4]PF_6$ (27.5 mg, 0.074 mmol, 0.97 eq.) and purged with N_2. CH_2Cl_2 (1.8 mL) and $^{i}Pr_2NEt$ (26 µL, 0.15 mmol, 2.0 eq.) were added and the resulting deep red solution was stirred at ambient temperature for 16 h. Then, MeOH (1.9 mL) and KCN as a solid (25 mg, 0.38 mmol, 5.0 eq.) were added and the resulting mixture was stirred vigorously for 1 h. The crude mixture was diluted with CH_2Cl_2 (5 mL) and washed with H_2O in two portions (10 mL and 5 mL). The combined aqueous phase was then extracted with CH_2Cl_2 (3 x 5 mL) and the combined organics were washed with brine (10 mL), dried over $MgSO_4$ and concentrated *in vacuo*. The residue corresponding to ($R_{co\text{-}c}$)-**S19** was dissolved in 99:1 $CHCl_3/H_2O$ (760 µL), then IBX (23.2 mg, 0.083 mmol, 1.1 eq.) and tetraethylammonium bromide (17.7 mg, 0.084 mmol, 1.1 eq.) were added. The resulting suspension was stirred for 16 h. The reaction mixture was then diluted with CH_2Cl_2 (5 mL), washed with 10% $NaHSO_3$ (5 mL), saturated $NaHCO_3$ (5 mL) and brine (5 mL), extracting all aqueous layers with CH_2Cl_2 (2 x 5 mL). The combined organics were dried over $MgSO_4$, filtered, and concentrated *in vacuo*. The residue was purified by column chromatography (SiO_2, petrol-EtOAc 0→50% then petrol-EtOAc (1:1) with MeOH 0→5%) to yield (R_{ma},$R_{co\text{-}c}$)-**9** (45.7 mg, 0.038 mmol, 50%) as an off-white foam. The absolute stereochemistry of the major diastereomer was assigned crystallographically (see 11.4). The mechanical stereochemistry of the minor diastereomer was assigned as opposite to that of the major diastereomer. The co-conformational stereochemistry of both is fixed by the absolute sterechemistry of (*R*)-**1**.

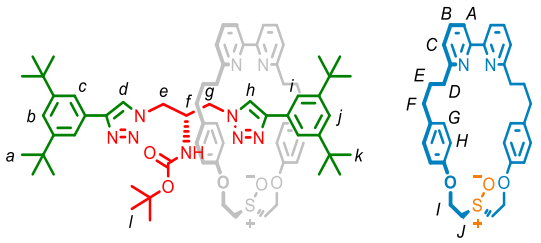

δ_H ($CDCl_3$, 400 MHz) 8.89 (s, 1H, H_h), 7.69 (app. td, J = 7.7, 3.1, 2H, H_B), 7.64 (d, J = 1.9, 2H, H_c), 7.60 (s, 1H, H_d), 7.55 (t, J = 1.3, 1H, H_A), 7.53 (t, J = 1.3, 1H, H_A), 7.51 (d, J = 1.9, 2H, H_i), 7.43 (t, J = 1.8, 1H, H_b), 7.32 (t, J = 1.8, 1H, H_j), 7.19 (dd, J = 2.8, 0.9, 1H, H_C), 7.17 (dd, J = 2.8, 1.0, 1H, H_C), 6.53 – 6.43 (m, 8H, H_G, H_H), 5.34 (d, J = 6.4, 1H, H_{NHBoc}), 4.71 – 4.61 (m, 2H, H_l), 4.60 – 4.49 (m, 2H, H_l), 4.18 (dd, J = 13.9, 4.5, 1H, H_e), 3.94 (dd, J = 13.8, 6.1, 1H, H_e), 3.88 – 3.71 (m, 4H, H_J, H_g), 3.77 – 3.72 (m, 1H, H_f), 3.17 – 3.08 (m, 2H, H_J), 2.65 – 2.49 (m, 4H, H_D), 2.49 – 2.32 (m, 4H, H_F), 1.84 – 1.59 (m, 4H, H_E), 1.38 (s, 18H, H_a), 1.34 (s, 9H, H_l), 1.32 (s, 18H, H_k); δ_C ($CDCl_3$, 101 MHz) 162.9, 162.9, 157.9, 157.9, 155.3, 155.2, 151.6, 150.8, 148.5, 147.5, 137.4, 137.3, 133.6, 133.4, 130.2, 129.9, 128.8, 128.7, 122.6, 122.4, 122.4, 121.5, 120.9, 120.5, 120.3, 120.2, 115.1, 115.0, 80.3, 61.1, 61.0,

52.2, 52.2, 51.09, 50.0, 49.8, 37.5, 35.1, 35.1, 34.7, 34.6, 31.8, 31.7, 31.7, 31.4, 28.5; LR-ESI-MS (+ve) m/z = 1196.7 $[M+H]^+$

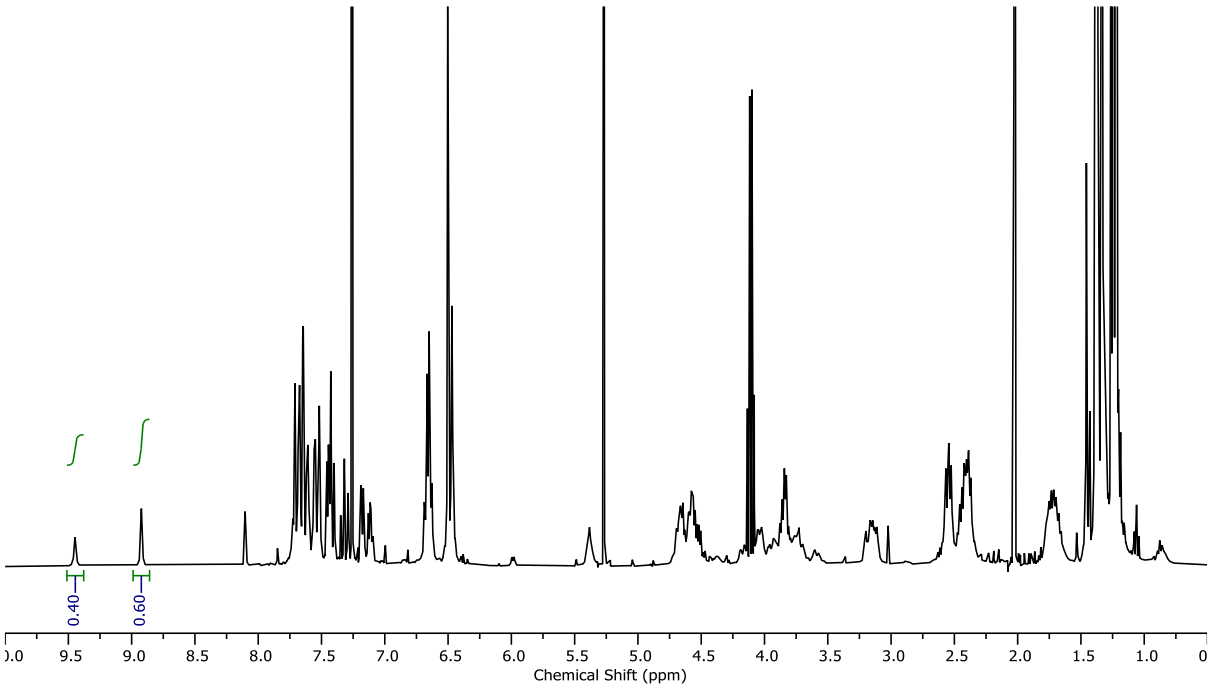

Figure 159: Crude ^{1}H NMR of **9** *via* oxidation of sulfide rotaxane ($R_{co\text{-}c}$)-**9** ($CDCl_3$, 400 MHz). Diastereoisomer integration: $\boldsymbol{H}_h$ protons (major 9.42 ppm, 0.40, minor 8.89 ppm, 0.60).

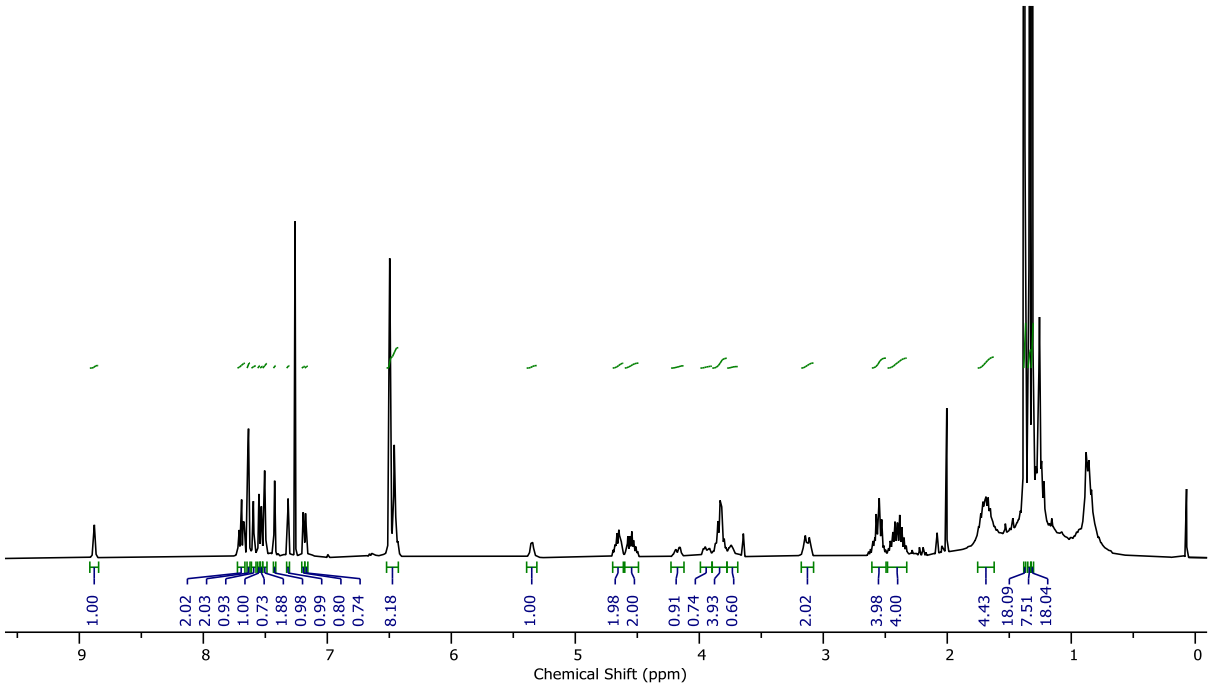

Figure 160: ^{1}H NMR ($CDCl_3$, 400 MHz) of (R_{ma},$R_{co\text{-}c}$)-**9**.

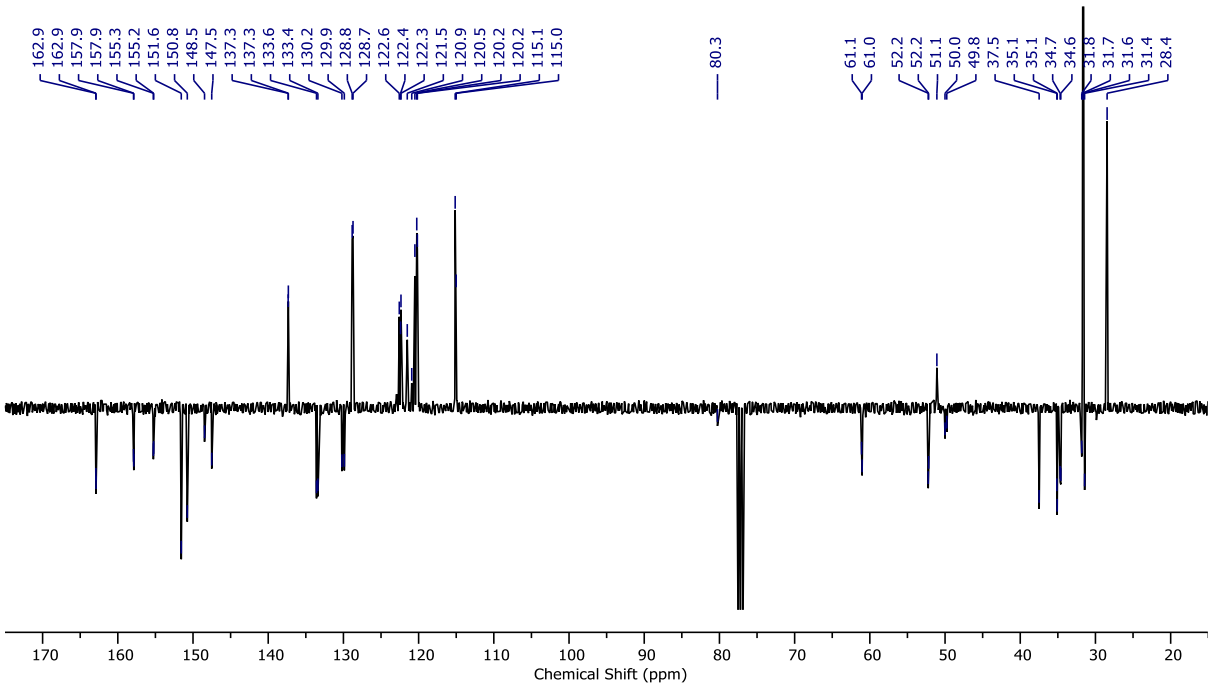

Figure 161: JMOD NMR ($CDCl_3$, 101 MHz) of (R_{ma},$R_{co\text{-}c}$)-**9**.

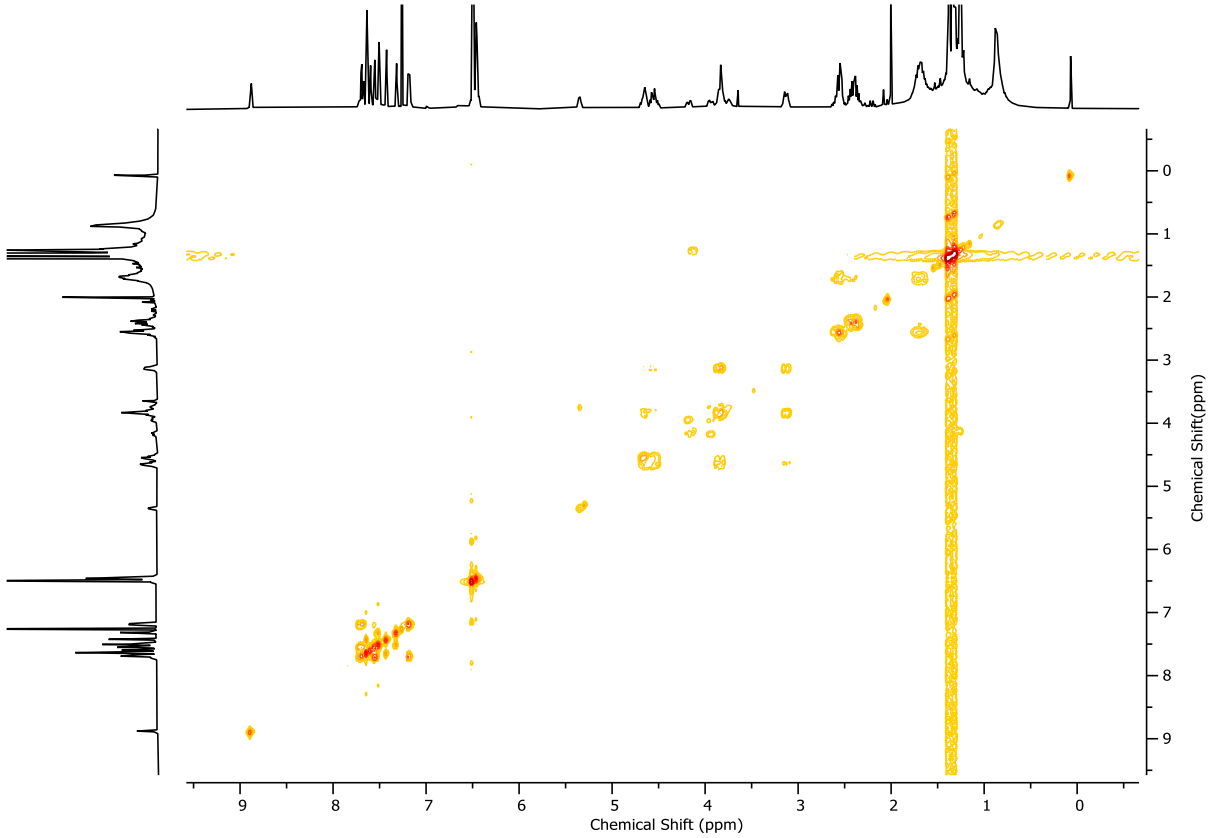

Figure 162: ^1H COSY NMR ($CDCl_3$, 400 MHz) of (R_{ma},$R_{co\text{-}c}$)-**9**.

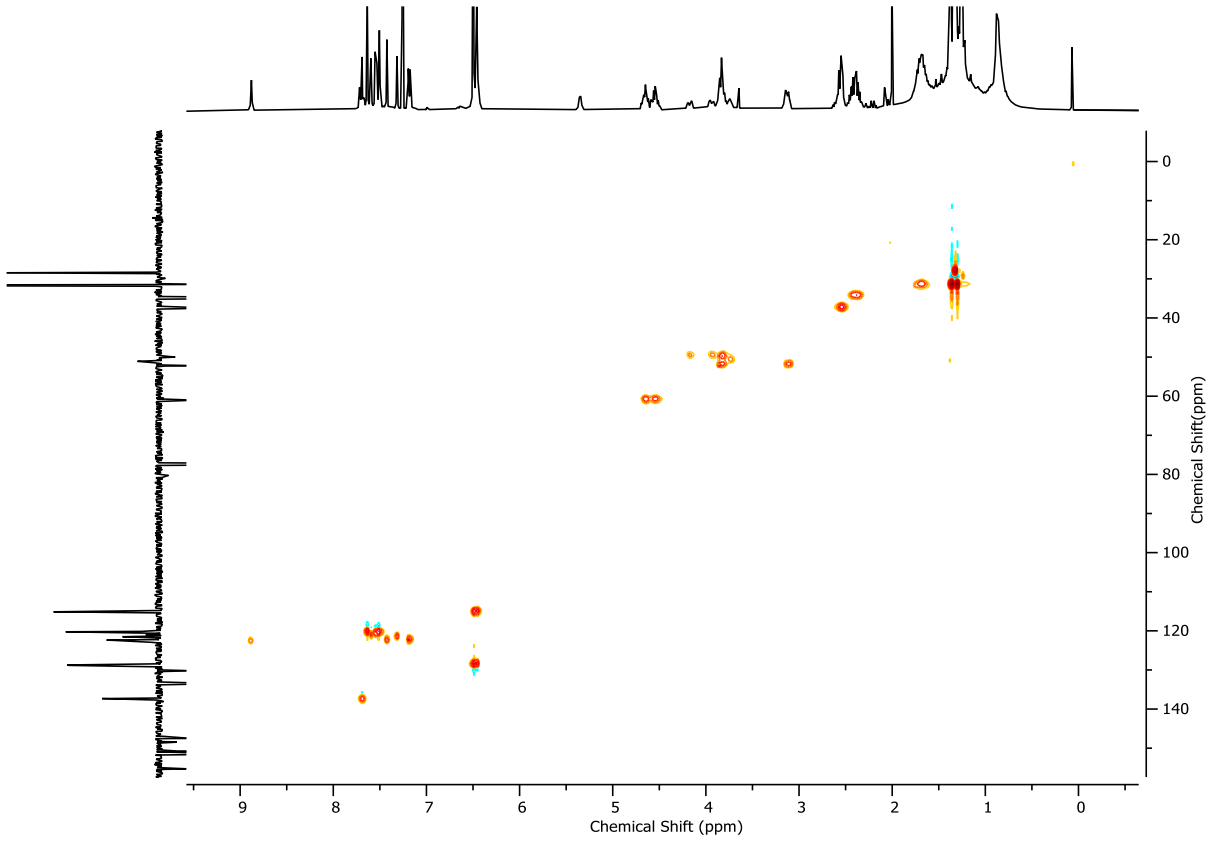

Figure 163: HSQC NMR ($CDCl_3$, 400 MHz) of (R_{ma},$R_{co\text{-}c}$)-**9**.

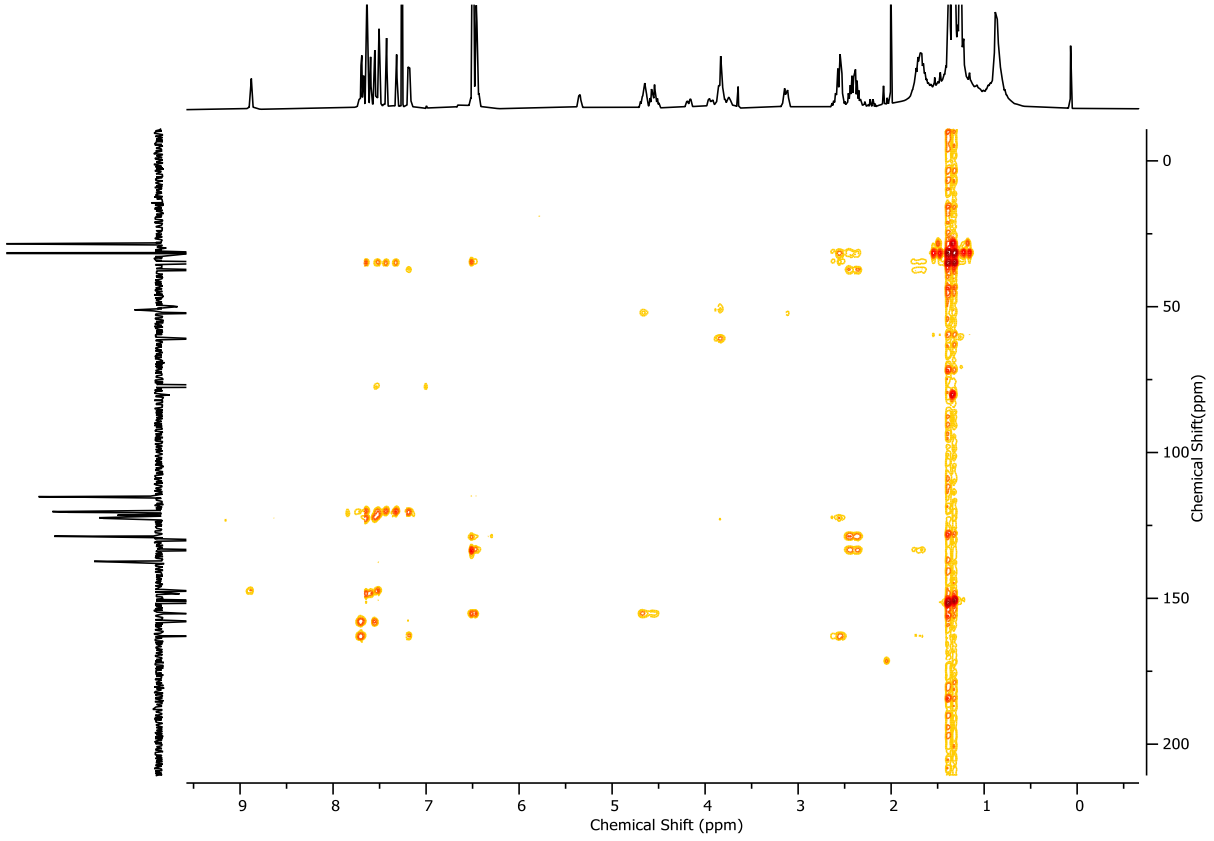

Figure 164: HMBC NMR ($CDCl_3$, 400 MHz) of (R_{ma},$R_{co\text{-}c}$)-**9**.

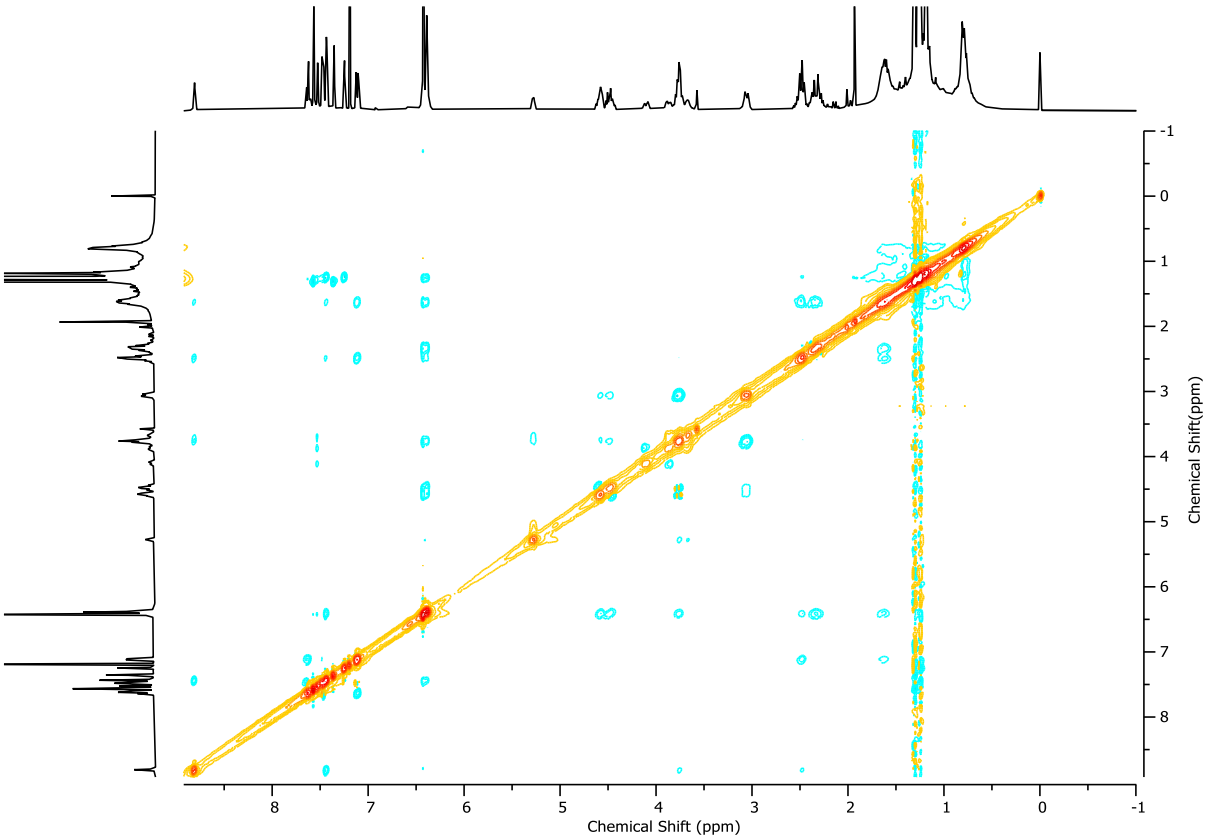

Figure 165: ^{1}H NOESY NMR ($CDCl_3$, 400 MHz) of (R_{ma},$R_{co\text{-}c}$)-**9**.

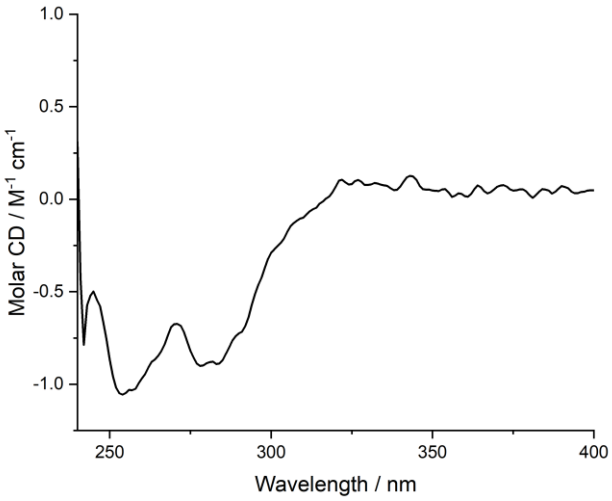

Figure 166: Circular Dichroism Spectra of (R_{ma},$R_{co\text{-}c}$)-**9** (25 µM) at 293 K in $CHCl_3$.

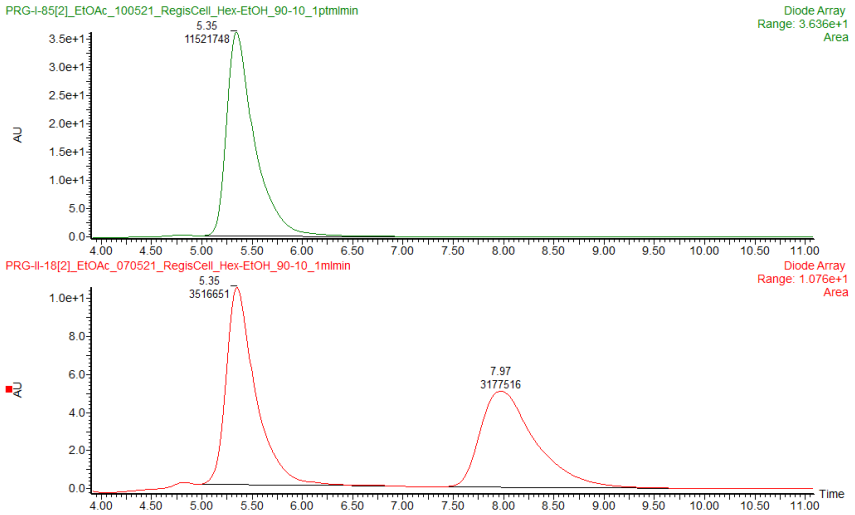

Figure 167: CSP-HPLC of (R_{ma},$R_{co\text{-}c}$)-**9** (loaded in EtOAc). RegisCell, *n*-hexane-EtOH 90 : 10, flowrate 1 mLmin^{-1}. (top) (R_{ma},$R_{co\text{-}c}$)-**9** (5.35 min, 11521748, >99.9%), (S_{ma},$S_{co\text{-}c}$)-**9** (not observed). (bottom) *rac*-**9**, (R_{ma},$R_{co\text{-}c}$)-**9** (5.35 min, 3516651, 52.5%), (S_{ma},$S_{co\text{-}c}$)-**9** (7.97 min, 3177516, 47.5%).

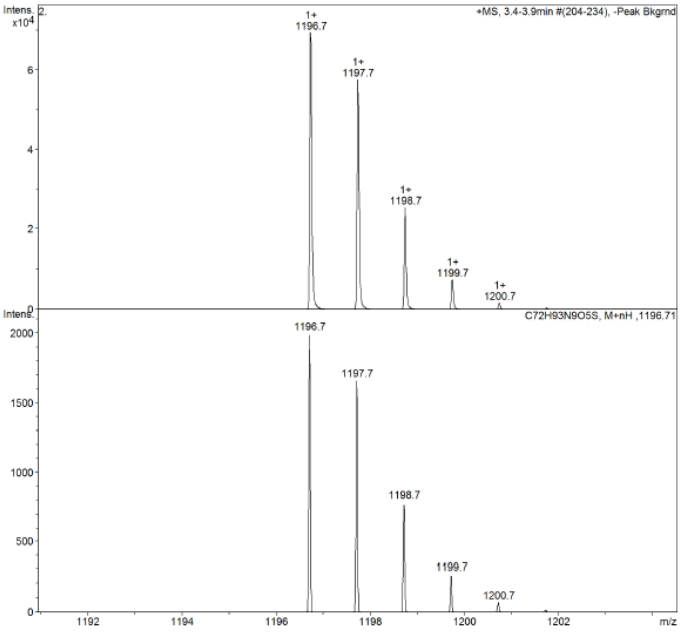

Figure 168: Observed (top) and calculated (bottom) isotopic patterns for (R_{ma},$R_{co\text{-}c}$)-**9**.

8.3. Axle S20

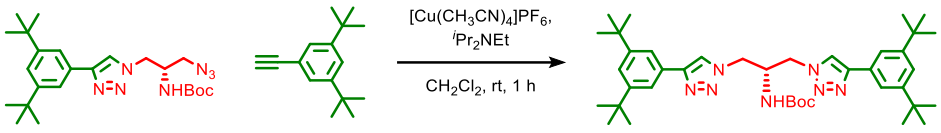

(*R*)-7 8 **S20** (quant.)

A CEM MW vial was charged with alkyne **8** (6.0 mg, 0.028 mmol, 1.1 eq.), azide (*R*)-**7** (11.4 mg, 0.025 mmol, and $[Cu(CH_3CN)_4]PF_6$ (1.9 mg, 0.005 mmol, 0.2 eq.) and purged with N_2. CH_2Cl_2 (0.5 mL) and $^iPr_2NEt$ (9 µL, 0.15 mmol, 2.0 eq.) then stirred at ambient temperature for 1 h. The crude mixture was diluted with CH_2Cl_2 (5 mL) and washed with EDTA-NH_3 solution (2 x 5 mL), and the combined organics were washed with brine (5 mL), dried over $MgSO_4$ and concentrated *in vacuo*. The residue was purified by column chromatography (SiO_2, petrol-EtOAc 0→30 %) to yield axle **S20** (16.5 mg, 0.025 mmol, quant.) as a white foam.

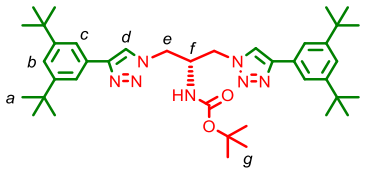

δ_H ($CDCl_3$, 400 MHz) 8.10 (s, 2H, H_d), 7.71 (d, J = 1.8, 4H, H_c), 7.45 (t, J = 1.8, 2H, H_b) 5.94 (d, J = 7.3, 1H, H_{NHBoc}), 4.58 (dd, J = 14.2, 4.2, 2H, H_e), 4.47 (dd, J = 14.2, 6.4, 2H, H_e), 4.34 (s, 1H, H_f), 1.47 (s, 9H, H_g), 1.38 (s, 36H, H_a); δ_C ($CDCl_3$, 101 MHz) 151.7, 149.2, 129.4, 123.0, 121.8, 120.4, 51.6, 49.5, 35.2, 31.7, 29.9, 28.5; HR-ESI-MS (+ve) m/z = 670.4819 $[M+H]^+$ (calc. m/z for $C_{40}H_{60}N_7O_2$ 670.4803).

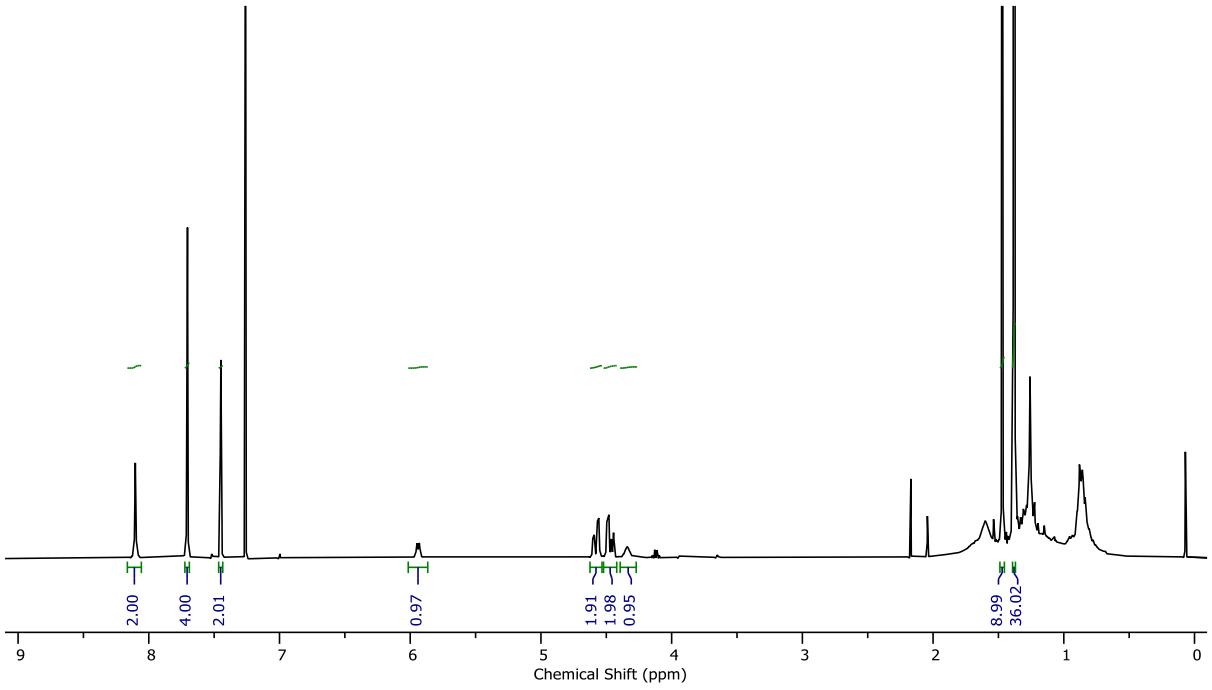

Figure 169: ^1H NMR ($CDCl_3$, 400 MHz) of **S20**.

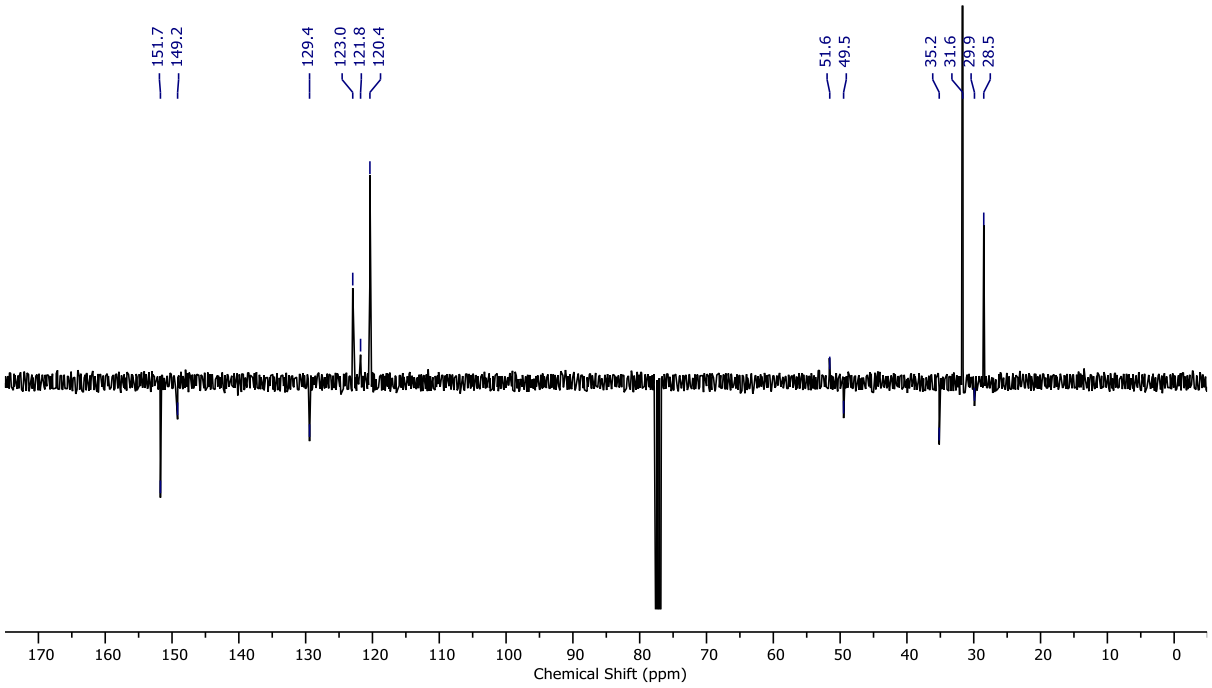

Figure 170: JMOD NMR ($CDCl_3$, 101 MHz) of **S20**.

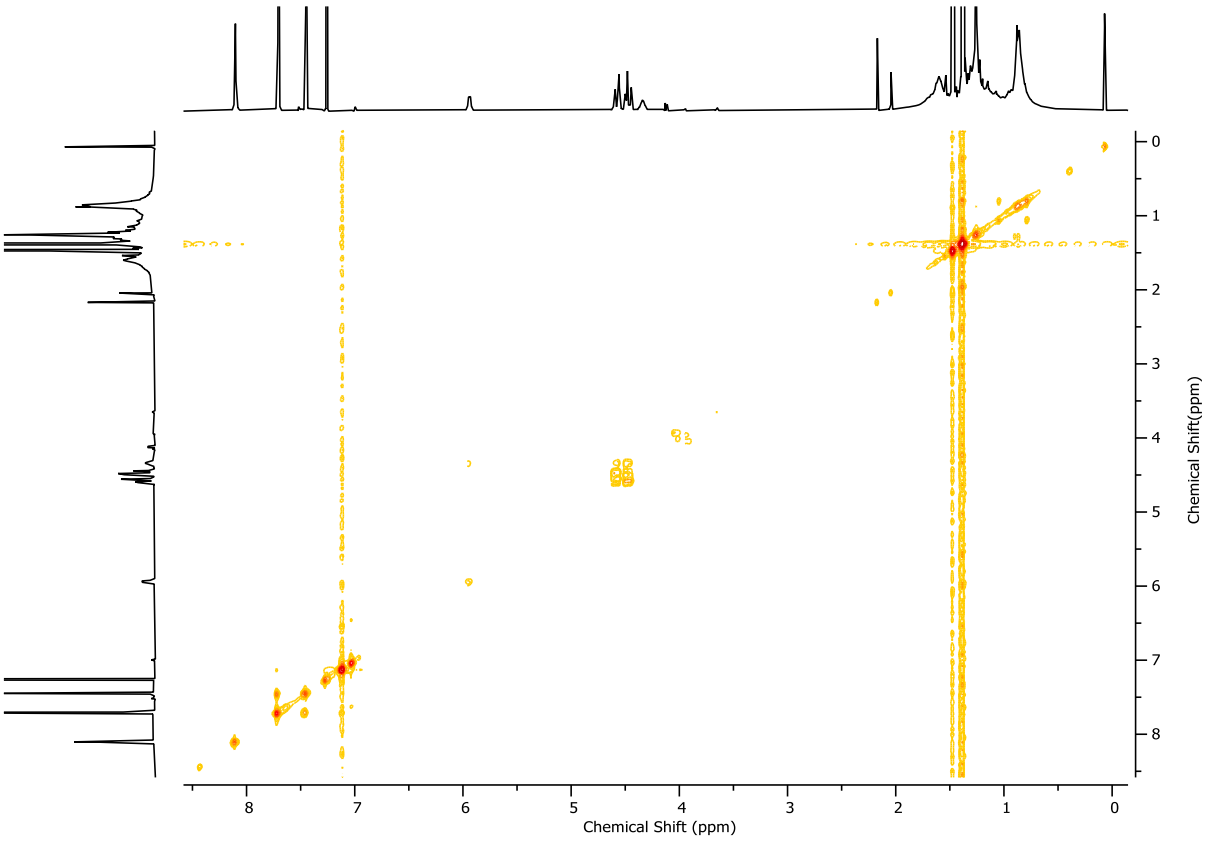

Figure 171: ^{1}H COSY NMR ($CDCl_3$, 400 MHz) of **S20**.

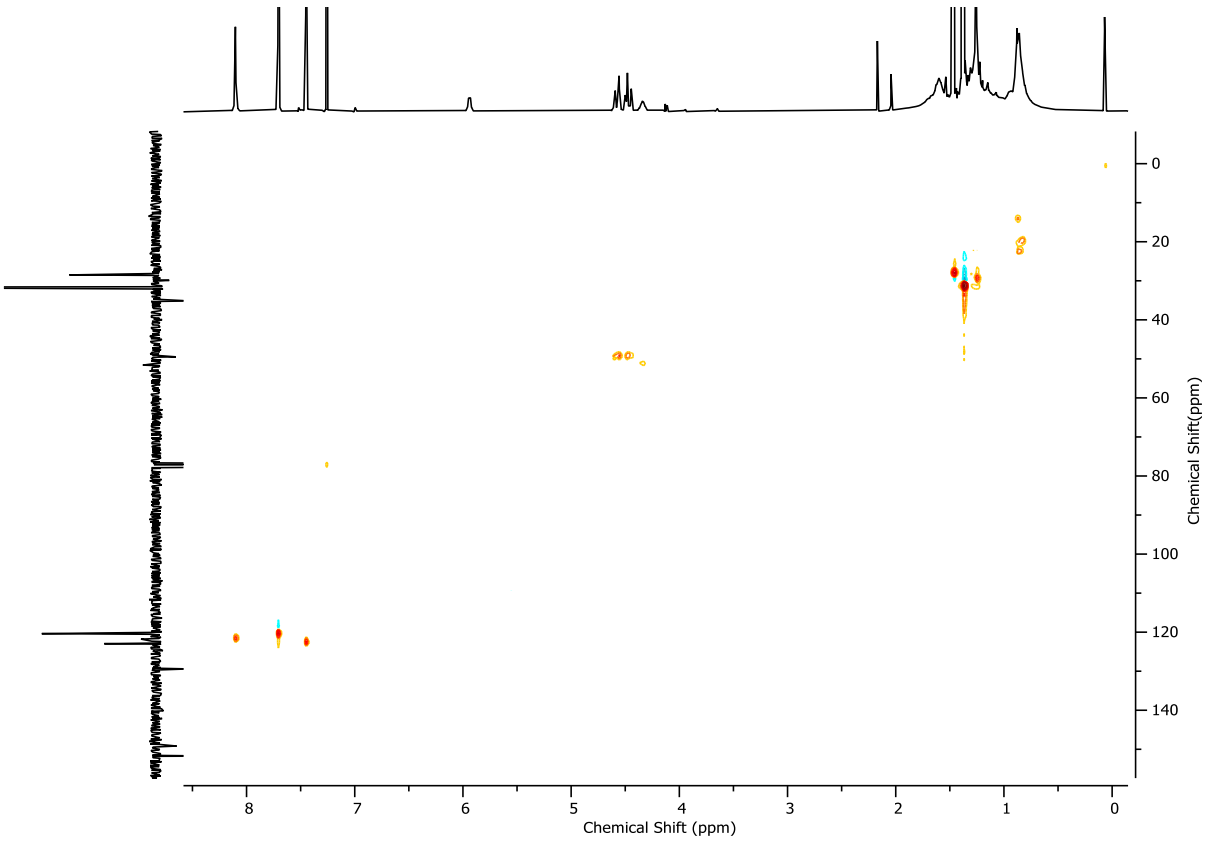

Figure 172: HSQC NMR ($CDCl_3$, 400 MHz) of **S20**.

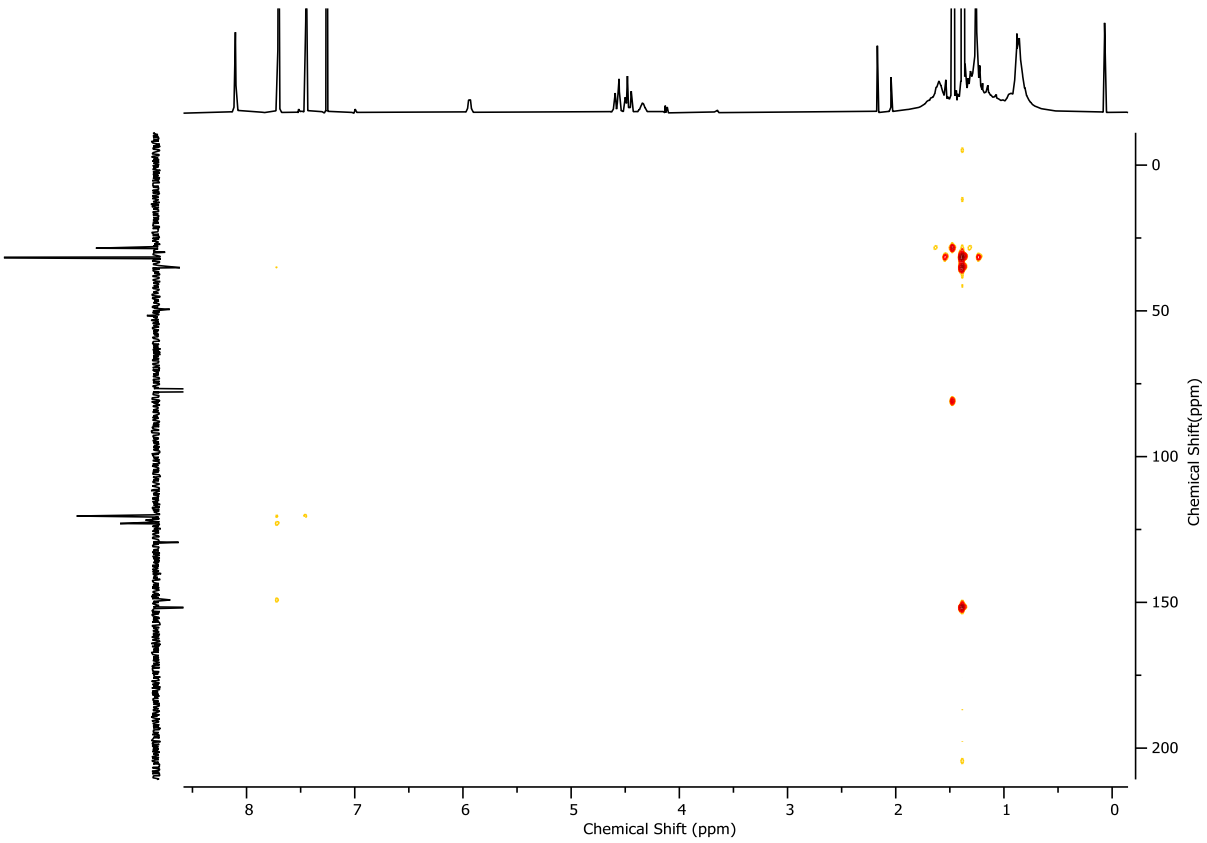

Figure 173: HMBC NMR ($CDCl_3$, 400 MHz) of **S20**.

9. Synthesis of enantiomeric rotaxanes (S_{ma})-10 and (R_{ma})-10

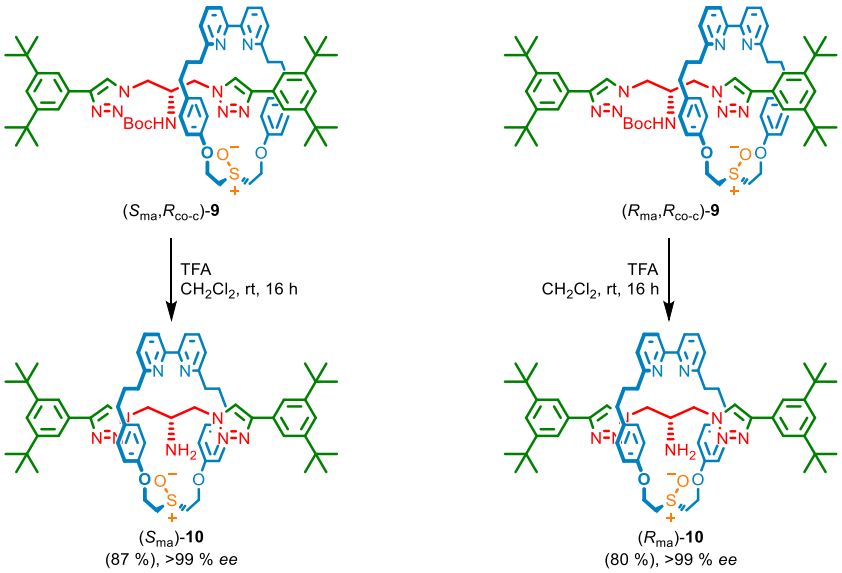

Scheme 8: Synthetic route to mechanically axially chiral enantiomeric rotaxanes (R_{ma})-**10** and (S_{ma})-**10**.

9.1. Rotaxane (S_{ma})-10

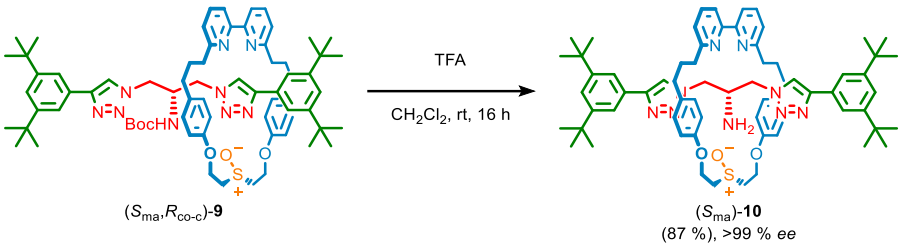

(S_{ma},$R_{co\text{-}c}$)-**9** (S_{ma})-**10** (87 %), >99 % *ee*

To a solution of rotaxane (S_{ma},$R_{co\text{-}c}$)-**9** (18.0 mg, 0.015 mmol, 1 eq.) in CH_2Cl_2 (300 µL) was added TFA (35 µL, 0.46 mmol, 31 eq.) dropwise, and the reaction mixture was stirred at ambient temperature for 16 h. The reaction mixture was then diluted with CH_2Cl_2 (5 mL) and poured into saturated $NaHCO_3$ (5 mL). The aqueous phase was extracted with CH_2Cl_2 (3 x 5 mL) and combined organics were washed with brine (5 mL), dried over $MgSO_4$, filtered and concentrated *in vacuo.* The residue was purified by column chromatography (SiO_2, CH_2Cl_2-CH_3CN 0→20% then CH_2Cl_2-CH_3CN (3:1) with MeOH 0→10%) to yield rotaxane (S_{ma})-**10** (13.8 mg, 0.013 mmol, 87%) as an off-white foam. The mechanical stereochemistry of the product was assigned by observing that this cannot change during the removal of the Boc group (or if it does, that the resulting product would be racemic, which was not observed).

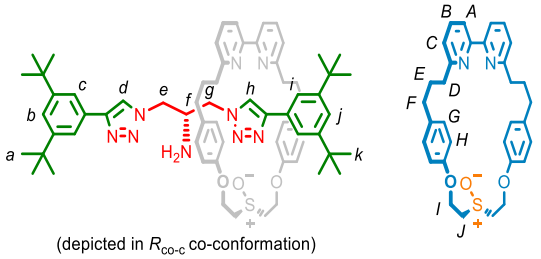

(depicted in $R_{co\text{-}c}$ co-conformation)

δ_H ($CDCl_3$, 400 MHz) 8.58 (s, 1H, H_h), 8.07 (s, 1H, H_d), 7.66 (d, J = 1.8, 2H, H_c), 7.65 –7.58 (m, 3H, H_I, H_B), 7.46 (dd, J = 2.9, 1.0, 1H, H_A), 7.44 (dd, J = 2.9, 1.0, 1H, H_A), 7.39 (t, J = 1.8, 1H, H_b), 7.35 (t, J = 1.8, 1H, H_j), 7.12 (dd, J = 7.7, 1.0, 1H, H_C), 7.09 (dd, J = 7.8, 1.0, 1H, H_C), 6.72 – 6.62 (m, 6H, H_G, H_H), 6.61 – 6.53 (m, 2H, H_H), 4.73 – 4.61 (m, 2H, H_I), 4.59 – 4.47 (m, 2H, H_I), 3.92 – 3.75 (m, 3H, H_J, H_e), 3.64 – 3.54 (m, 2H, H_e, H_g), 3.22 (dd, J = 13.8, 7.9, 1H, H_g), 3.16 – 3.09 (m, 2H, H_J), 2.70 – 2.63 (m, 1H, H_f), 2.54 – 2.40 (m, 9H, H_F, H_D), 1.79 – 1.67 (m, 4H, H_E), 1.37 (s, 18H, H_a), 1.29 (s, 18H, H_k); δ_C ($CDCl_3$, 101 MHz) 162.7, 162.7, 157.9, 157.8, 155.9, 155.7, 151.3, 148.3, 148.0, 137.3, 137.2, 134.0, 133.9, 130.4, 130.2, 129.6, 129.5, 122.7, 122.2, 122.2, 122.1, 122.0, 121.4, 120.6, 120.6, 120.3, 120.0, 115.0, 114.9, 61.0, 60.9, 54.2, 53.7, 53.1, 53.1, 51.5, 37.4, 37.2, 35.1, 35.1, 34.8, 34.7, 32.0, 31.9, 31.7, 31.6; LR-ESI-MS (+ve) m/z = 1196.7 $[M+H]^+$

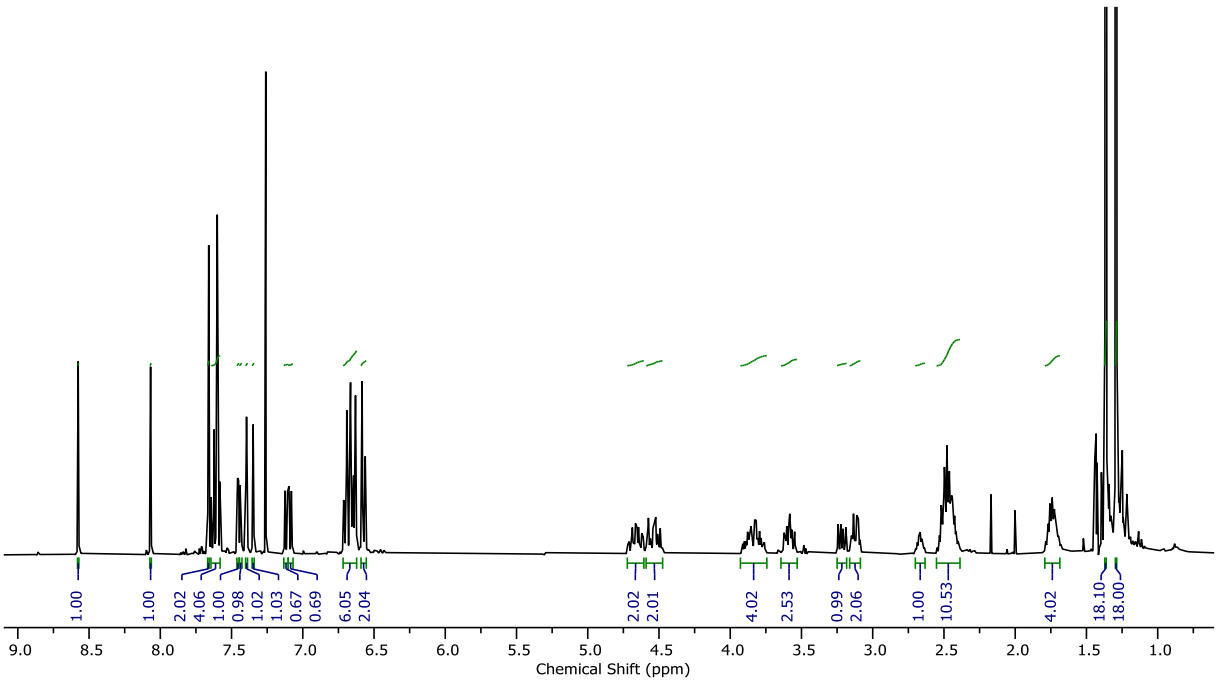

Figure 174: ^{1}H NMR ($CDCl_3$, 400 MHz) of (S_{ma})-**10**.

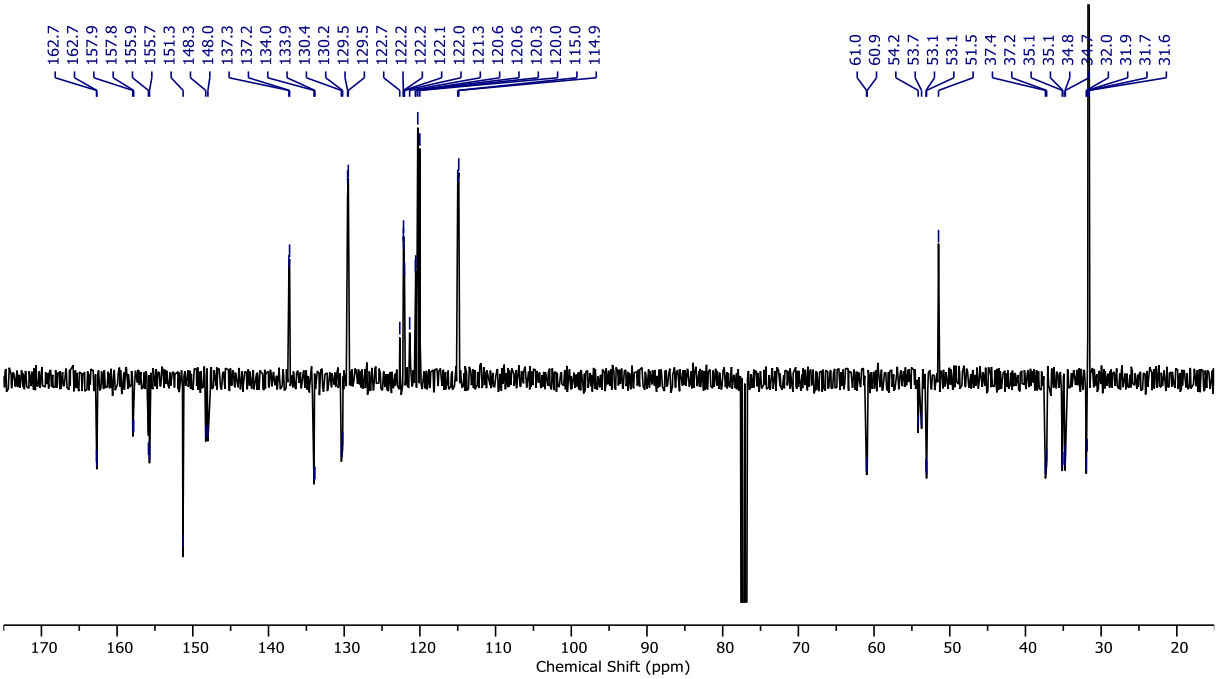

Figure 175: JMOD NMR ($CDCl_3$, 101 MHz) of (S_{ma})-**10**.

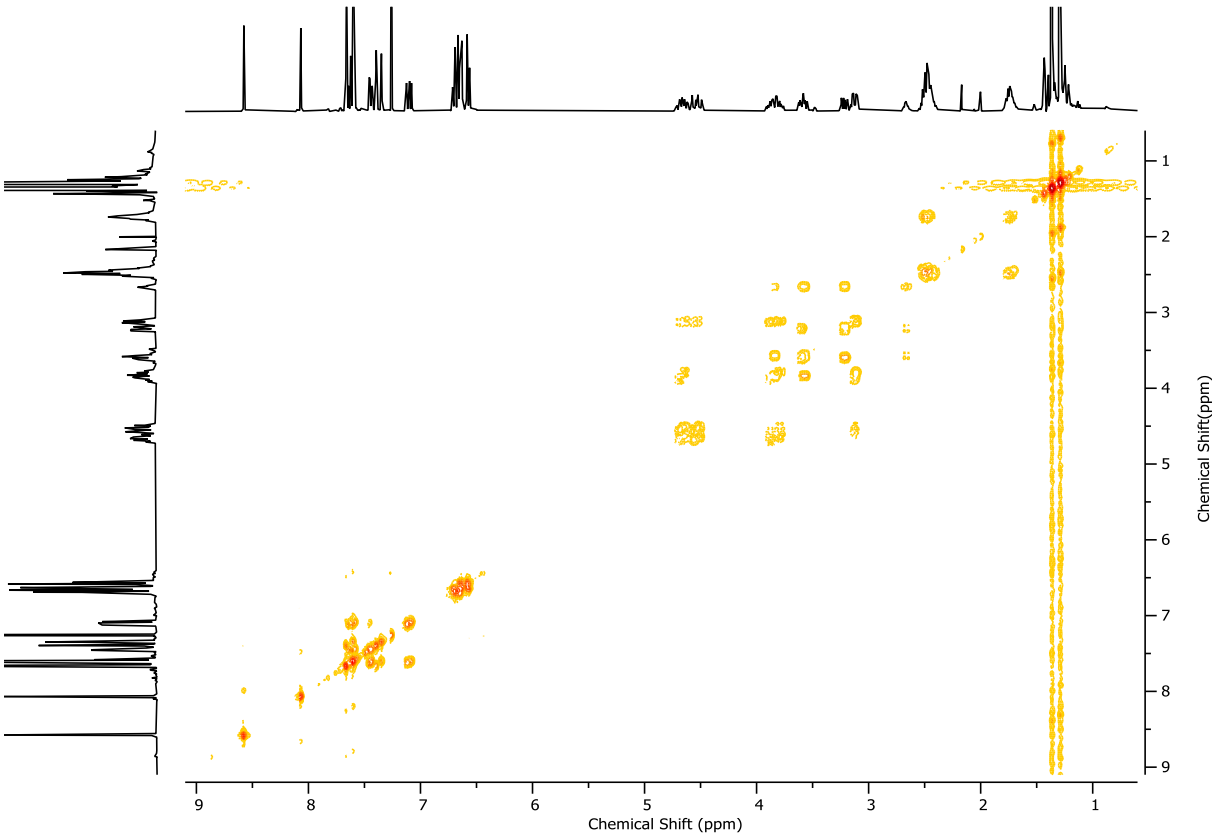

Figure 176: ^{1}H COSY NMR ($CDCl_3$, 400 MHz) of (S_{ma})-**10**.

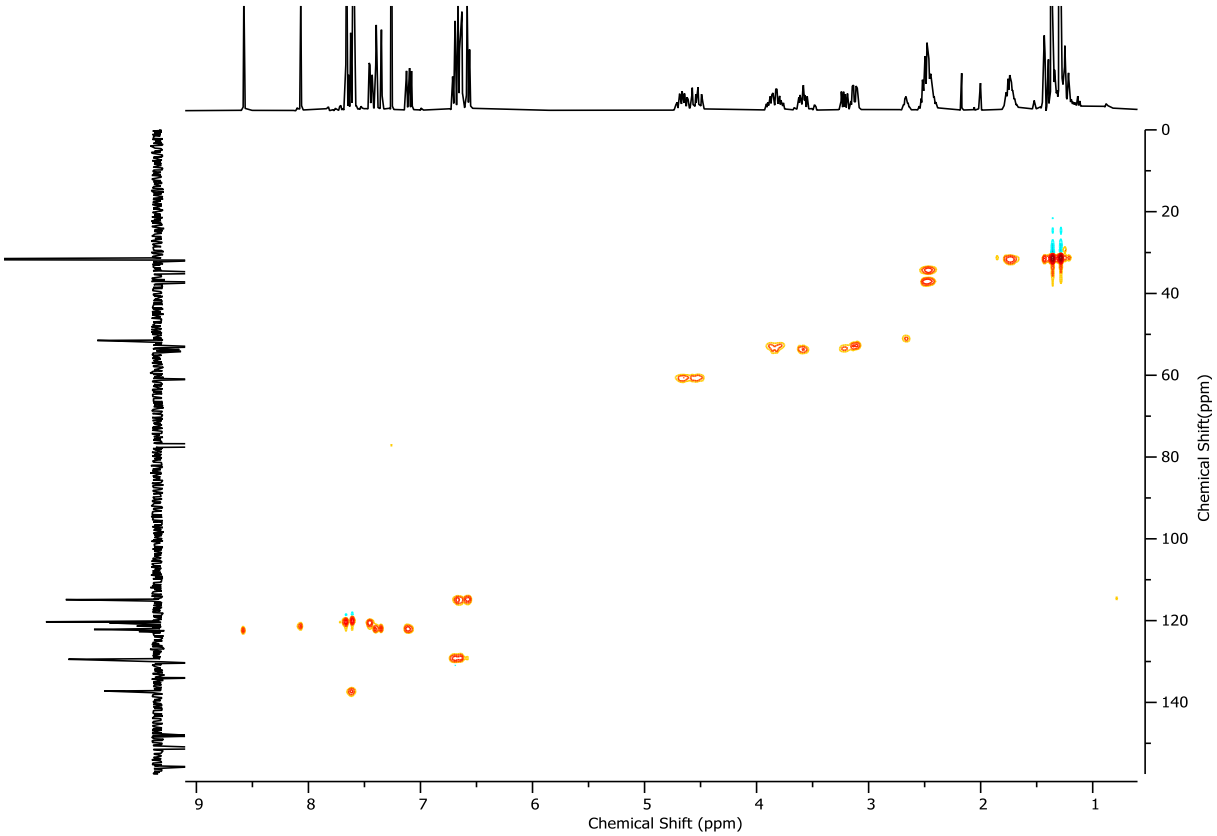

Figure 177: HSQC NMR ($CDCl_3$, 400 MHz) of (S_{ma})-**10**.

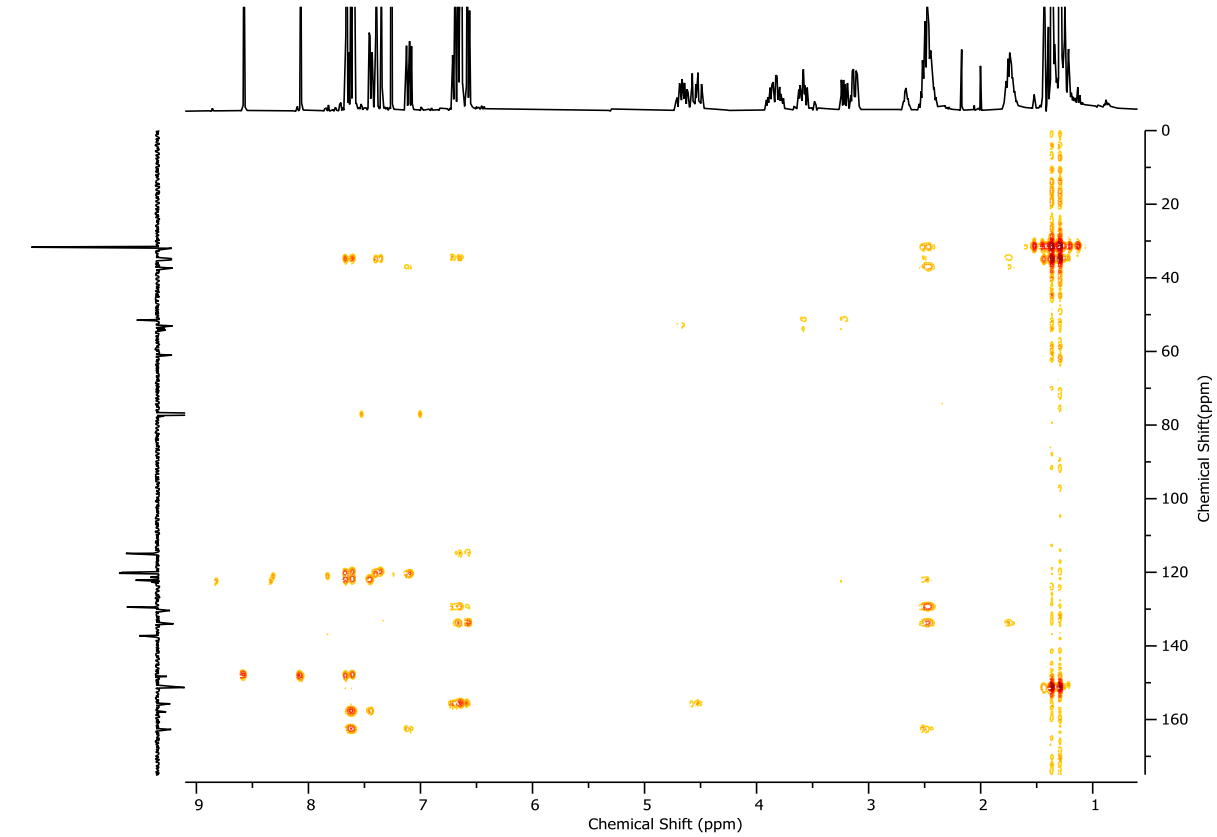

Figure 178: HMBC NMR ($CDCl_3$, 400 MHz) of (S_{ma})-**10**.

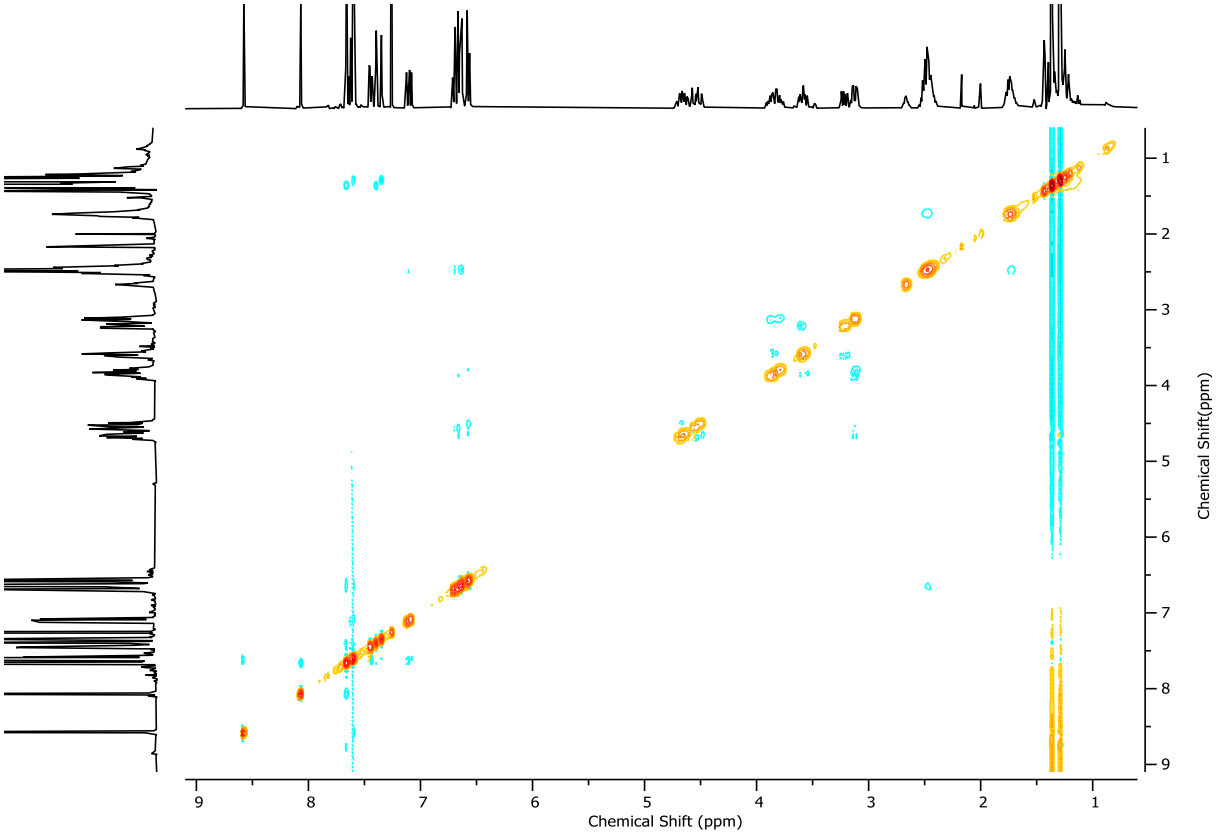

Figure 179: ^1H NOESY NMR ($CDCl_3$, 400 MHz) of (S_{ma})-**10**.

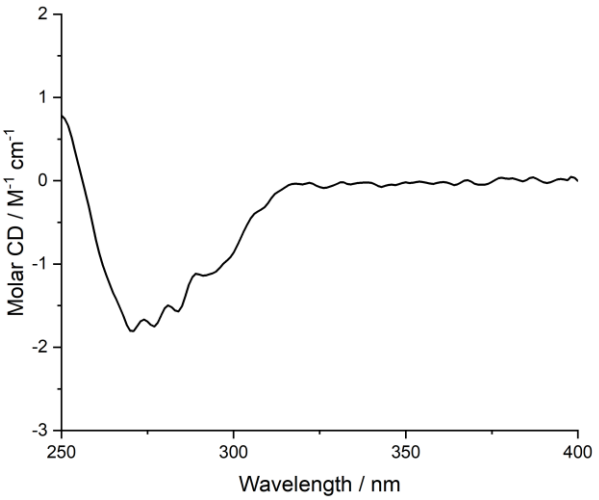

Figure 180: Circular Dichroism Spectra of (S_{ma})-**10** (26 µM) at 293 K in $CHCl_3$.

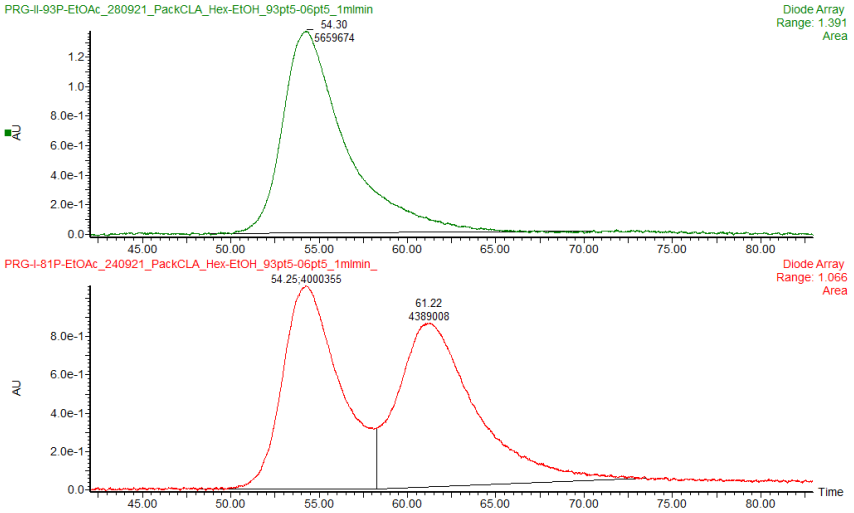

Figure 181: CSP-HPLC of (S_{ma})-**10** loaded in EtOAc). RegisPackCLA-1, *n*-hexane-EtOH 93.5 : 6.5, flowrate 1 mLmin^{-1}. (top) (S_{ma})-**10** (54.30 min, 5659674, >99.9%), (R_{ma})-**10** (not observed). (bottom) *rac*-**10**, (S_{ma})-**10** (54.25 min, 4000355, 47.7%), (R_{ma})-**10** (61.22 min, 4389008, 52.3%).

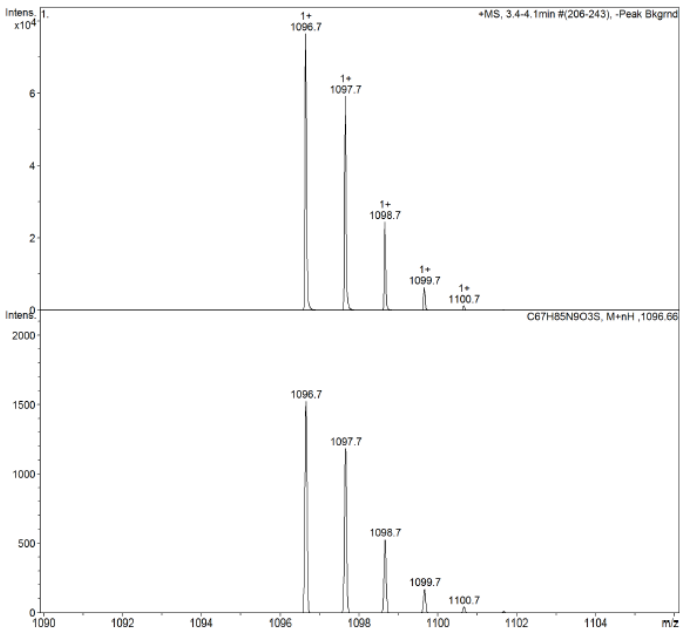

Figure 182: Observed (top) and calculated (bottom) isotopic patterns for (S_{ma})-**10**.

9.2. Rotaxane (R_{ma})-10

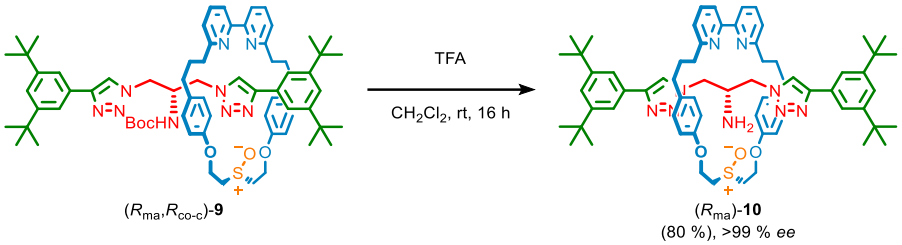

To a solution of rotaxane (R_{ma},R_{co-c})-**9** (12.2 mg, 0.010 mmol, 1 eq.) in CH_2Cl_2 (200 µL) was added TFA (23 µL, 0.30 mmol, 30 eq.) dropwise, and the reaction mixture was stirred at ambient temperature for 16 h. The reaction mixture was then diluted with CH_2Cl_2 (5 mL) and poured into saturated $NaHCO_3$ (5 mL). The aqueous phase was extracted with CH_2Cl_2 (3 x 5 mL) and combined organics were washed with brine (5 mL), dried over $MgSO_4$, filtered and concentrated *in vacuo.* The residue was purified by column chromatography (SiO_2, CH_2Cl_2-CH_3CN 0→20% then CH_2Cl_2-CH_3CN (3:1) with MeOH 0→10%) to yield rotaxane (R_{ma})-**10** (8.5 mg, 0.008 mmol, 80%) as an off-white foam.

All spectroscopic data is consistent with those reported for (S_{ma})-**10**, with the exception of circular dichroism spectra.

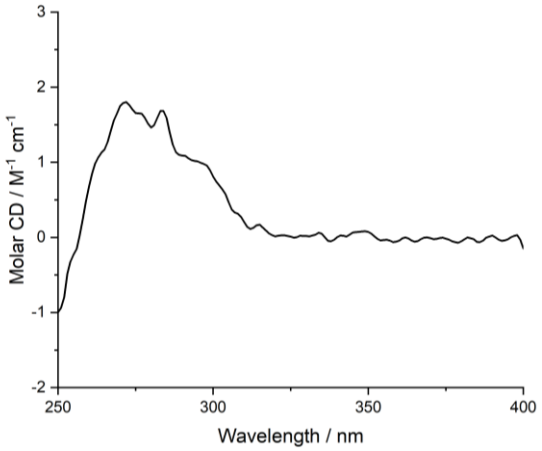

Figure 183: Circular Dichroism Spectra of (R_{ma})-**10** (23 µM) at 293 K in $CHCl_3$.

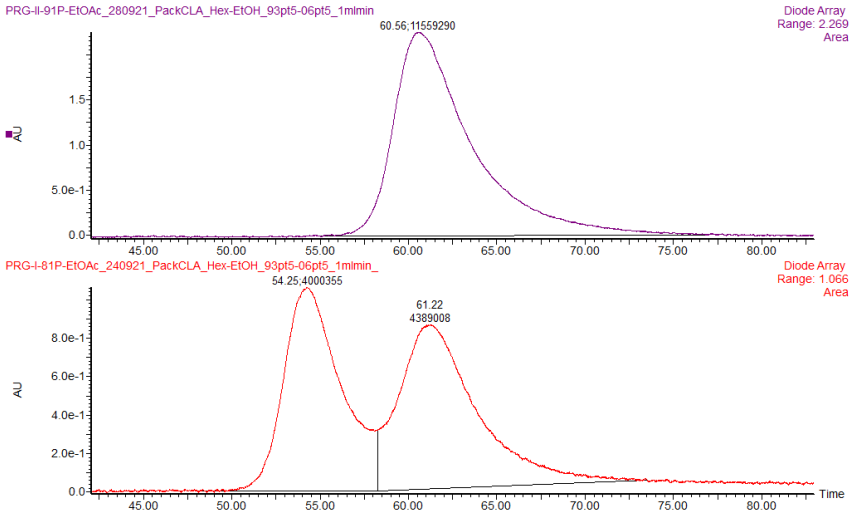

Figure 184: CSP-HPLC of (R_{ma})-**10** loaded in EtOAc). RegisPackCLA-1, *n*-hexane-EtOH 93.5 : 6.5, flowrate 1 $mLmin^{-1}$. (top) (S_{ma})-**10** (not observed), (R_{ma})-**10** (60.56 min, 11559290, >99%). (bottom) *rac*-**10**, (S_{ma})-**10** (54.25 min, 4000355, 47.7%), (R_{ma})-**10** (61.22 min, 4389008, 52.3%).

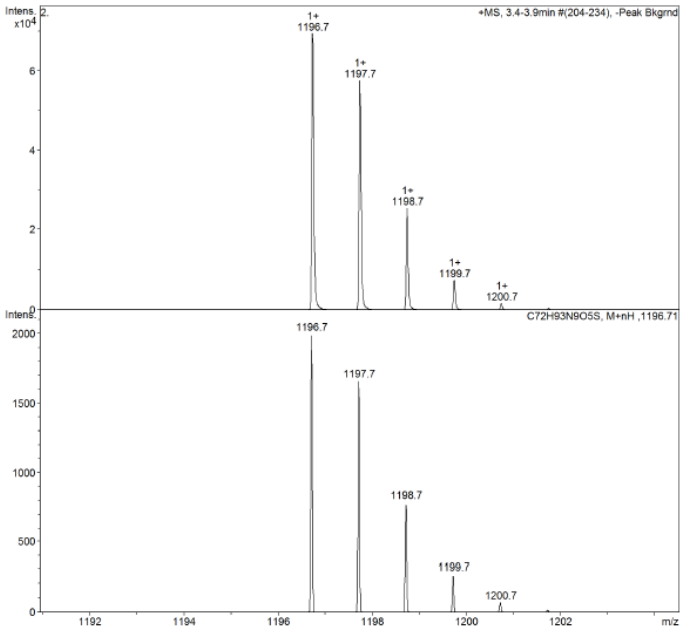

Figure 185: Observed (top) and calculated (bottom) isotopic patterns for (R_{ma})-**10**.

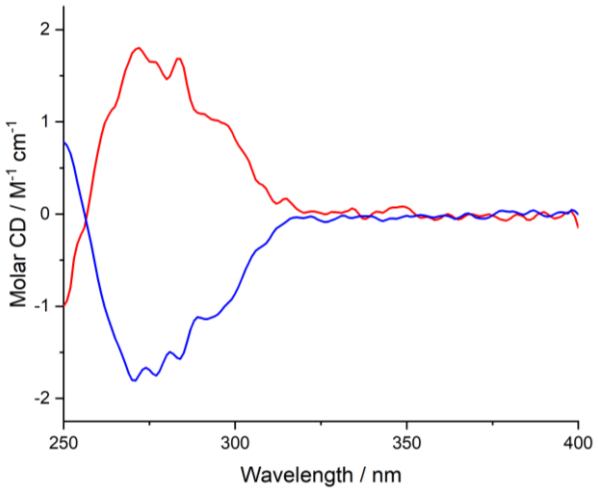

Figure 186: Circular Dichroism Spectra of (R_{ma})-**10** (blue, 23 µM) and (S_{ma})-**10** (red, 26 µM) at 293 K in $CHCl_3$.

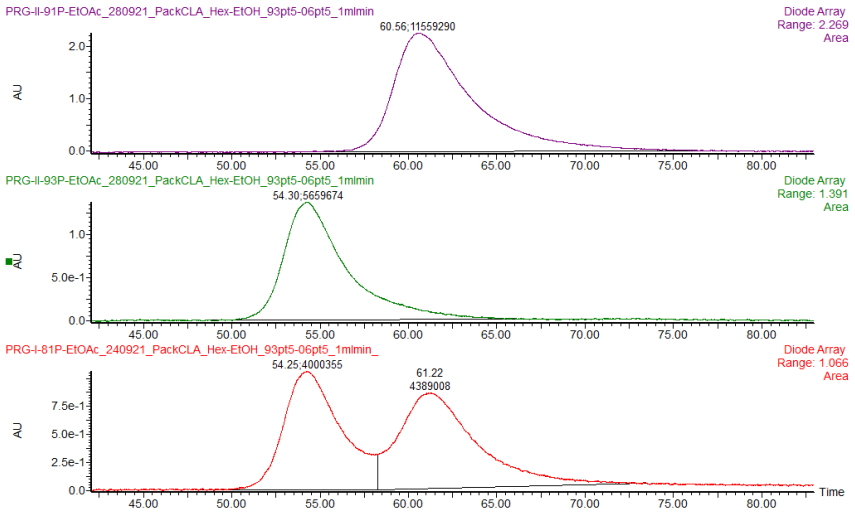

Figure 187: CSP-HPLC of (R_{ma})-**10** and (S_{ma})-**10** (loaded in EtOAc). RegisPackCLA-1, *n*-hexane-EtOH 93.5 : 6.5, flowrate 1 mLmin^{-1}. (top) (R_{ma})-**10** (not observed), (S_{ma})-**10** (60.56 min, 11559290, >99.9%); (middle) (R_{ma})-**10** (54.30 min, 5659674, >99.9%), (S_{ma})-**10** (not observed); (bottom) *rac*-**10**, (S_{ma})-**10** (54.25 min, 4000355, 47.7%), (R_{ma})-**10** (61.22 min, 4389008, 52.3%).

9.3. Axle S21

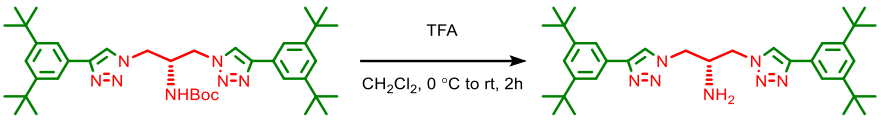

S20 **S21** (quant.)

A solution of **S20** (21.5 mg, 0.032 mmol) in CH_2Cl_2 (480 µL) was cooled to 0 °C, then TFA (160 µL) was added dropwise. After warming to ambient temperature, the reaction mixture was stirred for 2 h. The reaction mixture was then diluted with CH_2Cl_2 (5 mL) and poured into saturated $NaHCO_3$ (5 mL) with separation of aqueous and organic phases. The aqueous phase was extracted with CH_2Cl_2 (3 x 5 mL) and the combined organics were washed with brine (5 mL), dried over $MgSO_4$, filtered and concentrated *in vacuo* to yield **S21** (18.1 mg, 0.032 mmol, quant.) as a white foam without further purification.

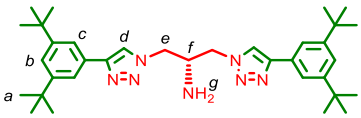

δ_H ($CDCl_3$, 400 MHz) 7.99 (s, 2H, H_d), 7.69 (d, J = 1.8, 4H, H_c), 7.44 (t, J = 1.8, 2H, H_b), 4.51 (dd, J = 14.0, 5.6, 2H, H_e), 4.42 (dd, J = 14.0, 5.7, 2H, H_e), 3.92 (p, J = 5.7, 1H, H_f), 1.68 (br. s, 2H, H_{NH2}), 1.37 (s, 36H, H_a); δ_C ($CDCl_3$, 101 MHz) 151.7, 149.0, 129.6, 122.8, 121.4, 120.4, 53.6, 51.9, 35.1, 31.6, 29.9, 17.9; HR-ESI-MS (+ve) m/z = 570.4281 $[M+H]^+$ (calc. m/z for $C_{35}H_{52}N_7$ 570.4279).

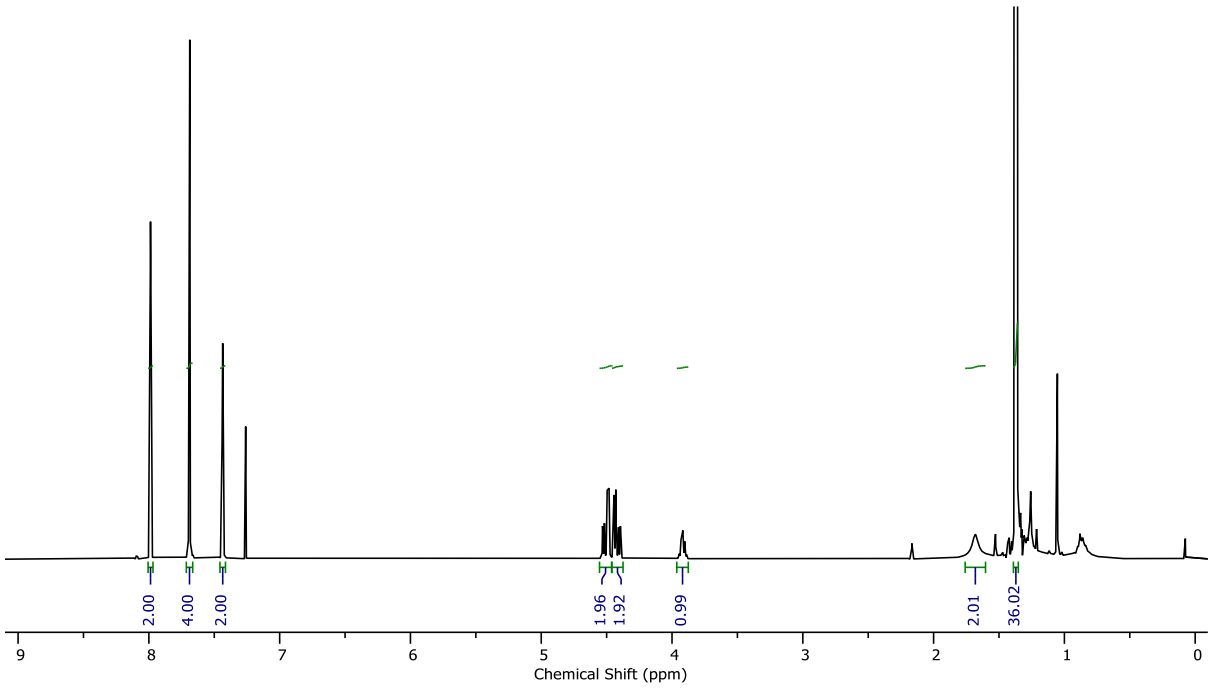

Figure 188: ^1H NMR ($CDCl_3$, 400 MHz) of **S21**.

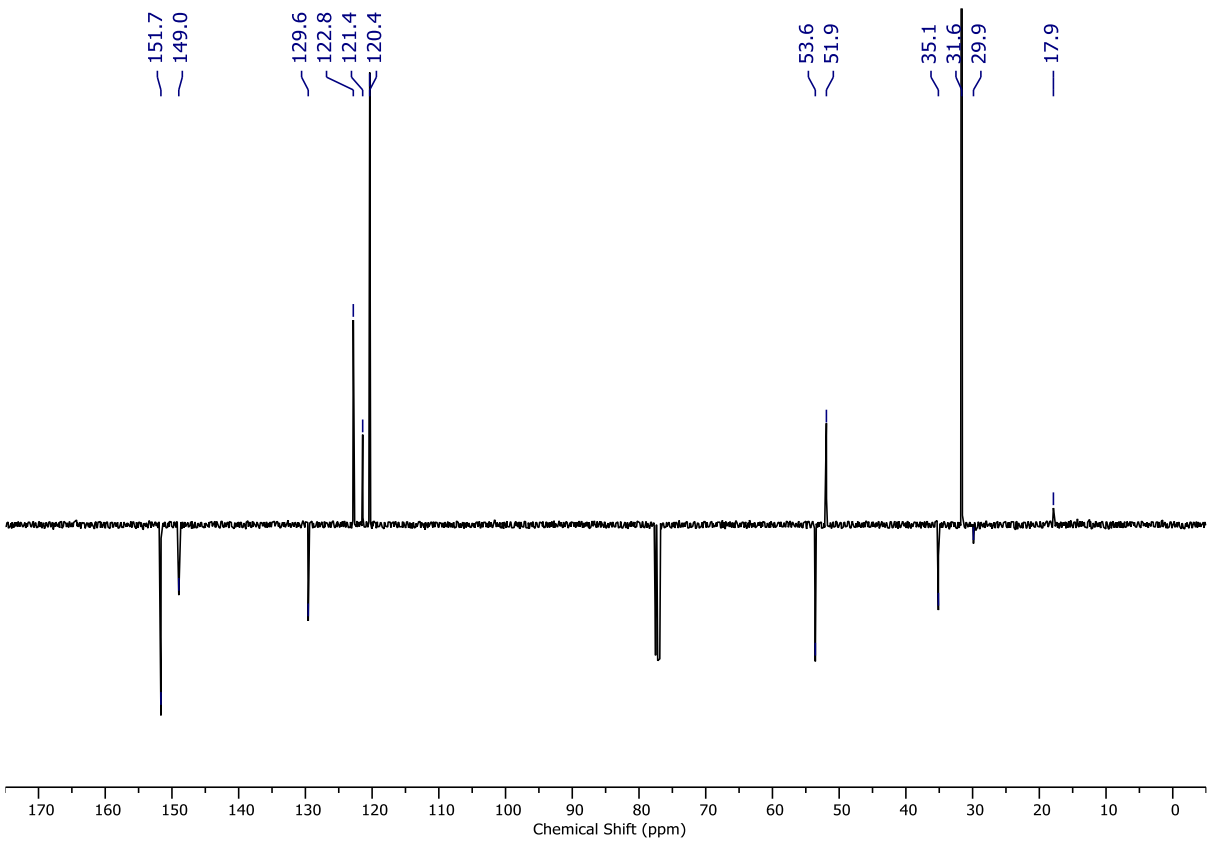

Figure 189: JMOD NMR ($CDCl_3$, 101 MHz) of **S21**.

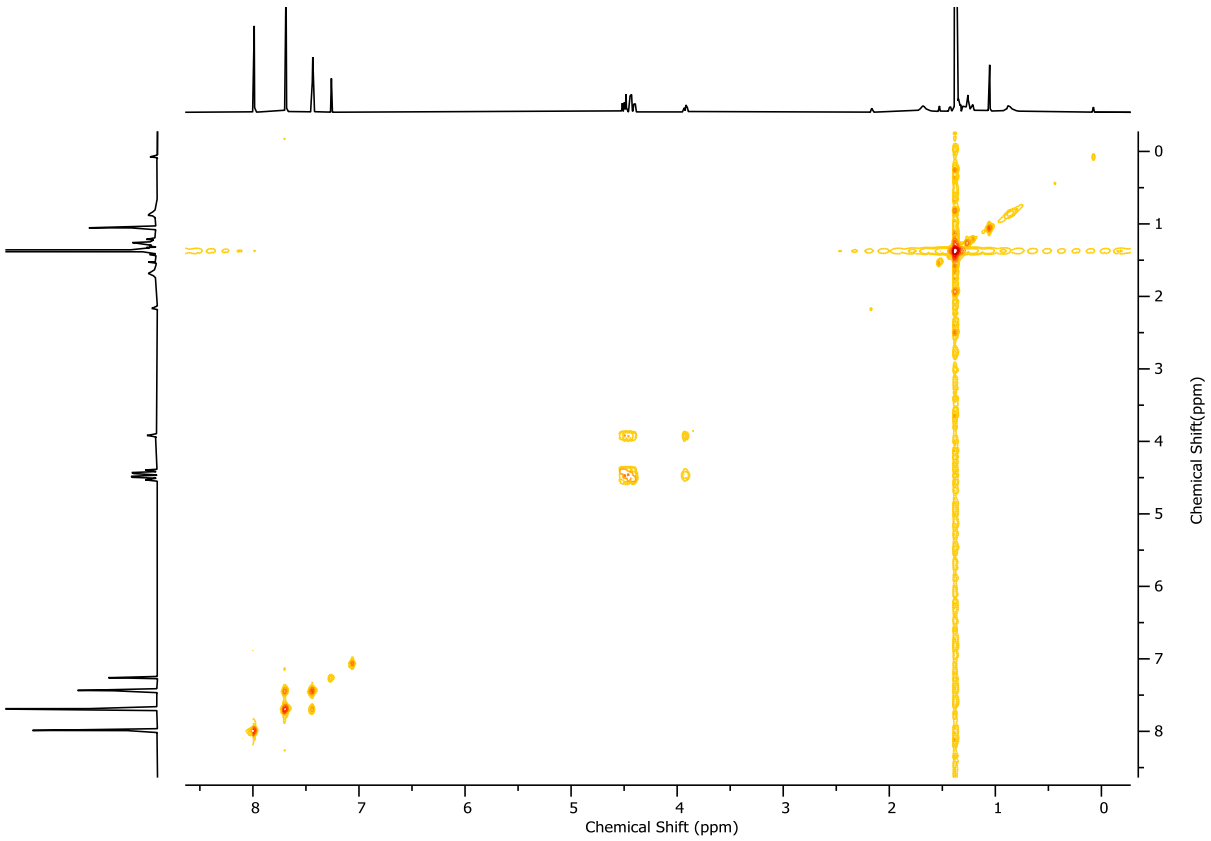

Figure 190: ^1H COSY NMR ($CDCl_3$, 400 MHz) of **S21**.

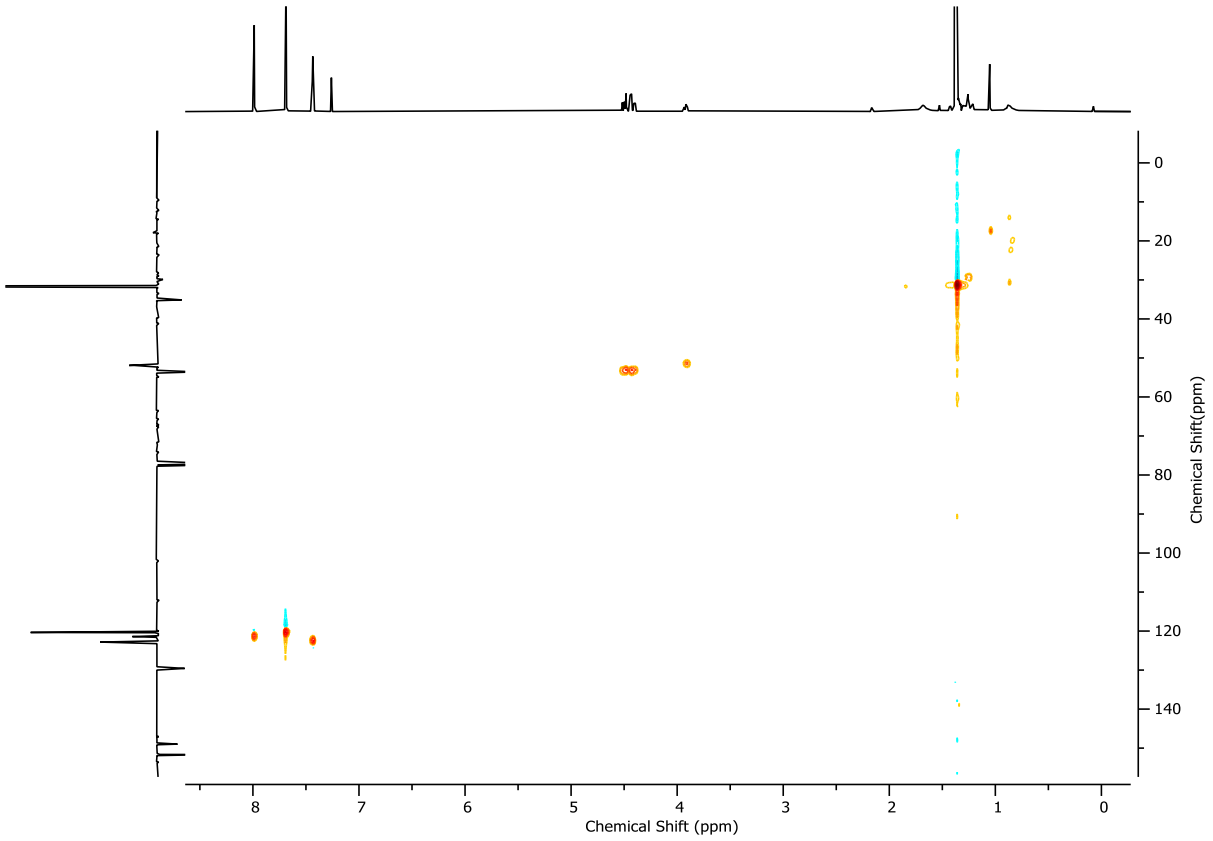

Figure 191: HSQC NMR ($CDCl_3$, 400 MHz) of **S21**.

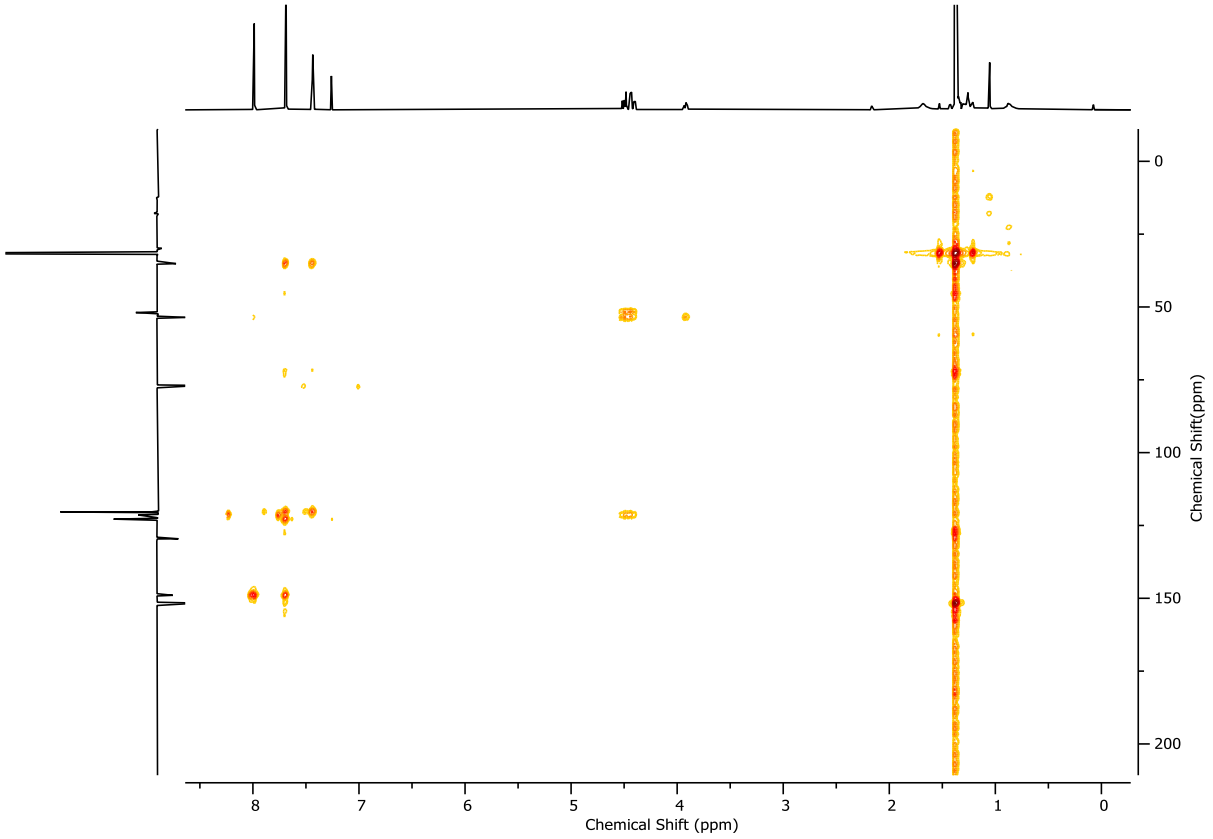

Figure 192: HMBC NMR ($CDCl_3$, 400 MHz) of **S21**.

10. Affect of conditions in the synthesis of catenane 3 and rotaxane 9

10.1. Effect of solvent on the direct synthesis of catenane 3 (route a)

Varying the solvent used in the AT-CuAAC synthesis of catenane **3** from pre-macrocycle (*R*)-**1** and macrocycle **1** did not lead to an improvement in the observed stereoselectivity (Table 1).

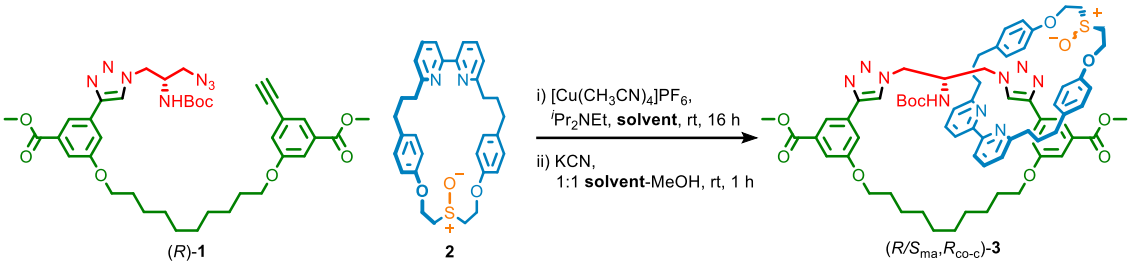

Scheme 9: Synthesis of catenane **3** from (*R*)-**1** and macrocycle **2** (route a)

Table 1: Effect of solvent in the direct synthesis of catenane **3**

Entry	Solvent	%conv.	*d.r.*
1	CH_2Cl_2	100	71 : 29
2	(1:1) CH_2Cl_2-PhMe	100	64 : 36
3	(1:1) CH_3Cl-EtOH	100	63 : 37

10.2. Oxidant screening for the oxidative synthesis of synthesis of catenane 3 (route b)

A brief screen of oxidants for route b was conducted. Initially mCPBA appeared to give high diastereoselectivity but closer inspection revealed this was at the expense of yield because over oxidation to the sulfone was observed (Table 2, entries 1 and 2). Oxone (entry 3) proved unselective but avoided over oxidation. IBX produced catenane **3** in reasonable diastereoselectivity (39 : 61) and with the opposite major stereoisomer to route a (entry 4). The chiral Davis oxaziridine reagent produced the opposite major stereoiomer in reasonable stereoselectivity (entry 5). Conditions reported by Sharpless for the enantioselective oxidation of sulfides did not result in any conversion. IBX oxidation (entry 4) was selected for the preparative reactions as it proceeds with the highest stereoselectivity and gives access to the opposite major stereoisomer from route a, facilitating access to the second enantiomer of **5**.

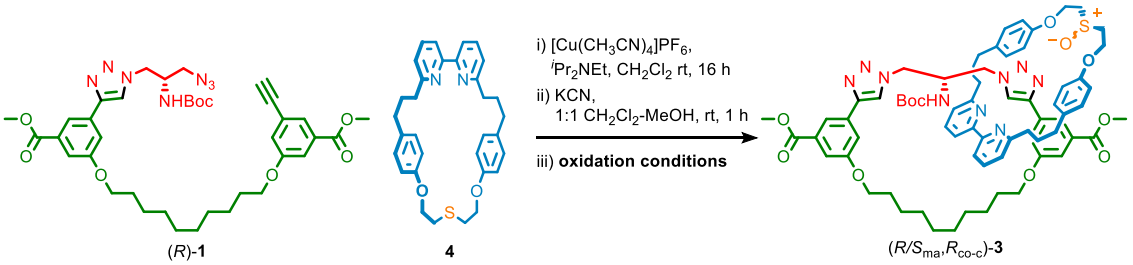

Scheme 10: Synthesis of catenane **3** from (*R*)-**1** and macrocycle **4** via oxidation (route b)

Table 2: Effect of oxidation conditions on the synthesis of catenane **3**

Entry	Conditions	%conv.	%sulfone	*d.r.*
1	mCPBA (1.2), CH_2Cl_2, -30 °C, 16 h	100	54	79 : 21
2	mCPBA (1.2), CH_2Cl_2, 25 °C, 2 h	100	27	58 : 42
3	Oxone (0.7), CH_3CN-H_2O, 25 °C, 16 h[6]	70	0	48 : 52
4	IBX (1.1), TEAB, $CHCl_3$-H_2O, 25 °C, 16 h[7]	100	0	39 : 61
5	Davis oxaziridine[a] (1.0), CH_2Cl_2, 25 °C, 16 h[8]	100	0	56 : 44
6	TBHP (1.0), $Ti(O^iPr)_4$, DET,[b] $ClCH_2CH_2Cl$, -20 °C, 16 h[9]	0	-	-

[a] (+)-(8,8-Dichlorocamphorylsulfonyl)oxaziridine. [b] Diethyltartrate

10.3. Effect of solvent on the direct synthesis of rotaxane 9 (route a)

Varying the solvent used in the AT-CuAAC synthesis of rotaxane **9** from half axle (*R*)-**7** and macrocycle **1** did not lead to an improvement in the observed stereoselectivity (Table 3).

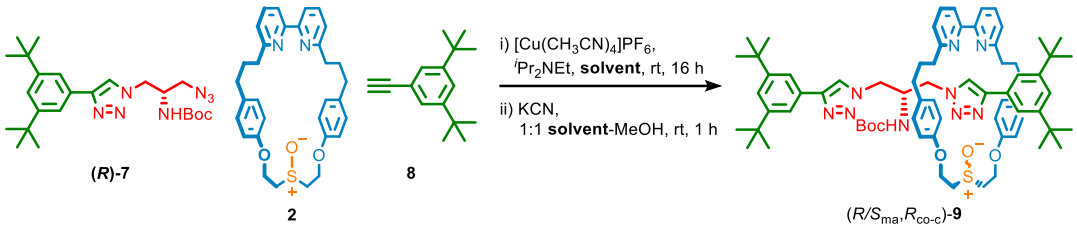

Scheme 11: Synthesis of rotaxane **9** from (*R*)-**7**, macrocycle **2** and alkyne **8** (route a)

Table 3: Effect of solvent in the direct synthesis of rotaxane **9**

Entry	Solvent	%conv.	*d.r.*
1	CH_2Cl_2	100	75 : 25
2	(1:1) CH_3Cl-EtOH	100	62 : 38

10.4. Oxidant screening for the oxidative synthesis of rotaxane 9 (route b)

As with the synthesis of catenane 3, varying the oxidant in the synthesis of rotaxane 9 (route b), resulted in different diastereoselectivity (Table 4). Once again, the use of IBX resulted in the highest diastereoselectivity for the oxidation of the sulfide rotaxane (entry 3) and produced the opposite major stereoisomer to route a. This method was selected for preparative scale reactions.

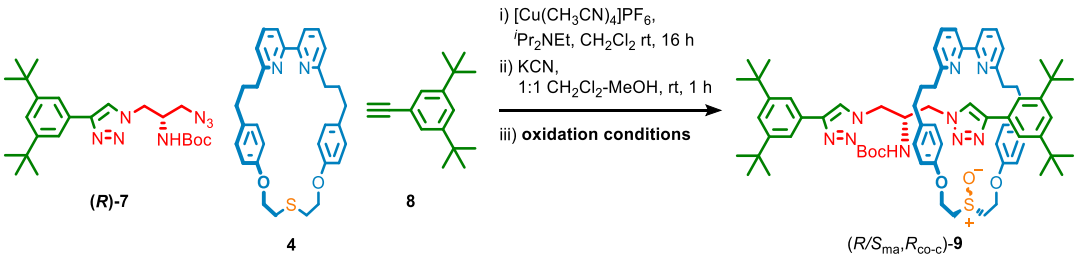

Scheme 12: Synthesis of rotaxane **9** from (*R*)-**7**, macrocycle **4** and alkyne **8** via oxidation (route b)

Table 4: Effect of oxidation conditions on the synthesis of rotaxane **9**

Entry	Conditions	%conv.	%sulfone	*d.r.*
1	mCPBA (1.2), CH_2Cl_2, 25 °C, 3 h	90	10	48 : 52
2	NBS (1.1), SiO_2, CH_2Cl_2, 25 °C, 1.5 h[10]	100	0	50 : 50
3	IBX/TEAB (1.1), $CHCl_3$-H_2O, 25 °C, 16 h[7]	100	0	40 : 60
4	Davis oxaziridine[a] (1.0), CH_2Cl_2, 25 °C, 16 h[8]	100	0	56 : 44
5	Ti(O^iPr)$_4$/BINOL/TBHP (2.0), PhMe-H_2O, 25 °C, 16 h[11]	50	9	57 : 43

[a] (+)-(8,8-Dichlorocamphorylsulfonyl)oxaziridine

11. NMR Stack Plots

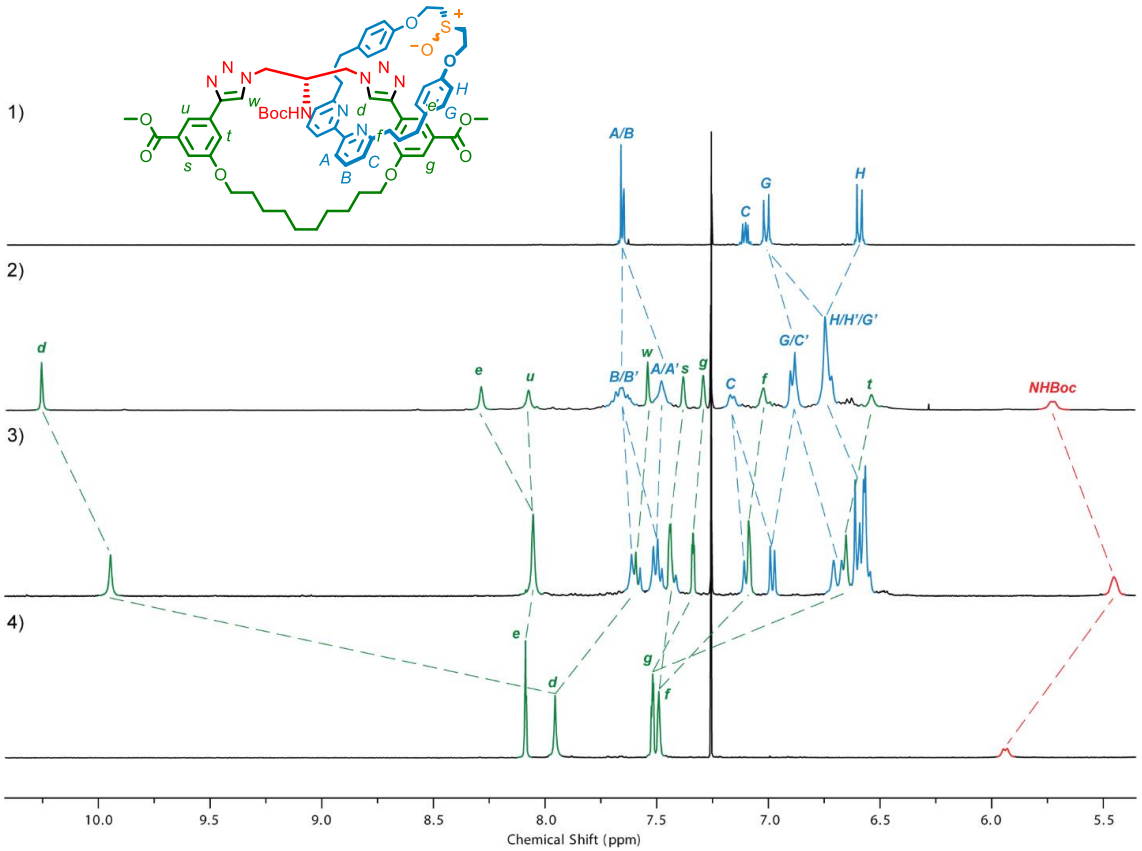

Figure 193: Stacked ^{1}H NMR ($CDCl_3$, 400 MHz): 1) macrocyle **2**, 2) catenane (S_{ma},$R_{co\text{-}c}$)-**3**, 3) catenane (R_{ma},$R_{co\text{-}c}$)-**3**, 4) macrocycle **S13**.

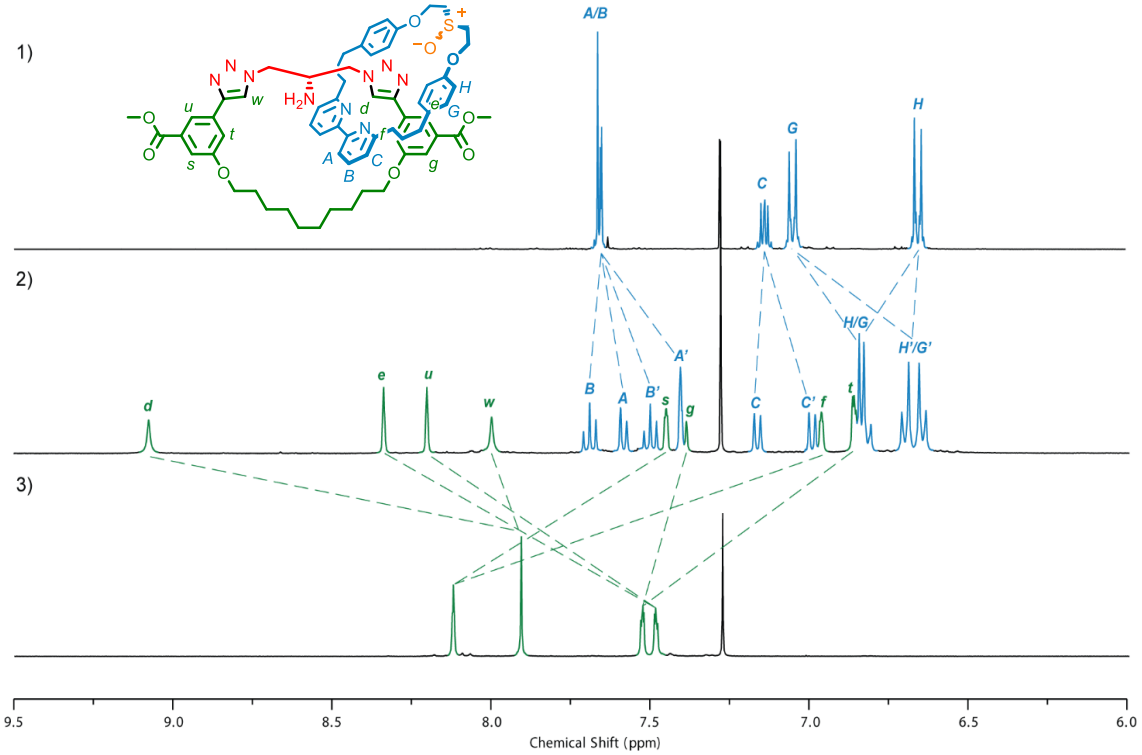

Figure 194: Stacked ^{1}H NMR ($CDCl_3$, 400 MHz): macrocyle **2**, 2) catenane (S_{ma})-**6**, 3) macrocycle **S13**.

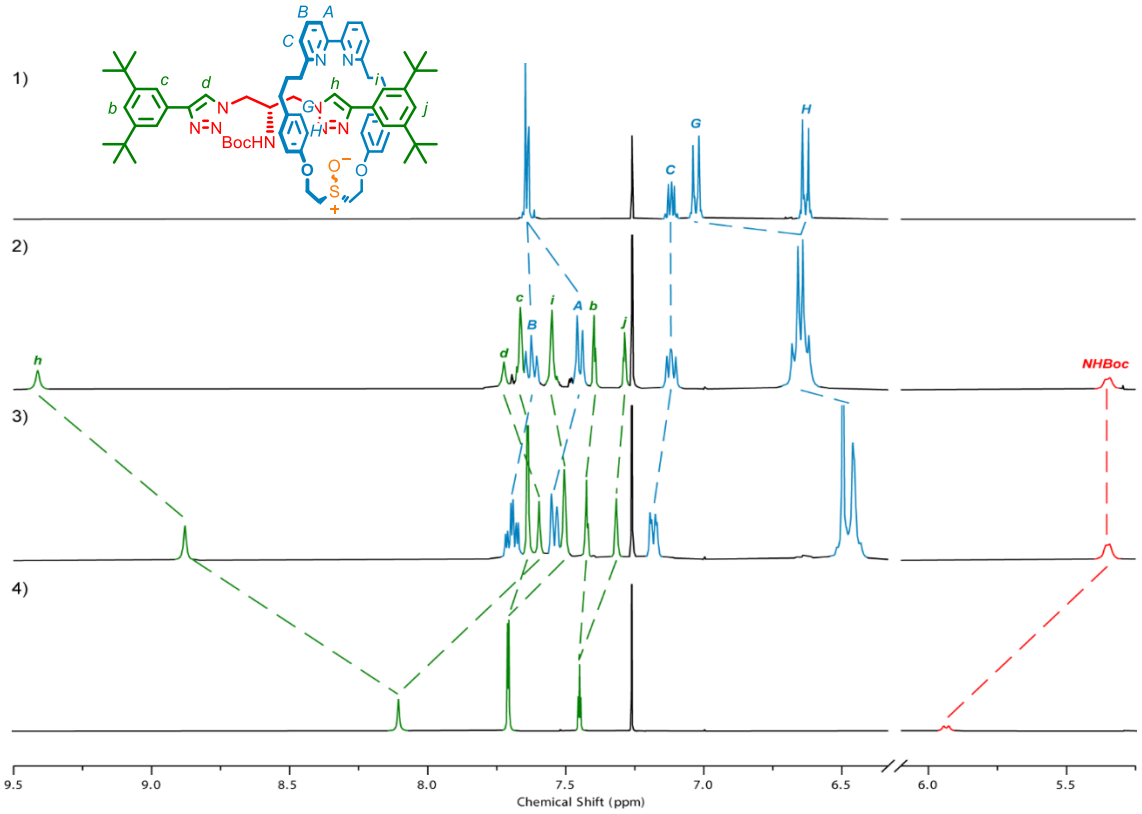

Figure 195: Stacked ^{1}H NMR ($CDCl_3$, 400 MHz): 1) macrocyle **2**, 2) rotaxane (S_{ma},$R_{co\text{-}c}$)-**9**, 3) rotaxane (R_{ma},$R_{co\text{-}c}$)-**9**, 4) axle **S20**.

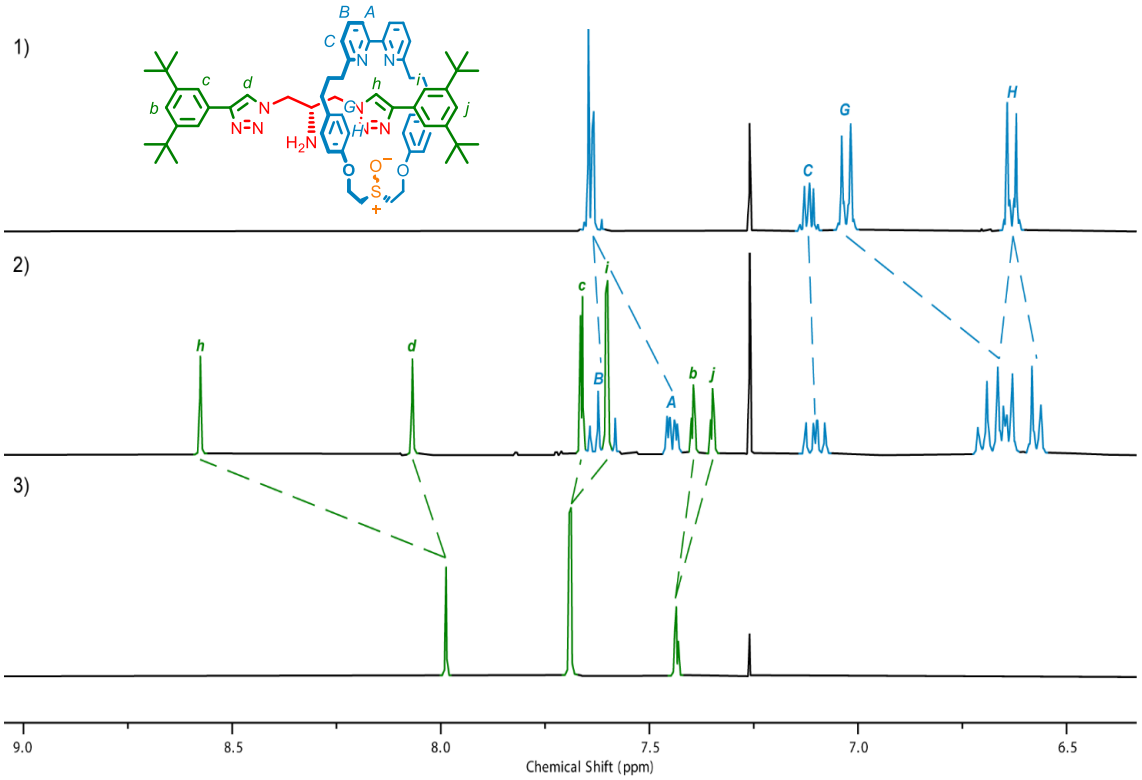

Figure 196: Stacked ^{1}H NMR ($CDCl_3$, 400 MHz): 1) macrocycle **2**, 2) rotaxane (S_{ma})-**10**, 3) axle **S21**

12. Single Crystal X-ray Diffraction Analysis

12.1. Single Crystal X-ray Diffraction Data for Catenane *rac*-(S_{ma},$R_{co\text{-}c}$)-3

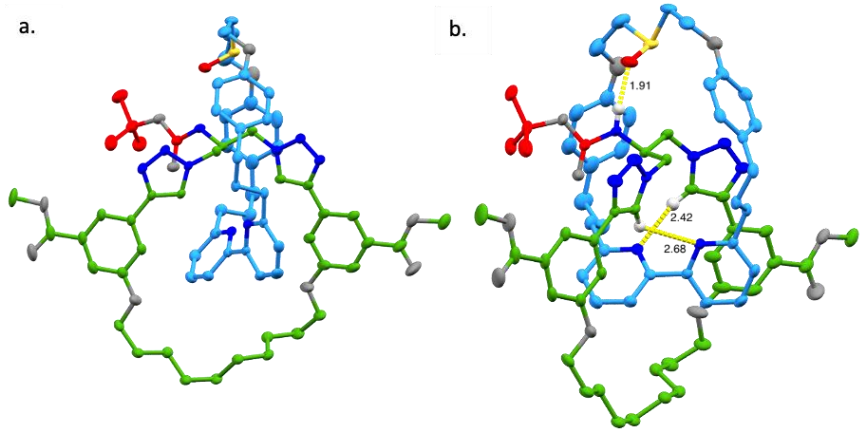

Figure 197: Ellipsoid plot of the asymmetric unit of *rac*-(S_{ma},$R_{co\text{-}c}$)-**3** with hydrogens omitted for clarity (a) and highlighting key interactions (b). Thermal ellipsoids at 50% probability.

Single crystals of racemic *rac*-(S_{ma},$R_{co\text{-}c}$)-**3** were grown by slow vapour diffusion of *n*pentane into a concentrated CH_2Cl_2 solution, yielding large colourless block crystals. Data was collected at 100 K on a Rigaku 007 HF diffractometer equipped with a HyPix 6000HE hybrid pixel array detector. Cell determination, data reduction, cell refinement, and absorption correction were processed by CrysalisPro[12]. The structure was solved within Olex2[13] by ShelXT[14] with refinement by ShelXL[15]. The asymmetric unit contained one molecule of $C_{70}H_{83}N_9O_{11}S$ (R_{ma},$S_{co\text{-}c}$)-**3** and disordered solvent. The unit cell contains both enantiomers related by an inversion centre. The disordered solvent was believed to contain primarily two dichloromethane molecules. There was also some indication of a low occupancy pentane molecule. Modelling of the disordered solvent molecules was attempted, however, the quality of the solution was significantly diminished, and thus the program SQUEEZE[16] implemented within PLATON[17] was used to account for the electron density within this region of the unit cell. SQUEEZE identified solvent accessible voids of 590 Å^3 and 192 electrons per unit cell were recovered.

Table 5 Crystal data and structure refinement for (*rac*)-(S_{ma},$R_{co\text{-}c}$)-**3**

CCDC Number	2109976	ρ_{calc} g/cm^3	1.120
Empirical Formula	$C_{70}H_{83}N_9O_{11}S$	μ/mm^{-1}	0.10
Formula Weight	1258.51	F(000)	1340
Temperature/K	100	Crystal size/mm^3	0.47 × 0.25 × 0.14
Crystal System	Triclinic	Radiation	Mo *K*α (λ=0.71073)
Space Group	*P*-1	2Θ range/°	4.0 – 64.2
a/Å	15.2504(3)	Index range	-21 ≤ *h* ≤ 22, -24 ≤ *k* ≤ 25, -24 ≤ *l* ≤ 25
b/Å	17.0326(4)	Reflections Collected	108399
c/Å	17.2393(3)	Independent Reflections	23034
α/°	106.910(2)	Data/parameters/restraints	23034/915/75
β/°	103.444(2)	Goodness-of-fit on F^2	1.025
γ/°	110.252(2)	Final R-factor [I ≥ 2σ(I)]	0.0616
Volume/Å^3	3732.34(15)	Final R indexes [all data]	R_1 = 0.0830, wR_2 = 0.1698
Z	2	Largest diff. peak/hole e Å^{-3}	0.88/-0.54

12.2. Single Crystal X-ray Diffraction Data for Catenane *rac*-6

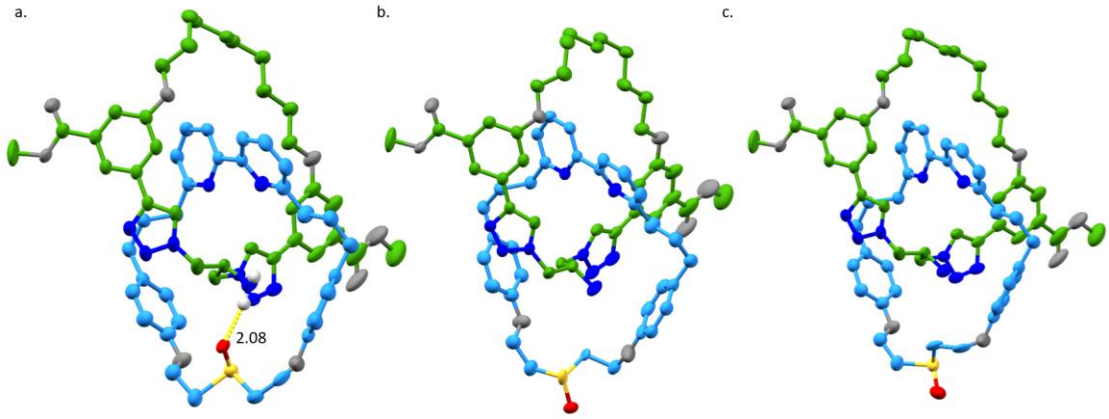

Figure 198: Ellipsoid plots of the asymmetric unit for rac-**6** depicting the three positions modelled for the sulfoxide disorder, which correspond to (a) (S_{ma},$R_{co\text{-}c}$)-**6**, (b) (S_{ma},$R_{co\text{-}c}$)-**6** and (c) (R_{ma},$R_{co\text{-}c}$)-**6** with ~50%, 30% and 20% occupancy respectively. Thermal ellipsoids at 50% probability, hydrogens omitted for clarity. Key intramolecular interactions are highlighted.

Single crystals of *rac*-**6** were grown by slow evaporation of a primarily ethyl acetate solution over a period of three months, yielding large colourless block crystals. Data was collected at 100 K on a Rigaku 007 HF diffractometer equipped with a HyPix 6000HE hybrid pixel array detector. Cell determination, data reduction, cell refinement, and absorption correction were processed by CrysalisPro. The structure was solved within Olex2[13] by ShelXT[14] with refinement by ShelXL[15]. The asymmetric units contained one molecule of $C_{65}H_{75}N_9O_9S$ and disordered solvent. The unit cell contained both enantiomers related by an inversion centre. The serendipity of the crystallization, in combination with disorder, precluded the identification of the solvent. Consequently, the electron density in this region of the unit cell was accounted for using the program SQUEEZE[16] implemented within PLATON[17]. SQUEEZE identified solvent accessible voids of 64 Å^3 and 23 electrons per unit cell were recovered. The sulfoxide group could be modelled reasonably as being disordered over three positions. A residual electron density peak (0.79 electrons) suggested the possibility of a fourth position corresponding to the second co-conformation of the inward pointing sulfoxide. However, this could not be modelled effectively.

Table 6: Single Crystal Diffraction and Refinement Statistics for *rac*-**6**

CCDC Number	2115463	ρ_{calc} g/cm^3	1.274
Empirical Formula	$C_{65}H_{75}N_9O_9S$	μ/mm^{-1}	1.00
Formula Weight	1158.40	F(000)	1232
Temperature/K	100	Crystal size/mm^3	0.45 × 0.33 × 0.22
Crystal System	Triclinic	Radiation	Cu $K\alpha$ (λ=1.54178)
Space Group	*P*-1	2Θ range/°	7.8 – 140.4
a/Å	9.9605(1)	Index range	-10 ≤ h ≤ 11, -15 ≤ k ≤ 16, -27 ≤ l ≤ 26
b/Å	13.4937(1)	Reflections Collected	35260
c/Å	22.5630(2)	Independent Reflections	11057
α/°	88.176(1)	Data/parameters/restraints	11057/889/306
β/°	86.450(1)	Goodness-of-fit on F^2	1.041
γ/°	86.543(1)	Final R-factor [I ≥ 2σ(I)]	0.0866
Volume/Å^3	3020.03(5)	Final R indexes [all data]	R1 = 0.0895, wR2 = 0.2219
Z	2	Largest diff. peak/hole e Å^{-3}	1.45/-0.65

12.3. Single Crystal X-ray Diffraction Data for Catenane *rac*-S15

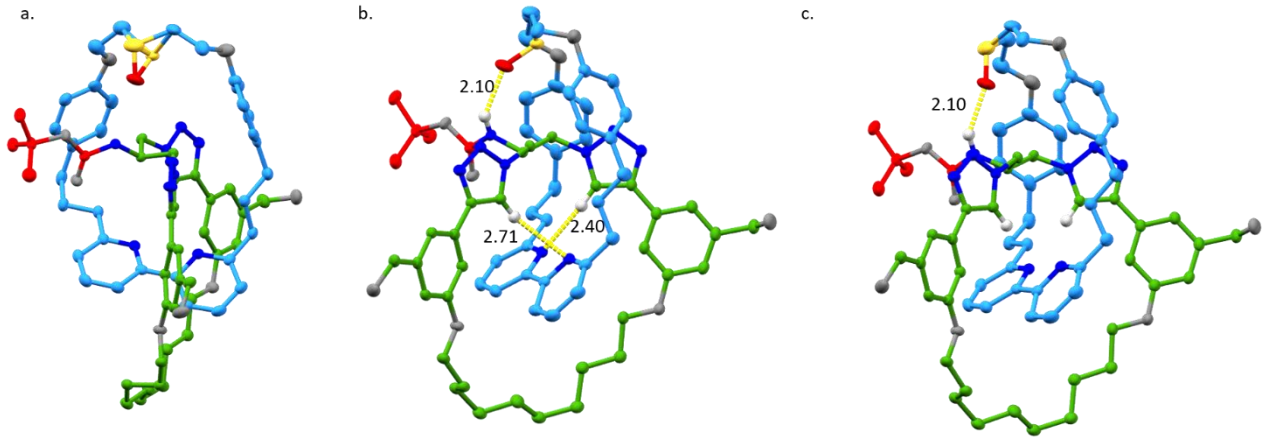

Figure 199: Ellipsoid plot of the asymmetric unit for rac-**S15**. (a) disorder of the sulfur atom between the two diastereomeric positions (hydrogens omitted for clarity), key interactions for (b) (S_{ma},$R_{co\text{-}c}$)-**S15** and (c) (R_{ma},$R_{co\text{-}c}$)-**S15**. Thermal ellipsoids at 50% probability, methanol solvent omitted for clarity.

Single crystals of *rac*-**S15** were grown by slow evaporation of a concentrated methanol solution, yielding colourless block crystals. Data was collected at 100 K on a Rigaku 007 HF diffractometer equipped with a HyPix 6000HE hybrid pixel array detector. Cell determination, data reduction, cell refinement, and absorption correction were processed by CrysalisPro. The structure was solved within Olex2[13] by ShelXT[14] with refinement by ShelXL[15]. The asymmetric unit contained one molecule of $C_{68}H_{83}N_9O_9S$ (**S15**) and one molecule of methanol. The unit cell contained enantiomeric structures related by an inversion centre. Modelling of the disorder is consistent with diastereomeric structures (R_{ma},$S_{co\text{-}c}$)-**S15** and (S_{ma},$S_{co\text{-}c}$)-**S15** occupying the same lattice positions with the occupancies refining to a ratio of ~80 : 20. A consequence of this disorder is a number of Hirshfeld test warnings for atom pairs in the alkyl chain, with one reaching a B-level alert on the checkcif report. We could remove these alerts by applying various restraints, however, in the context of the crystal we felt these were excessive. Moreover, the structure presented here agrees with all other experimental data. Therefore, we conclude that these alerts are a result of the disorder and not indicative of an incorrect atom-type assignment.

Table 7 Crystal data and structure refinement for (*rac*)-**S15**

CCDC Number	2109991	ρ_{calc} g/cm^3	1.257
Empirical Formula	$C_{69}H_{87}N_9O_{10}S$	μ/mm^{-1}	0.97
Formula Weight	1234.53	F(000)	1320
Temperature/K	100	Crystal size/mm^3	0.37 × 0.20 × 0.12
Crystal System	Triclinic	Radiation	Cu $K\alpha$ (λ=1.54178)
Space Group	*P*-1	2Θ range/°	6.2 – 140.4
a/Å	11.4186(1)	Index range	-13 ≤ *h* ≤ 13, -18 ≤ *k* ≤ 18, -24 ≤ *l* ≤ 24
b/Å	15.1215(1)	Reflections Collected	60775
c/Å	20.0942(1)	Independent Reflections	12119
α/°	95.432(1)	Data/parameters/restraints	12119/818/3
β/°	100.146(1)	Goodness-of-fit on F^2	1.034
γ/°	105.079(1)	Final R-factor [I ≥ 2σ(I)]	0.0468,
Volume/Å^3	3261.51(4)	Final R indexes [all data]	R_1 = 0.0480, wR_2 = 0.1145
Z	2	Largest diff. peak/hole e Å^{-3}	1.05/-0.42

12.4. Single Crystal X-ray Diffraction Data for Rotaxane (R_{ma},$R_{co\text{-}c}$)-9

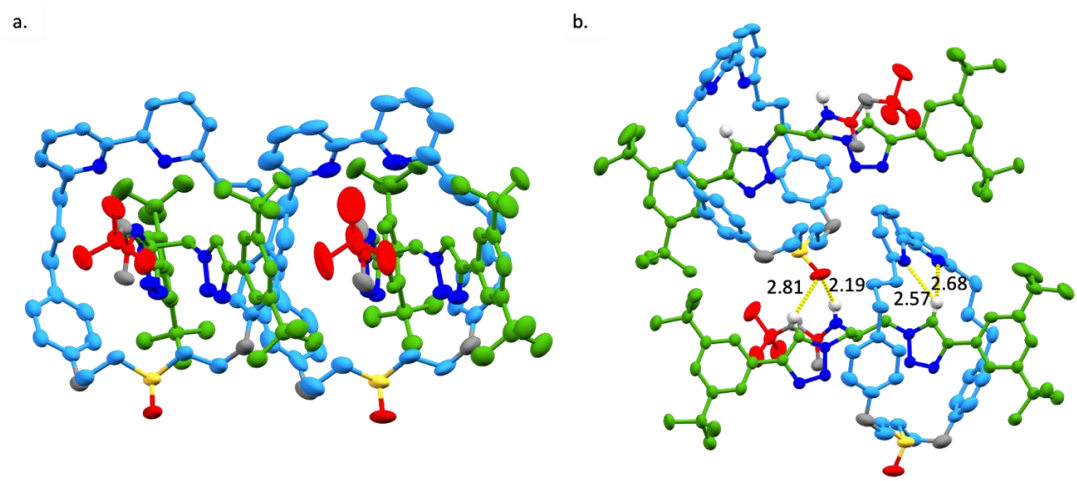

Figure 200: Ellipsoid plot of the asymmetric unit for (R_{ma},$R_{co\text{-}c}$)-**9** (a) and with key interactions (b). Thermal ellipsoids at 50% probability, hydrogens omitted for clarity.

Single crystals of (R_{ma},$R_{co\text{-}c}$)-**9** were grown by slow vapour diffusion of ^{n}pentane into a concentrated CH_2Cl_2 solution of (R_{ma},$R_{co\text{-}c}$)-**9** yielding colourless needle crystals. Data was collected at 100 K on a Rigaku 007 HF diffractometer equipped with a HyPix 6000HE hybrid pixel array detector. Cell determination, data reduction, cell refinement, and absorption correction were processed by CrysalisPro. The structure was solved within Olex2[13] by ShelXT[14] with refinement by ShelXL[15]. The asymmetric unit contained two crystallographically independent molecules of $C_{72}H_{93}N_9O_5S$ (R_{ma},$R_{co\text{-}c}$)-**9** and solvent accessible voids. The voids were accounted for using the program SQUEEZE[16] implemented within PLATON[17]. SQUEEZE identified solvent accessible voids of 565 Å^3 and 18 electrons per unit cell were recovered. The absolute stereochemistry of the structure is consistent with the configuration of the starting materials and supported by by refinement of the Flack parameter.

Table 8 Crystal data and structure refinement for (R_{ma},$R_{co\text{-}c}$)-**9**

CCDC Number	2109992	F(000)	2576
Empirical Formula	$C_{72}H_{93}N_9O_5S$	Crystal size/mm^3	0.48 × 0.13 × 0.06
Formula Weight	1196.61	Radiation	Cu Kα (λ=1.54178)
Temperature/K	100	2Θ range/°	5.8 – 140.6
Crystal System	Monoclinic	Index range	-22 ≤ h ≤ 23, -23 ≤ k ≤ 20, -24 ≤ l ≤ 16
Space Group	$P2_1$	Reflections Collected	67048
a/Å	19.0015(1)	Independent Reflections	22005
b/Å	19.5618(2)	Data/parameters/restraints	22005/1597/61
c/Å	19.8094(2)	Goodness-of-fit on F^2	1.068
β/°	102.508(1)	Final R-factor [I ≥ 2σ(I)]	0.0496
Volume/Å^3	7188.46(11)	Final R indexes [all data]	R1 = 0.0568, wR2 = 0.1425
Z	4	Flack parameter	0.027(7)
ρ_{calc} g/cm^3	1.106	Largest diff. peak/hole e Å^{-3}	0.51/-0.31
μ/mm^{-1}	0.81		

13. Discussion of the structural features of mechanically axially chiral molecules

13.1. Fundamental symmetry properties of the mechanical axial stereogenic unit

A mechanically axially chiral stereogenic unit arises when two covalent subcomponents with permanently distinguishable faces are directly mechanically bonded. The requirement for permanently distinguishable faces of the ring is achieved when its most symmetrical conformation has C_{nv} symmetry (rotational axis and mirror planes are perpendicular to the ring plane). Schematic structure **II** is the minimal representation of an axially chiral catenane (Figure 201a), the constituent rings (**I**) of which have $C_{\infty v}$ symmetry. Examining **II** allows us to identify how the mechanical axial stereogenic unit arises; in catenane **II** it is not possible to align any mirror plane of one ring with that of the other, which ensures that no improper symmetry operations of the subcomponents are maintained in the interlocked structure. In other words, it is the orthogonal arrangement of the rings enforced by the mechanical bond that ensures that the resulting structure is chiral.

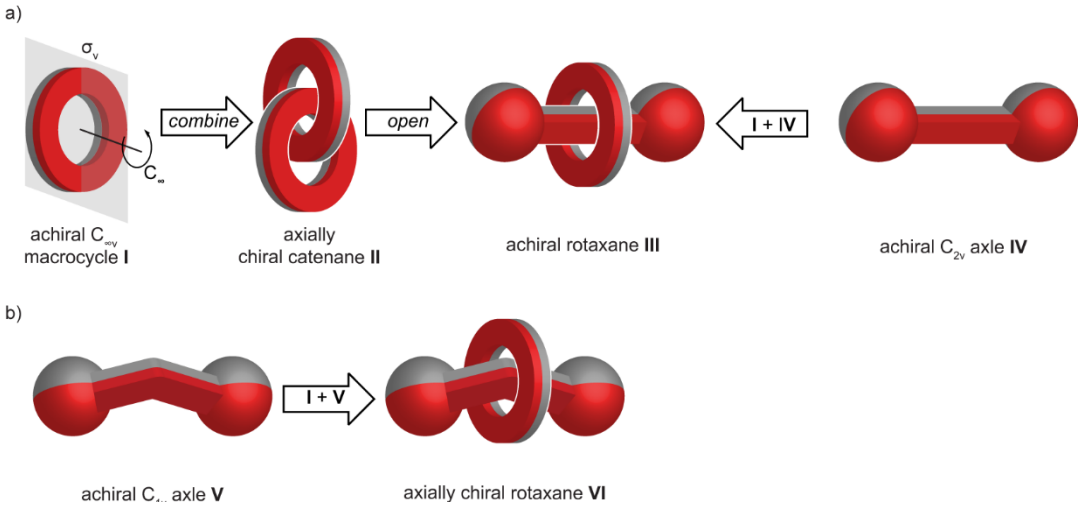

Figure 201: a) Minimal schematic representation of axially chiral catenane **II** based on $C_{\infty v}$ ring **I** and achiral rotaxane **III** that results from the notional ring opening of **II**. b) Minimal schematic respresentation of a mechanically axially chiral rotaxane based on C_{1v} axle **VI**.

Turning to the equivalent rotaxane stereogenic unit, it is tempting to consider the notional ring opening and stoppering of axially chiral catenane structure **II**, but this results in an achiral object (**III**) if the axle (**IV**) is assumed to have a linear structure, as is typical in such schematic representations (Figure 201a). Examining the symmetry of axle **IV** reveals the origin of this surprising result; it has C_{2v} symmetry and one of the σ_v mirror planes of the axle can be arranged to be coincident with that of the ring. As a consequence, representation **III** is achiral. An alternative way of considering this problem is simply to recognise that axle **IV** does not have distinguishable faces.

Returning to the definition of the catenane axial stereogenic unit, we can predict that an equivalent stereogenic unit will arise in a rotaxane if the axle component has no mirror planes along its long axis. This is the case if the axle component has C_{1v} symmetry (more commonly referred to as C_s) in which the only symmetry operation is a mirror plane perpendicular to the axle. In schematic form, this can be achieved by requiring that the axle adopts a fixed non-linear structure (**V**), although any structural feature that results in C_{1v} symmetry is sufficient (Figure 201b).

Based on the above discussion we define the mechanical axial stereogenic unit of catenanes as arising the mechanical bond between two C_{nv} rings, and the equivalent unit of rotaxanes arising from the combination of a C_{1v} (C_s) axle with a C_{nv} ring.

13.2. Prochirality in "real" mechanically axially chiral structures

The schematic representations above make no reference to how the required symmetry properties arise. Indeed, representation **I** effectively implies that the structure of the ring is continuous, whereas molecules are made up of atoms bonded together and so are granular.

The axles of mechanically axially chiral rotaxanes are required to be prochiral as this gives rise to the required C_{1v} symmetry. Thus, suitably embedded prochiral centres, axes and planes in the middle of an axle will give rise to a mechanically axially chiral rotaxane (**VI-VIII** respectively,Figure 202a). Alternatively, a meso structure (e.g. **IX**, Figure 202b) in which two or more stereogenic centres are related by a mirror plane that bisects the axle will also give rise to a C_{1v} axle and so mechanical axial chirality. It should be noted that the overall structure of **IX** is also potentially prochiral as any single modification that does not lie on the mirror plane gives rise to a chiral structure.

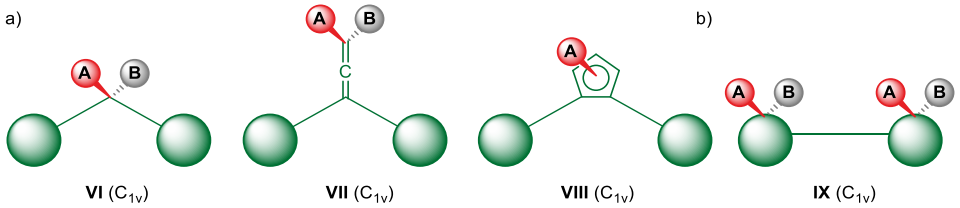

Figure 202: Semi-structural representations of axles suitable for inclusion in mechanically axially chiral rotaxanes based on (a) a single prochiral centre (**VI**), axis (**VII**) or plane (**VIII**) or (b) two stereogenic units related by an internal mirror plane to generate a meso structure (**IX**).

The simplest way to design a ring suitable for inclusion in a mechanically axially chiral structure is also to embed a single prochiral moiety (centre as shown, or axis/plane) such that the associated mirror plane lies perpendicular to the ring to generate a C_{1v} structure (e.g. **X**, Figure 203). Achiral rings containing multiple identical prochiral units also give rise to catenanes in which the mechanical axial stereogenic unit is the sole fixed source of stereochemistry (e.g. **XI**). It is also possible to achieve C_{1v} symmetry when a ring contains two or more stereogenic units related by a mirror plane to give a meso structure (e.g. **XII**). As with **IX**, ring **XII** is potentially prochiral as any modification that does not lie on the symmetry plane results in a chiral structure. If multiple non-identical prochiral units are present, the maximum rotational symmetry is determined by the lowest number in a set; for example, a ring containing two pairs of identical prochiral moieties can exhibit C_{2v} symmetry (e.g. **XIII**). The same groups connected such that the system is meso has C_{1v} symmetry (**XIV**).

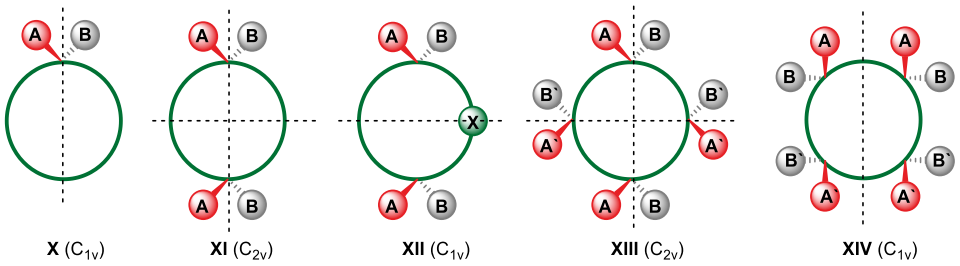

Figure 203: Semi-structural representations of rings suitable for inclusion in mechanically axially molecules based on a single prochiral centre (**X**), two identical prochiral (**XI**), two identical stereogenic units (XII), two pairs of prochiral units (**XIII**) or two pairs of stereogenic units (**XIV**).

Finally, it is interesting to consider if rings can be designed in which prochirality does not arise, as in minimal representation **I**. If a C_{nv} ring containing n identical prochiral moieties is designed such that every atom lies on a mirror plane the overall structure is pro-prochiral (i.e. two modifications are required to render the

structure chiral) but can still give rise to mechanically axially chiral structures (e.g. **XV**, Figure 204). Although a cyclohexane ring is obviously far too small to include in a catenane structure, the same holds for any cycloalkane substituted as shown. Such rings are obviously a special case, but it is important to note this exception to the general rule that the covalent subcomponents of mechanically axially chiral molecules exhibit prochirality. As n→∞ an equivalent symmetry to **II** would be achieved, although this is unphysical.

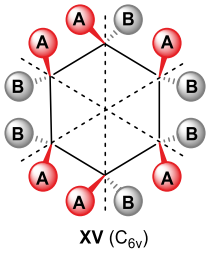

Figure 204: An example of a C_{nv} ring that does not display prochirality - as every atom and bond lies on a mirror plane two modification as required to generate a chiral structure.

13.3. Co-conformational covalent diastereomerism in mechanically axially chiral structures

Co-conformational covalent stereochemistry arises when the relative positions of the covalent sub-components in an interlocked structure result in the desymmetrisation of one or more covalent pro-stereogenic units (e.g. rotaxane **XVI** exists as an achiral and enantiomeric co-conformations, Figure 205). Given that prochirality is a common feature of mechanically axially chiral structures, it is thus unsurprising that they will be expected to display co-conformational diastereomerism (e.g. **XVII**) – although a highly symmetrical representation in which the mechanical axial stereogenic unit is the only source of stereochemistry is possible, it is not required to be the dominant co-conformation. Indeed, it is this property that we have taken advantage of in our approach to mechanically axially chiral rotaxanes and catenanes.

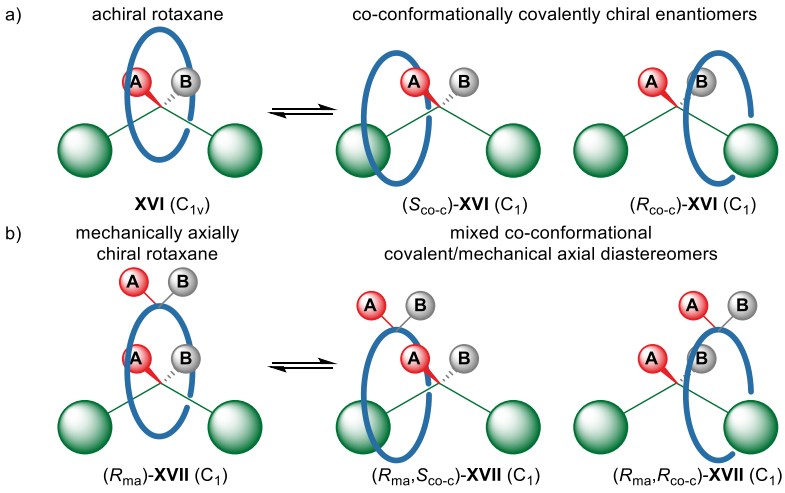

Figure 205: Co-conformational stereoisomerism in rotaxanes based on C_{1v} axles. (a) Co-conformational enantiomerism in rotaxane **XVI**. (b) Co-conformational diastereomerism in mechanically axially chiral rotaxane **XVII**.

The exception to this general rule would appear to be catenanes based on C_{nv} rings that contain n identical prochiral moieties – it has already been noted that such structures are pro-prochiral (Figure 204). However, although such molecules require two covalent modifications to generate a chiral structure, co-conformational desymmetrisation, which simply relies on the position of the other covalent subcomponent in space, can still give rise to diastereomers directly – the second component is not required to be located over an atom or a bond midpoint. Thus, although such rings are not prochiral, they can still exhibit co-conformational diastereomerism.

14. Assigning the absolute stereochemistry of mechanically axially chiral molecules

Although rules for assigning the absolute stereochemistry of mechanically axially chiral molecules have been proposed[18,19], as is often the case, attempts to apply these to real examples (as opposed to hypothetical cases or examples where the stereochemistry of the products was not determined), revealed their shortcomings. In particular, attempts to assign the stereochemistry of the molecules reported here highlighted that the outcome depended on the conformation of the covalent components considered. Here we propose a detailed approach that takes this complication into consideration.

14.1. Assigning the absolute stereochemistry of mechanically axially chiral molecules containing (pro)stereogenic centres

We propose that the absolute stereochemistry of axially chiral molecules based on a prochiral centre in each component can be assigned by correctly orienting their substituents. In the case of catenanes (e.g. **I**, Figure 206a), the in-plane substituents of the prochiral units should be oriented towards one another, whereas in the case of rotaxanes they should be oriented in the same direction (e.g. **II**, Figure 206b). The latter rule is to ensure that the notional ring opening of a catenane results in a rotaxane with the same absolute configuration. This arrangement is then viewed along the axis between prochiral centres to determine the orientation of the vectors connecting the out of plane substituents.

This approach can be readily extended to rings containing multiple identical prochiral moieties as any of these can be selected to achieve an identical result (e.g. **III,** Figure 206c). Similarly, catenanes based on rings containing multiple but non-identical prochiral moieties can be assigned by identifying the highest priority centre using CIP priorities for each centre and then following the same approach (e.g. **V**, Figure 206d). This approach can be extended to molecules based on a meso ring structure by orienting the in-plane substituents of the highest priority stereogenic units in the same way (e.g. **IV** and **VI**, Figure 206c and d respectively).

The step-by-step application of our approach for catenanes (e.g. **I**, Figure 206a) is given below. The same approach, with the prochiral moieties oriented in the same direction, can be applied to rotaxanes (e.g. **II**, Figure 206b):

Step 1: in each ring, identify the highest priority prochiral group (or stereogenic unit in meso structures) using the Cahn-Ingold-Prelog priority of the central atom.

Step 2: In each ring, identify the highest priority ligand of the identified center that lie outside of the macrocycle plane, again using CIP priority, and label it as "A"; label the lower priority group "B".

Step 2: redraw the molecule such that the in-plane substituents of both centres point towards one another with the macrocycles perpendicular to one another.

Step 3: define a vector A→B for each centre.

Step 4: View the relative orientation of the vectors along the axis connecting the centres and consider the direction of rotation from the head of the front vector to the tail of the rear vector, with a right-handed path assigned as (R_{ma}) and a left-handed path assigned as (S_{ma}).

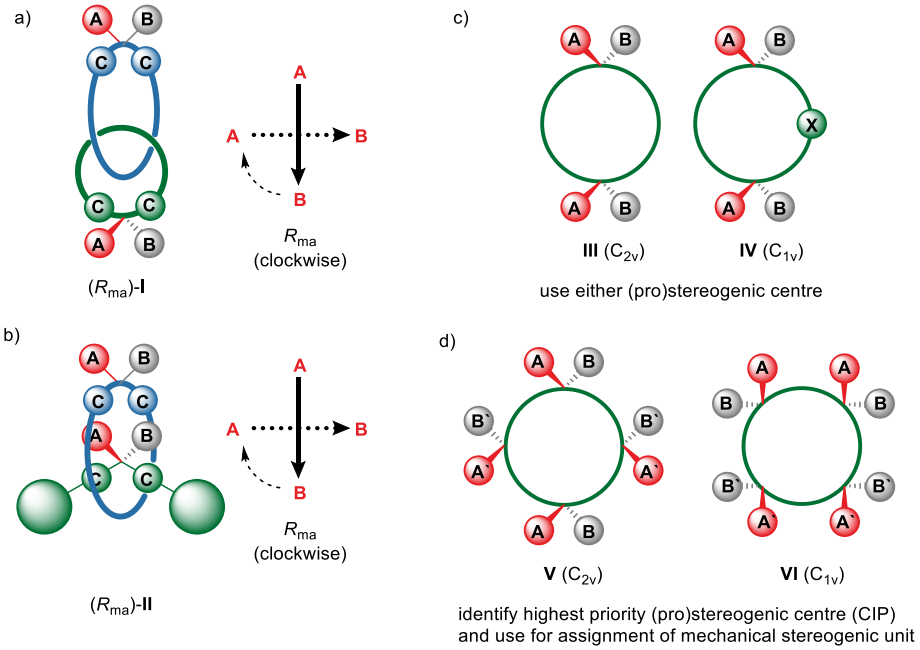

Figure 206: (a) Schematic representation of the method for assigning the stereochemistry of mechanically axially chiral catenane **I** whose rings each contain one prochiral centre. (b) Schematic representation of the method for assigning the stereochemistry of mechanically axially chiral rotaxane **II** whose ring and axle each contain one prochiral centre. (c) Examples of rings containing identical (pro)stereogenic centres - structures based on these rings can be assigned using any of the (pro)stereogenic units. (d) Examples of rings containing non-identical (pro)stereogenic centres - structures based on these rings can be assigned by first identifying the highest priority (pro)stereogenic unit based on the Cahn-Ingold-Prelog priority.

14.2. Assigning the absolute stereochemistry of mechanically axially chiral molecules based on other (pro)stereogenic units

The approach described above can be extended to rings based on (pro)stereogenic units other than centres (e.g. **VI**) by identifying that these can also be characterized as having (i) in plane substituents and (ii) at least one out of plane substituent. Indeed, this is a requirement for the appearance of permanent facial dissymmetry, the pre-requisite for mechanical axial stereochemistry.

In the case of axial (pro)stereogenic units, the approach can be extended without any significant modifications; the in-plane substituents that connect the (pro)stereogenic unit to the ring structure should be oriented towards one another and the out-of-plane substituents that define the (pro)stereogenic axis ranked using the CIP system, as in the assignment of a covalent axial stereogenic unit, and labelled A/B as above (e.g. **VII**, Figure 207). Planar (pro)stereogenic units (e.g. **VIII**, Figure 207) require a single modification to our general approach. Once again, the in-plane substituents that connects the (pro)stereogenic unit to the ring structure should be oriented towards one another. However, the plane is typically desymmetrised on only one face and so it is hard to identify the A and B substituents as in (pro)stereogenic centres and axes. In this case we propose that the A→B vector be replaced by a vector perpendicular to the ring plane pointing from (i.e. this is the tail of the vector) the highest priority out of plane ligand, the "pilot atom" in the context of the assignment of planar covalent stereogenic units, to the opposite face of the ring. Based on these arguments, all three prochiral units shown in Figure 207 result in the same **A→B** vector.

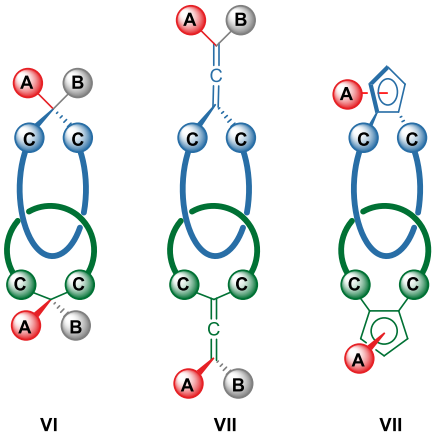

Figure 207: Three mechanically axially chiral catenanes with the same stereolabel based on prochiral centres (**VI**), axes (**VII**) and planes (**VIII**)

15. Mechanical stereochemistry in molecules containing prochiral and stereogenic centres

15.1. Stereochemical analysis of catenanes containing one prochiral and one chiral stereogenic unit

Having focused on how mechanical axial stereogenic units arise due to prochiral units, it is worth considering what happens when one of these is replaced by a chiral stereogenic unit (e.g. a stereogenic centre, Figure 208). If we consider what happens on substituent permutation[20], we see that such molecules can exist as four stereoisomers, which is consistent with them containing a covalent and a mechanical stereogenic unit. Exchanging C and D inverts the covalent absolute configuration whereas exchanging A` and B` inverts the mechanical absolute configuration. Interestingly, exchanging A and B inverts the absolute configuration of both stereogenic units. Based on this analysis, we propose that catenanes of this form are considered as containing a combination of mechanical axial and covalent stereogenic units and so, if a single diastereomer could be isolated, are viable precursors to axially chiral catenanes were the in-plane substituents of the stereogenic centre symmetrised through chemical modification.

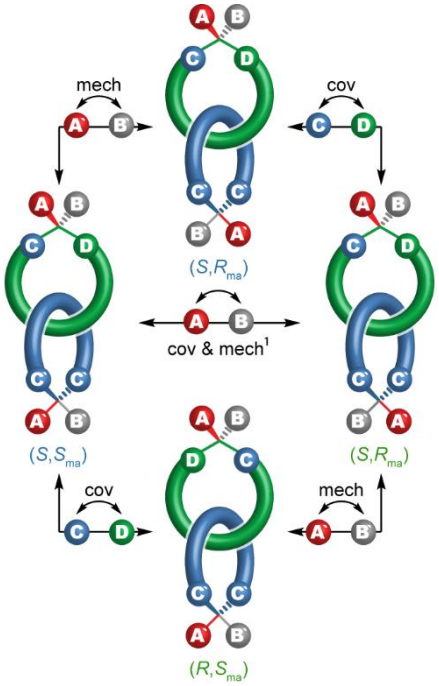

Figure 208: The four stereoisomers of a catenane in which one ring contains a prostereogenic centre and the other contains a stereogenic centre. cov = ligand exchange inverts covalent stereolable, mech = ligand exchange inverts mechanical stereolabel.

15.2. Catenanes containing one chiral stereogenic unit in each ring

The next logical step is to consider the stereochemistry of a catenane in which both rings contain a covalent stereogenic center (Figure 209). Intuitively, because each ring can exist in two enantiomeric forms, each of which can be interlocked with the other in two orientations, we can anticipate the potential for eight stereoisomeric forms and indeed, using the substituent permutation approach, this is what we find. Based on this, we can conclude that such molecules contain two covalent stereogenic units and one mechanical stereogenic unit but how to describe the mechanical stereochemistry is less obvious. In one interpretation, the facial desymmetrisation provided by the covalent stereogenic center gives rise to mechanical axial stereochemistry. In the other, the sequence of atoms within each ring as a result of the stereogenic center gives rise to a topological mechanical stereogenic unit. The labels arising from these interpretations behave differently under substituent permutation; exchanging the in-plane substituents inverts the topological and covalent stereogenic labels but leaves the axial stereodescriptor unchanged. Conversely, exchanging the out of plane substituents inverts the axial and covalent stereodescriptors but the topological label is unchanged.

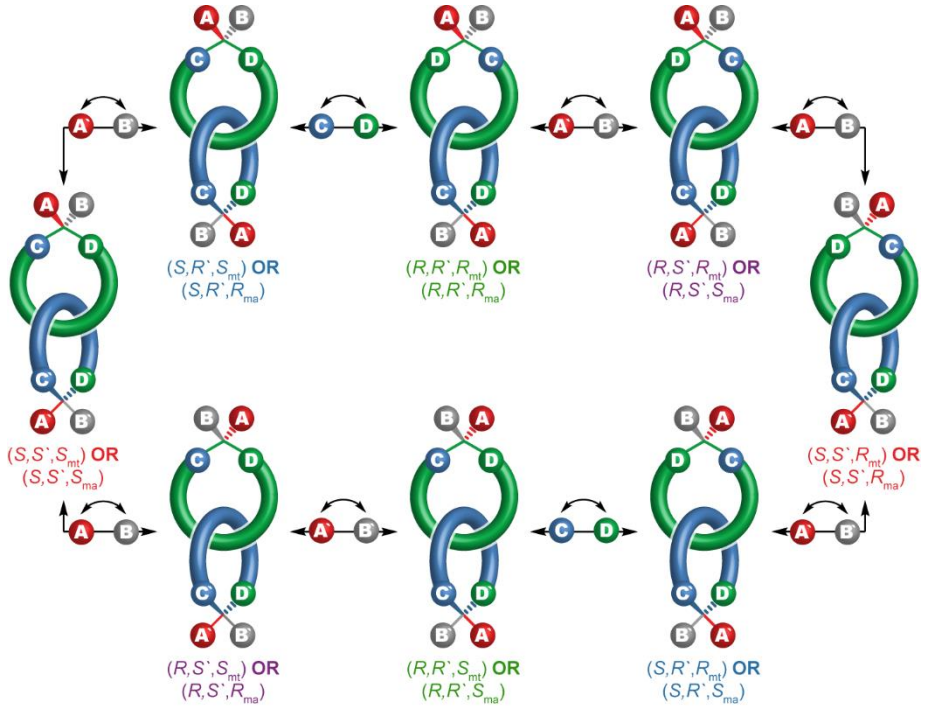

Figure 209: The eight stereoisomers of a catenane in which both rings contain a stereogenic centre. cov = ligand exchange inverts covalent stereolable, mech = ligand exchange inverts mechanical stereolabel. For each structure two mechanical stereolabels are provided, onl one of which is required to specify the structure.

Privileging one of these interpretations over the other is challenging but we propose that the covalent/topological description is more intuitively satisfying as it captures one of the more interesting properties of the system, the topological invariance of the mechanical stereogenic unit in such molecules; even when the Euclidean properties of the system are relaxed (i.e. bond angles and lengths), such catenanes remain chiral objects whereas axially chiral catenanes themselves do not. Indeed, it is chemically possible to epimerise the covalent stereocenters, for example through deprotonation/reprotonation or nucleophilic displacement, which would also invert the mechanical axial stereodescriptor, but a direct chemical process that exchanges the topological epimers is harder to envisage. Regardless of the interpretation, what is undoubtedly true is that the stereochemistry of such molecules can be fully described using two covalent and one mechanical stereolabel, confirming that the mechanical stereogenic unit should only be "counted" once

– it would be incorrect to assign both mechanical topologically and axial stereodescriptors simultaneously as this would, in effect, be double counting[21,22].

16. Other manifestations of mechanical axial stereochemistry

The manuscript describes an approach to molecules containing a fixed mechanical axial stereogenic unit. However, similar dynamic stereogenic units can arise due to co-conformational and conformational isomerism of the covalent subcomponents.

16.1. Co-conformational mechanical axial chirality

We have previously identified[18] that catenanes can display a co-conformational mechanical axial stereogenic unit when a ring whose highest symmetry representation is of C_{2h} or D_{nd} symmetry is combined with a C_{nv}, C_{2h} or D_{nd} ring. Such structures do not contain a fixed mechanical stereogenic unit but adopt chiral co-conformations that rely on the facial dissymmetry of the constituent rings, hence the analogy with the fixed mechanical axial stereogenic unit qualified by the co-conformational prefix. In schematic form, the required symmetry can be envisaged in rings that contain two or more prochiral moieties where the facial dissymmetry imparted by one is opposed by the other (e.g. **I** and **II**).

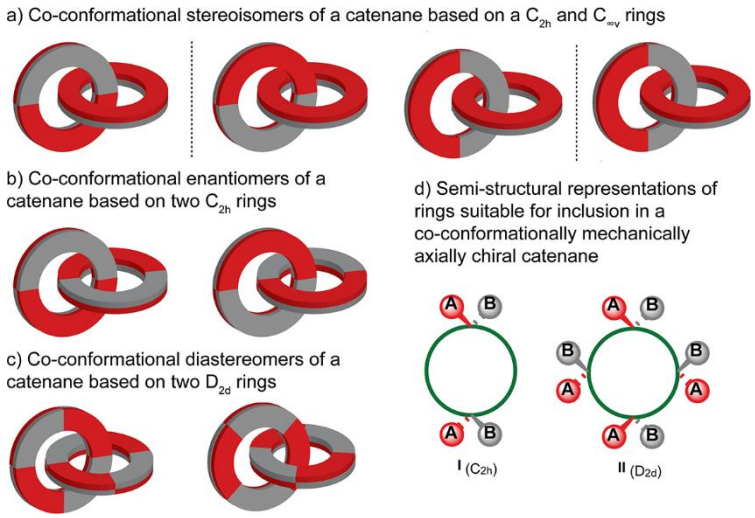

Figure 210: (a) Co-conformationally mechanically axially chiral enantiomers and diastereomers of a catenane based on a C_{2h} ring and a $C_{\infty v}$ ring. (b) Co-conformationally mechanically axially chiral enantiomers of a catenane based on two C_{2h} rings. (c) Co-conformationally mechanically axially chiral diastereomers of a catenane based on two D_{2d} rings. (d) Semi-structural representations of a C_{2h} ring containing two prochiral centres and a D_{2d} ring containing 4 prochiral centres.

The only example of such a structure we have been able to identify was reported by Puddephat and co-workers (Figure 211)[23]. The isolated ring, **IV**, of catenane **V** can exist in chiral and achiral forms, depending on the configurations of the binapthyl units, which are atropisomeric. When precursor **III** was combined with a Pd^{II} source, the resulting catenane was observed to contain meso rings **III** but the overall structure was found to be chiral, with both enantiomers observed in the solid state. The most symmetrical representation of the meso form of **IV** has C_{2h} symmetry and thus the observed stereochemistry can be recognised as arising from a co-conformationally mechanically axially stereogenic unit. The enantiomers of **V** can thus be exchanged by pirouetting one ring relative to the other.

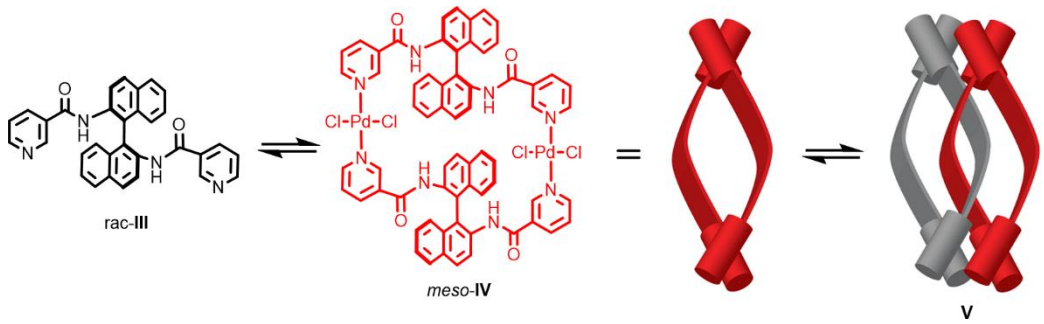

Figure 211: Puddephat's co-conformationally mechanically axially chiral catenane **V** constructed from C_{2h} rings **IV**.

16.2. Conformational mechanical axial chirality

Rings whose most symmetric representation is of higher symmetry than C_{nv} but whose stable conformations have C_{nv} symmetry can lead to interlocked structures that express what appears to be a mechanical axial stereogenic unit. The simplest example of this are structures containing a suitably embedded biphenyl unit (Figure 212). As this moiety adopts a non-planar conformation it behaves as a covalent axial prochiral moiety (e.g. **VI**). Such systems can be conformationally locked (i.e. atropisomeric) and so result in structures that functionally contain a fixed mechanical stereogenic unit, albeit a notional conformational exchange process can invert the enantiomers.

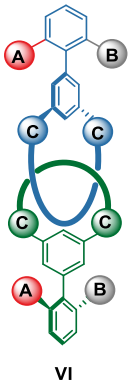

Figure 212: Conformationally mechanically axially chiral catenane **VI** whose stereochemistry relies on prochiral atropisomeric axial units.

Less obviously, any structural feature that enforces a C_{nv} symmetric conformation on the ring structure will result in the appearance of conformational mechanical axial stereochemistry. The earliest example we were able to identify that meets these criteria was reported by Sauvage and co-workers (Figure 213); the rings of catenane **VII** are too small to allow the alkyl chain to adopt the most symmetrical conformation in which it bisects the phenanthroline unit and so it is sits to one side. As a result, both rings adopt C_{2v} conformations that are enforced by the mechancial bond. The chiral nature of **VIII** could be detected when NMR analysis was carried out in the presence of a chiral anion, which led the appearance of diastereomeric signals.

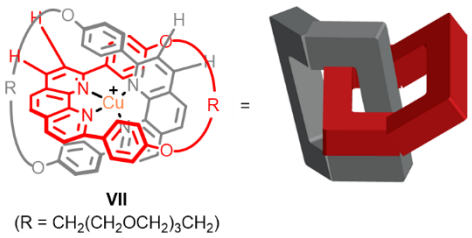

Figure 213: Conformationally mechanically axially chiral catenane **VII** whose stereochemistry arises due to the C_{1v} conformation of the rings that is enforced by the sterically crowded nature of the mechancial bond.

Cougnon and co-workers reported catenane **VIX** (Figure 214) that displays conformational mechanical axial stereochemistry (Figure 214)[24] (note: the schematic representations used in this manuscript suggest that the system displays co-conformational topological stereochemistry and the term "mechanical axial" is also used to describe the observed stereochemistry). The mechanical stereogenic unit arises because the naphthyl side panels of macrocycle **VIII** can adopt planar chiral conformations, the most stable of which is the meso form, at least in the catenane, and so the resulting ring structure has C_{1v} symmetry. The authors demonstrated that the conformational equilibrium could be biased by a chiral counteranion, which resulted in an unequal mixture of two diastereomeric structures. It is less clear whether isomerisation between the enantiomers occurs through bond rotation or if the structure is too crowded for this to occur and instead the isomerisation takes place by opening and closing the rings. It should be noted that the solid-state structure contains molecules in which the rings of the catenane are not perpendicular to one another and so a co-conformational helical stereogenic unit is also present and the meso conformational stereogenic units are also desymmetrised by the relative positions of the two rings.

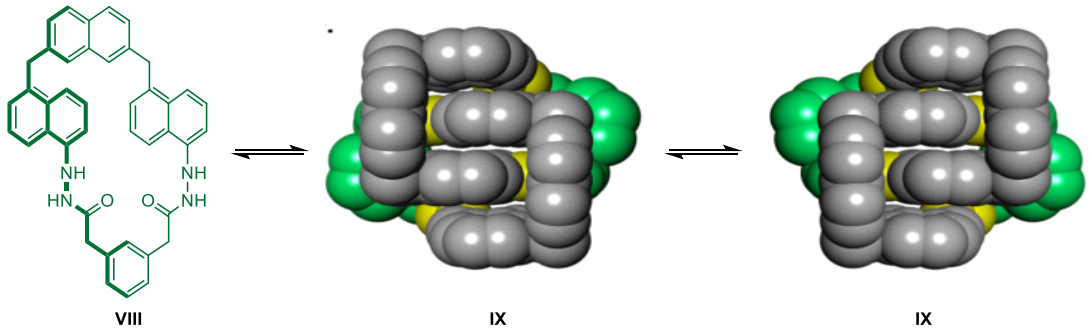

Figure 214: Conformationally mechanically axially chiral catenane IX constructed from macrocycle **VIII** that adopts a C_{1v} conformation.

16.3. Combining conformational and co-conformational isomerism

Although previously unrecognised (including by us)[18], if a ring adopts a preferred C_{2h} conformation, the resulting catenane can display a co-conformational mechanical axial stereogenic unit. This effect is most striking when the separated rings undergo fast conformational exchange which is slowed significantly in the interlocked structure due to steric crowding. Stoddart and co-workers demonstrated such a system in the case of catenane **XII** (Figure 215). The isolated rings of catenane **XII**, **X** and **XI**, are achiral but the naphthyl side panels are conformationally stereogenic. The rings can thus adopt conformations of different symmetry (Figure 215b), including an achiral C_{2h} structure, which results in co-conformationally mechanically axially chiral enantiomers that can be exchanged either by covalent bond rotation (i.e. inversion of the conformational stereogenic units) or co-conformational motion (relative rotation of one ring 180°).

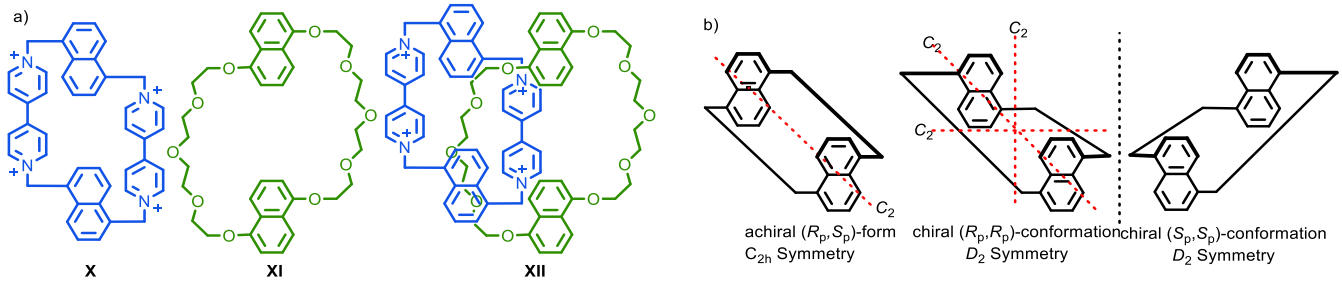

Figure 215: Catenane XII reported by Stoddart and co-workers in which the constituent macrocycles can exist in C_{2h} symmetry conformations, resulting in co-conformational mechanical stereochemistry.

17. References

(1) Pigorsch, A. & Köckerling, M. The Crystallization of Extended Niobium-Cluster Framework Compounds: A Novel Approach Using Ionic Liquids. *Cryst. Growth Des.* **16**, 4240-4246 (2016).

(2) Shibakami, M., Miyawaki, K., Harada, A. & Takagi, T. Design, Synthesis, and Self-Assembly of Parallel Cyclobolaphile that Contains Four Amide Groups as a Linkage between Polar Head Groups and Hydro-carbon Chain: A Mimetic of Archaeal Membrane Lipid. *Synlett*, 0349-0352 (2003).

(3) Do-Thanh, C. L., Vargas, J. J., Thomas, J. W., Armel, G. R. & Best, M. D. Design, Synthesis, and Evaluation of Novel Auxin Mimic Herbicides. *J. Agric. Food Chem.* **64**, 3533-3537 (2016).

(4) Lewis, J. E. M. *et al.* High yielding synthesis of 2,2′-bipyridine macrocycles, versatile intermediates in the synthesis of rotaxanes. *Chem. Sci.* **7**, 3154-3161 (2016).

(5) Ogi, S., Ikeda, T., Wakabayashi, R., Shinkai, S. & Takeuchi, M. A bevel-gear-shaped rotor bearing a double-decker porphyrin complex. *Chem. Eur. J.* **16**, 8285-8290 (2010).

(6) Kupwade, R. V., Khot, S. S., Lad, U. P., Desai, U. V. & Wadgaonkar, P. P. Catalyst-free oxidation of sulfides to sulfoxides and diethylamine catalyzed oxidation of sulfides to sulfones using Oxone as an oxidant. *Res. Chem. Int.* **43**, 6875-6888 (2017).

(7) Shukla, V. G., Salgaonkar, P. D. & Akamanchi, K. G. A mild, chemoselective oxidation of sulfides to sulfoxides using o-iodoxybenzoic acid and tetraethylammonium bromide as catalyst. *J. Org. Chem.* **68**, 5422-5425 (2003).

(8) Davis, F. A., ThimmaReddy, R. & Weismiller, M. C. (-)-.alpha.,.alpha.-Dichlorocamphorsulfonyloxaziridine: a superior reagent for the asymmetric oxidation of sulfides to sulfoxides. *J. Am. Chem. Soc.* **111**, 5964-5965 (2002).

(9) Pitchen, P., Dunach, E., Deshmukh, M. N. & Kagan, H. B. An efficient asymmetric oxidation of sulfides to sulfoxides. *J. Am. Chem. Soc.* **106**, 8188-8193 (2002).

(10) Hashmat Ali, M., Hartman, M., Lamp, K., Schmitz, C. & Wencewicz, T. Oxidation of Sulfides with N-Bromosuccinimide in the Presence of Hydrated Silica Gel. *Synth. Commun.* **36**, 1769-1777 (2006).

(11) Komatsu, N., Nishibayashi, Y., Sugita, T. & Uemura, S. Catalytic asymmetric oxidation of sulfides to sulfoxides using R-(+)-binaphthol. *Tetrahedron Lett.* **33**, 5391-5394 (1992).

(12) CrysAlisPro Software System, Rigaku Oxford Diffraction, (2020).

(13) Dolomanov, O. V., Bourhis, L. J., Gildea, R. J., Howard, J. A. K. & Puschmann, H. OLEX2: a complete structure solution, refinement and analysis program. *J. Appl. Cryst.* **42**, 339-341 (2009).

(14) Sheldrick, G. M. SHELXT - integrated space-group and crystal-structure determination. *Acta Cryst. A* **71**, 3-8 (2015).

(15) Sheldrick, G. M. Crystal structure refinement with SHELXL. *Acta Cryst. C* **71**, 3-8 (2015).

(16) Spek, A. L. PLATON SQUEEZE: a tool for the calculation of the disordered solvent contribution to the calculated structure factors. *Acta Cryst. C* **71**, 9-18 (2015).

(17) Spek, A. L. Single-crystal structure validation with the program PLATON. *J. Appl. Cryst.* **36**, 7-13 (2003).

(18) Jamieson, E. M. G., Modicom, F. & Goldup, S. M. Chirality in rotaxanes and catenanes. *Chem. Soc. Rev.* **47**, 5266-5311 (2018).

(19) Bruns, C. J. & Stoddart, J. F. *The Nature of the Mechanical Bond: From Molecules to Machines*. (Wiley, 2016).

(20) Mislow, K. & Siegel, J. Stereoisomerism and Local Chirality. *J. Am. Chem. Soc.* **106**, 3319-3328 (1984).

(21) Makita, Y., Kihara, N. & Takata, T. Synthesis and kinetic resolution of directional isomers of [2]rotaxanes bearing a lariat crown ether wheel. *Supramolecular Chemistry* **33**, 1-7 (2021).

(22) Schroder, H. V., Zhang, Y. & Link, A. J. Dynamic covalent self-assembly of mechanically interlocked molecules solely made from peptides. *Nat. Chem.* (2021).

(23) Burchell, T. J., Eisler, D. J. & Puddephatt, R. J. A chiral [2]catenane self-assembled from meso-macrocycles of palladium(II). *Dalton. Trans.*, 268-272 (2005).

(24) Caprice, K. *et al.* Diastereoselective Amplification of a Mechanically Chiral [2]Catenane. *J. Am. Chem. Soc.* **143**, 11957-11962 (2021).